LBL-1037

BIOPHYSICAL INVESTIGATION OF BIOMOLECULAR STRUCTURE AND INTERACTION:

I. CONFORMATION OF MONONUCLEOSIDES
II. CONFORMATION OF FLAVIN ADENINE DINUCLEOTIDE
III. ENZYME-SUBSTRATE INTERACTION OF A FLAVOPROTEIN - p-HYDROXYBENZOATE HYDROXYLASE
IV. PHOSPHOROUS-31 RELAXATION STUDY OF ADENOSINE TRIPHOSPHATE

Nelson Nan-Tsiung Teng
(Ph. D. Thesis)

RECEIVED
LAWRENCE
RADIATION LABORATORY

August 1972

LIBRARY AND
DOCUMENTS SECTION

AEC Contract No. W-7405-eng-48

TWO-WEEK LOAN COPY

This is a Library Circulating Copy which may be borrowed for two weeks. For a personal retention copy, call Tech. Info. Division, Ext. 5545

LAWRENCE BERKELEY LABORATORY
UNIVERSITY OF CALIFORNIA
BERKELEY

LBL-1037

DISCLAIMER

This document was prepared as an account of work sponsored by the United States Government. While this document is believed to contain correct information, neither the United States Government nor any agency thereof, nor the Regents of the University of California, nor any of their employees, makes any warranty, express or implied, or assumes any legal responsibility for the accuracy, completeness, or usefulness of any information, apparatus, product, or process disclosed, or represents that its use would not infringe privately owned rights. Reference herein to any specific commercial product, process, or service by its trade name, trademark, manufacturer, or otherwise, does not necessarily constitute or imply its endorsement, recommendation, or favoring by the United States Government or any agency thereof, or the Regents of the University of California. The views and opinions of authors expressed herein do not necessarily state or reflect those of the United States Government or any agency thereof or the Regents of the University of California.

BIOPHYSICAL INVESTIGATION OF BIOMOLECULAR STRUCTURE AND INTERACTION

Contents

	Page
Abstract	-vi-
Acknowledgements	-x-
CHAPTER I: CONFORMATION OF MONONUCLEOSIDES	1
A. INTRODUCTION	2
B. THEORETICAL CONSIDERATION OF OPTICAL ACTIVITY	3
Origin of Optical Activity	3
Definition of Rotational Strength	4
Monopole Approximation	7
Induced Dipole-Dipole Interaction	8
C. CALCULATION OF THE ROTATIONAL STRENGTH	9
Coordinates	9
Glycosidic Rotation	13
Transition Monopoles and Dipoles	13
Polarizabilities	15
D. RESULTS AND DISCUSSION	20
E. REFERENCES	31
CHAPTER II: CONFORMATION OF FLAVIN ADENINE DINUCLEOTIDE	34
A. INTRODUCTION	35
B. EXPERIMENTAL PROCEDURE	37
C. RESULTS AND DISCUSSION	39
Assignment of Lines	39
Intermolecular Interactions	47

Contents (continued)

	Page
Intramolecular Interactions	49
Temperature Studies	51
Solvent Effects	56
Temperature Dependence of Line Widths	60
D. REFERENCES	63
CHAPTER III. ENZYME-SUBSTRATE INTERACTION OF A FLAVOPROTEIN - *p*-HYDROXYBENZOATE HYDROXYLASE	65
A. INTRODUCTION	66
B. EXPERIMENTAL PROCEDURE	68
Material	68
Enzyme Preparation	68
Enzyme Assays	70
Kinetic Measurements	70
Optical Measurements	70
Nuclear Magnetic Resonance Measurements	71
Anaerobic Experiment	71
C. RESULTS	72
Chemical Structure of Substrate Analogues	72
Kinetic Study	72
Effect of Deuterium on the Activity of *p*-Hydroxybenzoate Hydroxylase	80
Circular Dichroism Study of the Enzyme-Inhibitor Complexes	85
Evidence for the Direct Binding of NADPH to *p*-Hydroxybenzoate Hydroxylase	89

Contents (continued)

Page

Nuclear Magnetic Resonance Study 92

D. DISCUSSION 96

E. REFERENCES 101

CHAPTER IV: PHOSPHOROUS-31 RELAXATION STUDY OF ADENOSINE TRIPHOSPHATE 103

A. INTRODUCTION 104

B. EXPERIMENTAL PROCEDURE 105

Material 105

NMR Spectra 108

Relaxation Time Measurement 108

C. RESULTS AND DISCUSSION 109

Orthophosphate 109

Adenosine Triphosphate 116

D. REFERENCES 135

APPENDICES 137

I. ^{31}P-HOMONUCLEAR FOURIER TRANSFORM DOUBLE RESONANCE 138

II. COMPUTER PROGRAMS

A. Program ROTSTRN 146

B. Program TEMROT 162

C. Program LESQW 166

III. REPRINTS 170

BIOPHYSICAL INVESTIGATION OF BIOMOLECULAR STRUCTURE AND INTERACTION

Nelson Nan-Hsiung Teng

Laboratory of Chemical Biodynamics
Lawrence Berkeley Laboratory
University of California
Berkeley, California

ABSTRACT

This thesis describes the investigation of the structure and interaction of biological molecules by various spectroscopic techniques. In Chapter I we present a theoretical treatment of the optical activities of mononucleosides in the hope to understand the following: a) The steric hindrance of the rotation of the bases about glycosidic bonds; b) the furanose contribution to the optical activities of polynucleotides and, hence, to facilitate the interpretation of the circular dichroism spectra of polynucleotides. The rotational strengths of the two longer wavelength transitions B_{2U}, B_{1U}, of four mononucleosides (adenosine, guanosine, uridine and cytidine) as a function of the glycosidic rotational angles have been calculated. The transition in each base is characterized by transition monopoles; the sugar is treated as a sum of bond polarizabilities. The interaction among these polarizabilities is also considered. Rotational strengths were calculated using three different sets of transition monopoles and many combinations of bond polarizabilities. We conclude that adenosine, uridine and cytidine may

have primarily one conformation, but that in guanosine the base is not definitely fixed with respect to the ribose. This finding may provide a physical explanation of the pairing of codon and anticodon. Calculation on different anomeric nucleosides of adenosine and uridine shows that the configuration at the anomeric carbon (C1') determines the sign of the optical rotation. The configuration at C2' influences the glycosidic angular dependence of rotational strength more profoundly than that at C3' and C5'. These results are in good agreement with experiments. The signs and magnitude of the calculated rotational strengths are in good agreement with experiment for the anti conformation of all the isomers of adenosine. As the conformation of the nucleosides in B-form DNA is quite different from the anti form, we calculate that the rotational strengths of the nucleosides in the polynucleotide are very different from those in solution.

In Chapter II the conformation of a slightly larger nucleotide, flavin adenine dinucleotide (FAD), is studied. Proton magnetic resonance have shown that FAD assumes a conformation where the adenine ring is folded over the isoalloxazine ring and the dinucleotides associate as dimers in solution at the concentration investigated. The determination of the temperature dependence of the FAD, flavin mononucleotide (FMN), and adenosine diphosphoribose (ADPR) proton shifts were found to be necessary for a correct assignment of the isoalloxazine protons in FAD and hence for determining the conformation. The FAD proton shifts in D_2O solutions have a sigmoid dependence on temperature which is discussed in terms of a two-state model, where an

equilibrium exists between the folded and unfolded states of the molecule. Sigmoid curves are not observed in D_2O/dioxane solutions, suggesting that dioxane lowers the transition temperature. Dioxane decreases the fraction of folded FAD molecules in solution by lowering the energy barrier between the two states and also reduces the intermolecular stacking of FAD and FMN.

Chapter III attempts to understand the mechanism of action of p-hydroxybenzoate hydroxylase from Pseudomonas putida, strain M-6. The aromatic substrate analogues, benzoate, p-fluorobenzoate, p-chlorobenzoate, p-nitrobenzoate, p-aminobenzoate, and 6-hydroxynicotinate, are found to be competitive inhibitors. This finding differs from the previously reported noncompetitive behavior in a different buffer system. Deuterium isotopic effect on the enzyme activity is presented.

The optical activity of the enzyme-inhibitor complex is studied. From the kinetic and circular dichroism (CD) measurements, we have found that the carboxyl moiety is necessary and sufficient for the enzyme-substrate binding, whereas the hydroxyl group alone will not lead to binding. There are two classes of inhibitory analogues: One causes changes in CD spectra of the enzyme similar to those evoked by the substrate, and the other does not cause significant changes. This difference may be understood in terms of a steric hindrance effect at the hydroxyl binding site. The CD of the enzyme-NADPH complex under anaerobic conditions suggests that the oxidized enzyme and reduced pyridine nucleotide form a complex, both in the absence and presence of the substrate p-hydroxybenzoate. NMR study of the enzyme-NADPH complex indicates that the adenine moiety of NADPH binds to the enzyme more

tightly than the nicotinamide region. Furthermore, evidence for a ternary complex is given.

In Chapter IV the NMR relaxation behavior of phosphorous-31 in orthophosphate and adenosine 5'-triphosphate (ATP) are studied. The longitudinal relaxation (T_1) times of phosphates are strongly influenced by low levels of paramagnetic metal ions and by pH. Deuterium isotopic effect on the phosphorous relaxation rate of both orthophosphate and ATP is presented. A detailed investigation of the phosphorous NMR chemical shift and T_1 relaxation rates as a function of pH and Fe^{3+} concentration is given. Fourier transform double resonance (FTDR) technique is illustrated. The NMR relaxation mechanism of phosphorous is discussed.

ACKNOWLEDGMENTS

Our very existence is a link in the continuous chain of biological evolution, our very contribution is only made possible by the inseperable, cooperative and accumulative efforts of others.

To the following I would like to express my gratitude and appreciation: Melvin Calvin, Keiichi Hosokawa, William Horsley, Martin Itzkowitz, the late Aharon Katchalsky, Melvin Klein, George Kotowycz, Evie Litton, Leonard Loeb, John Markley, John Neilands, Alex Nichols, Jo Onffroy, Irving Salmeen, Zin-may Sung, and Ignacio Tinoco, Jr.

This investigation was supported in part by a University of California Fellowship (1969-1970) and in part by the U.S. Atomic Energy Commission.

I. CONFORMATION OF MONONUCLEOSIDES

A. INTRODUCTION

The understanding of the chemical structure and molecular interaction of nucleic acids are fundamental in elucidating many of their biological functions. Since the nucleic acids are optically active, circular dichroism (CD) and optical rotatory dispersion (ORD) are useful techniques in studying the molecular structure. The theory of optical activity has been treated extensively in several articles.[1] A general consideration of the origin of optical activity will be given here. An optically active molecule must not possess a plane or a center of symmetry. Generally, optically active molecules can be separated into two classes, the class containing an inherently dissymmetric chromophore, and the class containing a symmetric chromophore in a dissymmetric molecular environment. Hexahelicene, skewed dienes, are examples of the inherently dissymmetric chromophore. Azosulfonamide is optically inactive; however, upon binding to carbonic anhydrase, a large visible CD is produced.[2] The resulting optical activity, apparently, is induced in the symmetric chromophore by the dissymmetric potential field of the protein. Four principal mechanisms have been proposed for the origin of optical activity: (1) The coulombic field of the substituents mixes the electronic states of the symmetric chromophore such that a magnetic dipole transition acquires a minor electric dipole character and <u>vice versa</u>. (2) The incident electromagnetic radiation producing an electronic excitation in the symmetric chromophore induces a transient

electric dipole moment in the substituent which, then couples with the magnetic or the electric dipole moment of the chromophore transition. (3) The electronic transitions of two chromophores interact as coupled oscillators. (4) In an inherently dissymmetric chromophore, each electronic transition will have both magnetic and electric dipole moments. The optical activity in the dissymmetric chromophore is, usually, much larger than those in (1), (2), and (3), where the optical activities are derived from vicinal perturbation of the symmetric chromophores.

Recently, theories have been developed to facilitate the interpretation of the spectra of polynucleotides.[3,4] However, in these theories, the CD and ORD of the monomer units themselves have been ignored. Therefore, the conformation of nucleosides has been the subject of interest, both experimentally and theoretically.[5-8] The optical activity of mononucleosides falls into mechanism (2) described above.

In this chapter we have used an improved version of Kirkwood polarizability theory to include the presence of a classical polarizability near a quantum system. The rotational strengths of mononucleosides are calculated using transition monopoles on the bases interacting with polarizable bonds of the sugars. We try to examine the calculations critically. Three different sets of transition monopoles have been employed with various degrees of success. The effect of different values of bond polarizability and variation of the positions of furanosyl OH groups has also been examined. The calculated rotational strengths as a function of the glycosidic angle are in qualitative agreement with calculations of Miles _et al._,[8] using bond transition dipoles on the bases.

In the next section a detailed description of the theoretical method is given; in section C we discuss the numerical methods and the data used, and in section D we demonstrate the application of the theory to the four mononucleosides found in nucleic acids and to various anomeric isomers of adenosine and uridine.

B. THEORETICAL CONSIDERATION OF OPTICAL ACTIVITY

Origin of Optical Activity

Condon[1] modified the familiar constitutive properties for a homogeneous, isotropic, optically inactive medium to incorporate time varying terms with proportionality constant g, thus:

$$\underset{\sim}{D} = \varepsilon \underset{\sim}{E} - g\dot{\underset{\sim}{H}} \tag{1}$$

$$\underset{\sim}{B} = \mu \underset{\sim}{H} + g\dot{\underset{\sim}{E}} \tag{2}$$

where ε is the dielectric constant, μ is the magnetic permeability, and $\mu \simeq 1$ for nonmagnetic media. $\underset{\sim}{D}$, $\underset{\sim}{B}$ are electric displacement and magnetic induction, respectively. $\underset{\sim}{E}$, $\underset{\sim}{H}$ are the electric and magnetic field intensities.

A solution of Maxwell's equations, then, yields

$$n_R = \varepsilon^{1/2} - 2\pi\nu\, g \tag{3}$$

$$n_L = \varepsilon^{1/2} + 2\pi\nu\, g \tag{4}$$

n_R, n_L are the indices of refraction for left and right circularly polarized light, and ν is the frequency of the incident light.

Then the rotation per unit length ϕ is given by definition

$$\phi = \frac{4\pi^2 c}{2}\, g \tag{5}$$

g can be related to the microscopic parameter β if

$$\mu = \alpha E^{eff} - \beta/c\ \dot{H} \tag{6}$$

E^{eff} is the local effective electric field, and, if one assumes Lorentz' expression, then

$$g = \frac{4\pi}{3} N_1 (\beta/c)\ (\varepsilon+2) \tag{7}$$

N_1 is the number of molecules per unit volume. The parameter β can be calculated by a quantum mechanical expansion of the expectation value of the electric dipole moment μ in the ground state as induced by the electromagnetic field. When the induced dipole moment is averaged over all occupied molecular states and then over all possible molecular orientations, β is given by the following expression:

$$\beta = \frac{c}{3\pi h} \sum_A \frac{\{\mathrm{Im}\ \langle 0|\ \mu\ |A\rangle\ \langle A|\ m\ |0\rangle\}}{\nu_A^2 - \nu^2} \tag{8}$$

$|o\rangle$ and $|A\rangle$ are the wave functions from the ground state and excited state respectively. Im denotes the imaginary part of a complex number.

Definition of Rotational Strength

Rosenfeld[9] characterized the optical rotation by the rotational strength for the optical transition from 0 to A, $R_{0A} = \mathrm{Im}(\mu_{0A} \cdot m_{A0})$. μ_{0A} is the electric dipole transition moment vector and m_{A0} is the magnetic dipole transition moment vector defined as follows:

$$\mu_{0A} = \sum_j \langle 0|\mu_j|\ A\rangle \tag{9}$$

$$m_{A0} = \frac{e}{2\ mc} \sum_j R_j \times \langle A|\ P_j\ |0\rangle + \sum_j \langle A\ |m_j'|\ \ 0\rangle \tag{10}$$

where R_j is the vector distance from an arbitrary origin to the origin of group j; μ_j is the electric dipole moment operator of group j; P_j is the

linear momentum operator of group j; $\underset{\sim}{m}_j$ is the magnetic moment operator of group j relative to the origin in group j (illustrated in Figure 1). The origin is usually selected to minimize the contribution of $\underset{\sim}{m}_j'$ to rotational strength. c, e, m are the usual notations for speed of light, electronic charge and electronic mass. The molecular wavefunctions for states 0 and A are $|0\rangle$ and $|A\rangle$. The expectation value of $\underset{\sim}{P}_j$ between state 0 and A can be related to $\underset{\sim}{\mu}_{j0A}$ by the relation

$$\underset{\sim}{P}_{j0A} = (-2\pi\ im/e)\ \nu_{0A}\ \underset{\sim}{\mu}_{j0A} \tag{11}$$

where $\underset{\sim}{\mu}_{0A}$ is the frequency of the transition from 0 to A. Therefore, for an electrically allowed, magnetically forbidden transition ($\langle A|\ \underset{\sim}{m}_j'|\ 0\rangle = 0$) the expression for rotational strength is

$$R_{0A} = (-\pi\nu_{0A}/2c) \sum_{i\neq j} \underset{\sim}{R}_{ij} \langle 0\ |\underset{\sim}{\mu}_i|\ A\rangle \times \langle A|\ \underset{\sim}{\mu}_j|\ 0\rangle \tag{12}$$

where $\underset{\sim}{R}_{ij} = \underset{\sim}{R}_j - \underset{\sim}{R}_i$.

It can be seen that the optical activity originates from the interaction between electric transition dipoles located asymmetrically with respect to one another. In equation (12) we have resolved R_{0A} into groups. The obvious separation into groups for mononucleosides would be to treat the base as the major chromophore and the furanose as an asymmetric substituent. The furanose is further subdivided into bonds. For a particular transition $0 \rightarrow A$ of the base, which is far removed in energy from any transitions in the furanose, it is a good approximation to replace the transition dipole from the bonds of the furanose by the dipole that would be induced in a classical polarizability placed within the transition field of the base.

$$\underset{\sim}{\mu}_{jA0} = \underset{\sim}{\alpha}_j \cdot \underset{\sim}{E}_j^{eff} \tag{13}$$

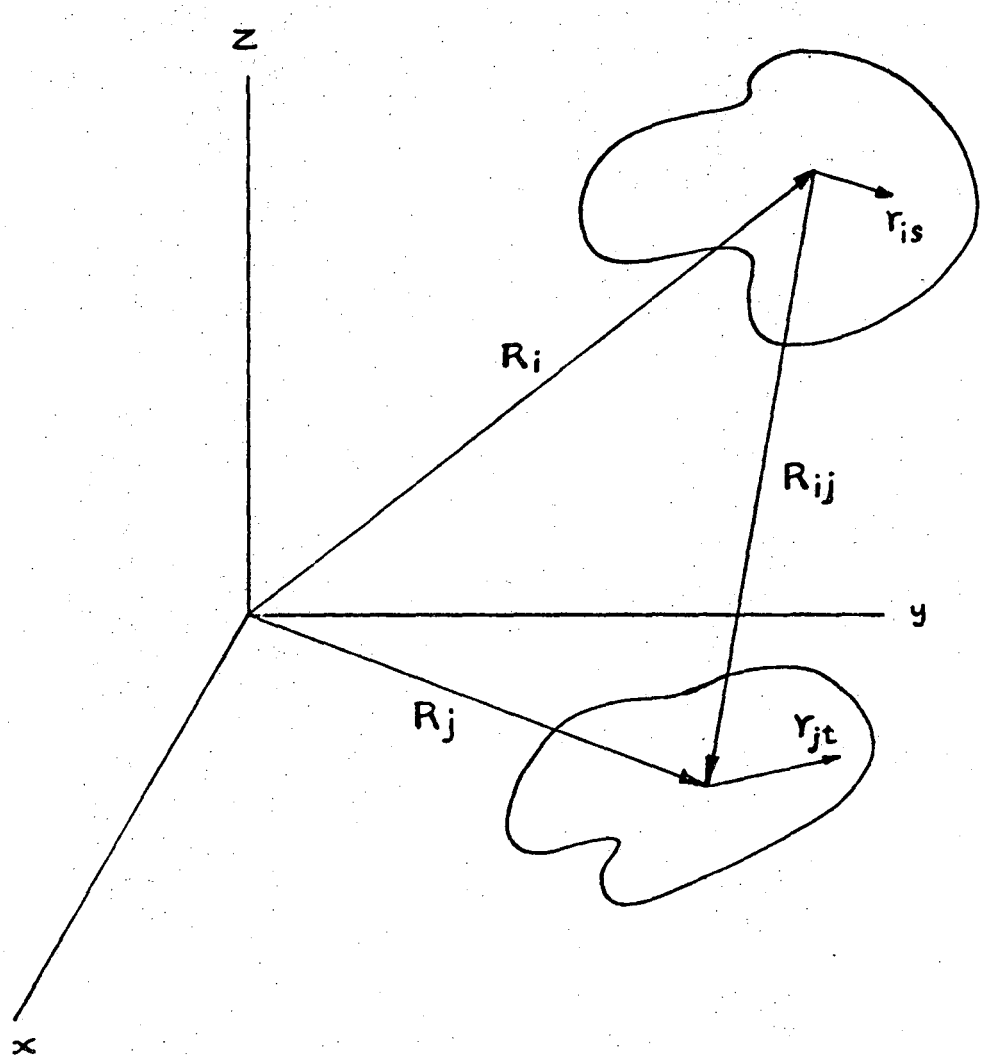

Figure 1. The vectorial relationship of group i,j and of electrons in the group (r_{is}, r_{jt}).

where $\underset{\sim}{\alpha}_j$ is the polarizability tensor of the jth furanose bond and $\underset{\sim}{E}_j^{eff}$ is the effective field at the jth bond due to the transition $0 \rightarrow A$.

Monopole Approximation

To evaluate the effective field $\underset{\sim}{E}_j^{eff}$, one expands the molecular wavefunctions in a linear combination of atomic orbitals,

$$|0\rangle = \sum_s C_{0s} \, |s\rangle$$

$$|A\rangle = \sum_s C_{As} \, |s\rangle$$

We obtain

$$\underset{\sim}{E}_j^{eff} = - \nabla_j \langle A| \frac{1}{r_j} |0\rangle$$

$$= - \nabla_j \sum_{s,t} C_{As}^* \, C_{0t} \cdot \langle s| \frac{1}{r_j} |t\rangle \qquad (14)$$

The standard point monopole approximation sets

$$\langle s| \frac{1}{r_j} |t\rangle = \delta_{st} \cdot \frac{1}{r_{sj}} \qquad (15)$$

where δ_{st} is the Kronecker δ.

Alternatively, one may treat $\psi_0|\psi_A$ as a charge distribution and do a multipole expansion ($\sum_j \underset{\sim}{E}_j^{eff}$) about the center of the charge. The practical limit in terms of computer programming on the CDC 6600 computer used for our calculations is the octupole term, and convergence is poor. We abandoned this method in favor of the use of equation (15). In the hopes of increased accuracy we calculated the integrals $\langle s|\frac{1}{r_i}|s\rangle$ in terms of Slater $2p\pi$ orbitals to obtain $\underset{\sim}{E}_j^{eff}$. This was found to make a negligible correction to rotational strengths; we therefore used for a zero order $\underset{\sim}{E}_j^{eff}$:

$$\underset{\sim}{E}_j^{eff} = \sum_s \rho_s \frac{\underset{\sim}{r}_{js}}{|r_{js}|^3} \qquad (16)$$

where $\rho_s \equiv C_{As}\, C_{Us}$ is the monopole charge of atom s due to the base transition $0 \rightarrow A$. $\underset{\sim}{r}_{js}$ is a position vector from the jth group to the sth monpole. By combining equations (12), (13) and (16), we have an expression for the rotational strength of transition $0 \rightarrow A$ in the base of a nucleoside. The base is represented by transition monopoles on each atom and the furanose is approximated by bond polarizabilities.

$$R_{0A} = \left(-\frac{\pi \nu_{0A}}{2c}\right) \sum_{i \neq j} \sum_{s} \rho_s \underset{\sim}{R}_{ij} \cdot (\underset{\sim}{\mu}_{iA0} \times \underset{\sim}{\alpha}_j \cdot \underset{\sim}{r}_{js}) / r_{js}^{\ 3} \qquad (17)$$

where $\underset{\sim}{R}_{ij}$ is the distance from the base transition dipole $(\underset{\sim}{\mu}_{iA0})$ to bond j in the furanose.

Induced Dipole-Dipole Interaction

Equation (17) is the most commonly used expression for calculating optical activity under conditions mentioned above. However, this expression has only considered the monopole field caused by the base and has ignored the interaction among the furanose bonds. This approximation may be good in situations where the asymmetric perturbation is an aliphatic chain.[10] But in the furanose ring, for the most part, the sugar bonds are much closer to each other than to the base, so each bond will feel the effect of the induced dipoles in all other bonds. To include this effect we replace $\underset{\sim}{E}_j^{eff}$ by a more complete expression

$$\underset{\sim}{\mu}_{jA0} = \underset{\sim}{\alpha}_j \cdot \underset{\sim}{E}_j^{eff} = \underset{\sim}{\alpha}_j \cdot \left[\sum_s \rho_s \frac{\underset{\sim}{r}_{js}}{|r_{js}|^3} - \sum_k \underset{\sim}{T}_{jk} \cdot \underset{\sim}{\mu}_{kA0}\right] \qquad (18)$$

where $\underset{\sim}{T}_{jk} = (\underset{\sim}{1} - 3\, \underset{\sim}{r}_{jk}\, \underset{\sim}{r}_{jk} / r_{jk}^{\ 2})\left(\frac{1}{r_{jk}^{\ 3}}\right)$ the dipole interaction tensor between points j and k.

These coupled linear equations can be solved for $\underset{\sim}{\mu}_{jA0}$.

$$\underset{\sim}{\mu}_{jA0} = \sum_k (1 + \underset{\sim}{\alpha}\underset{\sim}{T})^{-1}_{jk} \cdot \underset{\sim}{\alpha}_k \cdot \sum_s \rho_s \frac{\underset{\sim}{r}_{js}}{|r_{js}|^3} \qquad (19)$$

Substituting equation (19) in (12), we have the final expression for the rotational strength with the furanose interaction treated self consistently.

$$R_{0A} = \left(-\frac{\pi \nu_{0A}}{2c}\right) \sum_{i \neq j} \sum_{k} \sum_{s} \rho_s \, \underset{\sim}{R}_{ij} \cdot \underset{\sim}{\mu}_{iA0} \times \left(\underset{\sim}{1} + \underset{\sim}{\alpha} \underset{\sim}{T}\right)^{-1}_{jk} \cdot \underset{\sim}{\alpha}_k \cdot \underset{\sim}{r}_{ks} / |r_{ks}|^3 \quad (20)$$

For all calculations R_{0A} was evaluated using transition monopoles only as in equation (17) and also self consistently including the sugar bond-bond induced dipole coupling as in equation (20).

C. CALCULATION OF THE ROTATIONAL STRENGTH

All the computations were carried out on a CDC 6600 Computer. The listings of the computer programs used for the calculation of rotational strength as a function of glycosic rotation (ROSTRN) and temperature dependence of rotational strength (TEMROT) are given in Appendix IIA and IIB respectively.

We consider each base to have two $\pi \rightarrow \pi^*$ transitions with maxima between 240 mμ and 280 mμ. The transition frequency ν_{0A} is taken as the location of the major experimental UV absorption maximum.[4]

Coordinates. The coordinates used in the computation are taken from Spencer[11] for the bases (Table I) and Sundaralingam and Jensen[12] for the 2'endo ribose and 3'endo ribose. The coordinates for the α anomers were obtained by reflection from that of β nucleosides about the plane of C1', C2' and O' of the furanose. The numbering system and the nomenclature for the pentofuranoses is shown in Figure 2.

The conformation of the furanose has been subject of debate.[12-15] We have used 2'endo conformation, consistent with the majority of crystal structures of nucleosides, for most of the calculations. The 2'endo

Table I [11]

Atomic Coordinates of Purine and Pyrimidine Bases

Adenine			Cytosine		
Atom	X(Å)	Y(Å)	Atom	X(Å)	Y(Å)
N_1	-2.791	4.407	N_1	0.000	1.470
C_2	-3.201	3.134	C_2	-1.207	2.139
N_3	-2.391	2.078	N_3	-1.231	3.489
C_4	-1.079	2.298	C_4	-0.070	4.132
C_5	-0.604	3.583	C_5	1.157	3.504
C_6	-1.500	4.633	C_6	1.181	2.125
N_7	0.763	3.598	O_2	-2.253	1.511
C_8	1.055	2.280	N_4	-0.094	5.472
N_9	0.000	1.470			
N_6	-1.041	5.892			
Guanine			**Uracil**		
N_1	-2.799	4.348	N_1	0.000	1.470
C_2	-3.205	3.051	C_2	-1.207	2.139
N_3	-2.378	2.010	N_3	-1.159	3.518
C_4	-1.079	2.298	C_4	0.010	4.251
C_5	-0.604	3.583	C_5	1.205	3.504
C_6	-1.462	4.702	C_6	1.181	2.125
N_7	0.763	3.598	O_2	-2.269	1.538
C_8	1.055	2.280	O_4	0.010	5.471
N_9	0.000	1.470			
N_2	-4.523	2.807			
O_6	-1.045	5.848			

ribose and 3'endo deoxyribose coordinates are given in Table II. Coordinates of the other sugars were obtained by interchanging H and OH atoms and changing bond lengths. In solution, the positions of the hydroxyl groups of the furanose are not precisely known. In an effort to determine the influence of OH position on R_{OA}, we have rotated the OH groups about their individual CO axes for both adenosine and uridine. The effect on the calculated R_{OA} is small; the shape of the curve when R_{OA} is plotted

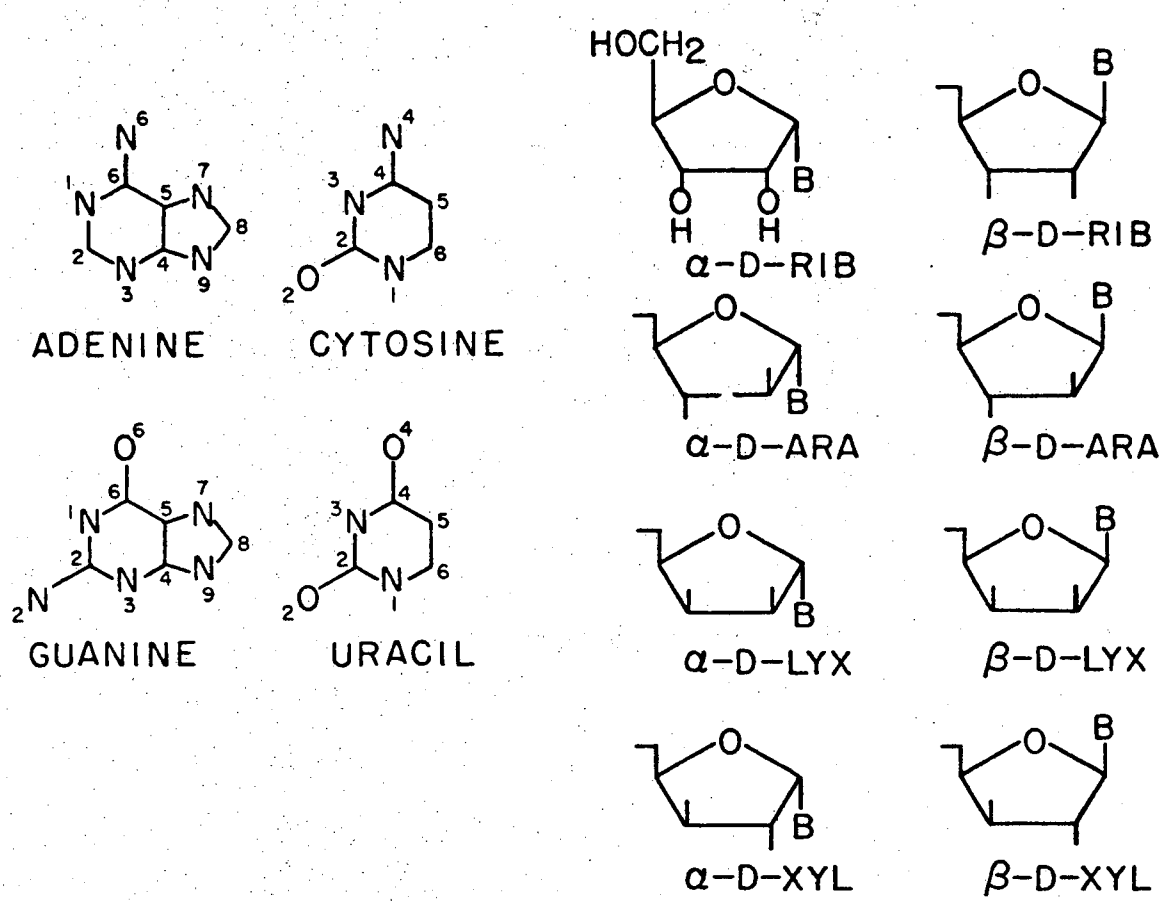

CONFIGURATION OF THE NUCLEIC ACID BASES AND THE PENTOFURANOSES

XBL709-5401

Figure 2. Nomenclatures and configurations of the nucleic acid bases and the pentafuranoses.

Table II. Coordinates of 2'endo ribose and 3' endo deoxy ribose[12]

Atoms	2'endo ribose x	y	z
C1	0.00	0.00	0.00
H1	-0.51	-0.16	0.74
O1	1.35	-0.43	0.00
C2	-0.62	-0.58	-1.25
H2	-0.26	0.08	-1.89
O2	-2.02	-0.57	-1.26
OH2	-2.60	-1.09	-0.59
C3	0.08	-1.94	-1.31
H3	0.02	-2.33	-2.02
O3	-0.53	-2.80	-0.34
OH3	-0.48	-3.80	-0.42
C4	1.51	-1.59	-0.86
H4	1.81	-2.46	-0.38
C5	2.48	-1.28	-1.97
H5	3.37	-0.73	-1.40
H5'	2.98	-2.14	-2.36
O5	1.95	-0.44	-3.00
OH5	1.88	-1.15	-3.69

Atoms	3'endo deoxyribose x	y	z
C1	0.00	0.00	0.00
H1	-0.40	-0.53	0.96
O1	1.37	-0.43	0.00
C2	-0.68	-0.65	-1.21
H2	-1.28	-1.47	-1.11
H2'	-1.35	-0.16	-1.86
C3	0.52	-1.08	-2.10
H3	0.87	-0.28	-2.80
O3	-0.24	-2.16	-2.96
OH3	0.06	-3.00	-2.40
C4	1.57	-1.37	-1.08
H4	1.20	-2.35	-0.70
C5	3.02	-1.26	-1.52
H5	3.71	-1.64	-0.80
H5'	3.28	-1.80	-2.39
O5	3.27	0.09	-2.04
OH5	4.06	0.23	-2.73

vs. the glycosidic angle (ϕ_{CN}) is not significantly altered. Slight variation in magnitude of R_{OA} is found when the OH at the C'2 position is rotated; however, no noteiceable change is observed in the case of C'3 and C'5. This finding is consistent with our conclusion (Section D) about the importance of configuration at C'2 position.

Glycosidic Rotation

We have chosen the definition of glycosidic rotation by Donohue and Trueblood.[16] The sugar-base torsion angle ϕ_{CN} is defined as the angle formed by the plane of the base and C_1'-O_1' bond of the furanose ring when viewed along the C_1'-N bond. ϕ_{CN} is taken as zero when C_2 of the base is anti-planar to O_1'. Positive rotation is clockwise rotation of C_1'-O_1' when one looks from C_1' to N. Donohue and Trueblood define "anti" conformation for ϕ_{CN} equal to -30° $\pm$45° and "syn" for ϕ_{CN} equal to +150° $\pm$45°. The "anti" and "syn" conformations of adenosine and uridine are illustrated in Figure 3.

Transition Monopoles and Dipoles

Three sets of monopoles for the various transitions of the four bases were used in the computation. We used monopoles described by Bush[17] and those calculated from self-consistent field with and without configuration interaction.[18] The monopoles obtained from Bush were calculated by a SCF-LCAO-CI method done by H. De Voe of National Institutes of Health. His method was that of Viellard and Pullman (1963) extended to the excited states. The monopoles selected by Bush were not just the lowest energy transitions but were chosen so that the transition moment directions were consistent with experimental directions, or what were inferred to be the most likely directions. Bush's procedure assumes the

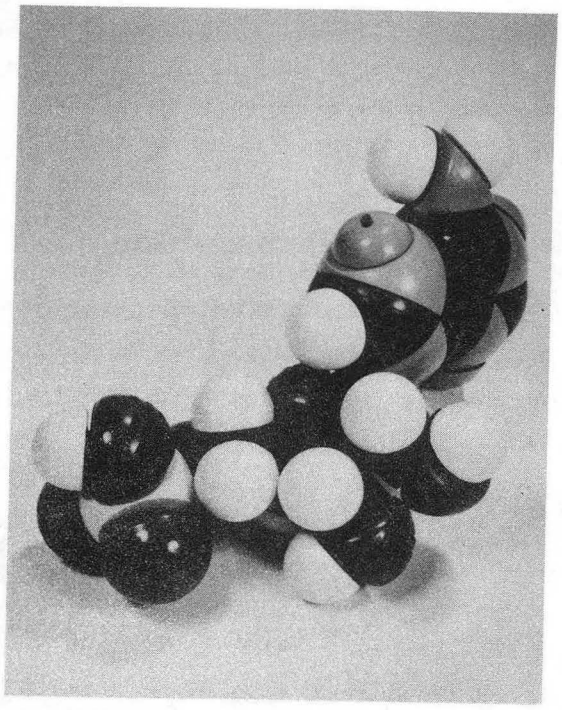

Anti 5'-AMP

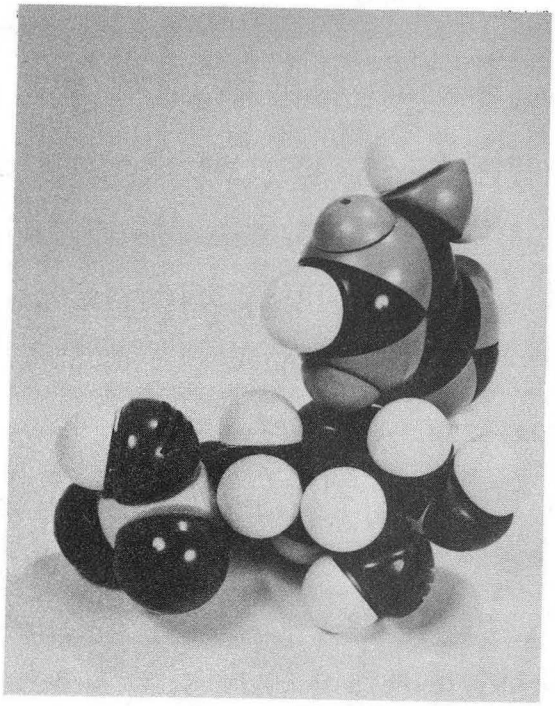

Syn 5'-AMP

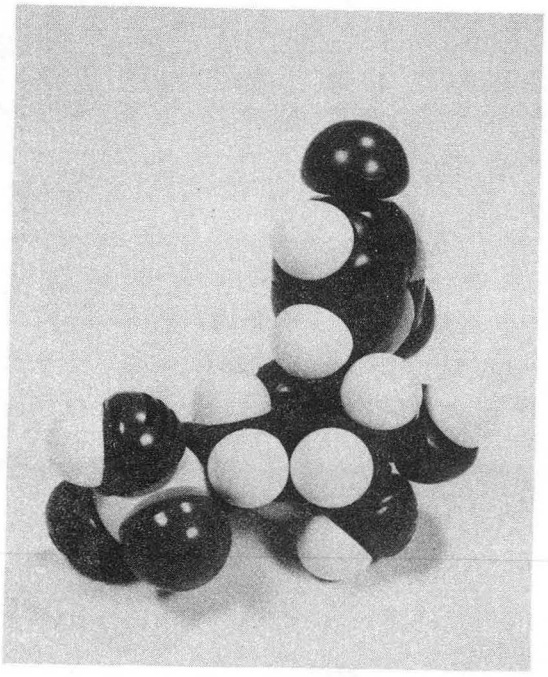

Anti 5'-UMP

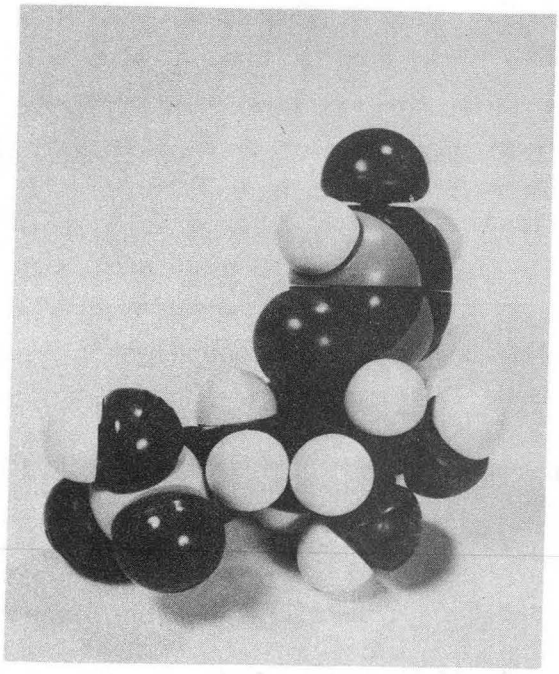

Syn 5'-UMP

Figure 3. The "anti" and "syn" conformation of 5'-AMP and 5'-UMP. The 5'-phosphorous is trans to C_4' as determined in Chapter IV.

XBB 727-3725

order of the excited state in energy may be incorrect. The magnitudes of all the monopoles were scaled to give the measured transition moment magnitudes. The scaled monopoles for the B_{2U} and B_{1U} transitions are given in Table III.

The base transition dipoles were calculated from the transition monopoles placed on each nucleus of the base. The point transition dipole is assumed to be at the center of transition charge of the base (Table IV).

The effect of different transition monopoles and the use of a self-consistent treatment of the furanose bond interactions is shown in Figure 4. One sees that the self-consistent theory for induced dipoles in the sugar [Equation (20)] gives very different results from Equation (17). We use Equation (20) for all the calculations discussed in this chapter.

Polarizabilities

Bond polarizabilities have always been the subject of controversy. The merits of different measurements of polarizability have frequently been discussed, especially by users wanting to evaluate optical activity.[4,8,22] Because of the uncertainties in the bond polarizabilities, the agreement between experiment and the result of any calculation which is sensitive to the values of bond polarizability should be examined critically.

Different sets of values of bond polarizabilities have been published (Table V). These values include those which have been proven satisfactory for other workers,[10] and those existing in the current literature. The rotational strength of uridine resulting from different

Table III.[a,b] Monopoles for the B_{2U} and B_{1U} transitions

	Trans. B_{2U}			Trans. B_{1U}		
Atom	SCF/CI[20]	SCF[19]	Bush/DeVoe[17]	SCF/CI	SCF	Bush/DeVoe
Adenine						
N1	-0.178	0.035	-0.030	0.023	-0.064	
C2	0.091	-0.072	-0.037	-0.063	-0.050	
N3	-0.129	0.140	-0.107	0.087	-0.014	
C4	-0.063	0.018	-0.291	-0.039	-0.051	
C5	-0.018	0.032	0.126	0.088	0.060	
C6	0.156	-0.114	0.232	-0.033	0.031	
N7	0.046	-0.085	0.055	-0.020	0.009	
C8	-0.180	0.134	-0.106	0.050	0.026	
N9	0.069	0.031	0.112	0.034	0.023	
N6	0.206	-0.117	0.046	-0.078	0.030	
Guanine						
N1	0.051	0.041	-0.032	0.116	0.039	-0.044
C2	0.100	0.101	0.030	-0.060	-0.013	-0.165
N3	-0.101	-0.080	-0.050	0.097	0.081	0.075
C4	0.090	0.060	-0.104	0.108	0.125	-0.151
C5	-0.112	-0.083	-0.034	-0.045	-0.079	0.165
C6	-0.013	-0.000	0.035	-0.008	0.007	0.003
N7	0.009	0.003	0.043	-0.039	-0.063	-0.042
C8	-0.060	-0.067	-0.291	0.207	0.099	0.127
N9	-0.009	-0.010	0.249	-0.088	0.000	0.028
O6	-0.003	-0.002	0.166	-0.243	-0.191	0.054
N2	0.049	0.039	-0.008	-0.046	-0.005	-0.049
Cytosine						
N1	-0.202	-0.135	-0.097	0.129	0.095	-0.007
C2	-0.006	-0.029	0.005	0.011	0.004	0.012
N3	0.311	0.256	-0.135	0.187	0.105	-0.043
C4	-0.121	-0.112	0.070	-0.043	-0.043	0.039
C5	0.167	0.079	0.044	0.021	0.175	-0.061
C6	-0.156	-0.118	-0.032	0.000	0.047	-0.078
N4	-0.117	-0.083	0.155	-0.215	-0.136	0.014
O2	0.123	0.142	-0.011	-0.089	-0.011	-0.111
Uracil						
N1	0.104	0.080	-0.090	-0.017	-0.085	0.008
C2	-0.006	-0.001	-0.003	0.000	0.034	0.001
N3	0.024	0.017	-0.006	0.151	0.292	-0.052
C4	-0.017	0.030	-0.008	0.054	0.129	-0.021
C5	-0.286	-0.185	0.262	0.012	0.132	0.001
C6	0.237	0.179	0.235	0.008	-0.013	-0.017
O4	-0.063	-0.136	0.086	-0.178	-0.365	-0.001
O2	0.005	0.016	-0.005	-0.029	-0.124	0.091

a The numbering system of the bases is given in Figure 1.
b The monopoles are scaled to experiments.

Table IV. Data for transition moments

Base	Monopoles	Trans. energy (ev) Theory	Trans. energy (ev) Exptl.[a]	Exptl. trans. moment magnitude[a] eÅ	Exptl. trans. moment magnitude[a] Debye	Calculated trans. vector[b]	Calculated trans. (eÅ)	Transition center[c] (Å) X	Transition center[c] (Å) Y
Adenine		B_{2U}							
	SCF/CI	4.8	4.77	0.813	3.90	+0.02 i	+ 0.81 j	1.24	3.65
	SCF	5.2				-0.14 i	- 0.8 j	1.02	3.47
	Bush/DeVoe	5.6				-0.22 i	+ 0.78 j	0.96	3.10
		B_{1U}							
	SCF/CI	5.0	5.17	0.35	1.68	-0.14 i	- 0.32 j	1.21	3.26
	SCF	5.5				-0.34 i	+ 0.08 j	1.41	3.47
	Bush/DeVoe								
Guanine		B_{2U}							
	SCF/CI	4.3	4.47	0.514	2.46	+0.51 i	+ 0.07 j	1.74	2.92
	SCF	4.4				+0.50 i	+ 0.10 j	1.73	2.85
	Bush/DeVoe	5.8				+0.22 i	+ 0.45 j	0.34	2.92
		B_{1U}							
	SCF/CI	5.1	4.94	0.806	3.87	-0.21 i	- 0.78 j	1.06	3.44
	SCF	5.4				+0.08 i	- 0.80 j	0.86	3.65
	Bush/DeVoe	4.2				-0.80 i	+ 0.07 j	1.33	3.04
Uracil		B_{2U}							
	SCF/CI	4.8	4.72	0.685	3.29	-0.09 i	- 0.68 j	0.76	2.94
	SCF	5.1				-0.06 i	- 0.68 j	0.57	3.27
	Bush/DeVoe	5.2				+0.05 i	+ 0.68 j	0.80	3.01
		B_{1U}							
	SCF/CI	5.4	5.17	0.241	1.16	-0.08 i	- 0.23 j	-0.50	4.14
	SCF	5.5				+0.04 i	- 0.24 j	-0.43	3.79
	Bush/DeVoe	6.3				-0.15 i	- 0.18 j	-1.29	2.52
Cytosine		B_{2U}							
	SCF/CI	4.1	4.57	0.632	3.04	-0.62 i	+ 0.09 j	-0.25	3.02
	SCF	4.2				-0.63 i	- 0.04 j	-0.47	2.95
	Bush/DeVoe	5.4				+0.18 i	+ 0.60 j	-0.22	3.64
		B_{1U}							
	SCF/CI	5.1	5.17	0.549	2.63	-0.00 i	- 0.55 j	-0.62	3.49
	SCF	5.3				-0.11 i	- 0.54 j	-0.09	3.52
	Bush/DeVoe	6.8				+0.40 i	+ 0.38 j	0.06	2.85

(a) Resolved from spectra of Pabst Laboratories.[21]
(b) Transition moment vectors are scaled to experimental magnitude. i, j are unit directional vectors referring to X,Y axes defined in Table I.
(c) Coordinates are defined in Table I.

Table V. Bond Polarizabilities ($Å^3$)

	Bond	α_{33}(a)	α_{11}(a)
I.[22]			
	C-H	0.46	0.77
	C-C	0.99	0.27
	C-O	1.23	0.27
II.[23]			
	C-H	0.8	0.6
	C-C	1.85	0.02
III.[24]			
	C-H	0.64	0.64
	C-C	0.99	0.27
	C-O	0.89	0.46
IV.[25]			
	C-H	0.77	0.59
	C-C	1.35	0.23

(a) α_{33} is along the bond and α_{11} is perpendicular to the bond.

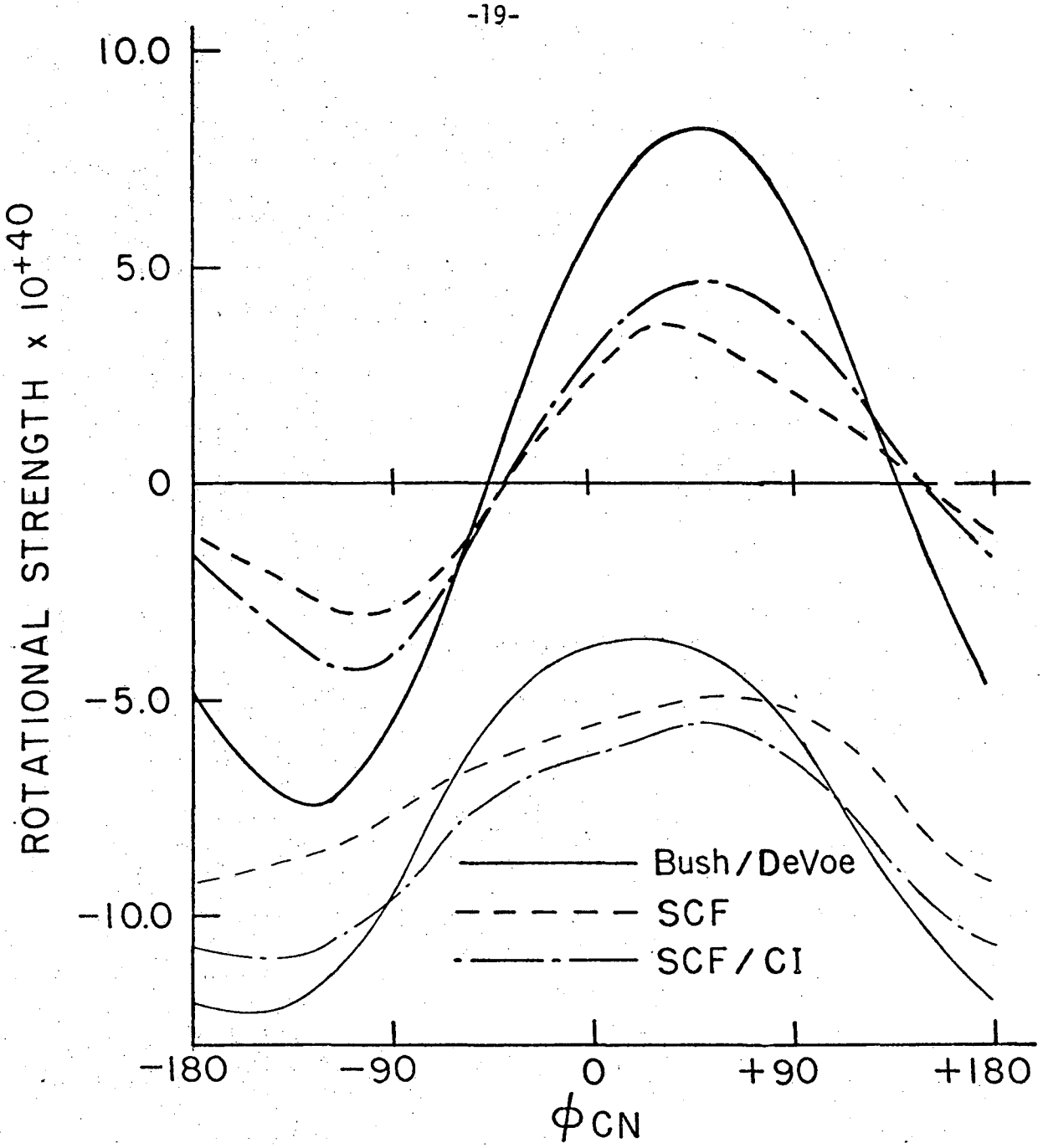

XBL709-5404

Figure 4. The effect of different transition monopoles and the self-consistent treatment of furanose bonds on $R_{B(2U)}$ vs. ϕ_{CN} of uridine. The top three curves are self-consistently treated as in equation (11). The bottom three curves are without the self-consistent furanose treatment [equation (17)].

combinations of possible values of bond polarizabilities, using the SCF/CI monopoles, is shown in Figure 5. The calculated R_{0A} is more sensitive to C-O and O-H bond polarizabilities than C-C and C-H bonds. The same conclusion is obtained with the other two sets of monopoles. This is unfortunate because the bond polarizabilities for C-O and O-H bonds are the least well known. For all the computations, unless otherwise stated, we have used Le Fevre's (1955) bond polarizabilities (set II in Table V) and treated carbon and oxygen equivalently (curve 6 in Figure 5).

D. RESULTS AND DISCUSSION

Results of the calculations are given in Tables VI, VII, VIII, and Figure 5. The rotational strengths of the B_{2U} and B_{1U} transitions were calculated using equation (20) for each of the four nucleosides (Table VI). The effect of the 2'endo and 3'endo furanose conformation is also included. From the results, it can be seen that the rotational strength calculation depends critically on the choice of wavefunctions. However, the rotational strengths from the SCF/CI and SCF monopoles nearly always agree in sign and magnitude with each other. Quantitative comparison with experiment is difficult, because of the uncertainty in assignment and resolution of the CD spectrum into bands. In Table VI the experimental rotational strengths are given to one significant figure, or the sign is simply given. The calculated values are shown for two conformations: <u>anti</u> (ϕ_{CN} = -30°) and <u>syn</u> (ϕ_{CN} = +150°). The experimental value, of course, represents an average value over the conformations actually present in solution. With SCF/CI or SCF monopoles the signs

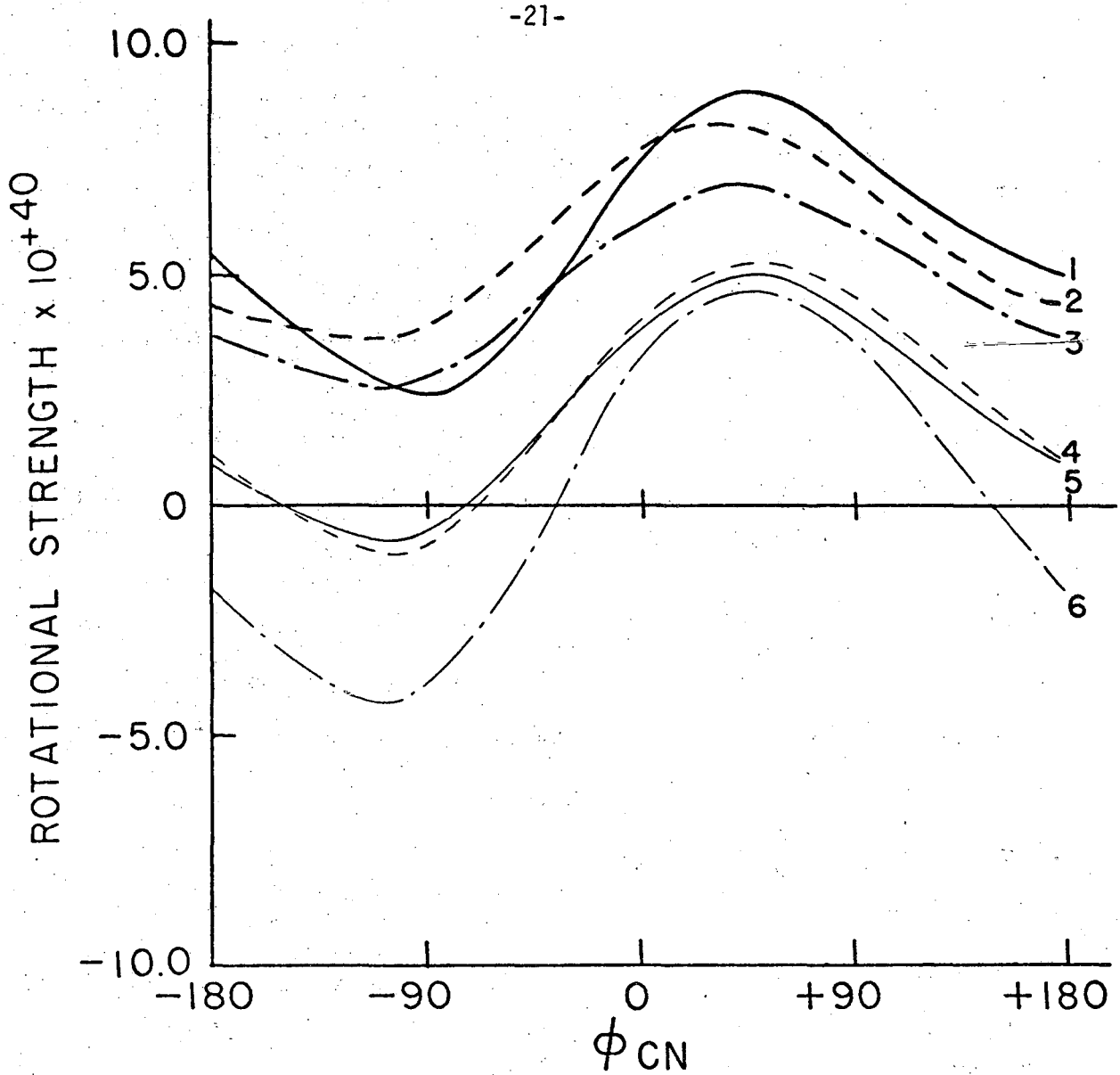

XBL709-5403

Figure 5. Calculated rotational strengths of B_{2U} transitions of uridine as a function of ϕ_{CN} using di-ferent values of polarizabilities. The various sets of polarizabilities are given in Table V. (1) Set I, treating OH equivalent to CH; (2) set III, treating OH equivalent to CH; (3) set II, approximating OH by α_{33}=0.8, α_{11}=0.6; (4) set IV, treating OH equivalent to CH and CO equivalent to CC; (5) set I, approximating OH by 0.8, 0.6; (6) set II, treating OH equivalent to CH and CO equivalent to CC.

Table VI. Calculated rotational strengths for different monopoles and Furanose configurations and conformations. The four ribonucleosides are in the 2'endo conformation.

Compound	Expl. $R_{0A} \times 10^{40}$ e.s.u.	Monopoles	Theoretical $R_{0A} \times 10^{40}$ e.s.u. B_{2U} Anti	B_{2U} Syn	B_{1U} Anti	B_{1U} Syn
Adenosine	$-2(B_{2U}+B_{1U})$	SCF/CI	-2	+3	+0	+0
		SCF	-2	+3	+2	-4
		Bush-DeVoe	+8	-8		
Guanosine	$-0(B_{2U})$	SCF/CI	+2	-4	-2	+3
	$-1(B_{1U})$	SCF	+2	-4	-2	+2
		Bush-DeVoe	-7	+7	+8	-16
Uridine	$+9(B_{2U})$	SCF/CI	+1	+0	+0	-0
	$-4(B_{1U})$	SCF	+1	+0	-2	+2
		Bush-DeVoe	+2	-1	+0	-1
Cytidine	$+12(B_{2U})$	SCF/CI	+27	-31	-7	+7
	$-6(B_{1U})$	SCF	+19	-24	-5	+5
		Bush-DeVoe	-6	+6	-2	+0
2'deoxy A	$-1(B_{2U}+B_{1U})$					
2' endo		SCF/CI	-2	+4		
3' endo		SCF/CI	-7	+0		
2'deoxy G	$-0(B_{2U})$					
	$-0(B_{1U})$					
2' endo		SCF/CI	+1	-5		
3' endo		SCF/CI	+5	-0		
2'deoxy U						
	$+3(B_{2U})$					
2' endo		SCF/CI	+5	+2		
3' endo		SCF/CI	+3	+1		
2'deoxy C	$+(B_{2U})$					
	$-(B_{1U})$					
2' endo		SCF/CI	+24	-34		
3' endo		SCF/CI	+35	+0		

Table VII. Comparison of calculated and experimental rotational strengths for different anomeric adenosines

Compound	λ_{max} (mu)	Exptl. Maximum molar ellipticities[a]	$R_{OA}(B_{2U}) \times 10^{+40}$ e.s.u. Expt.[a,b]	Theory[c] anti	syn
α-Lyx	260	3750	2.7 (c)	3	-7
β-Lyx	256	-3560	-2.7	-2	6
α-Ribo	256	5410	4.4	3	-6
β-Ribo	265	-2970	-2.5 (c)	-2	3
α-Ara	258	3570	2.8	1	-6
β-Ara	258	-5380	-4.1	-2	4
α-Xyl	258	6960	6.0	5	-7
β-Xyl	259	-2450	-2.0	-3	5

(a) The experimental results from Ingwall[28]. Molar ellipticities are in units of deg ℓ/mole cm.

(b) The rotational strengths are evaluated by fitting the spectrum by Gaussian curves on a duPont curve resolver and computed using the formula, $R_i = 1.23 \times 10^{-42} (\theta_i \Delta_i/\lambda_i)$ where Δ_i is the half width of the resolved Gaussian.

(c) Single Gaussian is not possible. Composite Gaussian curves are used. See Ref. 28.

(d) SCF/CI monopoles used.

Table VIII. Calculated $R_{OA}(B_{2U})$ of nucleosides[a] with glycosidic angle ϕ_{CN} present in polynucleotides

Base	$R_{OA}(B_{2U}) \times 10^{+40}$ e.s.u.		
	ϕ_{CN}[b] = -11° (RNA-11)	-14° (DNA-A)	-86° (DNA-B)
A	-3	-3	+5
G	+1	+1	-1
U (T)	+2	+6	+1
C	+31	+32	-25

(a) SCF/CI monopoles and 2'endo conformation for ribose and deoxyribose were used.

(b) ϕ_{CN}'s are from Ref. (26).

of the calculated rotational strengths for the first two transitions are consistent with three of the four mononucleosides in the anti conformation. Calculations for guanosine are not consistent with experiment for either syn or anti conformations.

Figure 6 shows what values of the glycosidic angle give correct results for the calculated signs of the B_{2U} and B_{1U} rotational strengths. For uridine and cytidine about half the possible range of angles ($+150° \phi_{CN} > -30°$) give the correct sign for both B_{2U} and B_{1U}. For adenosine only the anti range ($-10° > \phi_{CN} > -90°$) is consistent with the signs of the rotational strengths. For guanosine a very small overlap occurs ($\phi_{CN} \approx -100°$) between values of ϕ_{CN} which give the correct sign for both B_{2U} and B_{1U} rotational strengths. This probably indicates that guanosine does not exist mainly in one conformation, but instead, includes a wide range of conformations. There is some evidence that the conformation of guanosine depends on pH, as might be expected for a conformationally mobile molecule. We speculate that the conformation mobility of guanosine may explain some of the anticodon-codon degeneracy when the steric consideration is important. For example, the mobility may be the cause of inosine not pairing with guanosine at the third position of the codon, whereas inosine pairs with all other three nucleotides.[26a]

One way of testing this idea further is to calculate an average rotational strength by weighting each calculated rotational strength at angle ϕ_{CN} by the probability of finding the molecule with this value of ϕ_{CN}. We used a probability distribution for the glycosidic bond (ϕ_{CN}), which had been estimated earlier,[27] to obtain an average rotational strength for the B_{2U} transitions for each mononucleoside. The probability

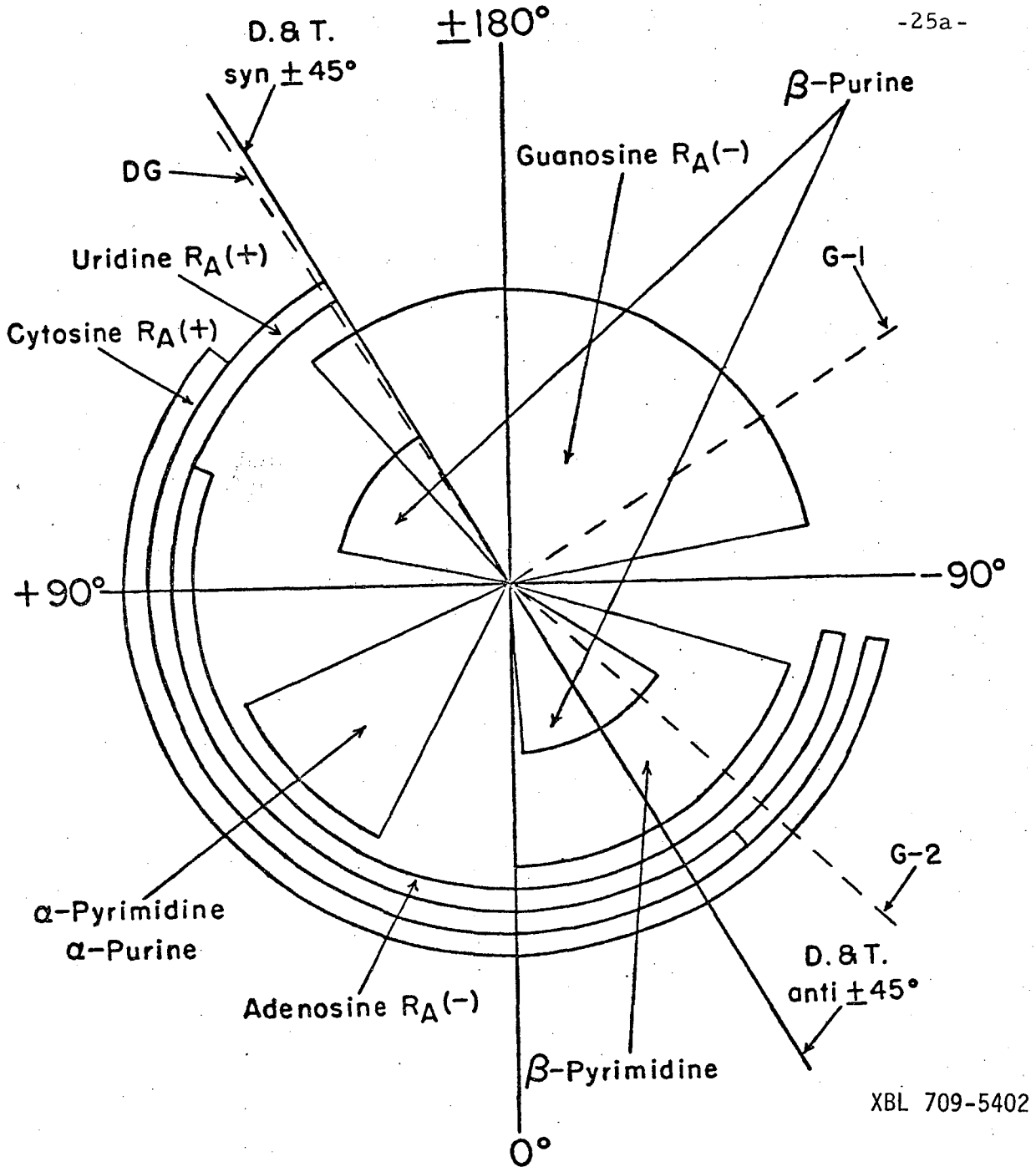

Figure 6. Glycosidic angle (ϕ_{CN}) and calculated sign of the rotational strength. The range of angles labeled α,β-purines and pyrimidines shown are those found in crystals by X-ray scattering.[26] The rotational strengths were calculated with SCF/CI monopoles. (a) Purines, the measured signs of the rotational strengths are minus for both B_{2U} and B_{1U} transitions of adenosine and guanosine; (b) pyrimidines, the measured signs are plus for the B_{2U} transitions and minus for the B_{1U} transitions of uridine and cytidine. DG, G-1, G-2 represent different glycosidic angles found in crystal structures of guznosine.[26]

distribution calculated by estimating the potential energy of interaction of each base with ribose as a function of ϕ_{CN} is reproduced in Figure 7. Although magnitudes were changed, no signs changes, so a positive B_{2U} rotational strength was still obtained for guanosine in disagreement with experiment.

The temperature dependence of the rotational strengths was also calculated. This gives an increase in rotational strengths with decreasing temperature as expected. It also gives the correct order of magnitude change[13] as the temperature is lowered from +90°C to -70°C. For cytidine there is a calculated 3% increase, for adenosine a calculated 30% increase.

In Table VII the results for the anomeric cis-trans isomers of adenosine are given. The calculated results for the anti conformation agree well with experiment. The agreement between theory and experiment is excellent when one considers the α and β pairs of the different isomers. The calculation gives not only the correct sign for each one of the pairs, but also provides the correct relative magnitudes. We see that experimentally the sign of the CD for the anomeric adenosine depends on the configuration at carbon C1': α gives a positive CD at high wavelength, β gives a negative CD. The good agreement with the calculated rotational strengths is strong evidence that all eight of these molecules are primarily in anti conformation.

We also carried out calculations on uracil with different sugars. Experimentally,[29] it was found the rotational strengths of β-D-ara-U and β-D-lyx-U were similar and approximately twice that of β-D-rib-U. The R_{0A} calculated for these compounds are $+10 \times 10^{-40}$, $+11 \times 10^{-40}$, and $+2 \times 10^{-40}$ for ara, lyx and rib U respectively. The Bush/De Voe monopoles were used and anti conformation was assumed.

distribution calculated by estimating the potential energy of interaction of each base with ribose as a function of ϕ_{CN} is reproduced in Figure 7. Although magnitudes were changed, no signs changes, so a positive B_{2U} rotational strength was still obtained for guanosine in disagreement with experiment.

The temperature dependence of the rotational strengths was also calculated. This gives an increase in rotational strengths with decreasing temperature as expected. It also gives the correct order of magnitude change[13] as the temperature is lowered from +90°C to -70°C. For cytidine there is a calculated 3% increase, for adenosine a calculated 30% increase.

In Table VII the results for the anomeric cis-trans isomers of adenosine are given. The calculated results for the anti conformation agree well with experiment. The agreement between theory and experiment is excellent when one considers the α and β pairs of the different isomers. The calculation gives not only the correct sign for each one of the pairs, but also provides the correct relative magnitudes. We see that experimentally the sign of the CD for the anomeric adenosine depends on the configuration at carbon C1': α gives a positive CD at high wavelength, β gives a negative CD. The good agreement with the calculated rotational strengths is strong evidence that all eight of these molecules are primarily in anti conformation.

We also carried out calculations on uracil with different sugars. Experimentally,[29] it was found the rotational strengths of β-D-ara-U and β-D-lyx-U were similar and approximately twice that of β-D-rib-U. The R_{0A} calculated for these compounds are $+10 \times 10^{-40}$, $+11 \times 10^{-40}$, and $+2 \times 10^{-40}$ for ara, lyx and rib U respectively. The Bush/De Voe monopoles were used and anti conformation was assumed.

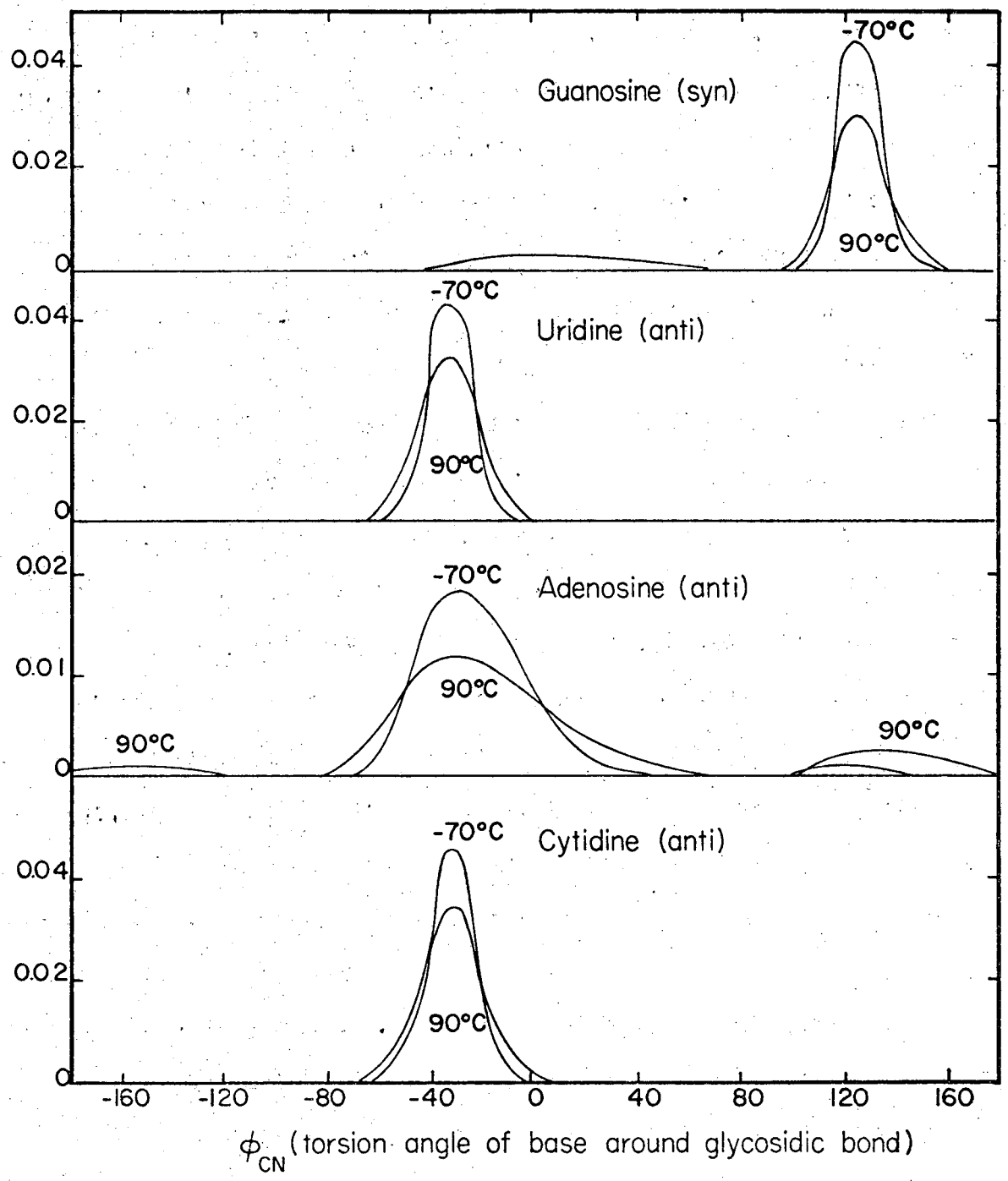

XBL 728-4712

Figure 7. Calculated probability of finding a mononucleoside in a particular conformation at two temperatures (Ref. 27).

We have found that a configuration change at the C2' position of the furanose alters the glycosidic angular dependence of R_{OA} more significantly than that at the C3' position. The calculated R_{OA} vs. ϕ_{CN} for ribo and xyl compounds are similar in curve shape, positions of maximum, minimum and zero crossing, whereas the same holds for ara and lyx compounds. Experimentally, it was found that the configuration at C2' profoundly affects the magnitude of the Cotton effect.[8,28,29] It was reported previously[30] that a cis-oriented hydroxyl group at C2' interacts with the base and that cis-nucleosides gave a Cotton effect larger in magnitude than the trans anomers. It was found that[29] the amplitudes of the Cotton effect of α-D-rib-U, α-D-UMP are larger than their β-anomers; however, the magnitudes of α-lyx nucleosides give smaller Cotton effects compared to their β-anomers. Examination of molecular model suggests that the C1'-C2' trans configuration allows the base to rotate more freely about the glycosidic bond. By inspection of the R_{OA} vs. ϕ_{CN} curve, it can be seen that a range of allowed values of ϕ_{CN} always results in decreasing the amplitude of a trans compound.

From X-ray studies of oriented fibers of DNA, three different geometrical structures designated by "A", "B" and "C" form have been observed.[31,32] These different structures are obtained by manipulating the chemical environment of the molecule, namely, the salt of the acid, salt concentration, and the relative humidities. The "A" form exists for Na salts of DNA at relative humidities ranging from 75 to 92% depending on the amount of Na and the "C" form is found for Li salts of DNA at similar range of relative humidities. The "B" form occurs

in very high hydration level and is believed to be the structure in solution. The CD and absorbance spectra of DNA, when manipulated into different geometrical structures, have been investigated recently.[4,33,34] In particular, the reversibility of CD spectra of DNA is demonstrated when condition of hydration of the DNA fiber is reversed.[35] Correlation of these observations with X-ray works have shown that the large differences observed in CD of DNA under different environmental conditions is caused by changes in the geometrical structure of DNA molecules. Another recent work[36] on the CD spectra of double-stranded RNA have indicated that it is not double-strandness of the molecule that could account for the difference of CD behavior between RNA and DNA. Some other factors must be postulated.

We have tablulated in Table VIII the rotational strengths, $R_{B(2U)}$, of the four bases of ribose and deoxyribose at the ϕ_{CN} for RNA-11, DNA-A and DNA-B given by crystal structures.[31,32] The monomer $R_{B(2U)}$ of RNA-11 and DNA-A are very similar, however, are significantly different from that of DNA-B. This finding is extremely interesting in light of the fact that the CD of DNA-A form is very similar to that of double-stranded rice dwarf virus RNA, whereas CD of the "A" and "B" form DNA are radically different.[33] This study suggests that the base-sugar interaction is important and should not be ignored, as commonly the case, in interpreting the differences of CD spectra of DNA vs. RNA. Furthermore, this result supports the experimental observation that base-sugar geometry is the main factor affecting the optical activity of DNA, and the differences of the base and sugar species only enter indirectly.[33] We would also like to point out that because of the different ϕ_{CN} for

the monomer and polymer it is not valid to account for the mononucleoside contribution to the optical activity of polymer by simply subtracting the CD of monomer in solution from that of polymer. Finally, it is our hope that although the "face" values in Table VIII cannot be taken directly to correlate the polymer CD spectra, a comparison on a relative basis may give fruitful insight to the interpretation of the optical activity of nucleic acid polymers.

E. REFERENCES

1. W. Kuhn, Trans. Faraday Soc. 26, 293 (1930); E. U. Condon, Rev. Mod. Phys. 9, 432 (1937); J. G. Kirkwood, J. Chem. Phys. 3, 479 (1937); D. D. Fitts and J. G. Kirkwood, Proc. Nat. Acad. Sci. U.S. 42, 33 (1956); W. Moffitt, J. Chem. Phys. 25, 467 (1956); W. Moffitt and A. Moscowitz, J. Chem. Phys. 30, 648 (1959); A. Moscowitz, Adv. Chem. Phys. 4, 67 (1962); I. Tinoco, Jr., Adv. Chem. Phys. 4, 113 (1962); J. A. Schellman, Accts. of Chem. Res. 1, 144 (1968).
2. J. E. Coleman, J. Biol. Chem. 243, 4574 (1968).
3. C. A. Bush and I. Tinoco, Jr., J. Mol. Biol. 23, 601 (1967).
4. W. C. Johnson, Jr., and I. Tinoco, Jr., Biopolymers 7, 727 (1969).
5. P. A. Hart and J. P. Davis, J. Amer. Chem. Soc. 91, 512 (1969).
6. G. T. Rogers and T. L. V. Ulbricht, Biochem. Biophys. Res. Commun. 39, 2, 414 (1970).
7. G. T. Rogers and T. L. V. Ulbricht, ibid. 419 (1970).
8. D. W. Miles, W. H. Inskeep, M. J. Robins, M. W. Winkley, R. K. Robins, and H. Eyring, J. Amer. Chem. Soc. 92, 3872 (1970), and references therein.
9. L. Rosenfeld, Z. Physik. 52, 161 (1928).
10. K. Philipson, S. Tsai, and K. Sauer, J. Phys. Chem. 75, 1440 (1971).
11. M. Spencer, Acta Cryst. 12, 59 (1969).
12. M. Sudaralingam and L. H. Jensen, J. Mol. Biol. 13, 914 (1965).
13. R. C. Davis, Ph.D. Thesis, University of California, Berkeley, 1967, p. 128 ff.
14. D. B. Davies and S. S. Danyluk, 14th Biophysical Society Meeting, Feb. 1970.

15. A. E. V. Haschemeyer and A. Rich, J. Mol. Biol. 27, 369 (1967).

16. J. Donohue and K. N. Trueblood, J. Mol. Biol. 2, 363 (1960).

17. C. A. Bush, Ph.D. Thesis, University of California, Berkeley, 1965, p. 62 ff.

18. W. C. Johnson, private communication.

19. H. Berthod, C. Giessner-Prettre, and A. Pullman, Theoret. Chim. Acta 5, 53 (1966).

20. H. Berthod, C. Giessner-Prettre, and A. Pullman, Int. J. Quan. Chem. 1, 123 (1967).

21. Circular OR-10 (1967), Pabst Laboratories, Milwaukee, Wisconsin.

22. C. Houssier and K. Sauer, J. Amer. Chem. Soc. 92, 779 (1970).

23. C. G. LeFevre and R. J. W. Le Fevre, Rev. of Pure and Appl. Chem. 5, 261 (1955).

24. R. J. W. Le Fevre, Adv. of Phys. Org. Chem. 3, 1 (1965).

25. R. J. W. Le Fevre, B. J. Orr, and G. L. D. Ritchie, J. Chem. Soc. (B) 273 (1966).

26. M. Sundaralingam, Biopolymers 7, 821 (1969).

26A. F. H. C. Crick, J. Mol. Biol. 19, 548 (1966).

27. I. Tinoco, Jr., R. C. Davis, and S. R. Jaskunas, "Molecular Association in Biology," B. Pullman, Ed., Academic Press, Inc., New York, N. Y., 1968, p. 77.

28. J. Ingwall, J. Amer. Chem. Soc., submitted for publication.

29. T. Nishimura, B. Shimizu, and I. Iwai, Biochim. Biophys. Acta 157, 221 (1968).

30. T. L. V. Ulbricht, T. R. Emerson, and R. J. Swan, Biochem. Biophys. Res. Commun. 22, 505 (1966).

31. R. Langridge, C. Wilson, C. W. Hooper, M. H. F. Wilkins, and L. D. Hamilton, J. Mol. Biol. 2, 19 (1960).

32. W. Fuller, M. H. F. Wilkins, R. H. Wilson, and L. D. Hamilton, J. Mol. Biol. 12, 60 (1965).

33. M. B. Tunis-Schneider and M. F. Maestre, J. Mol. Biol. 52, 521 (1970).

34. M. F. Maestre and J. C. Wang, Biopolymers 10, 1021 (1971).

35. M. F. Maestre, J. Mol. Biol. 52, 543 (1970).

36. W. A. Samejima, H. Hashizume, K. Imahori, I. Fujii, and K. Mivra, J. Mol. Biol. 34, 39 (1968).

II. CONFORMATION OF FLAVIN ADENINE DINUCLEOTIDE

A. INTRODUCTION

The flavoproteins constitute an important class of enzymes. The enzymes are dehydrogenation catalysts and utilize either flavin adenine dinucleotide (FAD) or flavin mononucleotide (FMN) as one of the cofactor requirements. The modes of action of the cofactors, therefore, are of great interest. The interest and importance of flavins and flavoproteins are evident at the three international symposia on flavins and flavoproteins.[1] From a spectroscopist's point of view, flavins are ideal structural probes because of the possession of a unique visible absorption spectrum which changes drastically upon reduction. The flavins also possess fluorescence, which is readily quenched upon binding to apoenzyme. The semiquinone in many flavin-catalyzed reactions can be detected by electron paramagnetic resonance (EPR) technique.

Among the flavins, FAD is particularly intriguing because of the adenylic moiety (AMP) in the FAD. This group does not participate in the oxidation-reduction reactions carried out by FAD nor does it modify its electromotive potential;[2] nonetheless, it is usually essential for normal enzymatic activity. For example, the flavoenzyme p-hydroxybenzoate hydroxylase, studied in the next chapter, is extremely specific for FAD.

The knowledge of the conformation of FAD is imperative in understanding the role of FAD in FAD-requiring enzymes. The quenching of

the fluorescence of riboflavin by non-hydrogen bond forming aromatic compounds leads to the proposal of a parallel stack model for the isoalloxazine and aromatic rings. The complex is speculated to be stabilized by electrostatic and dispersion forces between rings and by hydrophobic forces due to the solvent rather than via a charge-transfer mechanism. This is because no evident charge-transfer absorption band was found in the complex.[3] In this chapter we use NMR to investigate the structure of FAD further. NMR was chosen since it yields valuable structural and conformational information. For example, the pyridine dinucleotides have been studied alone,[4-7] and in a complex formation with several enzymes[6] in solution. In the present study, the FAD molecule is found to prefer a folded structure in D_2O, where the adenine ring is folded over the isoalloxazine ring. In the folded dinucleotide conformation the adenine C_2H proton is preferentially located over the aromatic ring (A)* of the isoalloxazine of FAD, whereas the isoalloxazine C_5H proton is in the proximity of the pyrimidine portion of adenine. The dinucleotide tends to unfold by a decrease of solvent polarity or by an increase in temperature. The dinucleotides associate as dimers in solution by way of vertical stacking of isoalloxazine rings. This folded structure agrees with the model proposed by Sarma, Dannies and Kaplan;[9] however, it differs from that proposed by CD study,[10] and also differs from that arrived at from X-ray investigation of adenosine-riboflavin complex.[11] Nevertheless, all the studies seem to agree on a folded structure with long axes of the adenine and isoalloxazine rings parallel to each other.

---

*See Figure 1.

B. EXPERIMENTAL PROCEDURE

The NMR spectra were obtained on a Varian high resolution HR 220 MHz spectrometer. The spectrometer was an axially symmetrical superconducting solenoid made of niobium alloy wire. A magnetic field strength of 52 kilogauss is achieved. The resolution of spectrometer is 1.1 Hz at full linewidth at half maximum amplitude. The sensitivity is such that a 55:1 signal to noise ratio can be obtained in 1% (by volume) of ethyl benzene solution. The shifts were measured with respect to sodium-2,2-dimethyl-2-silapentane-5-sulfonate (from Merck Sharp and Dohme of Canada) used as internal reference, and calibrations were carried out by side-band modulation. The precision of the measurements is ± 0.5 Hz. Temperatures were calibrated using the temperature dependent chemical shifts of ethylene glycol and methanol samples and the calibration charts provided by Varian Associates. The precision of the measurement is $\pm$ 2.0°C. Calibrations were carried out before and after all measurements. High temperatures had no effect on the ambient temperature (17°C) spectra of the molecules, indicating no irreversible conformational changes or decomposition of the molecules had occurred. All solutions were at neutral pH.

FAD and FMN were obtained from Sigma Chemical Co. and K&K Labs., Inc.; ADPR was obtained from Cal Biochem. These compounds were used without further purification but were lyophilized twice from D_2O to remove exchangeable protons. The solvents D_2O, dioxane-d-8, and methanol-d-4 are from the International Chemical and Nuclear Corp.

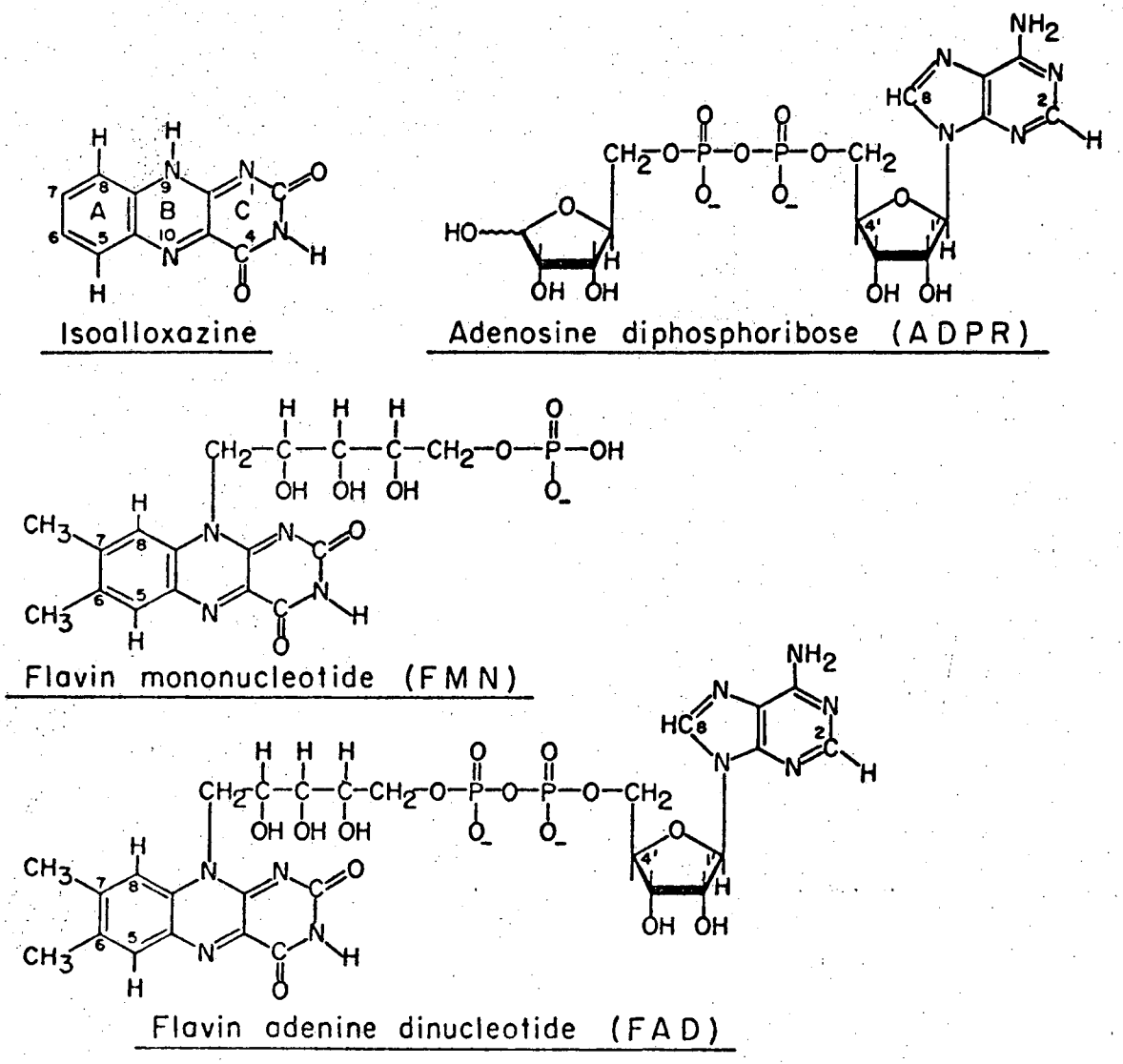

Figure 1. Structural formulae.

C. RESULTS AND DISCUSSION

Assignment of Lines

Selected regions of the 220 MHz proton magnetic resonance spectra of ADPR, FMN, and FAD (0.025 M) in a D_2O/dioxane-d-8 solution (70/30, v/v%) (pH 7.) are shown in Figure 2, and the concentration dependence of these proton shifts is illustrated in Figure 3. The peaks were assigned to their corresponding protons in the following manner: For ADPR, the singlet at lower field corresponds to the adenine C_8 proton (AC_8H) as shown by purine exchange experiments with D_2O.[12,13] The singlet at higher field is then assigned to the adenine C_2 proton (AC_2H) while the doublet arises from the C_1' ribose proton in adenosine ($AC_{1'}H$). The observed splitting corresponds to the coupling constant $J(H_1'-H_2')$ between the ribose protons.

Sarma *et al.*[9] assigned the isoalloxazine protons of FMN and FAD on the basis of the computed π-electron densities at the carbon to which the proton is bonded. The uncertainties involved will be described. Correlations between π-electron densities and aromatic proton chemical shifts have been discussed by several authors (14 and references therein). The proton bonded to the highest π-electron density carbon experiences the largest diamagnetic (high-field) shift. On this basis the lower of the two aromatic proton lines was assigned to the isoalloxazine C_5 proton in FMN (FC_5H) (C_5 π-electron density 1.004). The higher field line is then assigned to the C_8 proton (FC_8H) (C_8 π-electron density 1.063). Computed π-electron densities at the methyl

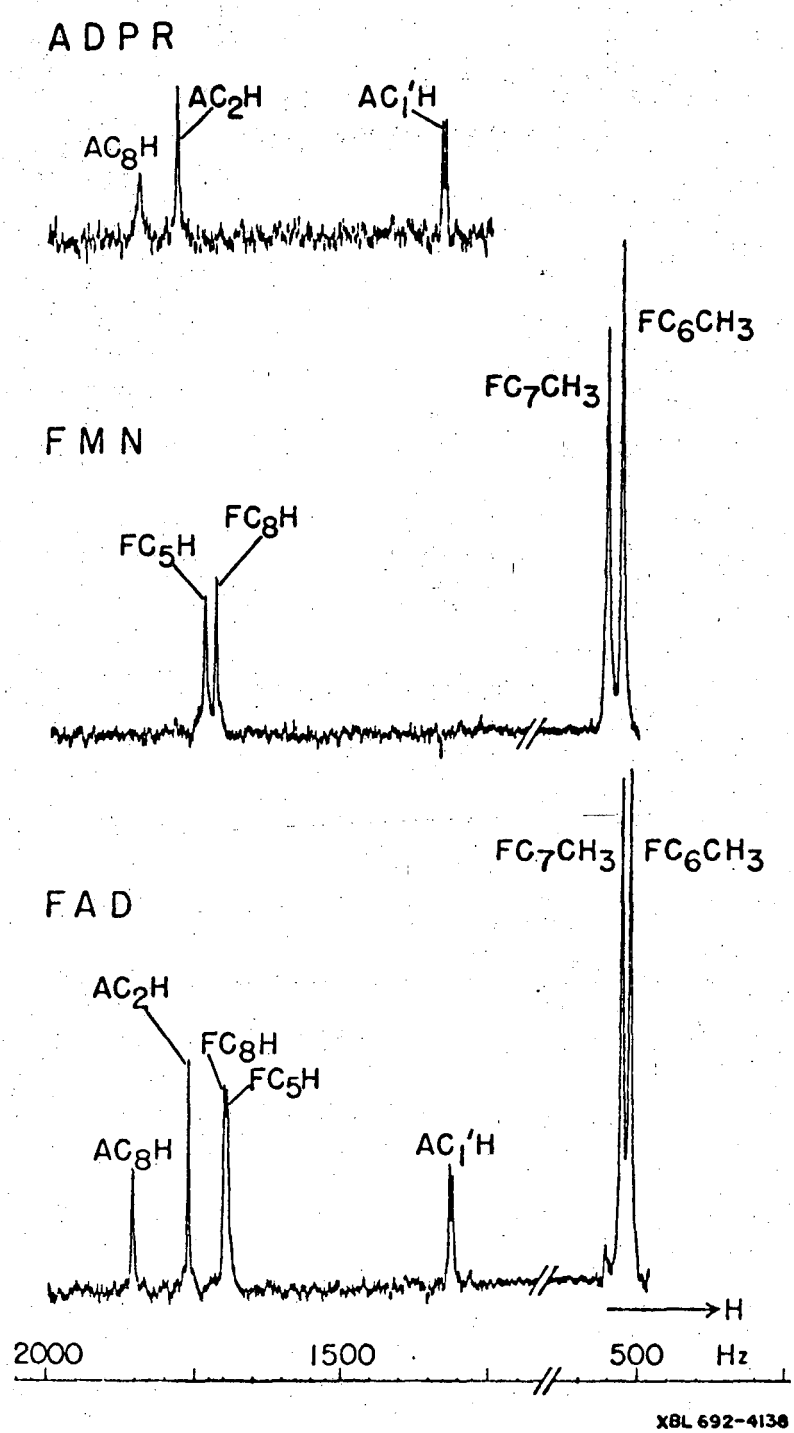

Figure 2. 220 MHz proton magnetic resonance spectra of ADPR, FMN and FAD (0.025 M) in D_2O/dioxane-d-8 (70/30 v/v%) at 17°C (pH 7.0). Only the aromatic, C_1'-ribose and methyl proton regions of the spectra are shown. All shifts are with respect to internal DSS.

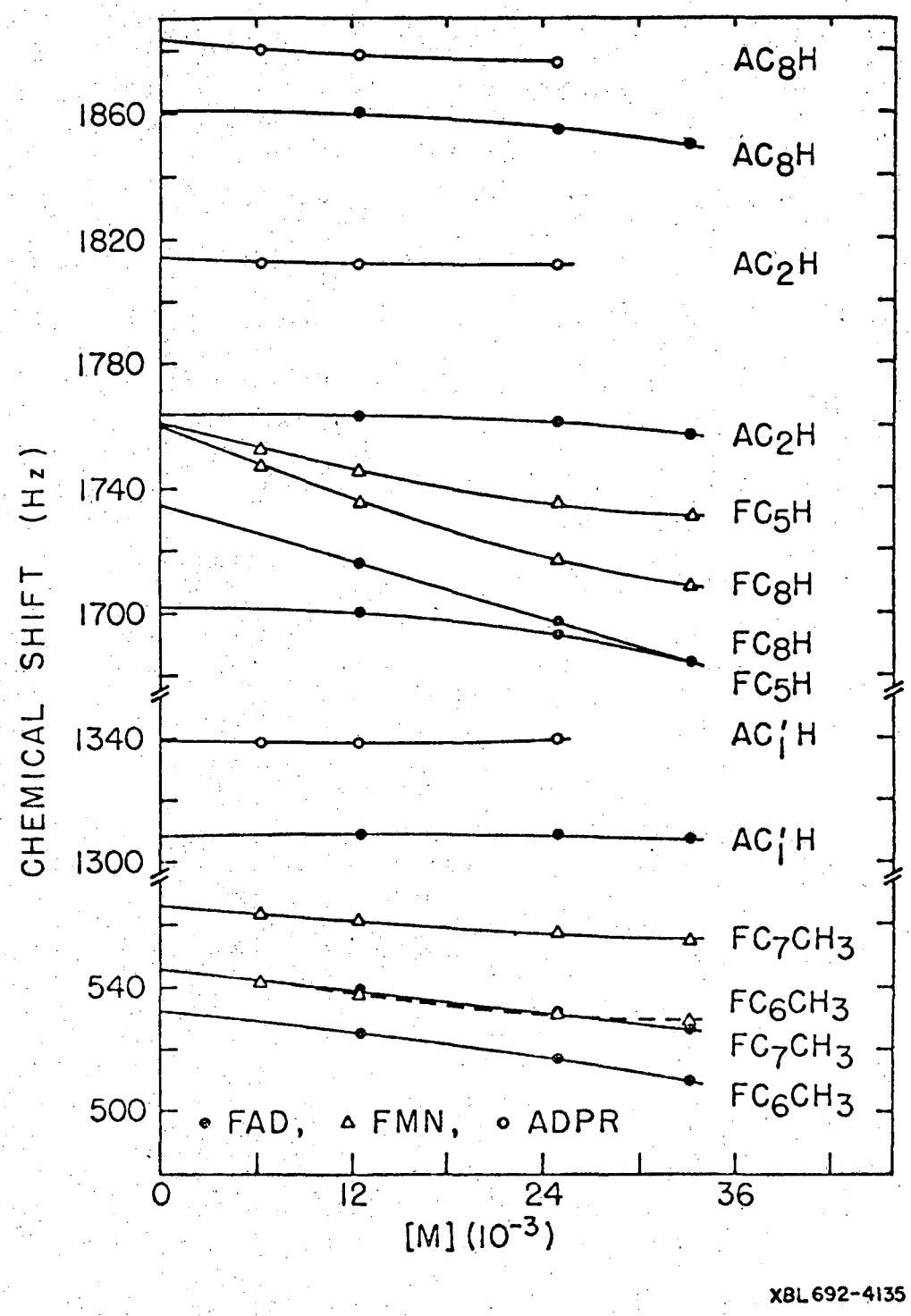

Figure 3. Concentration dependence of ADPR, FMN and FAD chemical shifts in D_2O/dioxane-d-8 (70/30 v/v%) solutions (pH 7.0, 17°C).

protons were used to assign the FMN methyl resonances. Hence the C_7 methyl protons (FC_7CH_3) occur to low field of the C_6 methyl protons (FC_6CH_3) (π-electron densities 0.943 and 0.949, respectively). These π-electron densities were calculated by Pullman and Pullman[15] for the oxidized form of the isoalloxazine ring of FMN.

The uncertainty in this approach is evident from Figures 3, 4, and 5. From Figure 3 the FMN FC_5H proton shifts appear to become equivalent in D_2O/dioxane solutions at infinite dilution. The temperature dependence shows that these two resonances collapse into a single line at 68°C in D_2O/dioxane solutions (0.025 M) (Figure 4), and at 91°C in D_2O solutions (0.025 M) (Figure 5). These results are unexpected from electron density considerations alone.

An unequivocal assignment of the FMN proton resonances has been carried out experimentally by Bullock and Jardetzky.[16] These authors observed the exchange of the FC_7CH_3 protons at 90-95° in D_2O solutions and a consequent decrease in the amplitude of the lower field methyl line. McAndless and Stewart report on similar deuterium exchange experiments of the methyl protons in two lumazine derivatives.[17] From a comparison of the spectra of lumiflavin and 8-deuteriolumiflavin, the higher field aromatic proton in the isoalloxazine ring was assigned to the FC_8H proton. This assignment (Figure 2) is in agreement with that predicted on the basis of the Pullmans' calculations.

In FAD, the resonances in the dinucleotide occur at higher fields than they do in the corresponding mononucleotide. This arises from the ring-current diamagnetic shielding effects of the dinucleotide protons in the folded structure as well as from intermolecular ring-

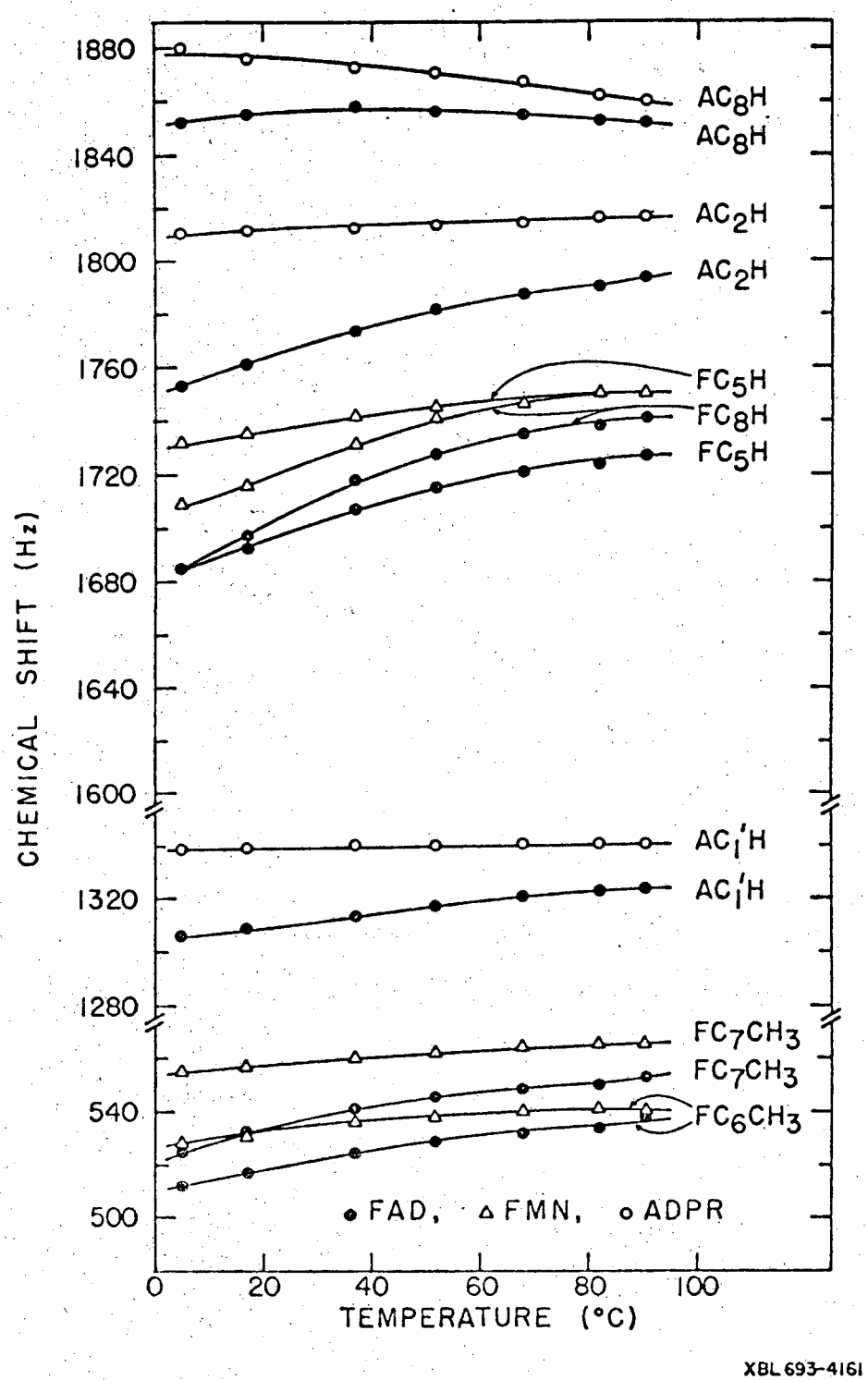

Figure 4. Temperature dependence of ADPR, FMN and FAD chemical shifts in D_2O/dioxane-d-8 (70/30 v/v%) solutions (0.025 M, pH 7.0).

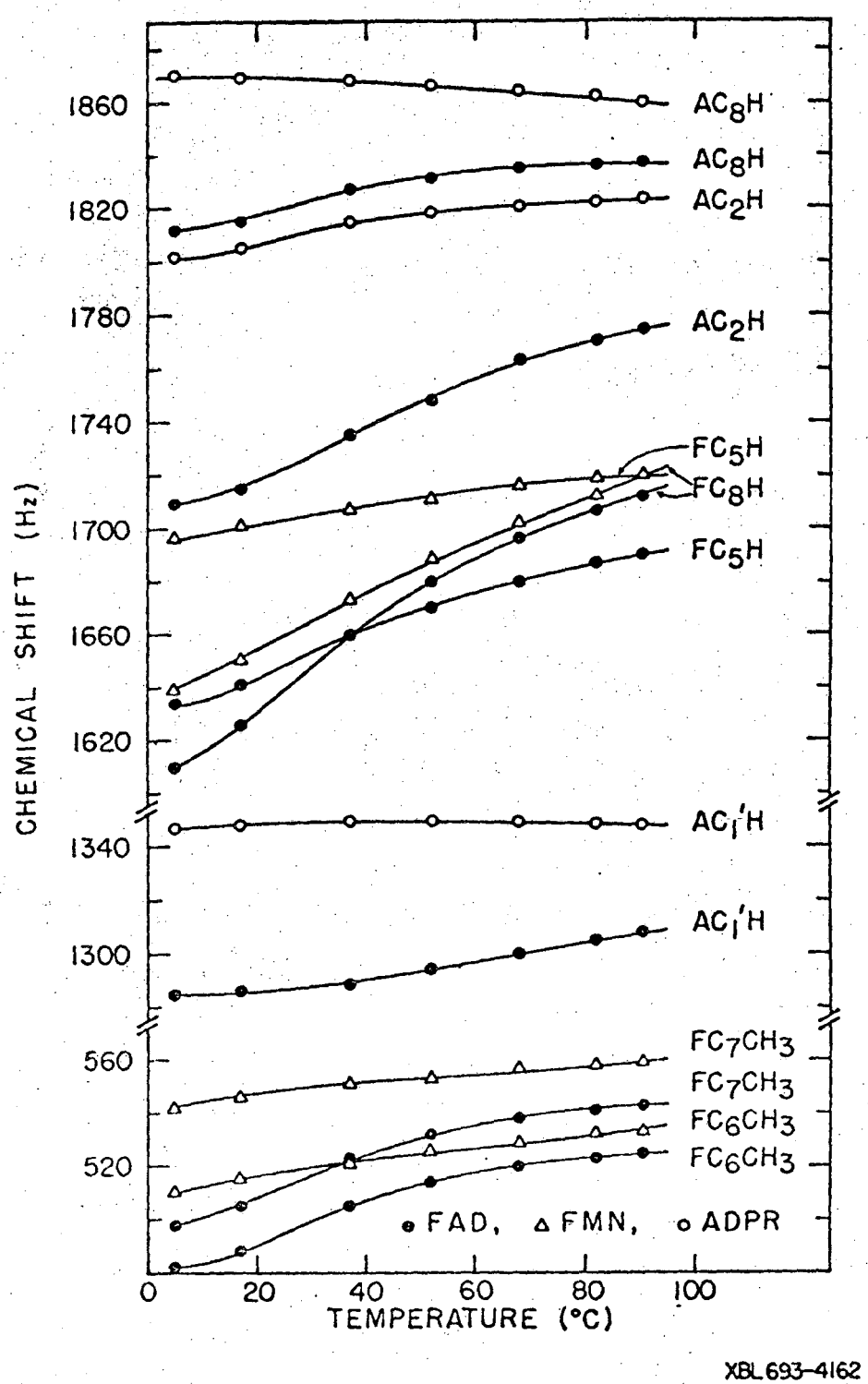

Figure 5. Temperature dependence of ADPR, FMN and FAD chemical shifts in D_2O (0.025 M, pH 7.0).

current interactions between isoalloxazine rings. The lowest field FAD resonance (Figure 2) is assigned to the AC_8H proton on the basis of our exchange experiments in which the D_2O/dioxane solution was kept at 85°C for 4 hours, resulting in the almost total disappearance of this line. The AC_2H proton is assigned to the next resonance; it is well removed from the flavin peaks and the shift difference between this resonance in FAD and in ADPR decreases as the temperature increases (Figures 4 and 5). This is interpreted as reflecting a partial unfolding of the dinucleotide with temperature which removes the AC_2H proton from the ring-current shielding influence of the neighboring isoalloxazine ring. The result is that at higher temperatures the FAD AC_2H proton shift tends to approach the observed shift for the corresponding proton in ADPR.

The most difficult assignment was that of the FAD FC_5H and FC_8H protons, and again the requisite information was derived from the temperature measurements. The temperature dependence of the chemical shifts (Figures 4 and 5) shows that the chemical shift differences between the corresponding AC_8H, AC_2H and $AC_{1'}H$ protons in ADPR and FAD decrease with increasing temperature. The shift differences between the FC_6CH_3 and the FC_7CH_3 protons in FMN and FAD also reveal a similar inverse temperature dependence. In fact, at higher temperatures several of the curves for the corresponding protons almost merge. Similar reasoning should also apply to the FAD and FMN FC_5H and FC_8H proton resonances. Using the assignments of the FC_5H and FC_8H proton resonances in FMN, we assigned the corresponding resonances in FAD. A correct assignment of the isoalloxazine protons in FAD would have

been very difficult without the temperature measurements. Finally, the FAD $AC_1'H$, FC_7CH_3, and FC_6CH_3 protons were assigned as in ADPR and FMN.

Recently, Kainosho and Kyogoku[18] published an article on the conformation of FAD using high-solution proton and phosphorous NMR. The authors, again, discussed the difficulty in assigning the FC_5H and FC_8H resonances. A nuclear Overhauser experiment was used to assign the flavin resonances. The nuclear Overhauser effect (NOE)[19,20] is observed during nuclear magnetic double resonance experiments. The intensity of the absorption of one member of a pair of spatially proximate nuclei is enhanced as a result of irradiating the other. NOE is very useful in studying nuclear-nuclear mutual relaxation processes (see Appendix IIIA) and conformational analysis.[21] Kainosho and Kyogoku have observed that when FC_6CH_3 groups are irradiated, the integrated intensity of the higher field resonance (FC_8H, our assignment) is enhanced by 9%, whereas that of the lower field resonance (FC_5H, our assignment) is only enhanced by 1%. Based on this finding, they concluded that the assignments should have been reversed from ours. However, when the FC_7CH_3 group is irradiated, the intensity of FC_5H is enhanced by 6% and that of FC_8H is enhanced by 4%. This finding is puzzling. One would expect the FC_8H resonance to be enhanced significantly more than the FC_5H resonance, because FC_7CH_3 is closer to FC_8H than to FC_5H judging from the CPK space filling model. Furthermore, the argument given by Kainosho and Kyogoku is difficult to comprehend. They claim that the "reversed" enhancement is due to the small chemical shift between FC_8H and FC_5H protons. We feel that because of the small

NOE enhancements observed and possible nuclear relaxation from adenylic ring protons in the folded conformation, their assignment is inconclusive. An NOE experiment on a FMN molecule with irradiation of the $FC_1'H_2$ protons on the ribitol side chain will, perhaps, determine the assignment unequivocally.

In order to arrive at a correct model for the folded conformation of FAD or the structure of the FMN and FAD stacked dimers in solution, an unambiguous assignment of the proton resonance is required. An example of an incorrect assignment that could easily be made is seen from the data in Figure 5. In D_2O solutions at low temperatures the FAD FC_8H resonance occurs to high field of the FC_5H resonance. With an increase in temperature these peaks coalesce and cross now with the FC_8H to lower field. Consequently, only at experimental temperatures below 40°C can a correct assignment of these FAD proton resonances be made based solely on electron density calculations.

Intermolecular Interactions

Intermolecular interactions may be studied by examining the concentration dependence of FAD, FMN, and ADPR proton shifts in D_2O/dioxane solutions. Table I and Figure 3 show that the flavin protons are the most sensitive to concentration and must therefore be involved in intermolecular associations. Since the FC_8H proton both in FAD and FMN experiences the greatest shift to low field with decreasing concentration, Sarma et al.[9] argued that in D_2O these molecules associate by way of vertical stacking of the isoalloxazine rings. The FC_8H proton of one of the isoalloxazine rings spends on the average a considerable

TABLE I

Concentration Dependence of the FAD, FMN, and ADPR Proton Chemical Shifts in D_2O/Dioxane-d-8 Solutions (70/30, v/v%) (17°C)

Compound	Conc. (M)	AC_8H	AC_2H	FC_5H	FC_8H	$AC_1'H$[b]	FC_7CH_3	FC_6CH_3
FAD	0.025	1855	1761	1693	1697	1309	531	517
	0.0	1862	1764	1703	1735	1309	546	533
δ[a]		7	3	10	38	0	15	16
FMN	0.025			1735	1716		557	531
	0.0			1762	1760		566	546
δ				27	44		9	15
ADPR	0.025	1876	1812			1339		
	0.0	1883	1815			1339		
δ		7	3			0		

(a) δ-Shift at 0.0 M-shift at 0.025 M; positive numbers represent a shift to high field.. Shifts are in Hz.

(b) The coupling constant $J(H_1'-H_2')$ is 5.5 ± 0.2 Hz in FAD, and 5.8 ± 0.2 Hz in ADPR.

time in the proximity of the aromatic ring A of another isoalloxazine ring, and vice versa. Then these protons experience the largest diamagnetic shielding arising from the ring currents in the A ring. In D_2O/dioxane solutions (Table I), the FC_8H proton also experiences the greatest diamagnetic shift (FAD: 38 Hz; FMN: 44 Hz). The data in Table I are consistent with the stacking model for FAD and FMN proposed for the D_2O solutions. Adenine protons both in ADPR and FAD are insensitive to concentration, and therefore are not involved in intermolecular associations.

Intramolecular Interactions

The shielding effect of one ring on the proton resonances of the second ring in FAD may be studied by a comparison of the respective mononucleotide and dinucleotide proton shifts at infinite dilution. This assumes that intermolecular interactions and their effect on the chemical shifts are zero at infinite dilution. The Δ(ADPR-FAD) and Δ(FMN-FAD) values represent the difference in chemical shift between respective protons in the mononucleotides and the dinucleotide. In D_2O/dioxane (Table II) all Δ values are positive, indicating that in FAD all protons are diamagnetically shielded. The AC_2H proton is more highly shielded (51 Hz) than the AC_8 proton (21 Hz). The FC_5H proton also experiences a larger diamagnetic shielding (59 Hz) as compared with the FC_8H proton (25 Hz). Therefore, the conformation of FAD in D_2O/dioxane is in agreement with the folded structure proposed for this molecule in D_2O solutions by Sarma *et al*.

TABLE II

The Difference in Chemical Shift between Respective Protons in the Dinucleotide FAD and the Mononucleotides FMN and ADPR in D_2O/Dioxane-d-8 (70/30, v/v%) (17°C)

	AC_8H	AC_2H	FC_5H	FC_8H	$AC_1'H$	FC_7CH_3	FC_6CH_3
Δ(ADPR-FAD) (a) 0.0 M	21	51			30		
Δ(FMN-FAD) 0.0 M			59	25		20	13

(a) Δ = Difference in the proton shifts at infinite dilution. The positive numbers represent a shift to high field.

Temperature Studies

In Figures 4 and 5 we have summarized the temperature dependence of the chemical shifts in both D_2O/dioxane and D_2O solutions. With an increase in temperature the proton lines shift to lower field (exception: the AC_8H protons in ADPR in both solutions and in FAD in D_2O/dioxane). Changes in temperature will affect both the inter- and intramolecular interactions and associated proton shifts. The shifts to low field may be explained by a decrease in the ring-current diamagnetic shielding of the protons when intermolecular associations decrease by partially destacking as well as by a partial unfolding of the FAD molecules.

The temperature dependence of the intramolecular interaction in FAD may be deduced by taking the difference between the mononucleotide and dinucleotide proton shift at every temperature. This assumes that chemical shifts for equivalent protons in both mononucleotides and dinucleotides, arising from any intermolecular associations, have the same dependence on temperature.

Several interesting features are evident from a comparison of the curves in Figures 4 and 5 and from the data in Table III. The first is the decrease in the chemical shift separation between corresponding protons in the mononucleotides and in FAD as the temperature is increased. For example, the shielding effect on AC_2H in FAD decreases from 92 Hz at 5°C to 49 Hz at 90.5°C (D_2O) (Table III) as the high temperatures tend to unfold the FAD molecules. However, even at 90.5°C the dinucleotide proton resonances are always at higher fields than they are in FMN and ADPR. This indicates that at this temperature adenine-isoalloxazine ring interactions are still present.

Table III

Temperature Dependence of the Difference in Chemical Shift between Respective Protons in the Dinucleotide FAD and the Mononucleotides FMN and ADPR

	AC_8H	AC_2H	FC_5H	FC_8H	$AC_1'H$	FC_7CH_3	FC_6CH_3
A. D_2O/dioxane-d-8 (70/30,v/v%)(0.025 M)							
1. 5°C							
Δ(ADPR-FAD) [a]	28	57			33		
Δ(FMN-FAD)			47	24		30	16
2. 90.5°C							
Δ(ADPR-FAD)	8	23			17		
Δ(FMN-FAD)			23	9		12	3
B. D_2O (0.025 M)							
1. 5°C							
Δ(ADPR-FAD)	59	92			62		
Δ(FMN-FAD)			63	29		44	28
2. 90.5°C							
Δ(ADPR-FAD)	23	49			40		
Δ(FMN-FAD)			30	8		16	8

(a) Δ = Difference in the proton shifts at 0.025 M. Positive numbers represent a shift to high field.

Secondly, the FAD temperature curves in D_2O solutions are roughly sigmoidal in shape, with apparent asymptotic limits at both high and low temperatures (Figure 5). Sigmoid curves are also obtained when the differences in the chemical shifts Δ(ADPR-FAD) and Δ(FMN-FAD) are plotted as a function of temperature (Figure 6). The sigmoidal dependence of the chemical shifts could arise from changes in the relative conformation of the two rings in FAD. Similar curves were obtained for adenylyl (3'-5') adenosine (ApA) by Chan and Nelson.[13]

Sigmoid curves and cooperative transitions have been discussed in terms of the "two-state" hypothesis or "all-or-none" processes. These terms imply a discontinuity in thermodynamic states such that only one thermodynamic state is stable below the "transition temperature" and one above. At any given temperature the molecules in the two states are in equilibrium. The best known two-state processes are the phase changes of solids and liquids and the conformational changes in proteins. The theory, character and properties of cooperative transitions have been developed for the conformational transitions of proteins, together with tests for the validity of the two-state approximation.[22]

The melting of dinucleoside monophosphates has been interpreted in terms of this model. The two states correspond to folded and unfolded molecules.[23] These results are based on temperature changes in the circular dichroism spectra.

Considering the proton chemical shift vs. temperature plot (Figure 6), the shifts at the two asymptotic limits at low and high temperatures approach the chemical shifts of the protons in the folded

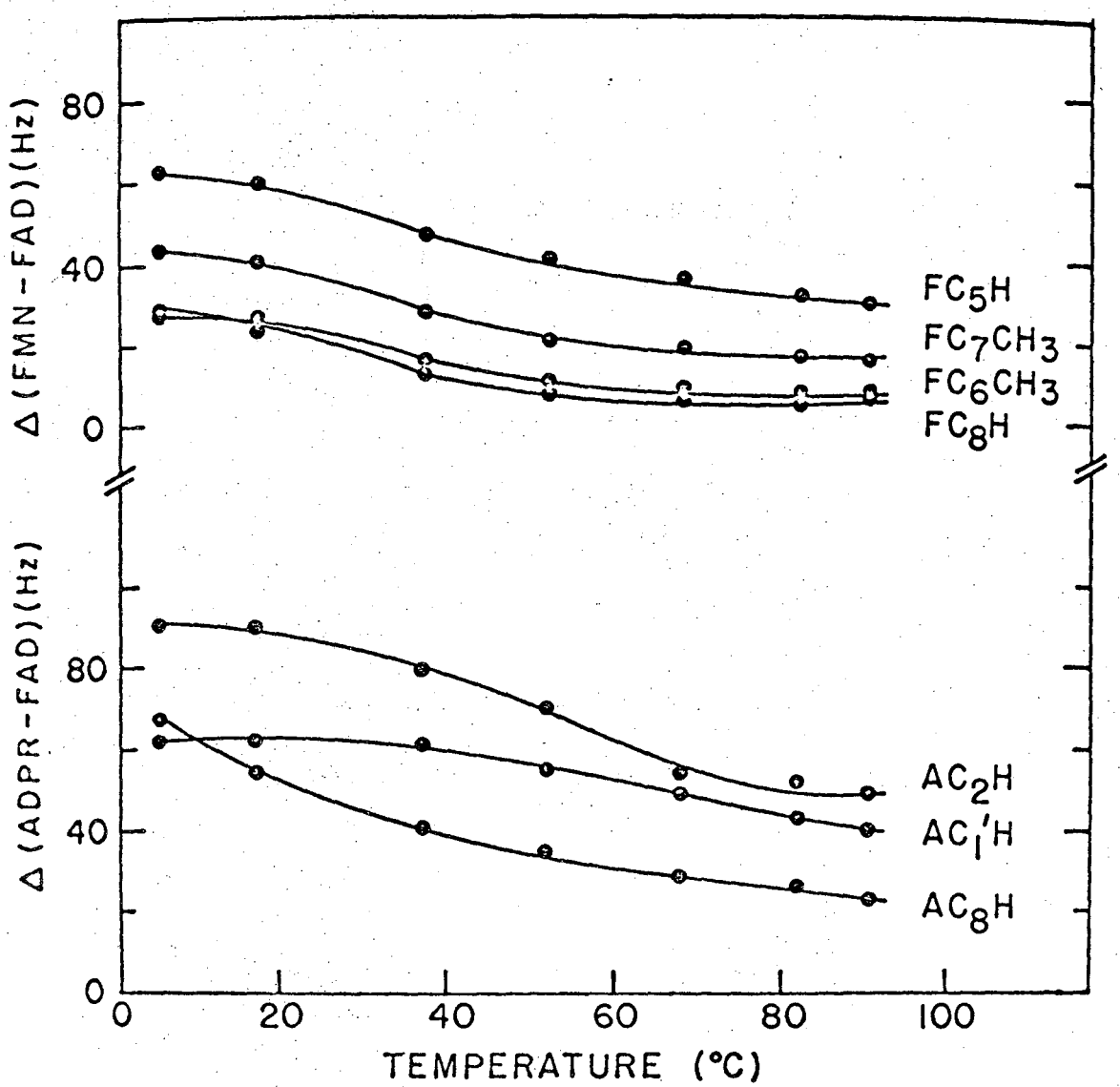

XBL693-4163

Figure 6. The correlation between the difference in the proton chemical shifts Δ(ADPR-FAD) and Δ(FMN-FAD) with temperature (0.025 M D_2O solutions, pH 7.0).

and unfolded states, respectively. Hence the sigmoid dependence of the shifts on temperature arises mainly from changes in the distance between the two rings, and therefore from changes in the ring-current shielding. The applicability of interpreting ring-current shift changes in ApA in terms of the two-state model has been discussed by Chan and Nelson.[13]

Patel[8] has applied NMR in studying the conformation of the coenzyme nicotinamide adenine dinucleotide (NADH). He suggests that a rapid equilibrium of open and one folded conformation of NADH favors the open form at higher temperatures and the folded form at lower temperatures. The observed NMR signal at any temperature is the weighted average of open and one folded conformation in rapid equilibrium at that temperature. We therefore suggest that FAD molecules in D_2O solutions are in a rapid equilibrium between a folded and an unfolded state.

Sigmoid curves are not observed in D_2O/dioxane solutions (Figure 4) nor when the difference in the chemical shifts Δ(ADPR-FAD) and Δ(FMN-FAD) are plotted as a function of temperature. Dioxane must therefore lower the energy barrier and hance the transition temperature between the folded and unfolded states. This results in a decrease in the intramolecular shielding of all FAD protons (Table III). For example, at the lowest and highest temperatures that were studied, the FAD AC_2H proton at 5°C in D_2O is shielded by 92 Hz and this shielding decreases to 49 Hz at 90.5°C, whereas in D_2O/dioxane the shielding decreases from 57 Hz to 23 Hz over this same temperature region.

Temperature dependencies of the coupling constant $J(H_{1'}-H_{2'})$ have been interpreted in terms of a conformational change of the ribose ring in several dinucleoside monophosphates.[24] In ApA this coupling increases from 2.3 to 4.7 Hz (4° to 71°C). In the molecules under consideration the temperature variation of this coupling is small. In D_2O the coupling constant increases from 4.5 to 5.2 Hz in FAD (5° to 90.5°C), and remains at 5.6 Hz in ADPR. In D_2O/dioxane, the coupling constant in FAD is 5.4 Hz but decreases in ADPR from 6.0 to 5.4 Hz (5° to 90.5°C). Because the changes are very small, no appreciable geometrical change in the relationship of $H_{1'}$ and $H_{2'}$ takes place in this temperature range.

Solvent Effects

A comparison of Figures 4 and 5, together with the data shown in Table IV, shows that the addition of dioxane to D_2O solutions of the solute molecules induces a shift to low field for the protons with the exception of the $AC_{1'}H$ proton in ADPR (17°C). These solvent shifts to low field may arise from (a) the decrease in the ring-current diamagnetic shielding of protons, and (b) hydrogen bond formation.

Solvent shifts of the FAD protons in going from D_2O to D_2O/dioxane arise since dioxane decreases both the fraction of folded molecules (all protons are deshielded and experience a shift to low field) as well as the fraction of intermolecularly stacked FAD molecules in solution (flavin protons experience an additional deshielding). Therefore, from Table IV, the solvent shifts are always greater for

TABLE IV

Solvent Effect on the FAD, FMN, and ADPR Proton Shifts

Δ = (D_2O/dioxane-d-8 (70/30, v/v%)) - D_2O proton shifts (0.025 M)

Compound	AC_8H	AC_2H	FC_5H	FC_8H	$AC_1'H$	FC_7CH_3	FC_6CH_3
Temp. 17°C							
FAD	40	46	52	71	23	27	29
FMN			34	66		11	16
ADPR	6.5	6.5			-9		
Temp. 90.5°C							
FAD	15	20	37	29	16	10	13
FMN			30	30		6	8
ADPR	0	-6			-7		

the dinucleotide than for the respective mononucleotide protons. For the AC_2H proton, these shifts are 46 and 6.5 Hz for FAD and ADPR, respectively.

Considering the intermolecular solute-solute stacking interactions further, the data in Table IV show that the FC_8H proton undergoes the greatest shift (66 Hz in FMN and 71 Hz in FAD). Since this proton shift is also the most concentration dependent (Table I) the dioxane must greatly disperse and decrease the fraction of stacked FMN molecules in solution. ADPR proton shifts are only slightly concentration dependent. Therefore, these molecules are not involved in intermolecular associations and experience a very small solvent shift (Table IV). These solvent shifts may be explained by the decrease in the ring-current diamagnetic shielding of protons as neighboring rings are dissociated by dioxane. An increase in temperature also increases the dissociation, as evidenced by the smaller (solvent) shifts at 90.5°C (Table IV).

FAD proton shifts were also studied in 50/50 (v/v%) D_2O/dioxane-d-8 solutions (Table V). All protons experience a further shift to low field with increasing concentrations of dioxane. This indicates that all dissociations are further enhanced.

Solvent shifts for the AC_2H, AC_8H, and $AC_1'H$ protons are in agreement with those observed b y Hruska _et al._[25] for purine, 6-methylpurine, and 9-ribosylpurine in D_2O/dioxane solutions for the solvent composition ratios under consideration. These authors also found that the AC_8H protons form hydrogen bonds with the solvent molecules, since the AC_8 carbon is the most electron-deficient center in purines.

Table V

FAD Proton Shifts as a Function of the D_2O/dioxane-d-8 ratio (v/v%) (0.025 M, 17°C)

Solvent ratio	AC_8H	AC_2H	FC_5H	FC_8H	$AC_1'H$	FC_7CH_3	FC_6CH_3
100/0	1815	1715	1641	1626	1286	505	488
70/30	1855	1761	1693	1697	1309	532	517
50/50	1867	1780	1722	1726	1319	542	526

Protons involved in hydrogen-bonding interactions are invariably shifted to low field.[26] The anomalous shifts to high field of the AC_8H proton as a function of temperature in ADPR and FAD in D_2O/dioxane (Figure 4) and in ADPR in D_2O solutions (Figure 5) may indicate the presence of this hydrogen bond. The FAD AC_8H proton in D_2O does not exhibit a shift to high field with an increase in temperature. This may arise because contributions to the chemical shift due to hydrogen-bond breaking (a net shift to high field) nearly equal the contributions from a decrease in the ring-current diamagnetic shielding of the protons (a net shift to low field). Shifts to high field of hydrogen-bonded protons are often observed with increasing temperature and result from a decrease in the fraction of hydrogen-bonded species.[27] The NAD AC_8H shift to high field with temperature (D_2O) may then also be ascribed to a decrease in the fraction of hydrogen bonded species in solution.[5]

Temperature Dependence of Line Widths

The line width at half height of the AC_8H proton in ADPR shows a temperature dependence (Table VI) which is not observed for the AC_2H proton in ADPR nor for the FAD protons. In D_2O/methanol, 50/50 (v/v%), a sharp AC_8H line is observed at low temperature (-29°C), broadens as the temperature is increased, and finally narrows again at temperatures above 60°C. In D_2O and D_2O/dioxane solutions this proton line width narrows with an increase in temperature (5°C to 68°C). Over this temperature region, the line widths of other protons in ADPR and FAD show a very slight temperature dependence. The ADPR AC_2H proton line width at 5°C is 3.0 Hz and decreases to 2.0 Hz at 90.5°C. Furthermore,

TABLE VI

Temperature Dependence of the ADPR Proton Line Widths* in Three Solvent Systems

	D_2O		D_2O/dioxane (70/30, v/v%)		D_2O/methanol (50/50, v/v%)	
T°C	AC_8H	AC_2H	AC_8H	AC_2H	AC_8H	AC_2H
-29					4.3	3.9
-13.5					4.4	3.8
5	8.0	3.5	8.2	3.0	5.8	3.7
17	6.5	2.5	7.0	3.0	6.0	3.0
37	4.5	3.0	6.5	2.5	8.0	3.5
52	3.0	2.0	5.5	2.0	5.3	2.5
68	2.5	2.0	3.5	2.0	4.0	2.0
82	2.0	2.0	2.5	2.0		
90.5	2.0	2.0	2.0	2.0		

*The numbers represent the proton full line widths at half height in Hz.

the line width of ADP AC_8H and AC_2H at ambient temperatures (17°C) are nearly equal.

These observations are, most probably, caused by the presence of paramagnetic metal impurities in ADPR (see Chapter IV for a detailed discussion). When ADPR is passed through a Dowex 50 column to remove metal contaminants, the preferential broadening of AC_8H to AC_2H is not observed. In ADPR the metal appears to bind closely to AC_8H, presumably, to N_7 of the adenine ring. A similar investigation by Berger and Eichhorn[28] on binding of copper (II) to adenine nucleotides shows the same result. A preferential broadening of AC_8H resonance peak to AC_2H is observed in 3'-AMP, 5'-AMP and poly(A). They postulate a binuclear 2:2 Cu-AMP complex in which the two bases are stacked with each Cu (II) bound to a phosphate of one AMP and N-7 of the other. This model is consistent with our temperature dependence study. In D_2O and D_2O/dioxane solution, when the temperature is raised, the AC_8H resonance of ADPR sharpens, possibly because of the dissociation of the binuclear complex. The observation in D_2O/methanol, however, is less clear. A possibility of solvent effect on the complex cannot be ignored. FAD proton resonances do not show any preferential broadenings can be attributed to either a cleaner sample or a different mode of metal binding.

D. REFERENCES

1. H. Kamin, ed., Flavins and Flavoproteins, Proceedings of the Third International Symposium on Flavins and Flavoproteins, University Park Press, Baltimore (1971); The Proceedings of the Second Conference on Flavins and Flavoproteins, K. Yagi, ed., University Park Press (1968); Flavins and Flavoproteins, E. C. Slater, ed., Elsevier Publishing Co., Amsterdam (1966).
2. G. R. Penzer and G. K. Radda, Quart. Rev. (London), 21, 43 (1967).
3. G. Weber, Biochem. J. 47, 114 (1950).
4. O. Jardetzky and N. G. Wade-Jardetzky, J. Biol. Chem. 241, 85 (1966).
5. R. H. Sarma, V. Ross, and N. O. Kaplan, Biochemistry 7, 3052 (1968).
6. D. P. Hollis, Biochemistry 6, 2080 (1967).
7. R. H. Sarma and N. O. Kaplan, J. Biol. Chem. 244, 771 (1969).
8. D. J. Patel, Nature 221, 1239 (1969).
9. R. H. Sarma, P. Dannies, and N. O. Kaplan, Biochemistry 7, 4359 (1968).
10. D. W. Miles and D. W. Urry, Biochemistry 7, 2791 (1968).
11. D. Vost and A. Rich, Proc. Natl. Acad. Sci. 68, 1151 (1971).
12. M. P. Schweizer, A. D. Broom, P. O. P. Ts'o, and D. P. Hollis, J. Am. Chem. Soc. 90, 1042 (1968).
13. S. I. Chan and J. H. Nelson, J. Am. Chem. Soc. 91, 168 (1969).
14. T. Schaefer and W. G. Schneider, Can. J. Chem. 41, 966 (1963).
15. B. Pullman and A. Pullman, Proc. Natl. Acad. Sci. 45, 136 (1959).
16. F. J. Bullock and O. Jardetzky, J. Org. Chem. 30, 2056 (1965).

17. J. M. McAndless and R. Stewart, Can. J. Chem. 48, 263 (1970).

18. M. Kainosho and Y. Kyogoku, Biochemistry 11, 741 (1972).

19. I. Solomon, Phys. Rev. 99, 559 (1955).

20. I. Solomon and N. Bloembergen, J. Chem. Phys. 25, 261 (1956).

21. R. E. Schirmer, J. H. Noggle, J. P. Davis, and P. A. Hart, J. Am. Chem. Soc. 92, 3266 (1970).

22. R. Lumry, R. Biltonen, and J. F. Brandts, Biopolymers 4, 917 (1966).

23. J. Brahms, J. C. Maurizot, and A. M. Michelson, J. Mol. Biol. 25, 481 (1967).

24. F. E. Hruska and S. S. Danyluk, J. Am. Chem. Soc. 90, 3266 (1968).

25. F. E. Hruska, C. L. Bell, T. A. Victor, and S. S. Danyluk, Biochemistry 7, 3721 (1968).

26. J. A. Pople, W. G. Schneider, and H. J. Bernstein, High Resolution Nuclear Magnetic Resonance, McGraw Hill, Toronto, 1969, Chapter 15.

27. J. W. Emsley, J. Feeney, and L. H. Sutcliffe, High Resolution Nuclear Magnetic Resonance Spectroscopy, Pergamon Press, New York, 1965, Chapter 9, p. 537.

28. N. A. Berger and G. L. Eichhorn, Biochemistry 10, 1847 (1971).

III. ENZYME-SUBSTRATE INTERACTION OF A FLAVOPROTEIN - *p*-HYDROXYBENZOATE HYDROXYLASE

A. INTRODUCTION

In Chapter II, we have pointed out that one of the advantages in the investigation of flavoproteins is that the characteristic chromophore - flavin - is contained in the coenzyme. Valuable information on enzyme-substrate interaction and mechanism of enzymatic catalysis can be obtained. In this chapter, we choose to study a flavoprotein, p-hydroxybenzoate hydroxylase. Hydroxylation plays an important role in the oxidative metabolism of aromatic compounds by bacteria. As a consequence, the mechanisms of action of those enzymes that mediate these hydroxylation reactions have stimulated profound interest. Two mono-oxygenases, p-hydroxybenzoate hydroxylase and salicylate hydroxylase, have been purified to homogeneity and investigated actively.[1-4] Both mono-oxygenases are inducible. They are flavoproteins requiring FAD and reduced pyridine nucleotides as cofactors; however, they differ in specificity. Salicylate hydroxylase is specific for NADH, whereas p-hydroxybenzoate hydroxylase is specific for NADPH.[2] The precise role of the flavin prosthetic group and the mechanism of action of the reduced pyridine nucleotide are not clear. Recently, investigation of the nature of the enzyme-substrate ternary complexes of salicylate hydroxylase by fluorometric methods have been reported by Takemori *et al.*[5-7] Nakamura, Higashi and co-workers have reported kinetic studies on the reaction mechanism of p-hydroxybenzoate hydroxylase from *Pseudomonas desmolytica*.[8,9]

p-Hydroxybenzoate hydroxylase was induced in *Pseudomonas putida*. The two subspecies, *putida* and *desmolytica*, have functionally the same *p*-hydroxybenzoate hydroxylases; however, they differ in the subsequent oxidation of protocatechuate. The former uses the *ortho* cleavage pathway, yielding β-carboxy-cis-cis-muconate;[10] the latter uses *meta* cleavage, yielding α-hydroxy-γ-carboxy-cis-cis-muconic semialdehyde.[11]

To elucidate the mechanism of enzymatic catalysis, it is pertinent to study the intermediate enzyme-substrate complexes and also the interactions of various analogues. Hesp *et al.*[2] reported that the CD spectrum of *p*-hydroxybenzoate hydroxylase was perturbed significantly upon addition of the substrate, *p*-hydroxybenzoate. CD measurements thus provide a sensitive method of studying the enzyme-substrate complexes. In this chapter, we present the results of a kinetic study which indicates the competitive inhibitory behavior of some of the substituted benzoates, contrary to previous findings,[1] and the CD and NMR studies which suggest the interaction of the substrate and the bound FAD.

B. EXPERIMENTAL PROCEDURE

Material

Reagents used routinely for enzyme preparation and assays were the purest grade available. Ammonium sulfate was the special enzyme grade reagent of Mann Research Laboratories. Calcium phosphate gel was prepared according to Keilin and Hartnee.[12] DEAE-cellulose was obtained from Mannex Company and washed with 0.005 M phosphate buffer (pH 6.85). Whatman Chromedia CF II cellulose powder was soaked in 10^{-3} M EDTA overnight and washed 10 times with deionized water. NADPH (grade II), NADH (Sigma grade), $NADP^+$ (grade III), NAD^+ (grade IV), FAD (grade III), p-fluorobenzoate, and p-aminobenzoate were purchased from Sigma. 6-Hydroxynicotinic acid was obtained from Aldrich. Phenol was from Mallinckrodt Chemical, and p-chlorobenzoate, p-nitrobenzoate were from Eastman Kodak. All the benzoate derivatives and phenol were twice crystallized from water before use. All other reagents were used directly without further purification.

Enzyme Preparation

p-Hydroxybenzoate hydroxylase from *Pseudomonas putida*, strain M-6 (ATCC 17428), was prepared and purified by a modification of the method described by Hosokawa and Stanier.[1] The method is similar to that reported in reference 2. The balance sheet for the purification procedure is given in Table I. The purified enzyme was stored in a stabilizing mixture at -70°C until use, as described previously.[2] The enzyme

TABLE I

Purification of p-Hydroxybenzoate Hydroxylase

Step	Volume	Total protein	Total Activity	Specific activity	Yield %
	ml	mg	units	units/mg	
1. Cell-free extract	3260	123,500	44,270	0.36	100
2. Protamine sulphate treatment and first ammonium sulphate fractionation 0.4 to 0.5 saturation	365	23,580	23,650	1.0	53.5
3. First Sephadex G-200 treatment and concentration by ammonium sulphate precipitation 0.3 to 0.6 saturation	52.5	3,150	14,700	4.67	33.2
4. Calcium phosphate gel column	115	1,960	13,200	6.75	29.8
5. DEAE-cellulose column and concentration by ammonium sulphate	17.5	590	3,600	6.1	8.1

was found to denature slowly over a period of one year. The preservation of the enzyme was improved by storing it under an oxygen-free helium atmosphere.

Enzyme Assays

p-Hydroxybenzoate hydroxylase was assayed by spectrophotometric measurement of the substrate-dependent oxidation of NADPH. The procedure has been described earlier.[1] The standard assay system is slightly modified from the previous method. The standard system contained in 3.0 ml, 67 mmoles K_2HPO_4-KH_2PO_4 (pH 7.0), 3.3 μmoles of FAD, 0.13 mmoles of NADPH, 0.67 mmoles of p-hydroxybenzoate, enzyme and deionized water. The unit of enzyme activity is defined as that amount of enzyme which oxidized 1.0 μmoles of NADPH/min under the conditions of the spectrophotometric assay.

Kinetic Measurements

The kinetics were studied spectrophotometrically by measuring the substrate-dependent oxidation of NADPH at 340 mμ. Various substrate analogues were incubated for 2 min (or longer) before the measurement. All substrate analogues were adjusted to pH 7.5. All experiments were carried out at 20°C ± 1°C. Each experiment was repeated at least twice until consistent results were obtained.

Optical Measurements

The absorption spectra were measured in a Cary Model 15 spectrometer. The circular dichroism measurements were obtained with a Cary Model 60 spectropolarimeter with a standard Model 6001 CD accessory attachment. A Cary thermostattable temperature cell compartment was used. CD spectra of the enzyme and p-fluorobenzoate and NADPH complexes

were studied at both 20°C and 2°C. Since spectra at the two temperatures were identical, subsequent experiments were carried out at 2°C ± 0.1°C. The slit width program was set for 15 Å resolution and the time constant and scan speed were adjusted for best signal:noise ratio for each individual experiment. In all cases, optical path length of 1.0 cm was used.

Nuclear Magnetic Resonance Measurements

The NMR spectra were obtained on a Varian high resolution HR 220 MHz spectrometer described in Chapter II. The enzyme was dialyzed against D_2O potassium phosphate buffer (pD 7.4)* extensively to remove the exchangeable hydrogen. The sample was freeze-thaw degased to remove molecular oxygen. The temperature for all measurements was maintained at 4°C ± 1.0°C. All measurements were made in D_2O potassium phosphate buffer system (pD 7.4) containing 0.001 M EDTA and 0.001 M DTT (dithioerythreitol).

Anaerobic Experiment

To efficiently achieve the anaerobic condition without denaturing the enzyme in a cuvette suitable for optical activity measurement and still permitting the addition of various reagents has been found to be difficult. We have used the method described previously.[2] The space above the enzyme solution in the cuvette is first flushed with oxygen-free helium for 30 min. The enzyme solution is then bubbled with O_2-free helium at a rate of 1.5 cc/min for 15 min. If the enzyme is noticed to denature during the assay procedure, the result is discarded. We have been able to achieve strict anaerobic condition with negligible amount of denaturation.

*The glass electrodes can be standardized with a correction factor of 0.4 unit added to the "pH" reading to give the pD value.[13]

C. RESULTS

Chemical Structure of Substrate Analogues

Several aromatic compounds which are structurally related to p-hydroxybenzoate, but cannot serve as a substrate, inhibit the enzyme. The benzoic acid derivatives vary in strength according to the nature of the substituent and its ring position. The relative strength of a substituted benzoic acid is characterized by a substituent constant σ. The more electron-attracting a substituent is, the more positive is its σ value (relative to benzoate as zero). Conversely, the more strongly a substituent donates electrons, the more negative is its σ value. These values for the inhibitory benzoates are given in Table II.

Kinetic Study

It was reported previously[1] that benzoate and a series of its analogues were inhibitory to the activity of p-hydroxybenzoate hydroxylase. Using Tris-HCl buffer system for assay, the inhibition was found to be non-competitive. However, enzyme activity drops very quickly during the assay in Tris buffer system (pH 8.0). Accordingly, there was inaccuracy in determining the initial velocity of the reaction. We could overcome this problem by replacing Tris-HCl buffer with a phosphate buffer system (pH 7.5), in which oxidation of NADPH proceeded almost linearly even at very low concentrations of NADPH and enzyme.

By employing the improved assay system, we have found that benzoate, p-fluorobenzoate, p-chlorobenzoate, p-nitrobenzoate, p-aminobenzoate, and 6-hydroxynicotinate are all competitive inhibitors. Figures 1-6

TABLE II[a]

Summary of Hammett Substituent Constants, σ

Compound	σ	Estimated limits of uncertainty
p-Aminobenzoate	-0.66	0.1
p-Hydroxybenzoate	-0.37	0.04
Benzoate	0	---
p-Fluorobenzoate	0.062	0.02
p-Chlorobenzoate	0.227	0.02
p-Nitrobenzoate	0.778	0.02

[a] σ values were based on ionization of substituted benzoic acids.[14]

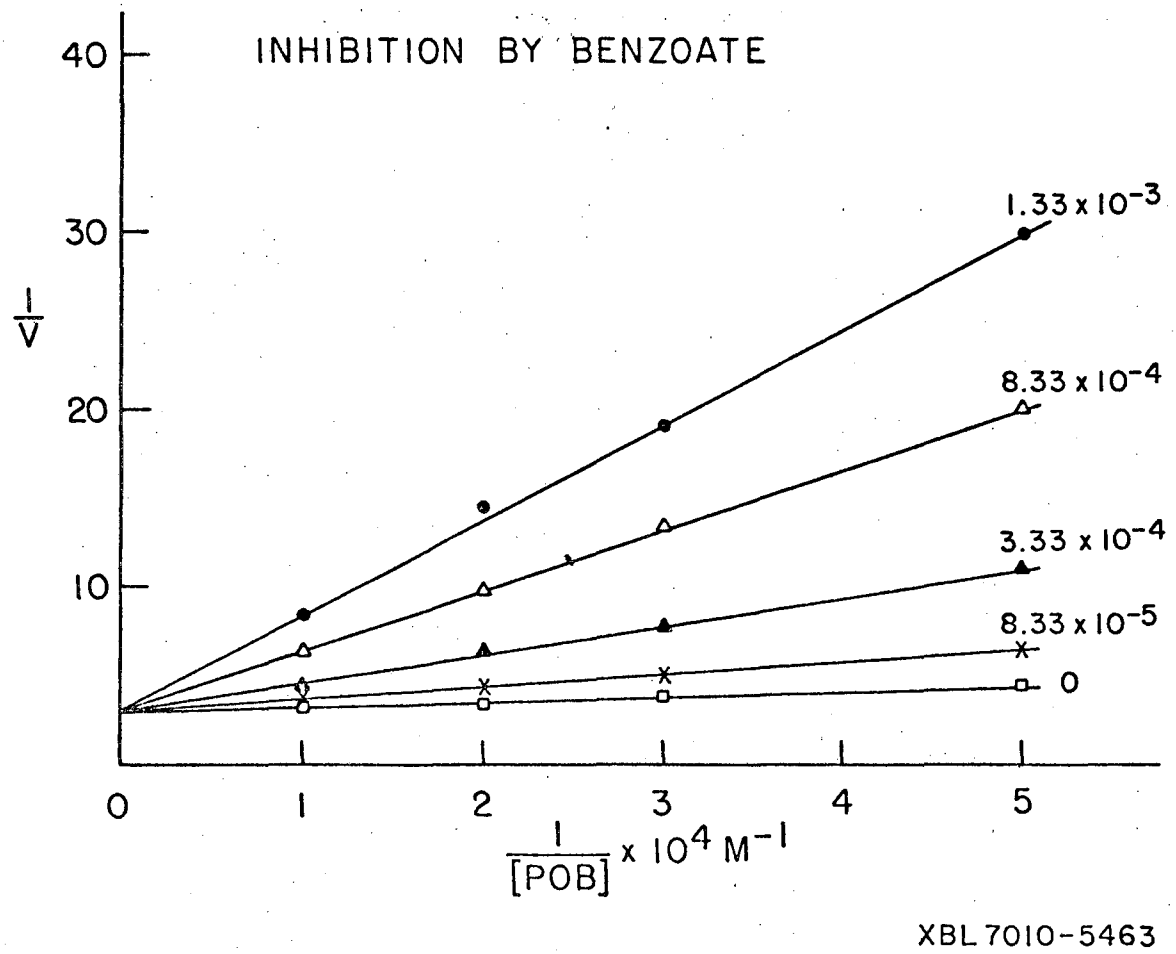

Figure 1. Effect of benzoate on the activity of p-hydroxybenzoate hydroxylase: double reciprocal plot. The data are plotted by the method of Lineweaver and Burk.[17] Assay conditions were described under "Experimental Procedure". The reciprocal velocity, 1/v, is in arbitrary units. The concentrations of benzoate in M are indicated on the plot. The same conditions stated above are used in Figures 2 through 6.

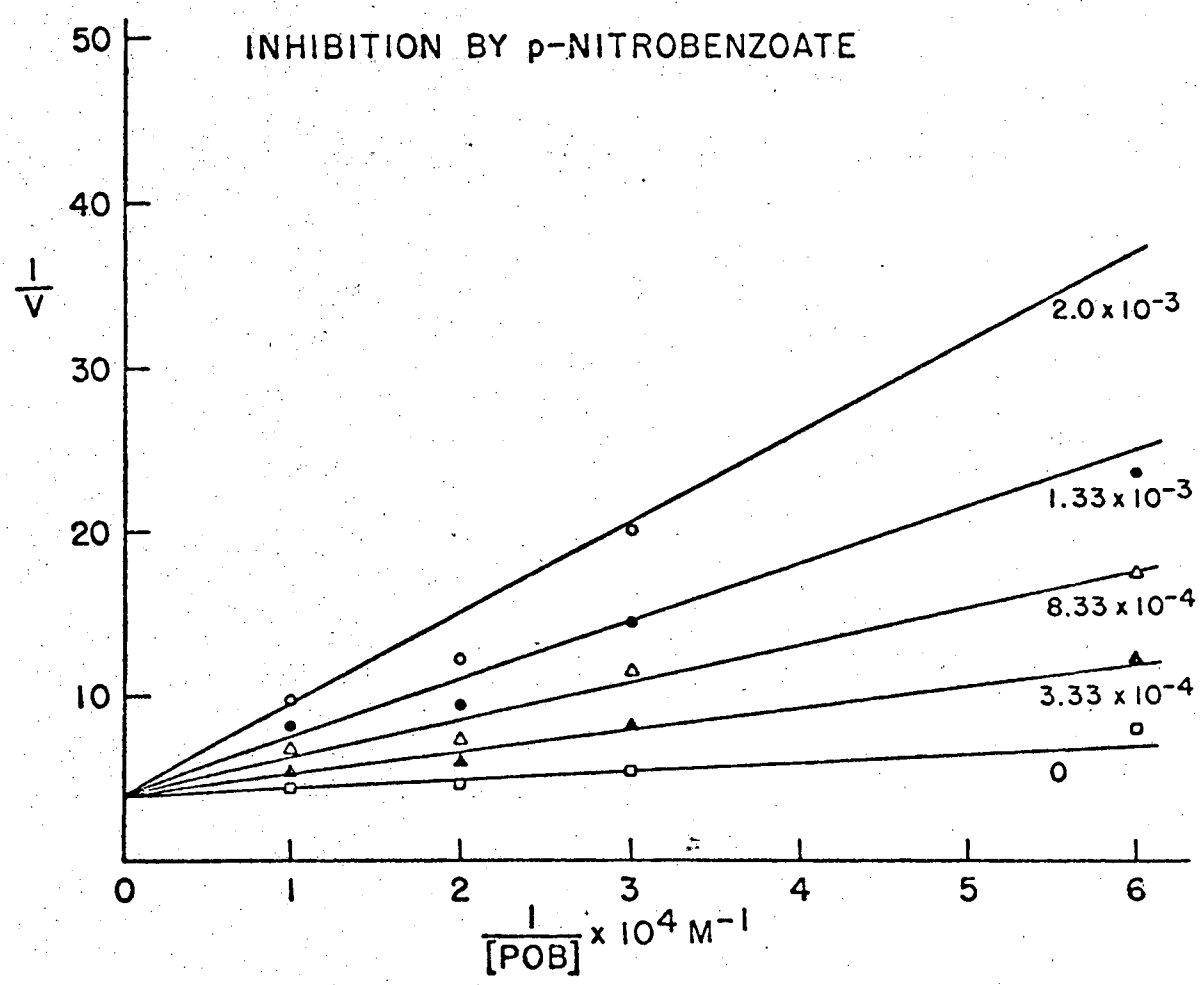

XBL 7010-5465

Figure 2. Effect of p-nitrobenzoate on the activity of p-hydroxybenzoate hydroxylase.

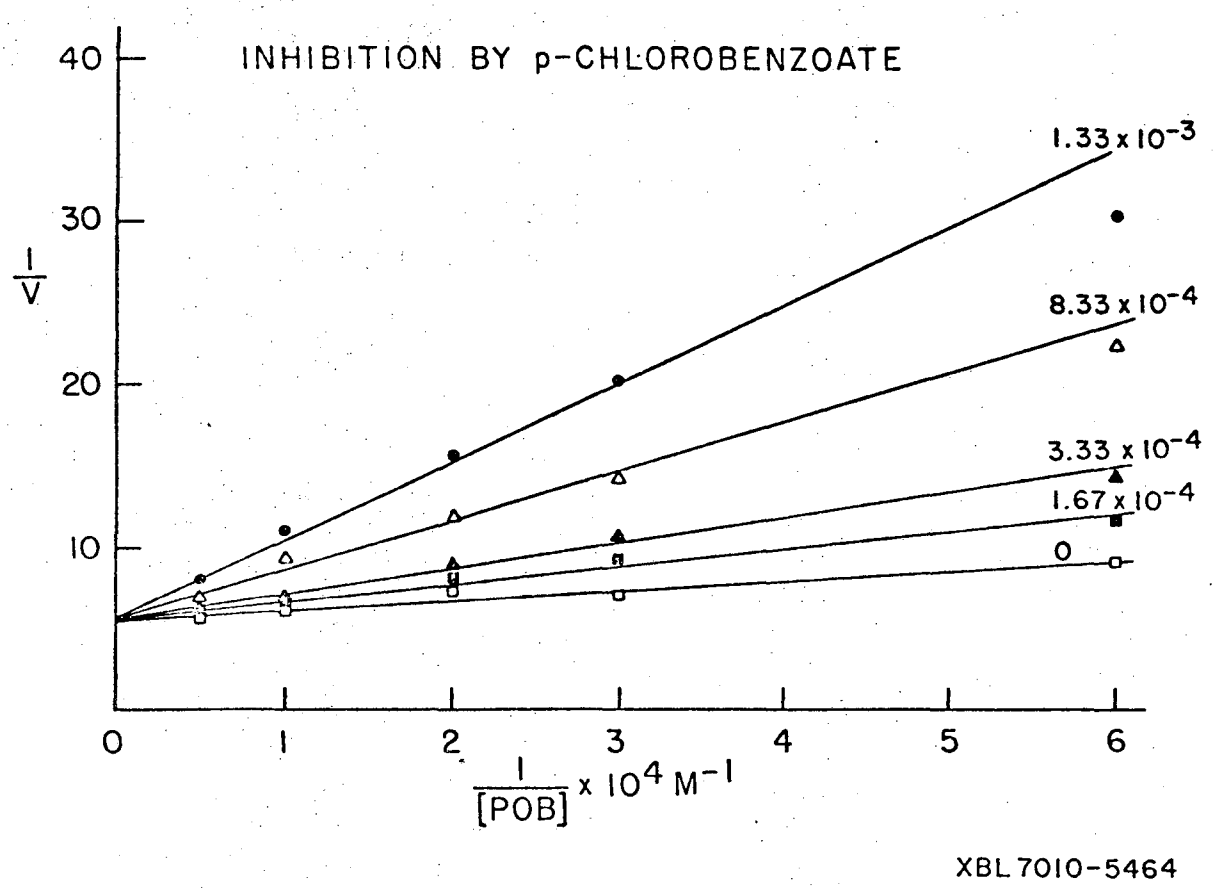

Figure 3. Effect of p-chlorobenzoate on the activity of p-hydroxybenzoate hydroxylase.

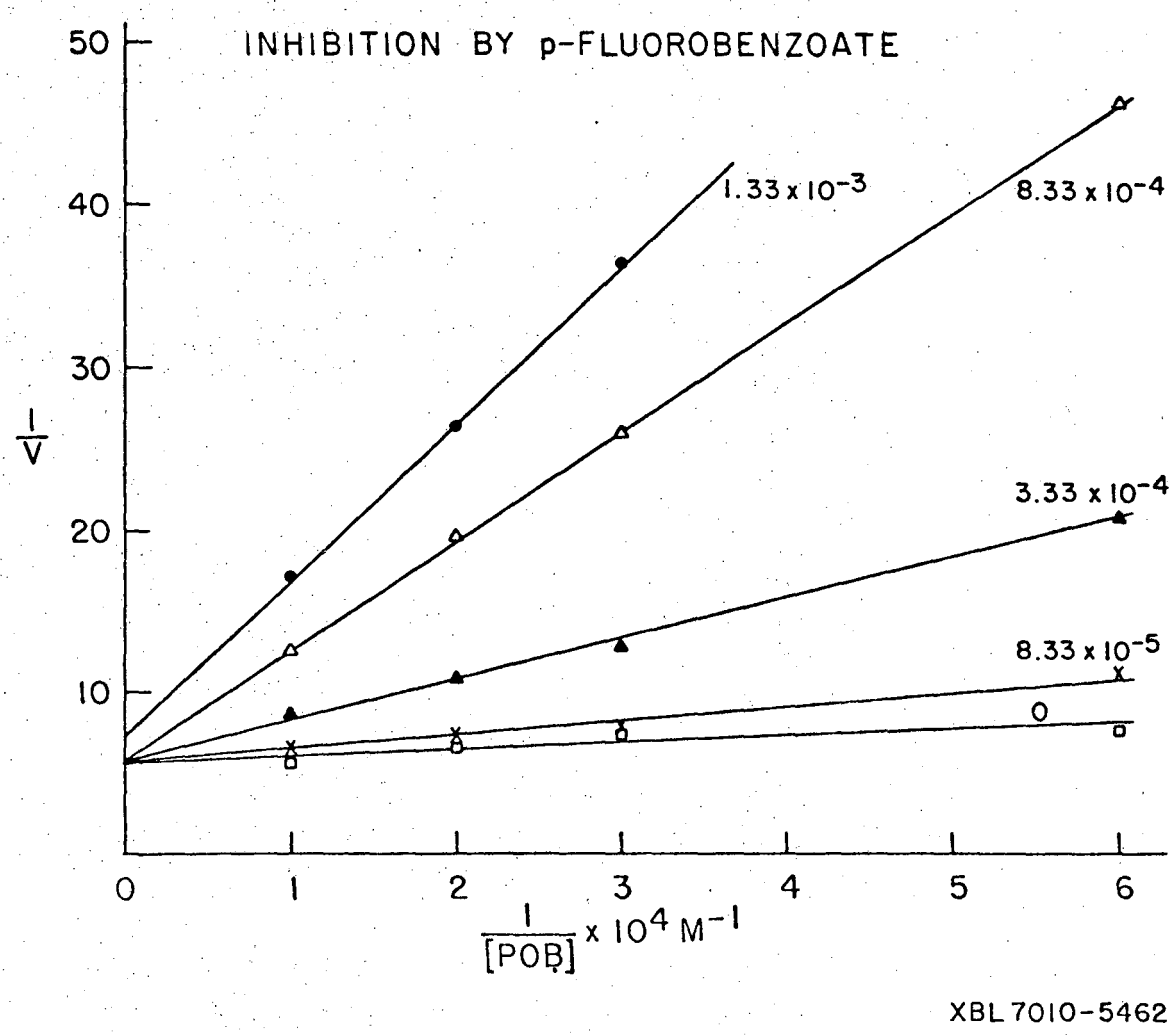

Figure 4. Effect of p-fluorobenzoate on the activity of p-hydroxybenzoate hydroxylase.

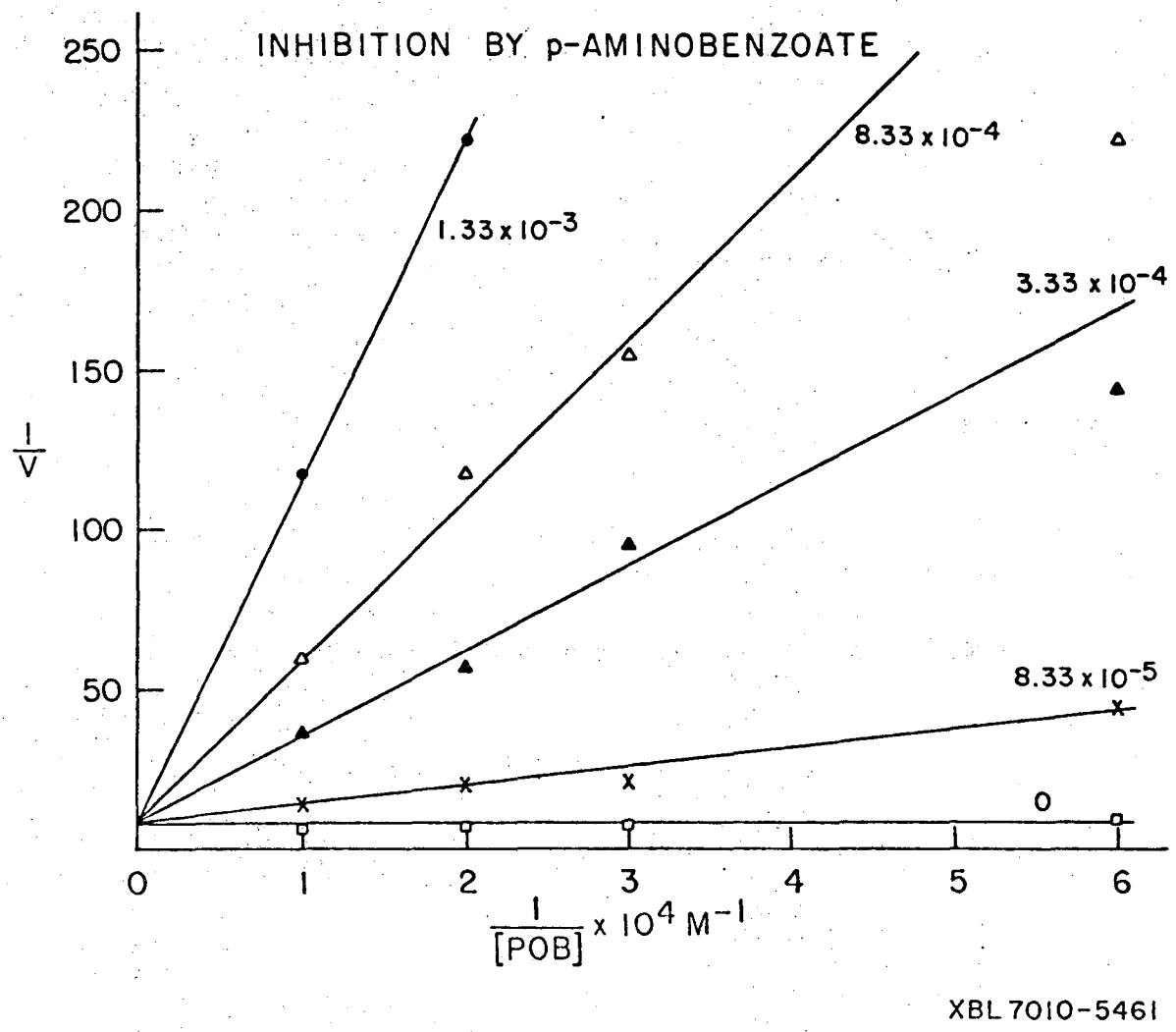

Figure 5. Effect of p-aminobenzoate on the activity of p-hydroxybenzoate hydroxylase.

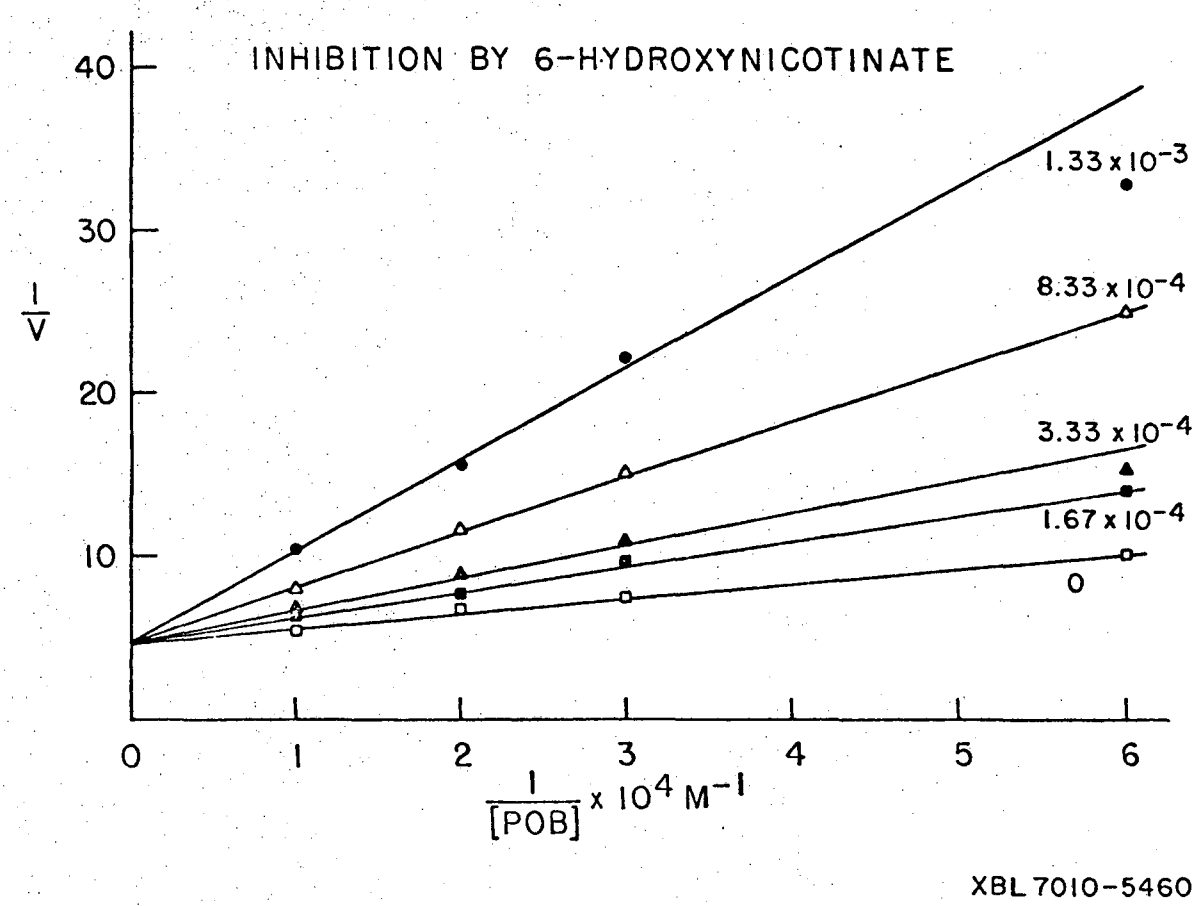

Figure 6. Effect of 6-hydroxynicotinate on the activity of p-hydroxybenzoate hydroxylase.

show the Lineweaver-Burk plots of the enzyme activity in the presence of these inhibitors. All of them are typical competitive inhibitions. The K_i values were determined by the method described by Wilkinson [13] and Cleland.[16] The results are given in Table III.

A Hammett plot of the action of the substituted benzoate derivatives is given in Figure 7, where the logarithms of the inhibition constants K_i's are plotted against their σ-values. They fit the Hammett equation very well. The "reaction constant", ρ, which is the slope of the Hammett plot, is estimated to be 1.78. The significance of ρ is that it measures the sensitivity of the reaction to the electrical effects of substituents in the meta and para positions. A positive ρ value suggests that the inhibition is favored by increasing the nucleophilic reactivity of the carboxyl group.

Phenol shows no inhibition at concentrations below 0.01 M. Inhibitory effects occur at concentrations greater than 0.01 M, due presumably to nonspecific binding to the enzyme. The results are given in Table IV.

The above findings suggest strongly that the carboxyl group is necessary for the substrate analogue to inhibit the enzyme and possibly is involved in the binding at the active site.

Effect of Deuterium on the Activity of p-Hydroxybenzoate Hydroxylase

It is well known that biological systems are affected by isotopic substitution. Enzymatic activity has been shown to be influenced by deuterium replacement.[18] Because of the necessity of substituting D_2O for H_2O to reduce solvent proton signal in NMR experiments, the enzymatic activity in D_2O is tested. A time dependent study of deuterium effect on enzymatic reaction is given in Table V. The assay is

TABLE III

Inhibitory Effect of Substrate Analogues

Substrate analogues	Inhibition (%)[a]	K_i[b]
p-Nitrobenzoate	16	$(4.2 \pm 1.3) \times 10^{-4}$ M
6-Hydroxynicotinate	17	$(3.1 \pm 0.4) \times 10^{-4}$
p-Chlorobenzoate	12	$(1.8 \pm 0.3) \times 10^{-4}$
p-Fluorobenzoate	35	$(7.6 \pm 1.9) \times 10^{-5}$
Benzoate	25	$(5.9 \pm 0.5) \times 10^{-5}$
p-Aminobenzoate	81	$(4.2 \pm 0.9) \times 10^{-6}$

(a) Inhibition was measured by the p-hydroxybenzoate-dependent oxidation of NADPH in the presence of 3.44 μg enzyme, 0.1 mM p-hydroxybenzoate, 0.33 mM substrate analogue and the other conditions were the same as the standard assay system mentioned in section on experimental procedure.

(b) K_i values were calculated, assuming a completely competitive inhibition, by a linear regression analysis of the equation

$$\frac{[S]}{v} = \frac{[S]}{V_{max}} + \frac{K_m}{V_{max}} \left(1 + \frac{[I]}{K_i}\right)$$

where S and I denote the substrate, p-hydroxybenzoate, and inhibitory substrate analogue, respectively, v and V_{max} are the reaction velocity and maximal reaction velocity, K_m is the Michaelis-Menten constant and K_i is the inhibitor dissociation constant. In our kinetic measurement, the velocity determinations, probably are reasonably homogeneous in variance. If the variance of v is σ^2, the variance of [S]/v can be shown to be $\sigma^2[S]^2/v^4$.[15] Therefore, in fitting the linear form to the above equation, the proper weight $v^4/[S]^2$ is used. The standard error of K_i is estimated by standard procedure of propagation of error. All computations were done on a CDC 6600 computer. The listing of the computer program (LESQW) used for the calculation is given in Appendix III C.

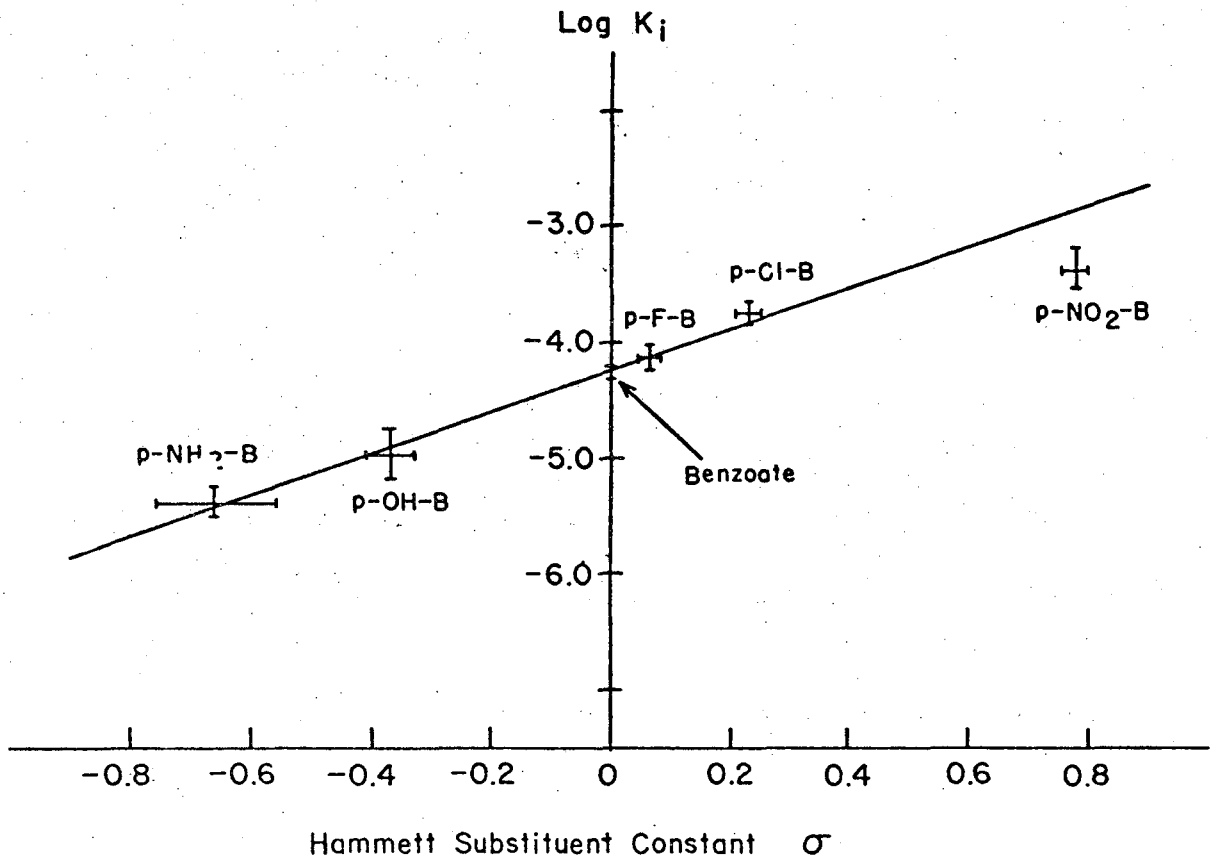

XBL 712-5036

Figure 7. Action of the substituted benzoate derivatives. K_i are the inhibition constants evaluated in Table III. The standard errors in log K_i are indicated by the vertical error bars. The Hammett substituent constants σ are summarized in Table II. The estimated errors of σ are plotted as horizontal error bars. The slope of the line is 1.78.

TABLE IV

Phenol Inhibition[a]

Phenol concentration	% Inhibition
10^{-1} M	78
5×10^{-2} M	51.5
10^{-2} M	0
10^{-3} M	0
8.3×10^{-5} M	0
0	0

[a] The standard enzyme assay system was utilized with 1 mM *p*-hydroxybenzoate.

TABLE V

Time dependent study of deuterium effect on p-hydroxybenzoate hydroxylase[a]

Time (min)	V_{H_2O} (O.D./min)	V_{D_2O} (O.D./min)	V_{D_2O}/V_{H_2O} (%)
0	0.348	0.184	52.9
80	0.322	0.176	54.6
175	0.327	0.174	53.2
275	0.322	0.188	58.4
15 (hrs)	0.294	0.159	54.1

[a]Enzyme was kept at 0°C. The assay was carried out at room temperature (or 23°C) in a standard assay system with 99.9% D_2O replacing H_2O

performed in the standard assay mixtures described in Section B with D_2O replacing H_2O. The reaction velocity in D_2O (v_D) decreases to approximately half of that in H_2O (v_H), immediately, and the ratio v_D/v_H remains constant over a period of 15 hours. This observation is similar to a study by Thomson and Bummert[18] on the reduction of pyruvate by NADH in the presence of lactate dehydrogenase. When the reaction rates were compared at the pH or pD of maximum velocity, an isotope effect of $v_D/v_H = 0.53$ was observed, which is identical to our result of $v_D/v_H = 0.529$ at zero time.

Circular Dichroism Study of the Enzyme-Inhibitor Complexes

The CD spectrum of the holoenzyme of p-hydroxybenzoate hydroxylase has been reported previously.[2] The effect of the substrate, p-hydroxybenzoate, on the holoenzyme manifests itself in the visible region of the FAD absorption. The perturbation of the holoenzyme CD spectrum upon addition of p-hydroxybenzoate was given in reference 2. The CD spectra of the enzyme-bound FAD holoenzyme in the absence and presence of the inhibitors and substrate, p-hydroxybenzoate, are given in Figures 8 and 9. The effect of benzoate on the CD spectrum of p-hydroxybenzoate hydroxylase was described earlier.[2] A large change was observed in the CD spectrum of p-hydroxybenzoate hydroxylase upon addition of benzoate.

p-Fluorobenzoate

The CD spectrum of the enzyme was changed by the addition of 10^{-3} M p-fluorobenzoate. The 367 nm CD was slightly shifted and decreased. The 455 nm band also decreased. Addition of 10^{-3} M p-hydroxybenzoate to the enzyme pfluorobenzoate system produced the familiar change of the CD spectrum characteristic of the enzyme p-hydroxybenzoate complex.

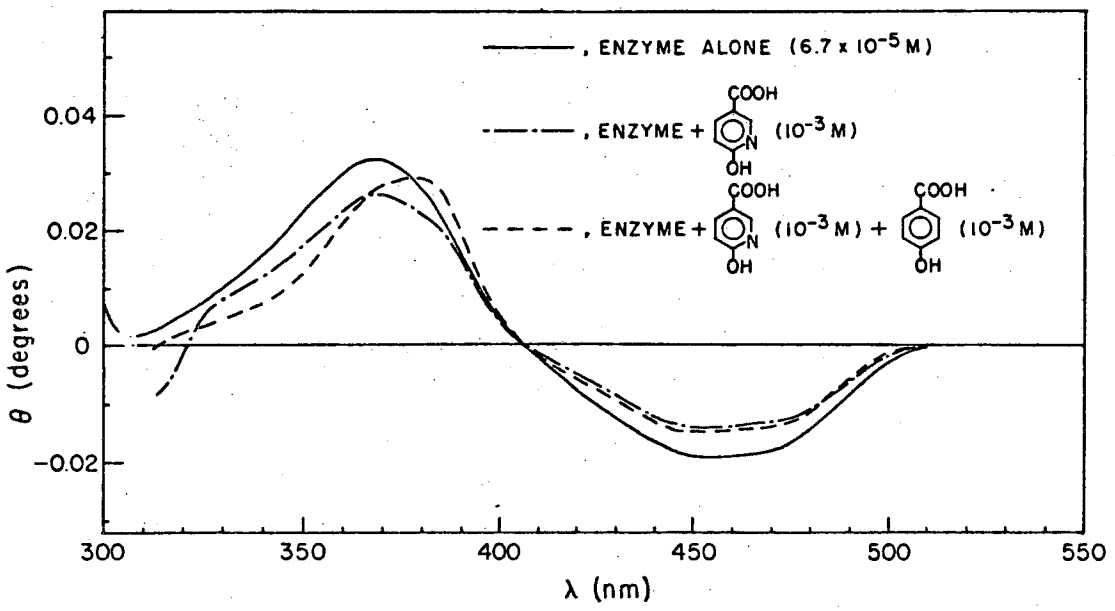

Figure 8. CD spectrum of p-hydroxybenzoate hydroxylase in the presence of 6-hydroxynicotinate and p-hydroxybenzoate. The enzyme (6.7×10^{-5} M) is in 0.05 M potassium phosphate buffer, pH 7.5; temperature 2°C; path-length, 1.0 cm.

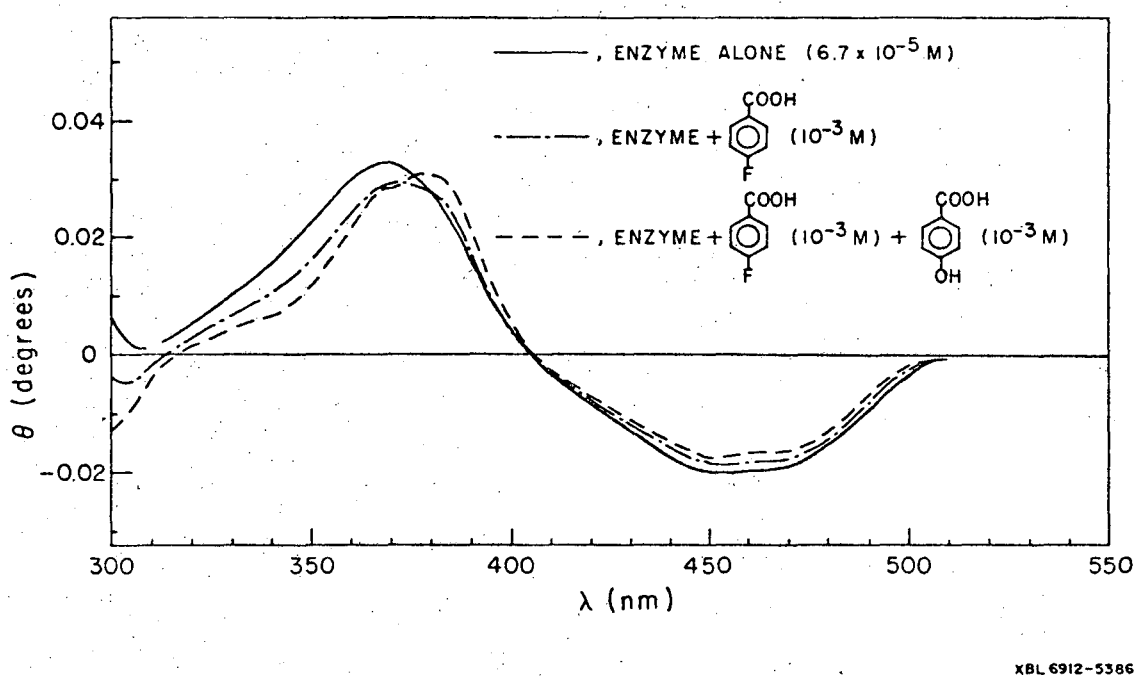

Figure 9. CD spectrum of p-hydroxybenzoate hydroxylase in the presence of p-fluorobenzoate and p-hydroxybenzoate. The enzyme (6.7×10^{-5} M) is in 0.05 M potassium phosphate buffer, pH 7.5; temperature 2°C; path-length, 1.0 cm.

6-Hydroxynicotinate

The effect on the CD spectrum of the enzyme caused by addition of 10^{-3} M 6-hydroxynicotinate was significant. Both the 367 nm and 455 nm CD bands decreased markedly. When 10^{-3} M p-hydroxybenzoate was added to the system, enhancement of the 455 nm band was observed. The general appearance of the CD spectrum resembled that of the enzyme p-hydroxybenzoate system.

p-Aminobenzoate

In contrast to the effect produced by p-fluorobenzoate, benzoate, and 6-hydroxynicotinate, the addition of 10^{-3} M p-aminobenzoate caused almost no modification of the CD spectrum of the enzyme except a slight decrease of the shoulder at 340 nm. Even after the addition of 10^{-3} M p-hydroxybenzoate, no further change was observed. This experiment was repeated with the order of addition of p-aminobenzoate and p-hydroxybenzoate reversed. The same final CD spectrum was obtained. Since p-aminobenzoate did inhibit the enzyme, this may suggest that the interaction of p-aminobenzoate with the enzyme is such that it does not manifest itself in a CD modification. This result indicates the possibility of a different mode of binding between the enzyme and p-aminobenzoate than that between the enzyme and p-fluorobenzoate.

p-Chlorobenzoate and p-Nitrobenzoate

These have been shown to be the weakest inhibitors (Table II). The CD spectra of the substrate analogue-enzyme mixtures are not significantly modified.

Evidence for the Direct Binding of NADPH to p-Hydroxybenzoate Hydroxylase

Circular Dichroism Study

Since CD spectra of p-hydroxybenzoate hydroxylase served as a sensitive means of detecting the formation of the enzyme-substrate complex, we now extend CD measurements for studying the interaction of NADPH with the enzyme. A summary of the results is in Table VI.

Under anaerobic condition, produced by flushing the system with helium, the effect of NADPH on the CD spectra of plain p-hydroxybenzoate hydroxylase was examined. Upon addition of NADPH, there were marked changes, as shown in Figure 10, in the CD spectra of the enzyme. In the presence of NADPH, both the negative and positive CD bands of the plain enzyme (maxima at 455 nm and 367 nm, respectively) are blue shifted. In addition, a negative contribution to the optical rotation is observed. When p-hydroxybenzoate is added in addition to NADPH under anaerobic condition, the broad negative band of the CD spectrum of the enzyme-NADPH mixture becomes even more negative. The results suggest that p-hydroxybenzoate hydroxylase forms a complex with NADPH both in the absence and presence of p-hydroxybenzoate.

In order to find whether NADPH or its oxidation product, NADP, is responsible for this binding, the effect of NADP on the CD spectra of the enzyme was examined. Under anaerobic conditions, there are no significant changes in the CD spectra of the enzyme upon addition of NADP. NADP does not affect the familiar substrate-induced changes in CD spectra of the enzyme under aerobic conditions. These facts indicate that there is probably no interaction between NADP and p-hydroxybenzoate hydroxylase or, at least, it does not manifest itself in a CD modification.

TABLE VI

Effect of reduced and oxidized pyridine nucleotides on the CD spectrum of p-hydroxybenzoate hydroxylase

Condition	p-Hydroxy-benzoate	NADPH	NADP	NADH
Aerobic	absent	No changes, but the conclusion cannot be deduced, because NADPH is oxidized in this system.	No changes.	---
	present	NADPH is oxidized quickly.	Familiar changes.	---
Anaerobic	absent	Marked changes.	No effect.	No significant changes.
	present	Further changes, more than above.	---	Slightly affected.

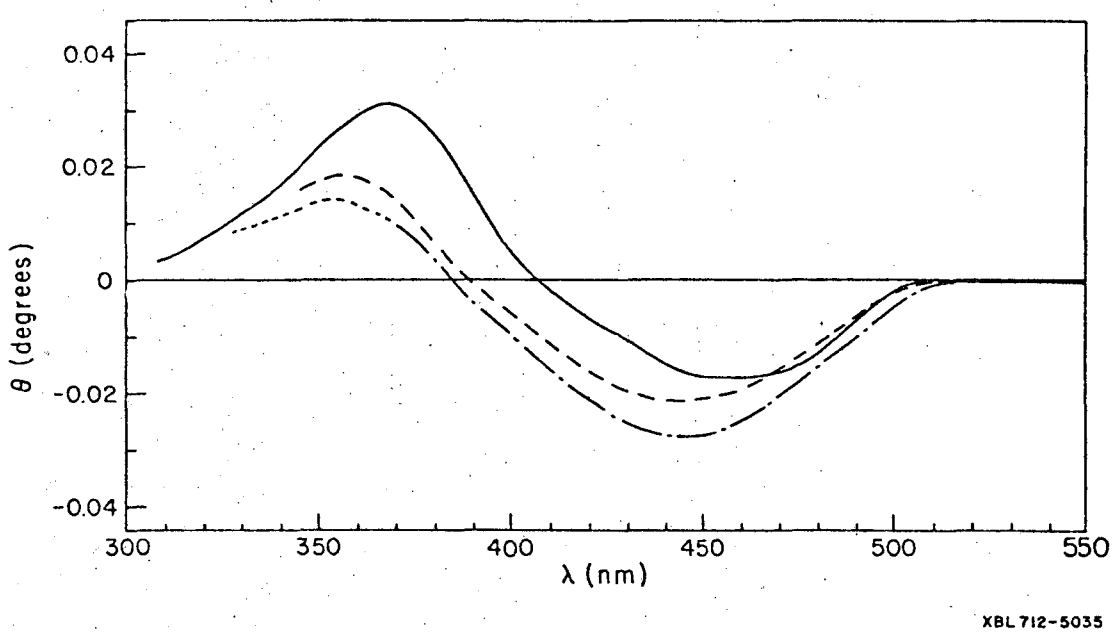

Figure 10. The effect of NADPH on the CD spectrum of p-hydroxybenzoate hydroxylase. The enzyme is in 0.05 M potassium phosphate buffer, pH 7.5; temperature 2°C; pathlength, 1.0 cm; anaerobic condition. ——— enzyme alone (6.9×10^{-5} M); ------- enzyme in the presence of 10^{-3} M NADPH; — — — — enzyme in the presence of 10^{-3} M NADPH and 10^{-3} M p-hydroxybenzoate. ····· indicates region of the curve where signal/noise is poor.

NADH does not induce significant changes in CD spectra of plain enzyme solution under anaerobic condition. Therefore, the enzyme-NADPH complex is highly specific, which is consistent with previous reports.[1,2]

From the results described above, we cannot determine the order of the binding of the substrates, NADPH and p-hydroxybenzoate, to the homoenzyme in the ternary enzyme-p-hydroxybenzoate-NADPH complex.

Nuclear Magnetic Resonance Study

The line widths in NMR spectra can, potentially, provide important information concerning binding of small molecules by macromolecules. A review of the subject[19] and a number of applications of the method[20-22] have appeared. In theory, the linewidths in NMR spectra are sensitive to the degree and kinds of molecular motion present in the sample. An increase in line widths can be interpreted as a restriction of molecular motion, provided the other broadening factors have been properly taken into consideration (for example, presence of paramagnetic metals, magnetic field inhomogeneity). Using this method, Jardetsky et al.,[20] Hollis[21] and Sarma[22] have reported the investigations of NAD and NADPH binding to alcohol dehydrogenose and lactate hydrogenose.

Jardetsky suggests that the pyridine moiety interacts with the enzyme and, to the contrary, Hollis proposes that the adenine moiety is involved. Sarma, utilizing a 220 MHz NMR system, concludes that both adenine and pyridine are involved in the binding and, furthermore, NADH remains in a folded conformation. Table VII summarizes our NMR results of NADPH and NADP binding to p-hydroxybenzoate hydroxylase. In the absence of p-hydroxybenzoate, it appears that the oxidized pyridine nucleotide, NADP, does not bind to the enzyme, because no significant broadening effect of the proton resonances is observed. This confirms

Table VII

NMR line width measurement of reduced and oxidized pyridine nucleotides in p-hydroxybenzoate hydroxylase

p-Hydroxybenzoate hydroxylase (7×10^{-4} M)	NADPH (5×10^{-3} M)			NADP[c] (2×10^{-3} M)				
	AC_8H[a,b]	AC_2H	PC_2H	AC_8H	AC_2H	PC_2H	PC_4H	PC_6H
Absent	1.3	0.8	3.5	3	3	4	4	4
Present	11.0	7.0	8.0	3	3	5	5	4

[a] A and P denote adenine and pyridine rings respectively; the numbering system is given in Figure 11.

[b] The line widths are full width at half maximum height of each peak, and are expressed in Hz.

[c] Due to the low concentration of NADP, the signal/noise does not permit line width measurement more accurately than 3 Hz.

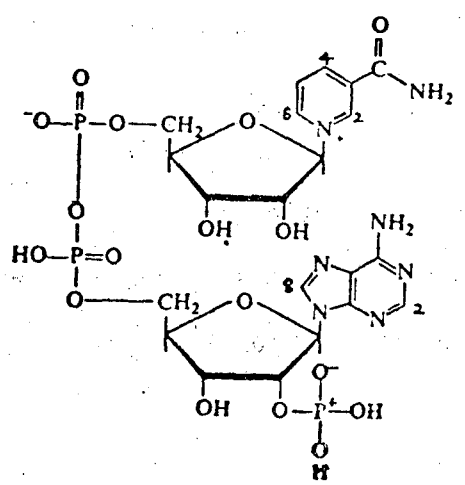

the CD finding that there is probably no interaction between NADP and the enzyme. However, NADPH shows definitive line width broadening in the NADPH + enzyme system. Comparing the relative extent of broadening of each proton, the adenine moiety of the pyridine nucleotide seems to interact with the enzyme more strongly than the nicotinamide portion. Assume a fast exchange between enzyme and NADPH[20,22] and using $\Delta\nu = \frac{1}{\pi T_2}$, where $\Delta\nu$ is the line width at half maximum amplitude and $\frac{1}{T_2}$ is the transverse relaxation rate, the bound line width $\Delta\nu_b$ can be estimated from the formula $\frac{1}{T_2} = \frac{P_f}{T_{2f}} + \frac{P_b}{T_{2b}}$, where $\frac{1}{T_2}$ is the observed relaxation rate, $\frac{1}{T_{2f}}$ and $\frac{1}{T_{2b}}$ are the relaxation rates of the molecules in the free and bound phases; P_f and P_b are the corresponding fractions of molecules in each phase. P_f and P_b can be estimated from Figure 12, knowing the total concentration of the enzyme (E_o), the total concentration of the substrate (NADPH)(S_o) and the dissociation constant for the enzyme-NADPH complex ($K_d = 2.27 \times 10^{-5}$)*.[1]

Figure 12 indicates approximately 14% of NADPH should be bound. The calculated line widths of bound AC_8H, AC_2H and PC_2H are 71 Hz, 45 Hz and 35 Hz, respectively. These values seem to reflect a less mobile molecular environment for the AC_8 and AC_2 protons than for PC_2 protons. This finding may suggest a model where adenine moiety interacts more strongly with the enzyme. The model is reasonable in view of the fact that the enzyme is very specific for NADPH and NADH cannot substitute NADPH for enzymatic activity. The adenine part of NADPH with its C_2'-phosphate group must serve as a recognition site and, perhaps, acts as an "anchor" for the pyridine nucleotide in the enzyme-NADPH complex.

---

*The dissociation constant K_d is estimated in H_2O buffer system.

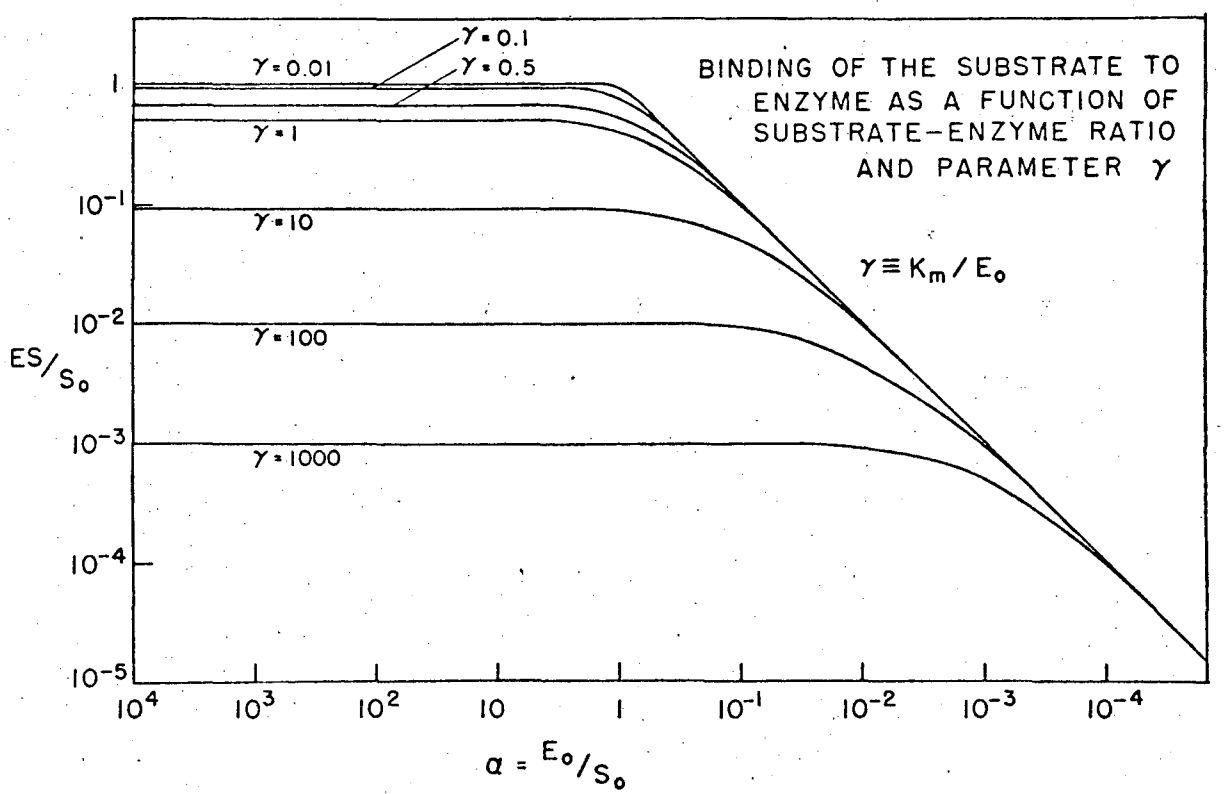

Figure 12. Binding study of the enzyme-substrate complex. The binding of substrate to enzyme is computed according to the equation $ES \overset{K_d}{\rightleftharpoons} E + S$; K_d, E_0 and S_0 are the dissociation constant, total enzyme concentration and total substrate concentration, respectively.

D. DISCUSSION

As has been reported, discrepancies were found among the modes of inhibition of p-hydroxybenzoate hydroxylase by a number of substrate analogues. The analogues, such as p-fluorobenzoate, p-aminobenzoate, benzoate and others; inhibited p-hydroxybenzoate hydroxylase from *Ps. putida* A3.12 in a non-competitive manner,[1] whereas these analogues were competitive inhibitors to the p-hydroxybenzoate hydroxylase from *Ps. putida* M-6 (this chapter) and *Ps. desmolytica*.[8] These discrepancies may be ascribed to the different buffer systems used. In the Tris-HCl buffer, pH optimum is 8.0 as compared to 7.5[1] and 7.0[2] found in potassium phosphate buffer system, and furthermore, the enzyme activity is found to be inhibited, increasingly and markedly, during the assay due to the presence of chloride ion.* This inhibitory action of chloride ion made the calculation of enzyme activity inaccurate and resulted earlier in an erroneous interpretation of the mode of inhibition. Recently, Howell and Massey,[23] using flavin fluorescence, have demonstrated the 6-hydroxynicotinate binding in competitive with the substrate p-hydroxybenzoate. This is consistent with our present finding.

The competitive behaviors of the benzoate derivatives indicate strongly that the carboxyl group is essential in the binding. Phenol does not inhibit the enzyme up to a very high concentration where non-specific binding may take place. The above findings, in conjunction with the fact that the enzyme will only catalyze p-hydroxybenzoate and

---

*Roland G. Kallen and Keiichi Hosokawa, unpublished results.

will not catalyze the other analogues to any significant extent,[1] lead to the following hypotheses: the carboxyl moiety participates in binding with the primary site, providing an "anchoring" and, subsequently, the hydroxyl group is bound to a secondary site to facilitate the catalytic activity. This is in agreement with the two binding sites model proposed before.[2,8,9] The positive "reaction constant" (ρ = 1.78) obtained from the Hammett plot (Figure 7) suggests that the primary binding site is favored by a nucleophilic attack.

Examination of the enzyme-inhibitor complex by CD spectrum showed that there are two classes of substrate analogues which competitively inhibit enzyme activity. One class of substrate analogues causes changes in CD spectra, and the other class shows no significant changes. p-Fluorobenzoate belongs to the former, and p-aminobenzoate is an example of the latter. A summary of the substrate analogues, their structure, formulae and effects on the enzyme is given in Table VIII.

p-Fluorobenzoate binds to the enzyme, as evidenced by a remarkable change in CD spectrum upon addition to free enzyme. If p-hydroxybenzoate is added to the p-fluorobenzoate-enzyme complex, the CD spectrum is converted to the one similar to p-hydroxybenzoate-enzyme complex. This indicates that p-fluorobenzoate binds to the same site as the substrate, and can be displaced by the p-hydroxybenzoate. On the other hand, p-aminobenzoate does not produce significant changes in CD spectrum of the free enzyme, although it inhibits the enzyme activity in a competitive manner. p-Aminobenzoate may bind to a site other than the one binding p-fluorobenzoate, and thus interfere with the overall reaction of p-hydroxybenzoate hydroxylase. Furthermore, the CD spectrum of the p-aminobenzoate-enzyme mixture is not affected significantly upon

Table VIII. Summary of Substrate Analogues

A. Substrate analogues which perturb the CD spectrum of p-hydroxybenzoate hydroxylase		Bond angle and length of para-substituent[a]	Inhibition constant K_I
1. Benzoate	H-⟨⟩-COOH	C-H = 1.081 Å	5.9×10^{-5}
2. Salicylate	H-⟨⟩(OH)-COOH		+
3. p-Hydroxybenzoate	HO-⟨⟩-COOH	C-O = 1.36	1.2×10^{-5}
4. 6-Hydroxynicotinate	HO-⟨N⟩-COOH	O-H = 0.96	3.1×10^{-4}
5. p-Hydroxybenzoate[b] methyl ester	HO-⟨⟩-C(=O)-CH_3	∢COH = 107.3°	+
6. p-Flurobenzoate	F-⟨⟩-COOH	C-F = 1.328	7.6×10^{-5}
B. Substrate analogues which do not perturb the CD spectrum of p-hydroxybenzoate hydroxylase			
1. p-Aminobenzoate	H_2N-⟨⟩-COOH	C-N = 1.426 N-H = 1.036	4.2×10^{-6}
2. p-Nitrobenzoate	NO_2-⟨⟩-COOH	N-O = 1.24	4.2×10^{-4}
3. p-Chlorobenzoate	Cl-⟨⟩-COOH	C-Cl = 1.70	1.8×10^{-4}
4. p-Methoxybenzoate[b]	CH_3-O-⟨⟩-COOH	C-O = 1.428	+ (weak)
5. Phenol	HO-⟨⟩-H		-

[a] Reference 24

[b] Reference 2

addition of p-hydroxybenzoate. Conversely, the CD spectrum characteristic of the enzyme-substrate complex is converted to the one similar to free enzyme spectrum by the addition of p-aminobenzoate. The results show that the binding of p-aminobenzoate to the enzyme causes a secondary effect on the substrate binding site so that p-hydroxybenzoate can no longer bind to its site, resulting in the inhibition of activity.

The different modes of bindings may be understood in terms of a steric hindrance effect at the hydroxyl binding site. Examination of the CPK space filling models (Figure 13) and interatomic distances and configurations (Table VIII) of the inhibitors (Class B) which does not modify the CD spectrum of the enzyme has a benzoate substituent ($-NH_2$, $-NO_2$, $-OCH_3$, -Cl), bulkier than that of the other class (Class A) (-H, -F, -OH).

By CD studies, we obtained evidence that NADPH binds to free p-hydroxybenzoate hydroxylase. The binding is so specific that NADH does not become associated with the enzyme. These findings will explain the specific requirement of NADPH for the enzymatic hydroxylation of p-hydroxybenzoate.

Proton magnetic resonance study of the relaxation times of the oxidized and reduced pyridine nucleotides in the presence of p-hydroxybenzoate hydroxylase reveals NADPH binding with the enzyme, but not NADP. This result supports the above described CD study that NADPH specifically interacts with the enzyme. Furthermore, the NMR result indicates a preferential binding of the adenine moiety with the enzyme, which provides a physical understanding of the biological specificity for NADPH as a coenzyme rather than NADH.

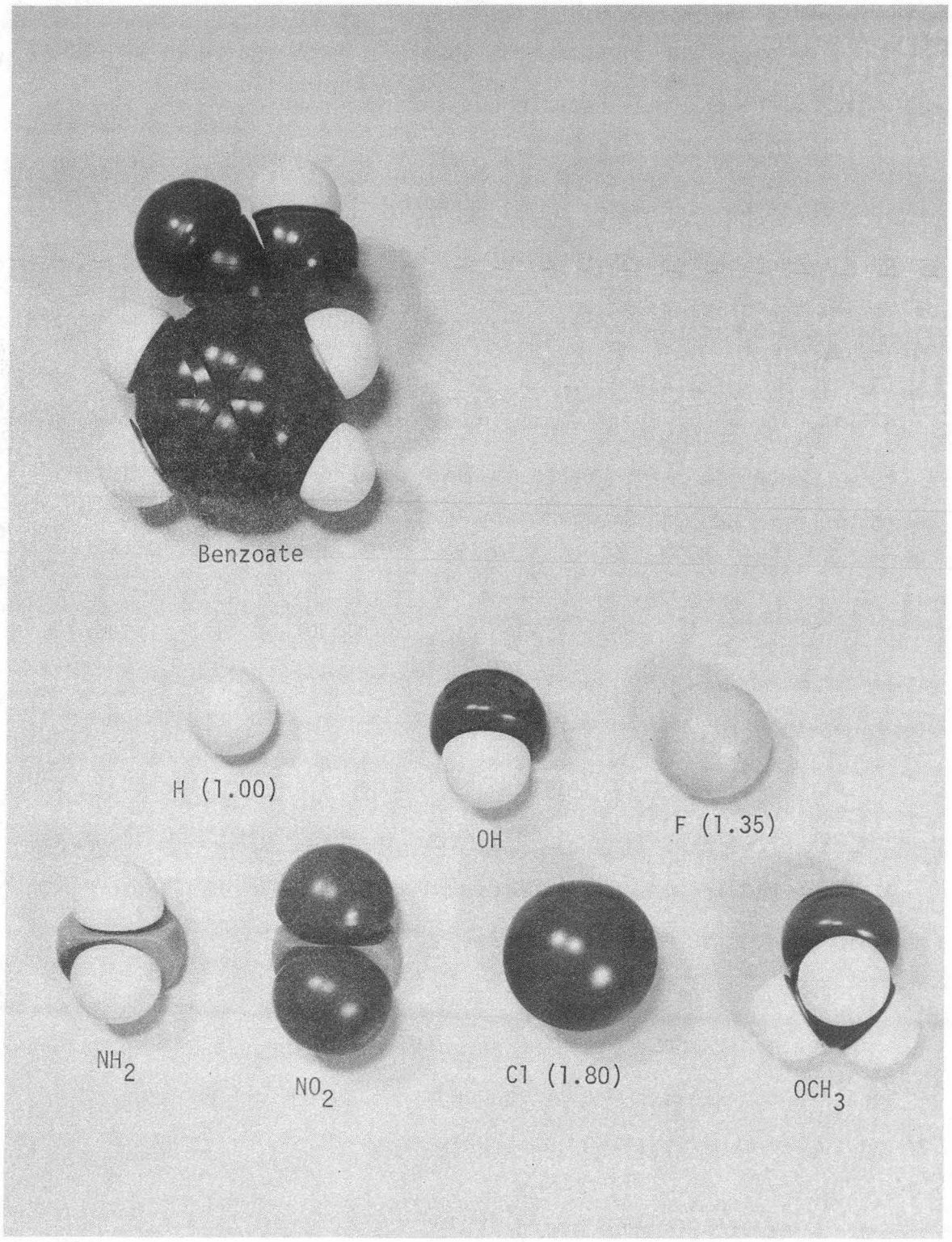

Figure 13. Corey-Pauling and Kolton (CPK) models of benzoic acid and various para-substituents and van der Wall radii, Å.

XBB 727-3724

E. REFERENCES

1. K. Hosokawa and R. Y. Stanier, J. Biol. Chem. 241, 2453 (1966).
2. B. Hesp, M. Calvin, and K. Hosokawa, J. Biol. Chem. 244, 5644 (1969).
3. S. Yamamoto, M. Katagiri, H. Maeno, and O. Hayaishi, J. Biol. Chem. 240, 3408 (1965).
4. M. Katagiri, H. Maeno, S. Yamamoto, O. Hayaishi, T. Kitao, and S. Oae, J. Biol. Chem. 240, 3414 (1965).
5. S. Takemori, H. Yasuda, K. Mihaya, K. Suzuki, and M. Katagiri, Biochim. Biophys. Acta 191, 58 (1969).
6. Ibid., 69.
7. K. Suzuki, S. Takemori, and M. Katagiri, ibid., 77.
8. N. Higashi, S. Nakamura, K. Yano, and K. Arima, Arg. Biol. Chem. 34, 964 (1970).
9. S. Nakamura, Y. Ogura, K. Yano, N. Higashi, and K. Arima, Biochemistry 9, 3225 (1970).
10. D. L. MacDonald, R. Y. Stanier, and J. L. Ingraham, J. Biol. Chem. 210, 809 (1954).
11. K. S. Trippett, S. Dagley, and D. A. Stophen, Biochem. J. 76, 97 (1968).
12. D. Keilin and E. F. Hartree, Proc. Roy. Soc. (London) Ser. B., 134, 397 (1938).
13. P. K. Glasoe and F. A. Long, J. Phys. Chem. 64, 188 (1960); K. Mikkelson and S. O. Nielsen, J. Phys. Chem. 64, 634 (1960).

14. D. H. McDaniel and H. C. Brown, J. Org. Chem. 23, 420 (1958).

15. G. N. Wilkinson, Biochem. J. 80, 324 (1961).

16. W. W. Cleland, Adv. in Enzymology 29, 1 (1967).

17. H. Lineweaver and D. Burk, J. Amer. Chem. Soc. 56, 658 (1934).

18. P. Alexander and Z. M. Bacq, ed., Biological Effects of Deuterium, International Series of Monographs on Pure and Applied Biology, 19, p. 29ff, p. 50ff, and references therein.

19. O. Jardetzky, Advan. Chem. Phys. 1, 499 (1964).

20. O. Jardetzky, N. G. Wade, and J. J. Fisher, Nature 197, 183 (1963).

21. J. J. Fischer and O. Jardetzky, J. Amer. Chem. Soc. 87, 3237 (1965); P. P. Hollis, Biochemistry 6, 2080 (1967); G. Navon, R. G. Shulman, B. J. Wyluda, and T. Yamane, Proc. Natl. Acad. Sci. 60, 86 (1968); B. D. Sykes, J. Amer. Chem. Soc. 91, 949 (1969) and references therein.

22. R. H. Sarma and N. D. Kaplan, Proc. Natl. Acad. Sci. 67, 1375 (1970).

23. L. G. Howell and V. Massey, Biochem. Biophys. Res. Commun. 40, 887 (1970).

24. L. E. Sutton, Table of Interatomic Distance and Autogenation in Molecules and Ions, Special Publication No. 18, The Chemical Society, London, 1965, p. 525.

IV. PHOSPHOROUS-31 RELAXATION STUDY OF ADENOSINE TRIPHOSPHATE

A. INTRODUCTION

The recent advance in Fourier transform nuclear magnetic resonance[1] has virtually opened up an entirely new dimension in magnetic resonance. In the past, the biophysical use of NMR spectroscopy has been mainly limited to the static information of chemical shifts and spin coupling constants. The dynamic aspect of NMR has not been widely investigated except for line width measurements (Chapter III) and occasional application of transient NMR method, usually done by way of adiabatic rapid passage. The Fourier transform technique enables the experiment to be performed at a great saving of time which in studying biological systems is necessary. Furthermore, this method provides a direct measurement of the relaxation times T_1 and T_2 of each individual nucleus within a biological molecule in an elegant fashion. The measurement of the relaxation times and their temperature dependence can furnish the much needed biological exchange rates.[2] For example, the forward and backward reaction rate constants K_{+1} and K_{-1} in a substrate-enzyme complex can be determined.[3] The relaxation data can, potentially, provide information about molecular structure and dynamics that is difficult to obtain by other physical techniques. For example: (i) changes in the mobility of parts of a flexible molecule may be deduced from relaxation rates;[4] (ii) distances between a paramagnetic center and nuclei giving NMR signals may be calculated from the paramagnetic enhancement of NMR relaxation;[5] (iii)

slow equilibria between conformational states may be identified and characterized by relaxation measurements.[6]

As a background for future ^{31}P-NMR relaxation studies of biological molecules we have investigated the influence of ionic strength, sample concentration, pH or pD, and paramagnetic ion concentration on phosphate chemical shifts and T_1 (longitudinal) relaxation. We have studied orthophosphate (P_i), tripolyphosphate, and adenosine triphosphate (ATP). ^{31}P-NMR titration curves have previously been published for P_i[7] and ATP.[8] In addition, the effect of metal ion binding on the ^{31}P-NMR chemical shifts,[9] linewidths[9-11] and relaxation times[10,11] of ATP have been reported. We have extended these studies by making use of the conveniences afforded by Fourier transform spectroscopy[12] for signal enhancement and T_1 determination.[13,14] We present here more detailed phosphate chemical shift data and data pertaining to the mechanisms underlying phosphorous T_1 relaxation in phosphates. Although a detailed interpretation is not yet possible, several general comments are in order.

B. EXPERIMENTAL PROCEDURE

Material

Na_2HPO_4 (Baker), sodium pyrophosphate (Baker), sodium tripolyphosphate (Alfa), and ATP (Sigma) were purified by passage through a Chelex-100 column (9.2 x 99 cm) at pH 6-8. Metal ion impurities were removed from some ATP samples by repeated extraction with 8-hydroxyquinoline.[15] Levels of paramagnetic ion contaminants (largely iron

and copper) were monitored by X-ray fluorescence spectroscropy. Purified samples contained less than 1 ppm iron or copper which was the lower limit of detection by X-ray fluorescence. Metal levels in purified Pi samples were well below 1 ppm since it was found that addition of 0.1 ppm Fe^{3+} to these samples produced significant enhancement of T_1 relaxation. Table I gives the results of X-ray fluorescence analysis of ATP samples.

Great care was exercised to exclude metal ion contaminants from the samples. Solutions were prepared using column deionized, glass-distilled water. The conductivity of the deionized water is $2 \times 10^{-6}\ \Omega^{-1}\ cm^{-1}$. The pH of H_2O solutions was adjusted with high purity HCl and NaOH (Alfa); the pD of D_2O (Biorad) solutions was adjusted with DCl and NaOD (Diaprep). Glassware was acid washed and rinsed with deionized water.

The concentrations of nucleotide solution was measured spectrophotometrically. The orthophosphate solution used for titration studies contained 0.3 M NaCl (Mann, high purity) added to mask changes in ionic strength and sodium ion concentration on titration. Metal ions were introduced by adding microliter quantities of concentrated metal salt solutions.

The pH measurements were made at room temperature on a Corning Model Digital 110 pH meter with a small combination electrode (Instrumentation Laboratories). Titrations were carried out with concentrated acid or base dispensed with micrometer syringes (Cole Parmer) equipped with teflon needles (Hamilton). The pH values in D_2O solutions are actual pH meter readings uncorrected for the deuterium isotope effect at the glass electrode.

TABLE I

X-ray Fluorescence Analysis of Metal Contaminants in 5'ATP

Source	Fe*	Cu	Zn	Pb
Sigma (Lot #110C -7410)	42 ppm	9	3	5
Cal Biochem (Lot #800685)	275	1	4	4
8-Hydroxyquinoline (treated once)	16	2	4	3
Chelex 100 column (treated at pH 6)	1	1	3	3

* All contaminants are expressed in parts per million.

NMR Spectra

Spectra were obtained at 24.3 MHz using a home-built Fourier transform NMR instrument based on a Varian DP-60 magnet and V-2100-B power supply. The field was stabilized by means of a proton external lock. The width of a 90° pulse was typically 40 μsec. Pulse programming was accomplished with a series of time base oscillators. The free induction decays were digitized into 2048 12-bit words and accumulated on a PDP-8 computer with disc storage. Completed experimental data was transferred to magnetic tape and processed later by a large computer using a fast Fourier transform program. The spectra were plotted on a Calcomp recorder.

All spectra were taken at 30°C. Sample volumes were 1 ml. The samples were placed in glass spheres that fit snugly inside a standard 15 mm NMR cell. The NMR cell holding the sphere was spun by a Wilmad turbine. The signal-to-noise ratio for a 0.1 M phosphate solution was generally 10 for a single 90° pulse. Spectra were usually the result of 10-25 passes. A thin capillary containing 50% H_3PO_4 was inserted in the sphere as an external reference. Chemical shifts are reported in Hz from 50% H_3PO_4 which, within experimental error, is the same as that of 85% H_3PO_4. 50% H_3PO_4 is a more satisfactory reference than 85% H_3PO_4 because it is less viscous and provides a sharper peak.

Relaxation Time Measurement

T_1 measurements were made either by the spin inversion[13] or spin saturation[14] method, depending on the length of T_1. Both methods gave similar results. Relaxation times were determined by a computer program, TIFIT, that gave a least squares fit of the data to an

exponential recovery of the magnetization vactor. The errors reported are based on standard deviation from the best fit. However, the reproducibility of the T_1 experiments was generally only within 5% from one sample to another. Thus the actual errors in the T_1 values are probably determined by contamination of samples rather than by the T_1 measurements themselves.

C. RESULTS AND DISCUSSION

Orthophosphate

pH and Solvent Dependence of Relaxation Rate and Chemical Shift

Control experiments were carried out to test the influence of metal ion contamination, dissolved oxygen, sample concentration, ionic strength, and proton concentration (D_2O vs. H_2O) on P_i T_1 relaxation (Table II). The P_i relaxation is extremely sensitive to metal ion contaminants which can be removed by passage of the sample through a Chelex-100 column. The T_1 value of purified P_i does not increase significantly when 10^{-3} M EDTA is added, indicating the removal of metal ions is complete. T_1 relaxation appears to be relatively insensitive to P_i concentration in the range 0.1-0.3 M and ionic strength in the range μ 0.9-1.2. The T_1 value increases two-fold at pH 7 when D_2O is used as the solvent instead of H_2O.

The pH dependencies of the relaxation rate (T_1^{-1}) and chemical shift of P_i in H_2O and D_2O are given in Figure 1. The chemical shifts of P_i are very similar in D_2O and H_2O. The close correspondence of the first and second inflections indicates that the deuterium isotope

TABLE II

Phosphate Relaxation Values

Sample	T_1 (sec)	T_1^{-1} (sec^{-1})
0.3 M unpurified Na_2HPO_4 pH 7.00		
H_2O	0.69	1.5
0.3 M purified (Chelex) Na_2HPO_4 pH 7.00		
H_2O	11.8 ± 0.5	0.085 ± 0.004
Purified (Chelex) H_2O	12.3 ± 0.1	0.081 ± 0.001
H_2O, degassed	10.1 ± 0.1	0.099 ± 0.001
D_2O	25.0 ± 0.7	0.040 ± 0.001
D_2O, degassed	23.2 ± 0.2	0.043 ± 0.001
0.1 M purified (Chelex) Na_2HPO_4 pH 7.0		
H_2O	12.1 ± 0.3	0.083 ± 0.002
D_2O	26.8 ± 0.9	0.037 ± 0.001
0.3 M purified (Chelex) Na_2HPO_4 + 0.3 M NaCl		
H_2O	13.7 ± 0.1	0.073 ± 0.001
0.3 M purified (Chelex) Na_2HPO_4 + 10^{-3} M EDTA		
H_2O	13.0 ± 1.7	0.077 ± 0.010

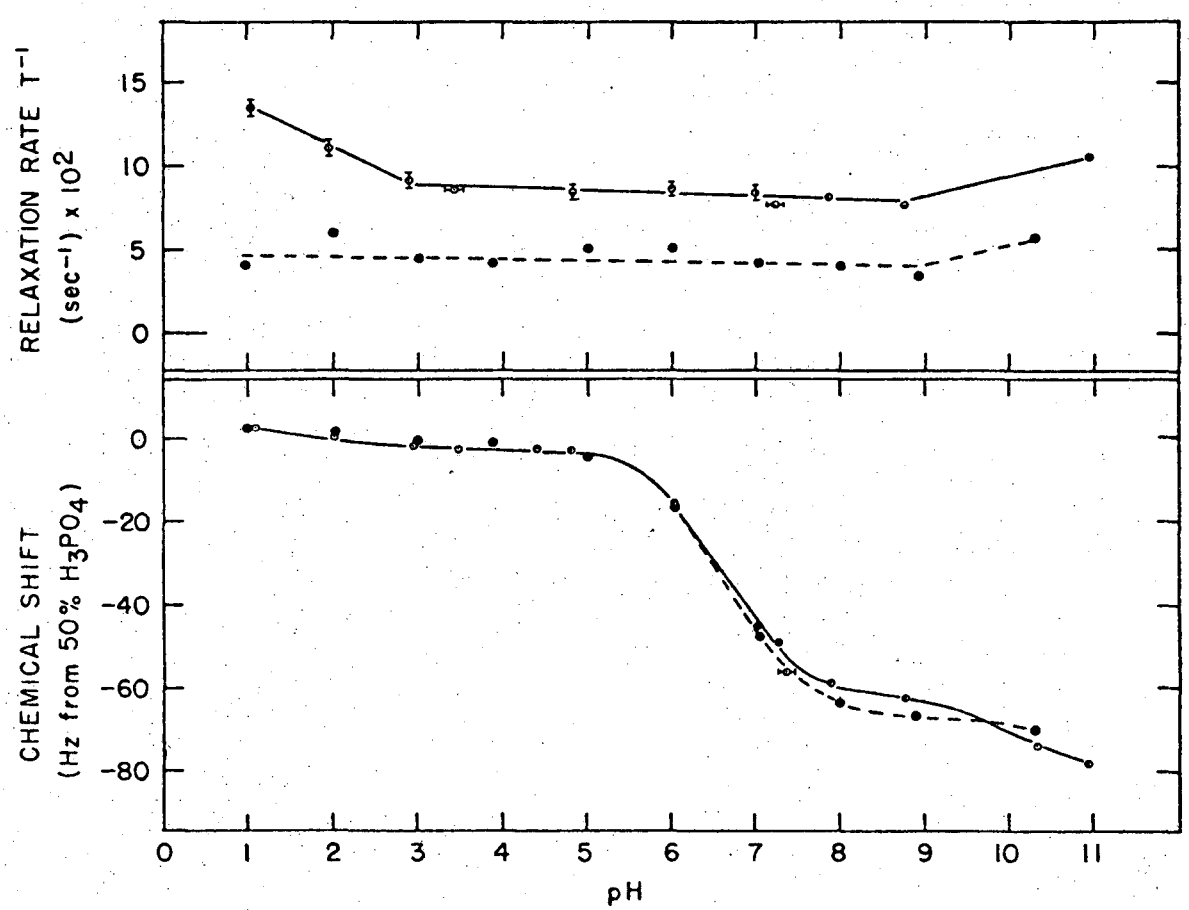

XBL721-4500

Figure 1. Dependence of chemical shift (bottom) and T_1 relaxation rate (top) of purified 0.3 M Na_2HPO_4 in H_2O (solid) and D_2O (dashed) solutions containing 0.3 M NaCl. The pH values for the D_2O solutions are actual pH meter readings uncorrected for the deuterium isotope effect at the glass electrode.

effects on pK_1 and pK_2 of P_i are nearly equal and opposite to the deuterium isotope effect on the glass electrode (+0.4 pH units).[16]

Because of the absolute necessity of removing metal ion contaminants from samples in NMR relaxation measurements, we chose P_i as a model study. Consequently, Fe^{3+} was added to purified P_i, and the T_1 relaxation rate was measured as a function of pH (Figure 2). The results indicate that very low levels of Fe^{3+} (0.2-1.0 ppm) have a pronounced influence on P_i relaxation. An explanation of the observed curves may be based on the following equilibria:

$$\begin{array}{ccccccc} & pK=1.5 & & pK=6.8 & & pK=10.5 & \\ H_3PO_4 & \overset{H^+}{\rightleftharpoons} & H_2PO_4^- & \overset{H^+}{\rightleftharpoons} & HPO_4^{2-} & \overset{H^+}{\rightleftharpoons} & PO_4^{3-} \\ & & Fe^{3+}\downarrow\uparrow & & Fe^{3+}\downarrow\uparrow & & Fe^{3+}\downarrow\uparrow \\ & & FeH_2PO_4^{2+} & & FeHPO_4^{+} & & FePO_4 \end{array} \qquad (1)$$

$$Fe^{3+} + 3OH^- \rightleftharpoons Fe(OH)_3 \text{ , } pK_{solubility} = 36$$

The amount of ferrous ion in solution should be negligible since the ferric ion binds much more strongly to phosphate.

At low pH, the phosphate is predominantly in the fully protonated uncharged form which does not bind Fe^{3+}. At higher pH, hydrous ferric oxide forms and Fe^{3+} is removed from solution. Above pH 9 the PO_4^{3-} species is formed which appears to compete with ferric oxide for some of the Fe^{3+}. The data at 0.2 ppm Fe^{3+} fit this model very well

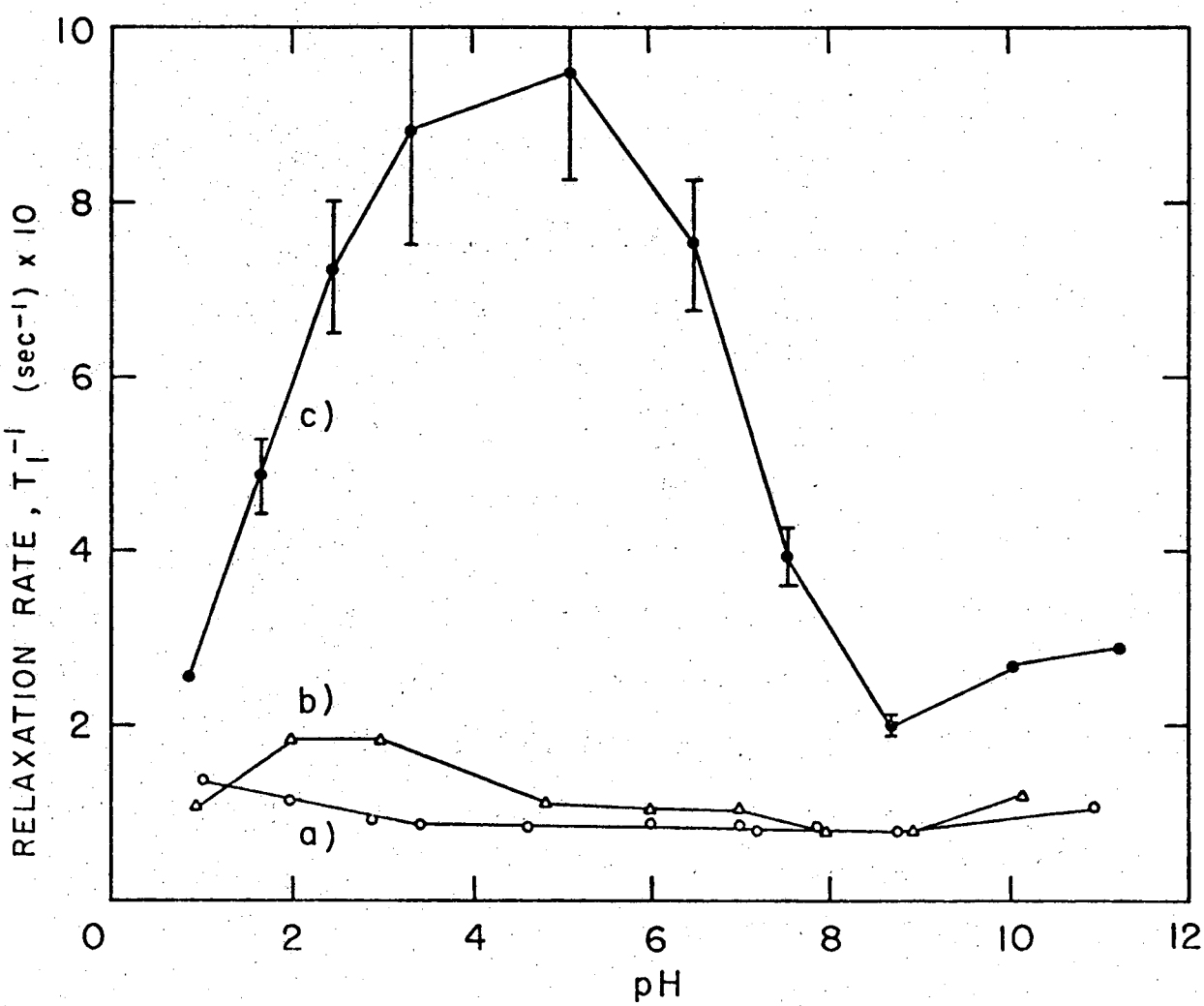

XBL728-4719

Figure 2. Influence of added Fe^{3+} on the T_1 relaxation rate of phosphate ion as a function of pH. The solutions contained 0.3 M Na_2HPO_4 in 0.3 M NaCl. (a) No added Fe^{3+}. (b) 0.2 ppm Fe^{3+}/P_i added. (c) 1.0 ppm Fe^{3+}/P_i added.

(Figure 2b). On the basis of the solubility product of hydrous ferric oxide one expects a fall in free [Fe^{3+}] to occur about pH 4. In view of the large errors in the data at 1.0 ppm Fe^{3+}, the apparent shift in the pH maximum from 2.5 to 5 may not be significant. It is puzzling, however, that the relaxation enhancement does not seem to be linear in Fe^{3+} concentration.

Relaxation Mechanisms

The relaxation mechanism(s) of ^{31}P in phosphorous compounds is (are) not well understood. Several investigators[11,18] have investigated small phosphorous compounds and concluded that spin-rotation interaction is the dominant relaxation mechanism in compounds such as PBr_3, PF_3, and $POCl_3$. The spin-rotation interaction arises from magnetic fields generated at a nucleus by the motion of a molecular magnetic moment which arises from the electron distribution in a molecule. Since this interaction is proportional to the angular velocity of rotation, and inversely proportional to the moment of inertia of the molecule, in general, the smaller the molecule the more dominant will be the spin-rotation relaxation. Furthermore, symmetric molecules with no intermolecular interaction will be most affected. Our T_1 observation of P_i in D_2O and H_2O seems to reject the magnetic moment of the proton as a significant relaxer. This is because of the small variation of T_1 in going from H_2O to D_2O. A factor of 2 change is observed, instead of $I(I+1)\ \gamma_H^2/S(S+1)\ \gamma_D^2 = 15.9$ as in the case of proton dipolar interaction, where I, and S are the spin quantum numbers of proton and deuteron; γ_H and γ_D are the magnetogyric ratios of proton and deuteron. The lack of pH dependent relaxation rates also supports the notion that

proton makes no significant contribution to the relaxation rates. The chemical shift anisotropy can also provide a relaxation mechanism via the local fluctuating magnetic field caused by the anisotropic chemical shift tensor. We feel in a relatively symmetric molecule, P_i, this mechanism is unlikely. In addition, the relaxation rate via chemical shift anisotropy is proportional to the molecular correlation time τ_c which can be related to the viscosity η and the "radius" of the molecule by the Debye formula $\tau_c = \frac{4\pi\eta a^3}{3kT}$, where k is the Boltzmann's constant and T is the absolute temperature. Therefore, the relaxation rate would be directly proportional to the viscosity if chemical shift anisotropy prevails. The observation that T_1^{-1} is shorter in D_2O than in H_2O is opposite to what one would expect from chemical shift anisotropy, knowing the viscosity of D_2O is 20% greater than that of H_2O at 30°C. The other possible relaxation mechanism is spin-rotation which is inversely dependent on τ_c and, hence, the viscosity η. This would explain the shortening of T_1^{-1} in D_2O; however, the mechanism cannot account for a factor of 2 change in magnitude of T_1. Nevertheless, we propose spin-rotation as an important relaxation mechanism of P_i at the temperature the measurements were made. A small contribution from the proton-dipolar interaction could compensate for the discrepancy in magnitude of T_1. We gain further confidence by noting that the magnitudes of the relaxation rates observed in PBr_3, PF_3 and $POCl_3$ at the same temperature as our measurements are comparable to the values we observe. A definitive test of spin-rotation interaction is a detailed study of the relaxation rate as a function of η/T. The temperature dependence of spin-rotation relaxation is opposite to that observed for all other relaxation mechanisms.

Adenosine Triphosphate

Spectrum

Figure 3 shows a first order ^{31}P NMR spectrum of ATP which consists of three peaks from the alpha, beta and gamma phosphates. Beta and gamma phosphorous give rise to a sharp triplet and doublet respectively. Alpha phosphorous resonance is a doublet broadened by proton hyperfine structure from the $C_5'H_2$ of the ribose. The phosphorous-phosphorous $JI_1 \cdot I_2$ spin interaction is observed to be 19.0 Hz for all the peaks. The spin coupling constant is pH dependent. As acidity increases, the coupling constant decreases from 19.0 at pH 12.0 to 18.0 Hz at pH 2.0. The decrease of coupling constant seems to be caused by the formation of H-O-P bonds of some covalent character in the acidic solution. Similar decrease has been observed in condensed polyphosphate.[19] The coupling constant is, however, independent of the concentration over the range tested (0.33-0.05 M). The proton-phosphorous spin interaction is 5.2 $\pm$ 0.5 Hz. This value is similar to those observed in inosine-5'-monophosphate and guanosine-5'-monophosphate, and is appreciably lower than the J_{PH} values for phosphates of normal alkyl alcohols.[20] Tsuboi, Kainosho and Nakamura[20] estimated J_{PH} for phosphorous trans in relation to the proton to be 22.1 Hz and gauche in relation to the proton to be 2.3 Hz. We therefore conclude that the ATP molecule assumes mostly a conformation in which the alpha phosphorous is gauche in relation to the methylene protons of C_5' of the ribose or trans to C_4', as shown in Figure 3 of Chapter I. From a general consideration of internal rotation about the C-O single bond,[21] three potential energy minima corresponding to the staggered conformations are usually found.

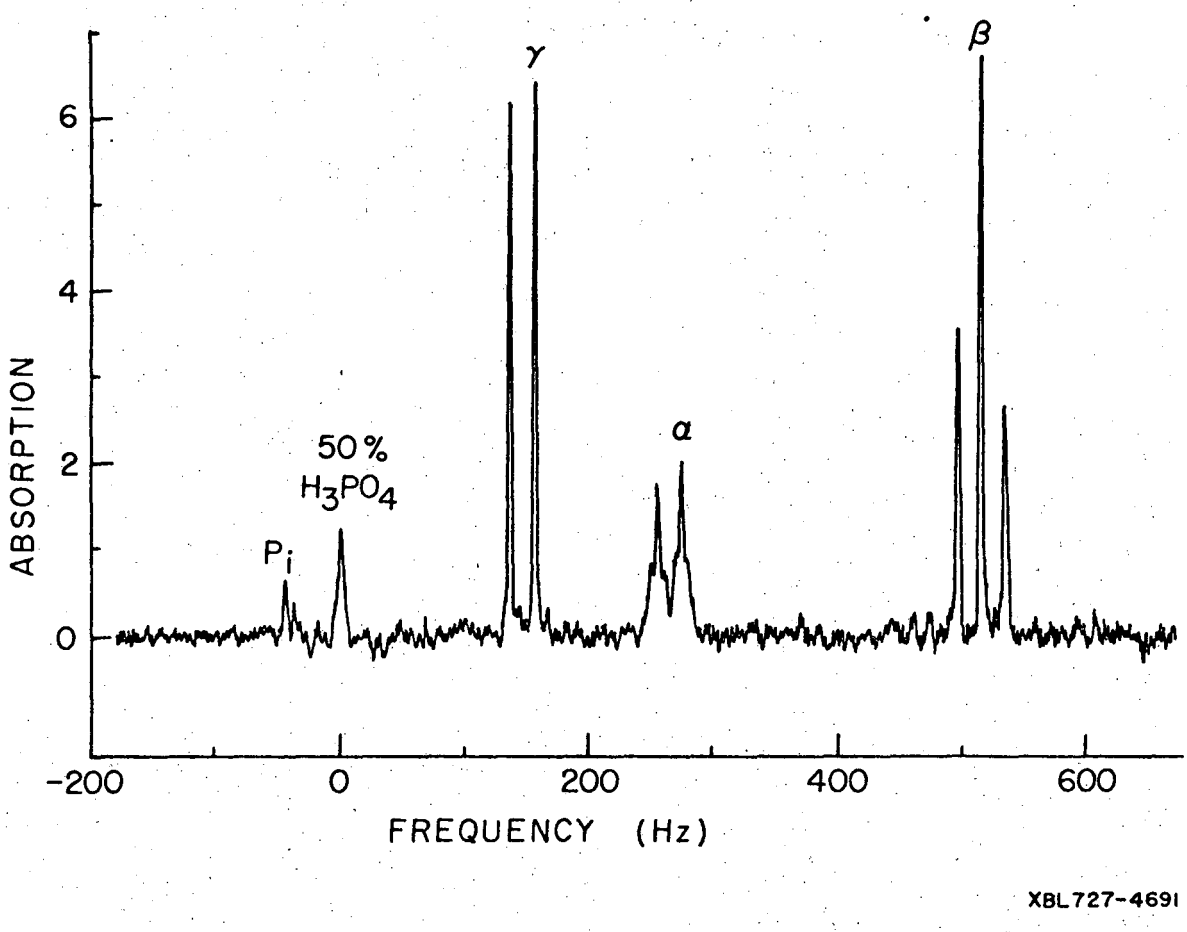

Figure 3. ^{31}P-NMR spectrum of 0.3 M 5'-ATP at pH 7.00. The spectrum is the Fourier transform of 10 averaged free induction decay spaced 40 seconds apart. The reference is 50% H_3PO_4 in an external capillary. P_i is an impurity present in the sample.

They are illustrated schematically in Figure 4. If we let P_t represent the population of the conformation, in which the α-phosphorous is trans to C_4', then $1/2(1-P_t)$ corresponds to the population of conformation

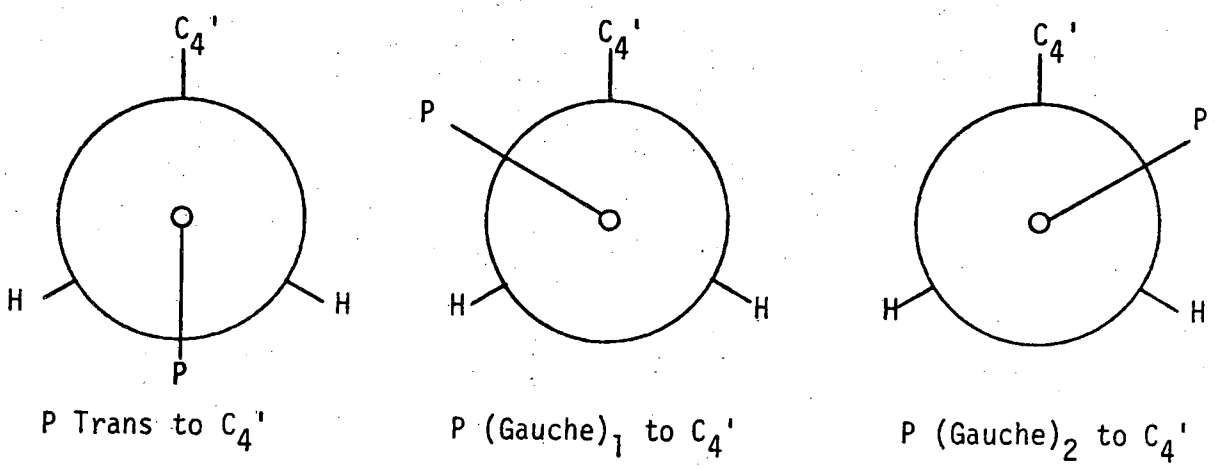

Figure 4. A schematic drawing of the three energetically favored rotamers when looking along C_5'-O bond in 5'-ATP.

where α-phosphorous is gauche to C_4'. Remembering J_t and J_g are defined as the coupling constants when P is trans and gauche to the proton, respectively, then the observed J_o is given by the relation,

$$J_o = \frac{1 - P_t}{2} J_t + \frac{1 + P_t}{2} J_g$$

Using the estimated value of J_t and J_g,[20] we calculate P_t to be 0.71. The P-H coupling does not seem to be dependent on pH and concentration in the limit of our resolution. The spectrum of ATP, however, is dependent on the concentration of nucleotide, the pH and trace metal concentration.

Concentration Dependence

Figures 5 and 6 and Table III show the chemical shifts and relaxation rates of ^{31}P in ATP as a function of concentration. The chemical shift changes are presumably due to intermolecular diamagnetic shielding of the ring current in the adenine moiety. This is consistent with the proton magnetic resonance findings. Ts'o et al.[22] have shown that the chemical shift of the proton resonances of the base is a sensitive probe for intermolecular association in nucleotides. Furthermore, the nucleotides are known to form stacked dimers with a concentration as low as 20 mM. The relaxation values extrapolated to zero concentration are presented in Table III.

Table III and Figure 7 show the α-^{31}P having the most concentration dependent T_1 and γ-^{31}P having the least. This is probably because γ-^{31}P is at the end of the phosphate chain and has, relatively, unrestricted and independent motion. The α and β-^{31}P, because of a closer proximity to the adenine ring, are more influenced by intermolecular association. A discussion of the relaxation mechanisms will be given after the presentation of pH dependent study.

pH Dependence of Chemical Shifts

Figure 7 shows the effect of pH variation on the chemical shifts of demetalized ATP. This result is a refinement of that of Cohn and Hughes.[9] In those previous investigations, which were limited by low resolution and possible presence of trace metal, the chemical shift of the alpha phosphorous appeared to be independent of pH and the chemical shift of the beta phosphorous showed a linear dependence of pH, shifting approximately 1 ppm downfield with decreasing acidity. Our data indicate that,

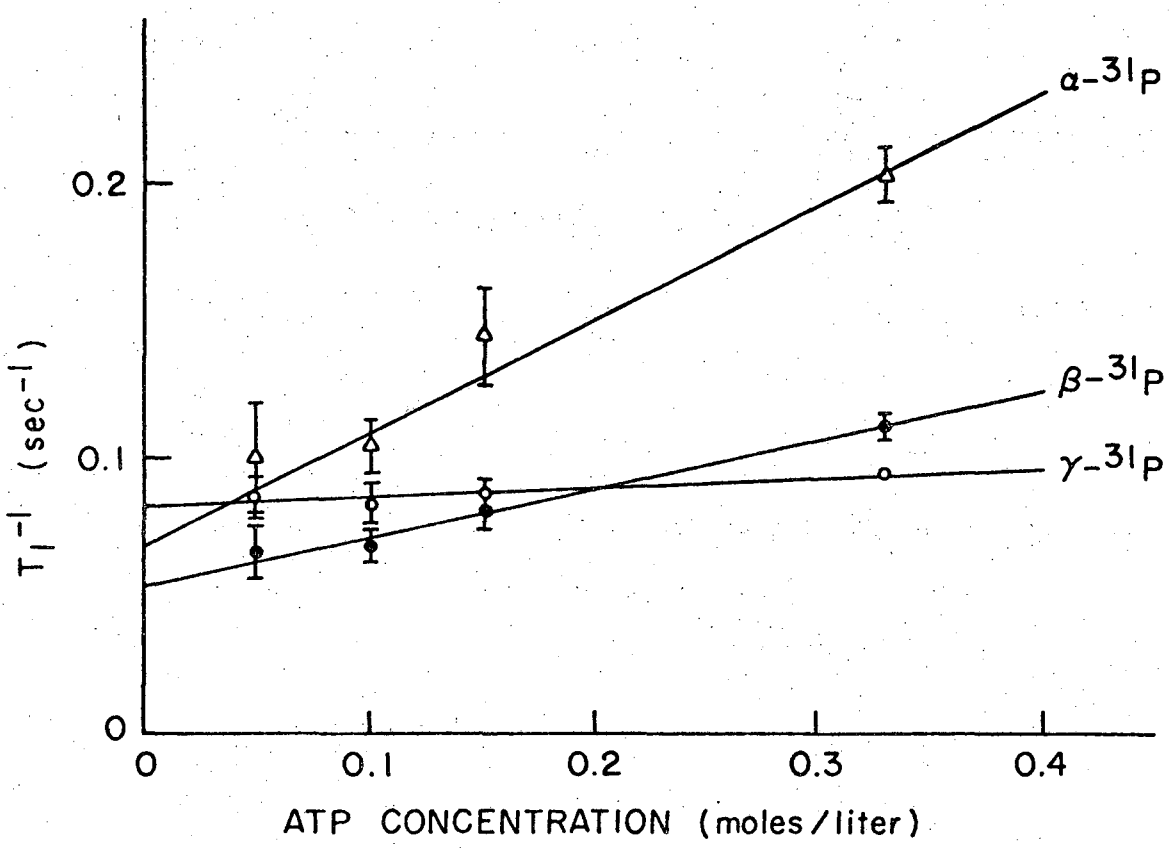

XBL 727-4693

Figure 5. Relaxation rate (T_1^{-1}) of ATP as a function of concentration. The concentration is determined by UV absorption at 259 nm.

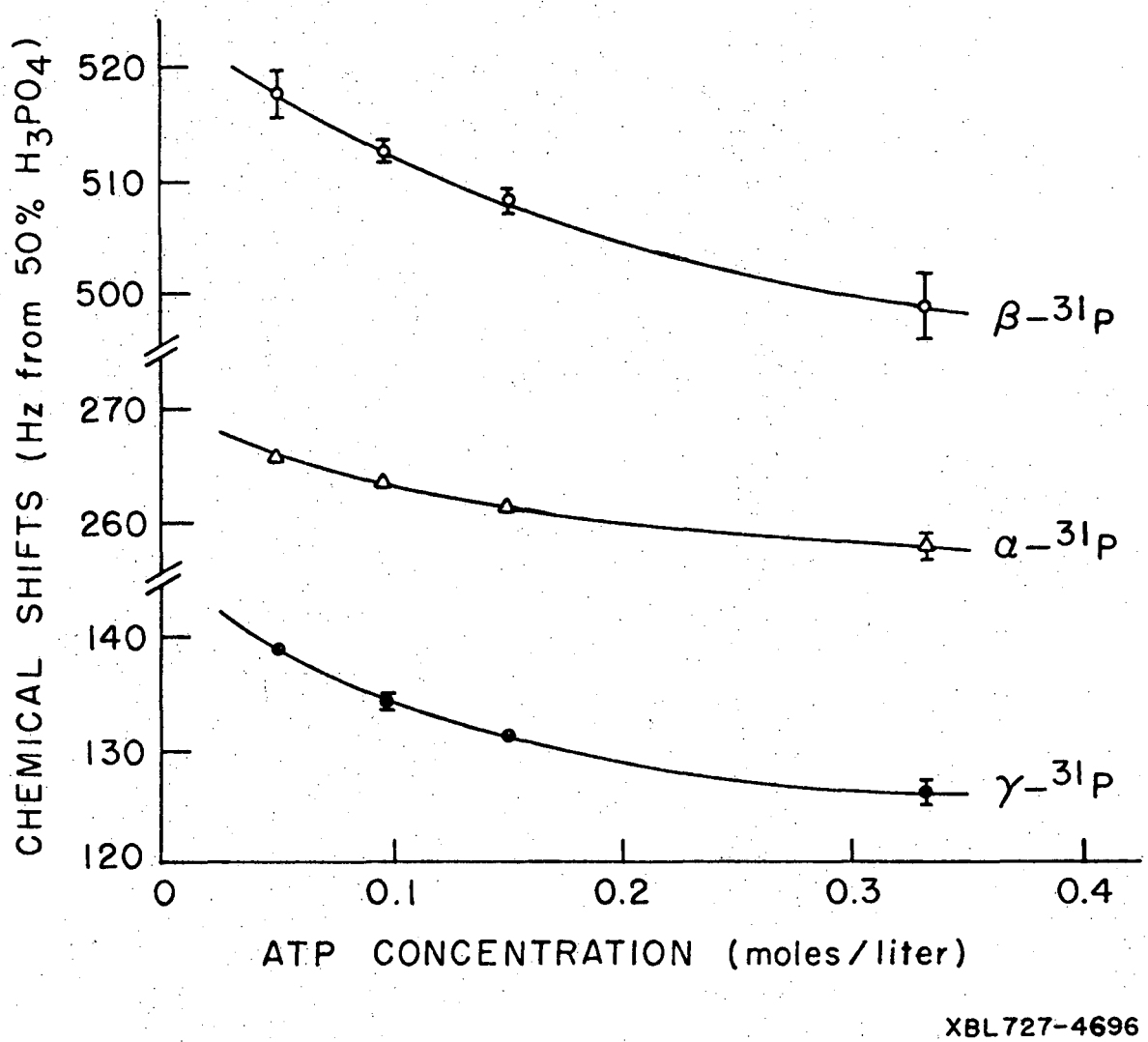

Figure 6. ^{31}P NMR chemical shifts of ATP as a function of concentration.

TABLE III

Concentration Study of ^{31}P Relaxation Value in 5'-ATP (pH 10.0)

[ATP]	α-P		β -P		γ-P	
M^{-1}	T_1 (sec)	T_1^{-1} (sec^{-1})	T_1 (sec)	T_1^{-1} (sec^{-1})	T_1 (sec)	T_1^{-1} (sec^{-1})
0.33	4.95 ± 0.31	0.20 ± 0.01	8.64 ± 0.41	0.11 ± 0.005	10.57 ± 0.26	0.0946 ± 0.002
0.0	14.7	0.068	18.5	0.054	12.05	0.083

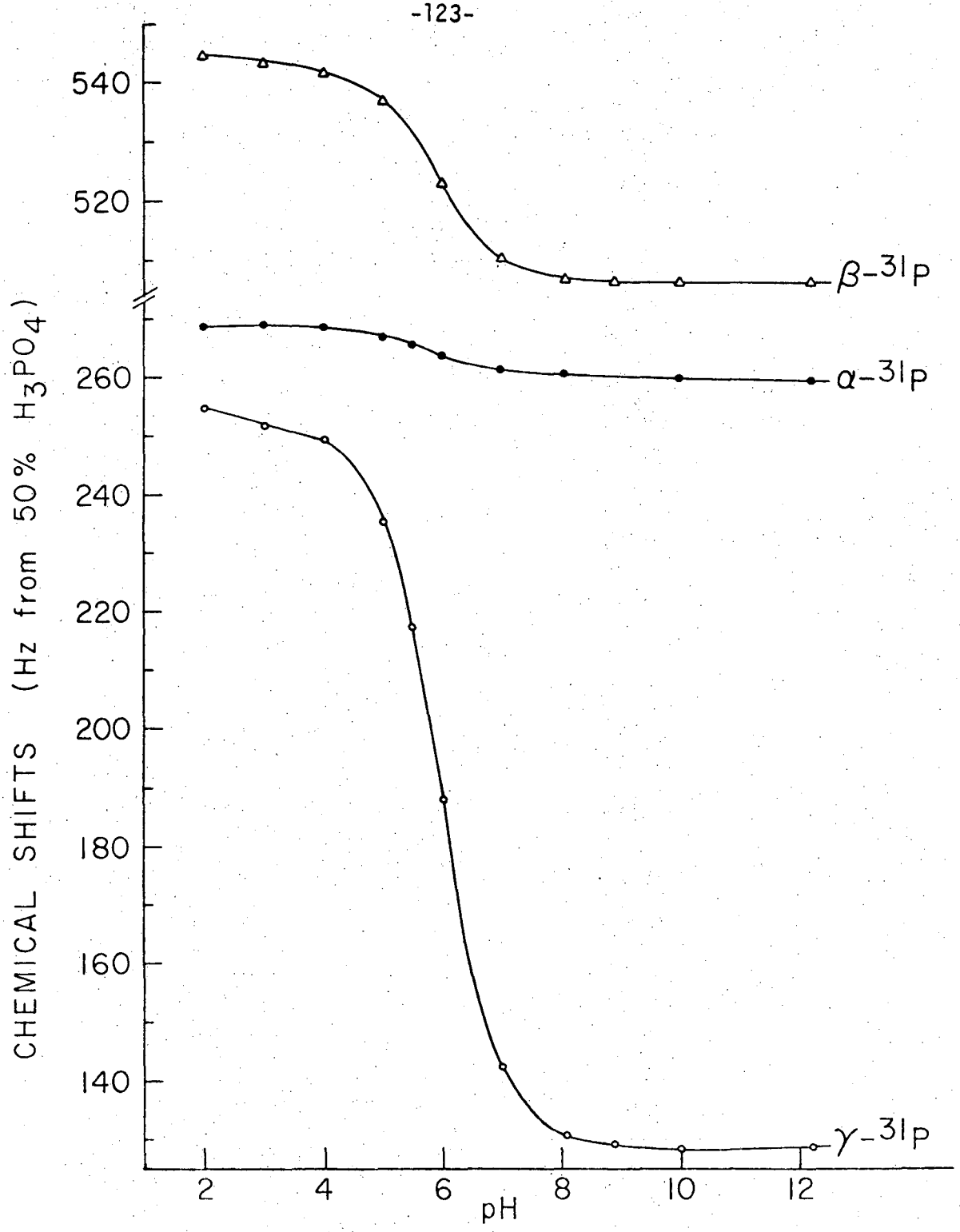

XBL727-4697

Figure 7. ^{31}P NMR chemical shifts of 0.3 M ATP in H_2O solution. The pH values given are uncorrected for the deuterium isotope effect at the glass electrode.

in the demetalized ATP sample, the chemical shifts of all the phosphorous resonances have a sigmoidal dependence on the pH with inflection points around pH 6.0. This apparent pK_a is considerably lower than the 6.48-7.68 values reported from glass electrode and other spectroscopic investigations.[23] This pK_a value corresponds, perhaps, to the dissociation of a proton on the γ phosphate group. The reason for the discrepancy is yet to be determined. It should be remembered, however, that glass electrode titration curves reflect the effect of overall acid-base equilibria on the concentration of free hydronium ion, whereas NMR data reflects a localized perturbation caused by the bound protons.

pH Dependence of Relaxation Times

Previous ^{31}P studies of ATP[24] had shown a strong dependence of the relaxation rate on pH in the range 4-6. It was of interest to investigate whether this was a special feature of the ATP molecule or whether the pH dependence could simply be explained by interaction of unremoved metal ion contaminants with the phosphates. The results of a pH dependent relaxation study on both demetalized and undemetalized commercial ATP are presented in Figures 8 and 9 and Table IV. Because of the high binding constant of iron to ATP, a dependable demetalization procedure is crucial. We have found treatment of ATP over freshly regenerated Chelex-100 column is able to produce 11 second T_1 relaxation time of β and γ phosphorous in 0.3 M ATP at pH 10.0 or higher. From observations of many samples we establish as a criterion of purity the requirement that the relaxation times for the β and γ phosphorous nuclei in the above stated conditions be at least 11 seconds to within the limits allowed by the signal-to-noise ratios.

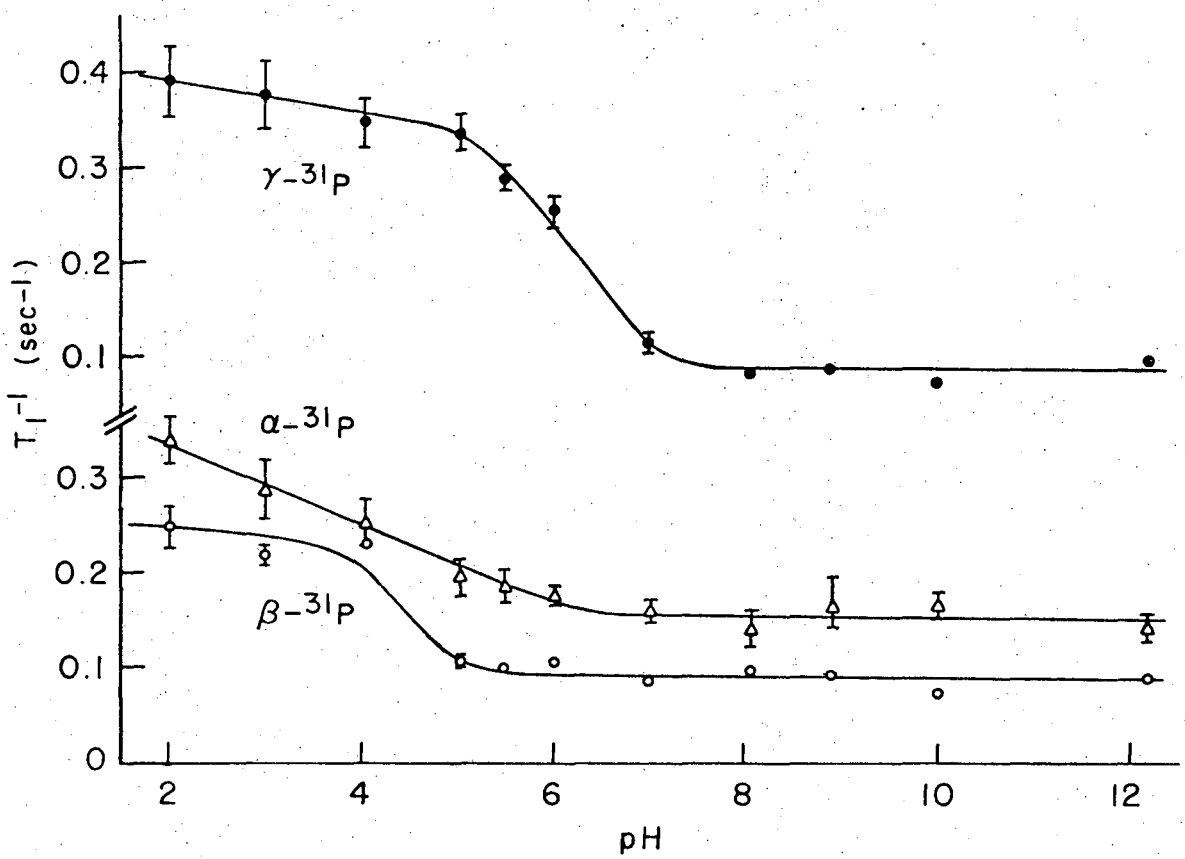

XBL727-4695

Figure 8. T_1 relaxation rate (T_1^{-1}) of 0.3 M demetalized ATP. The pH values are uncorrected for the deuterium isotope effect at the glass electrode.

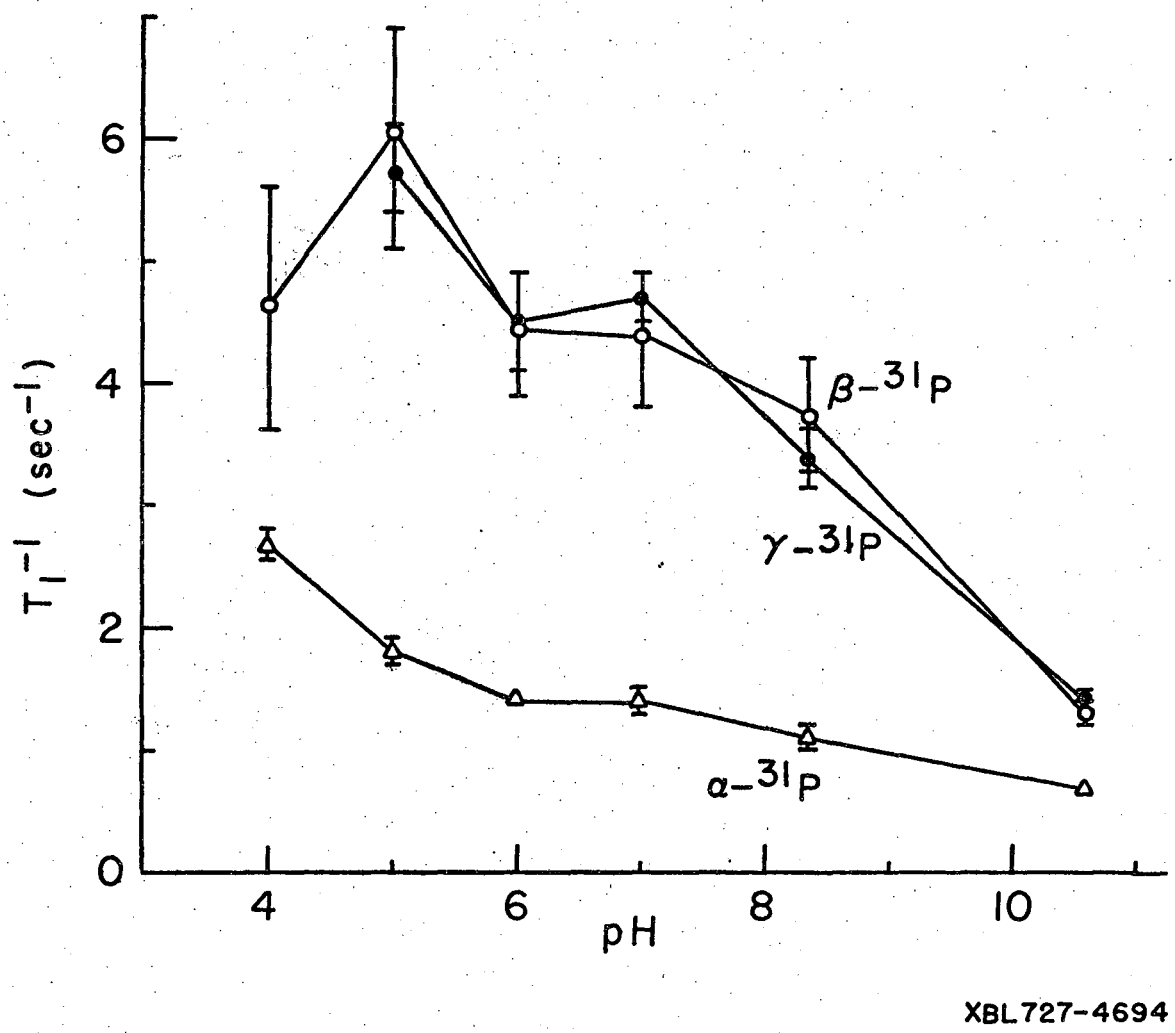

Figure 9. The T_1^{-1} relaxation rate of commercial ATP sample (Sigma) without demetalization.

TABLE IV

The pH Dependence of ^{31}P Relaxation Values of Demetalized and Undemetalized ATP

Sample	pH	α-P		β-P		γ-P	
		T_1 (sec)	T_1^{-1} (sec^{-1})	T_1 (sec)	T_1^{-1} (sec^{-1})	T_1 (sec)	T_1^{-1} (sec^{-1})
Demetalized (Chelex) ATP (0.3 M)	10.0	6.13 ± 0.54	0.163 ± 0.014	14.1 ± 0.74	0.071 ± 0.004	13.58 ± 0.34	0.074 ± 0.002
	7.0	6.34 ± 0.51	0.157 ± 0.013	11.67 ± 0.81	0.085 ± 0.006	8.74 ± 0.93	0.114 ± 0.012
	2.0	3.00 ± 0.25	0.336 ± 0.027	4.57 ± 0.28	0.218 ± 0.014	2.55 ± 0.23	0.39 ± 0.036
Undemetalized (Sigma) ATP (0.3 M)	10.6	1.48 ± 0.05	0.676 ± 0.025	0.77 ± 0.06	1.30 ± 0.09	0.71 ± 0.03	1.41 ± 0.06
	7.0	0.72 ± 0.06	1.398 ± 0.113	0.24 ± 0.03	4.37 ± 0.55	0.21 ± 0.01	4.73 ± 0.25

Figure 9 shows the relaxation rates of α and β phosphorous nuclei in the undemetalized ATP have almost identical pH dependence and the rates of all three phosphorous nuclei decrease as the acidity is increased. A similar explanation as that in the case of orthophosphate can be applied here - i.e., at high pH, hydrous ferric oxide starts to form and Fe^{3+} is removed from solution and, consequently, T_1 relaxation rates become shorter. Because of the complexity of the ATP-iron equilibria and large number of equilibrium species involved, it is not possible to establish the equilibrium constants from our data. It is most curious to observe, in the undemetalized ATP sample, that β and γ-^{31}P have much larger relaxation rates than α-^{31}P in the whole pH range tested (4.0-10.6). Furthermore, the line widths of the β and γ-^{31}P resonances are affected significantly more than that of α-^{31}P. The P-P splitting of β and γ-^{31}P resonances cannot be resolved for pH lower than 8.5, whereas the α-^{31}P resonance stays as a doublet until pH 5.0. The broadening of the phosphorous peaks due to the presence of paramagnetic impurities is illustrated in Figure 10. Considering that β and γ-^{31}P resonances are, intrinsically, much sharper than the α resonance which is broadened by the C_5' methylene protons (Figure 3), the broadening effect on the β and γ-^{31}P peaks due to paramagnetic transition metal impurities is remarkable. These evidences suggested that the β and γ phosphates are involved more strongly in the binding of metal ions (presumably, Fe^{3+} and Cu^{2+}) than the α phosphate (see discussion in Chapter II, section C). This finding agrees with the study of Sternlicht et al.[11] on Cu-ATP complex, where they proposed that the Cu^{2+} binds predominantly to the β and γ phosphates.

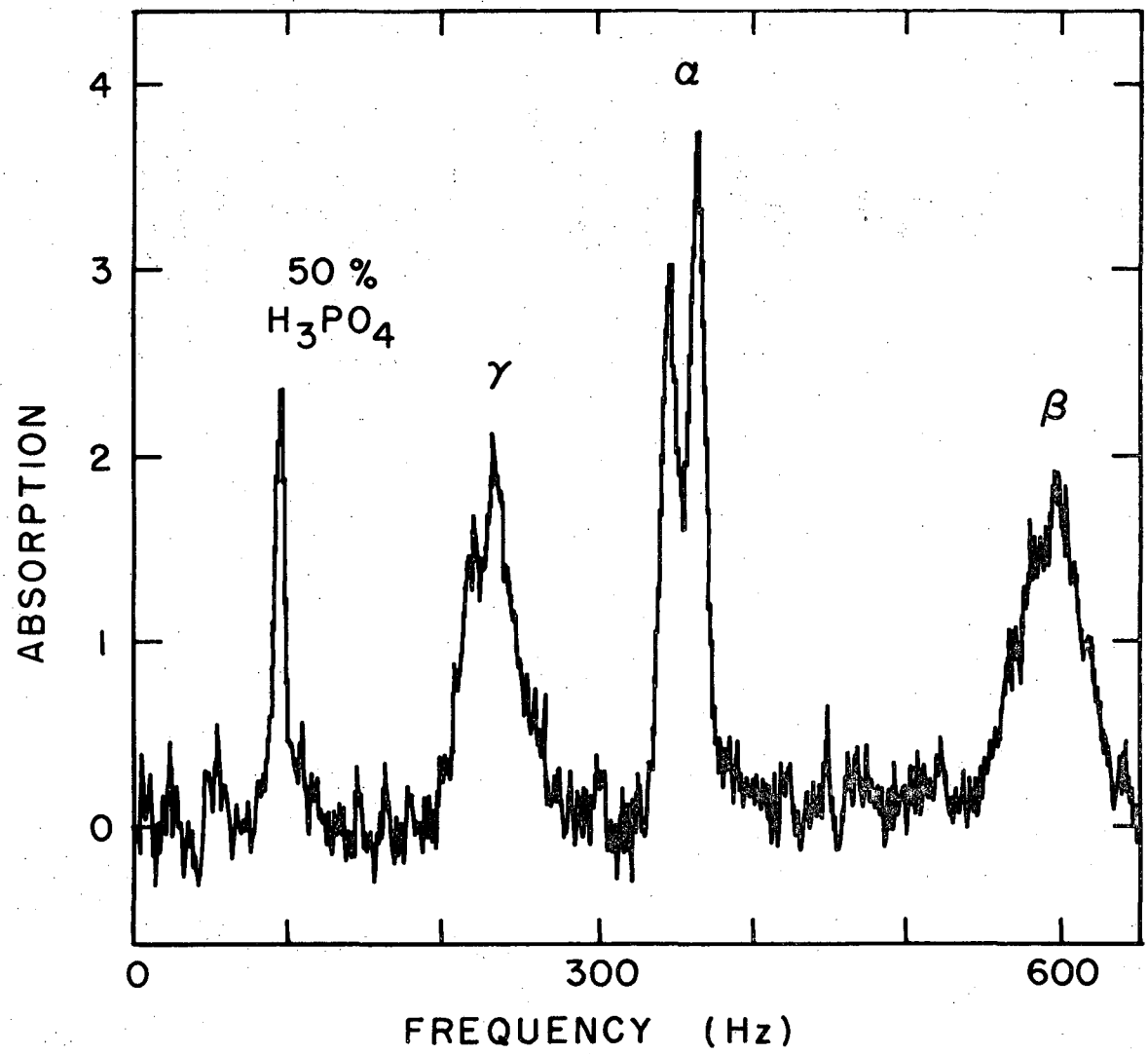

XBL728-4718

Figure 10. ^{31}P-NMR spectrum of 0.3 M undemetalized ATP at pH 8.5. The spectrum is the Fourier transform of 6 averaged free induction decay at 15 seconds apart.

As a result of demetalization, the relaxation times of phosphorous nuclei are an order of magnitude longer. The α-^{31}P has the shortest T_1 in contrast to the undemetalized ATP in which α-^{31}P has the longest T_1. We believe this is an evidence of the success in removing trace metal ions. Figure 8 shows that the T_1^{-1} curves of β and γ phosphorous nuclei as a function of pH have inflection points around pH 4.4 and 6.4 corresponding, approximately, to the pK_a's observed by glass electrode. The α phosphorous, however, has a T_1^{-1} that linearly increases when the pH is lowered below 6.0. The relaxation time measurements indicate an ionization scheme where first protonation (pK_a 6.5) corresponds to adding a proton to the γ phosphate group and the second protonation (pK_a 4.0) corresponds to adding to the β phosphate. The protonation of the α phosphate is not observed (pK_a <2.0) in our measurements.

Relaxation Mechanisms

It was observed that samples of ATP dissolved in D_2O relaxed with the same rates as samples dissolved in H_2O and in addition showed a dependence on pD similar to the pH dependence. Relaxation rates of tripolyphosphate in D_2O were also the same as those measured in H_2O.[24] The observation that the measurements yield the same results in D_2O as in H_2O shows that the magnetic moment of the proton which is being titrated makes no significant contribution to the relaxation rates. This is not surprising, since the phosphorus-oxygen bond prevents protons from approaching very near to the ^{31}P nuclei.

Since ATP at high concentrations is known to be extensively associated,[25] a possible explanation for the pH-dependence of the relaxation rates is to assume that the state of association is pH dependent.

Therefore, the random motion of the molecule which determines the relaxation rate is pH dependent. However, the following observation tends to argue against concentration effects as being responsible for the pH dependence of the relaxation rates. Ts'o et al.[11] have shown that a sensitive probe for intermolecular association in nucleotides is the concentration dependence of the chemical shift of the proton resonances corresponding to the 2 and 8 positions of the base. Any change in the state of association should be reflected by a change in chemical shift of these proton resonances. Recent measurements[26] of the pH dependence of the chemical shifts of the 2 and 8 positions of the adenine base in ATP as a function of concentration show that in the pH range of 5.0 to 9.0 the chemical shifts of these proton resonances are independent of pH in the concentration range of 0.5 to 0.001 molar. However, these proton resonances are strongly concentration dependent. Thus, changing the pH from 5 to 9 does not appear to change the state of association. Therefore, although the magnitude of the ^{31}P relaxation rates in ATP is concentration dependent, but at any given concentration the rates would not be affected by pH changes in the range 5 to 9.

If the extent of intermolecular association is rejected as the explanation for the relaxation-titrations, two other mechanisms, both of which could be pH dependent, are possible. These are: (i) chemical shift anisotropy, and (ii) spin-rotational interaction.

The anisotropy in the chemical shift as a relaxation mechanism offers an explanation for the pH dependence of the relaxation rates in ATP. The lack of pH dependence in orthophosphate and tripolyphosphate could be rationalized on the basis of the chemical shift anisotropy by noting that these two molecules are symmetrical at the position

being titrated, whereas ATP is not. Therefore, changes in the pH might be expected to change the anisotropy in the chemical shifts of ATP but not in these other two molecules. The chemical shift anisotropy in pyrophosphate has been measured.[27] The ^{31}P chemical shift tensors in the pyrophosphate group show axial symmetry about the bond between the phosphorous and bridging oxygen atoms. It would be reasonable to assume a chemical shift anisotropy of similar order of magnitude (100 ppm) exists in tripolyphosphate and ATP, and hence, causing relaxation. In the extreme narrowing limit, which is the situation in our case, the relaxation rate due to chemical shift anisotropy is given by[5]

$$T_1^{-1} = \frac{2}{15} \gamma^2 H_o^2 (\sigma_{\parallel} - \sigma_{\perp})^2 \tau_c \qquad (2)$$

where H_o is the dc magnetic field, $\sigma_{\parallel}$ and $\sigma_{\perp}$ are the parallel and perpendicular components of the chemical shift tensor $\underset{\sim}{\sigma}$. Assume $\tau_c = 10^{-10}$ sec, T_1^{-1} is estimated to be $\sim 10^{-3}$ sec. This is certainly insignificant. However, without an accurate determination of the values of $(\sigma_{\parallel} - \sigma_{\perp})$ and τ_c, relaxation <u>via</u> chemical shift anisotropy cannot be rejected.

Spin-rotational interaction has been invoked to explain ^{31}P relaxation of orthophosphate earlier. Considering the size of ATP compared with P_i and other small molecules, it is difficult to see how the spin-rotational interaction would be significant, unless the localized motion of the phosphorus nuclei in each molecule were responsible for the dominant relaxation process. However, since this mechanism depends on the electronic charge distribution around the ^{31}P nucleus, the pH dependence could be explained.

Either of these mechanisms can explain the concentration dependence study. In the case of spin-rotational interaction, if Hubbard relation[28] and Debye formula are used to express the angular momentum correlation time, then, for molecules undergoing isotropic molecular reorientation the relaxation rate is given by

$$T_1^{-1} = (I^2KT/h^2)\ C^2_{eff}/4\eta a^3 \qquad (3)$$

where $I = Ma^2$ is the moment of inertia of the molecule, M is the mass and a is the effective radius of the rotating molecule, h is the Planck's constant. C_{eff} is the effective spin-rotation constant for molecules in liquid state. Assume C_{eff} and η remain constant upon dimerization of ATP and, furthermore, assume the mass and radius of the dimer molecule are approximately twice those of the monomer, Eq. (3) yields

$$T_{1D}^{-1} \cong 8T_{1M}^{-1} \qquad (4)$$

where D and M denote the dimer and monomer unit of ATP. Knowing the association constant of ATP dimer ($K_A = 5M^{-1}$),[25] we estimate that the degree of dimerization at 0.33 M of total ATP concentration should be about 41 per cent. Assume a fast exchange, and use Eq. (4), the observed relaxation rate, T_{10}^{-1}, at 0.3 M is given by

$$T_{10}^{-1} = 3.8\ T_{1M}^{-1}$$

This result agrees with the α-P relaxation rate change (Table III), where a factor of 3 change was observed between T_1^{-1} at 0.33 M and

T_1^{-1} at infinite dilution. However, this agreement could be fortuitous. In the case of chemical shift anisotropy, the same relation as in Eq. (4) can be obtained from Eq. (2). Therefore, a similar argument can be given.

From the measurements completed so far, definite conclusions are not possible. However, a study of the temperature and magnetic field dependence of these relaxation-titration effects should lead to an explanation for these observations.

D. REFERENCES

1. T. C. Farrar and E. D. Becker, Pulse and Fourier Transform NMR, Academic Press, New York (1971) and references therein.
2. Z. Luz and S. Meiborn, J. Chem. Phys. 39, 366 (1963).
3. B. D. Sykes, J. Amer. Chem. Soc. 91, 949 (1969).
4. O. Jardetzky, Advan. Chem. Phys. 7, 494 (1964).
5. A. Abraham, The Principles of Nuclear Magnetism, Oxford Univ. Press, Oxford (1961).
6. H. M. McConnell, J. Chem. Phys. 28, 430 (1958).
7. H. M. Crutchfield, C. F. Callis, R. R. Irani, and G. C. Roth, Inorg. Chem. 1, 813 (1962).
8. M. Cohn and T. R. Hughes, Jr., J. Biol. Chem. 235, 3250 (1960).
9. M. Cohn and T. R. Hughes, Jr., J. Biol. Chem. 237, 176 (1962).
10. R. G. Shulman, H. Sternlicht, and B. J. Wyluda, J. Chem. Phys. 43, 3116 (1965).
11. M. Sternlicht, R. G. Shulman, and E. W. Anderson, J. Chem. Phys. 43, 3123 (1965).
12. R. R. Ernst and W. A. Anderson, Rev. Sci. Instr. 37, 93 (1966).
13. R. L. Vold, J. S. Waugh, M. P. Klein, and D. E. Phelps, J. Chem. Phys. 48, 3831 (1968).
14. J. L. Markley, W. J. Horsley, and M. P. Klein, J. Chem. Phys. 55, 3604 (1971).
15. J. E. Maling, L. T. Taskovich, and M. S. Blois, Jr., Biophys. J. 1, 79 (1963).

16. P. K. Glascoe and F. A. Long, J. Phys. Chem. 64, 188 (1960).

17. D. W. Aksnes, M. Rhodes, and J. G. Powles, Mol. Phys. 14, 333 (1968).

18. M. Rhodes, D. W. Aksnes, and J. H. Strange, Mol. Phys. 15, 541 (1968).

19. M. M. Crutchfield, C. F. Callis, R. R. Irani, and G. C. Roth, Inorganic Chem. 1, 813 (1962).

20. M. Tsuboi, M. Kainosho, and A. Nakamura, Recent Development of Magnetic Resonance in Biological Systems, ed. S. Fujimara and L. H. Pietle (1968).

21. S. Mizushima, Structure of Molecular and Internal Rotation, Academic Press, New York (1964).

22. A. Broom, M. Schweizer, P.O.P. Ts'o, Amer. Chem. Soc. 89, 3612 (1967).

23. R. Phillips, Chem. Rev. 66, 501 (1966).

24. I. Salmeen and M. P. Klein, 15th Annual Biophysical Society Meeting, New Orleans, La. (Feb., 1971).

25. H. Sternlicht, D. G. Jones, K. Kustin, J. Amer. Chem. Soc. 90, 7110 (1968).

26. I. Salmeen and T. Cole, in preparation.

27. P. S. Hubbard, Phys. Rev. 131, 1155 (1963).

28. W. Derbyshire, J. P. Stuart and D. Warner, Mol. Phys. 17, 449 (1969).

APPENDICES

APPENDIX I

^{31}P-HOMONUCLEAR FOURIER TRANSFORM DOUBLE RESONANCE

Several forms of homonuclear multiple resonances are commonly employed in conventional continuous wave NMR spectroscopy. A nuclear magnetic double resonance employing the Fourier transform technique with continuous wave preirradiation (H_2) has been reported by Freeman.[1] We report here an analogous experiment of Fourier transform double resonance (FTDR). The experimental procedure combines the standard pulsed-Fourier[2] and time-shared[3] modes of operation, for which an appropriate pulse sequence is shown in Figure 1. A non-selective pulse at ν_1 mutates the complete spectrum through a suitable angle followed by digitizing pulses at rates appropriate to the frequency width of the spectrum. In the present experiments, however, the receiver is held off for a short time during which a low-level pulse of R_f at ν_2 is applied to the system. For digitizing rates large compared with indirect coupling constants, and for values of γH_2 less than the couplings, lines which are coupled to that at ν_2 exhibit spin-tickling[4] effects. For values of γH_2 greater than the J's, decoupling of the other lines results, and ultimately for appropriate values of γH_2, relaxation rates, and relaxation mechanisms, Overhauser enhancements will ensue.

The time-sharing prevents the R_f at ν_2 from entering the receiver while permitting observation of the signal resulting from spins precessing at this frequency, an observation normally precluded. The effects

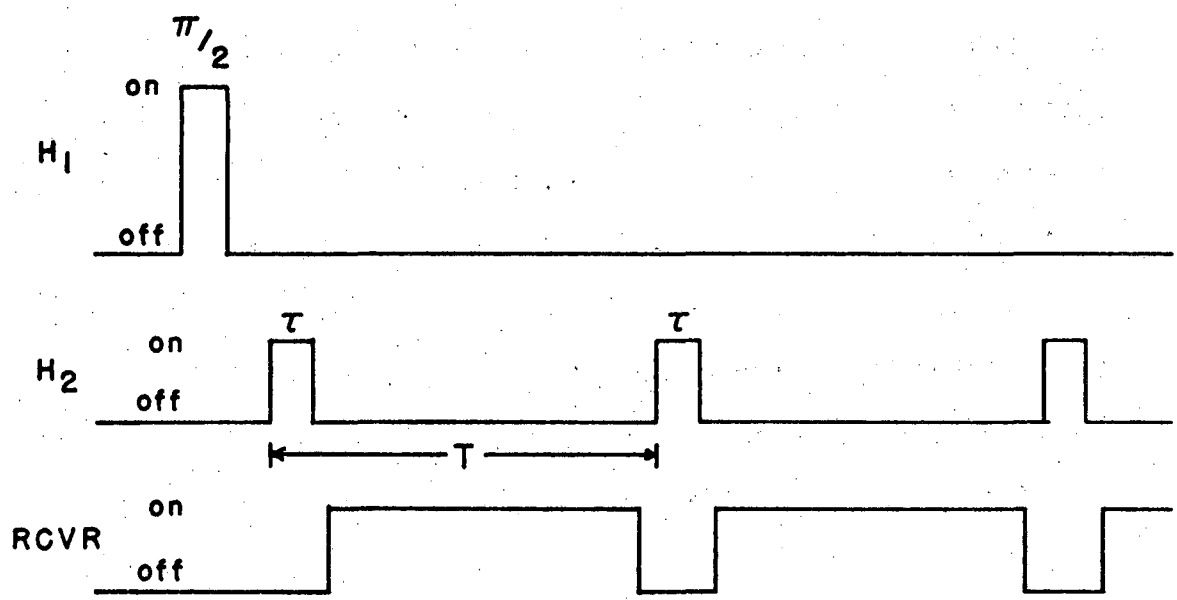

XBL727-4692

Figure 1. The pulse sequence of H_1, H_2 and receiver used in FTDR experiments. t is the pulse length of H_2 and T is the digitizing rate. A typical length of = 10 μsec, T = 500 μsec and π/2 H_1 pulse is 40 μsec.

of double irradiation of a single line[5] are manifest in the ^{31}P FTDR experiments and illustrated in the accompanying Figure 2. The experiments have been carried out on an extensively modified Varian HR-60 spectrometer with a PDP-8 computer and Data Disc. R_f pulse lengths and timing intervals are derived from external programmable time bases commanded by the PDP-8 computer. Two Hewlett-Packard frequency synthesizers are used and the transmitter amplifiers are isolated from each other by a R_f relay switch (Daico Industries). An external proton reference provides the field-frequency lock for the system.

In Figure 2, the irradiation of the lower field resonances of tripolyphosphate by ν_2 have produced two side bands for each resonance of the doublet placed symmetrically about ν_2. The resonance condition of the side bands has been derived for a weakly coupled system[5,6] and is given by

$$\nu = \nu_2 \pm \{(\nu_a-\nu_2)^2 + (\gamma H_2 t/2\pi T)^2\}^{1/2}$$

where ν is the observed resonance frequency, ν_a is the resonance frequency of group A phosphorous nuclei in the unirradiated spectrum, t is the length of the ν_2 pulse and T is the digitizing rate. Qualitatively, the side bands can be understood by considering the spin system in a frame rotating with the angular velocity $-\nu_2$. The magnetic moments perform a precession in the effective field

$$H_{eff} = 1/g\ \{(\nu_2-\nu_a)^2 + (\gamma H_2 t/2\pi T)^2\}^{1/2} \quad .$$

This motion when projected into the x,y plane appears to be an ellipse which can be decomposed into two couterrotation components with the same

Legend to Figures 2a and 2b

The FTDR spectra of tripolyphosphate (Alfa Inorganics), 0.3 M, pH 10.0, ambient magnetic temperature 30°C. The effective R_f irradiation $\gamma H_2 t/2\pi T$ is given in Hz in each spectrum. The theoretical calculated line positions and intensities are given below each spectrum.

(a) is the unirradiated spectrum with J_{PP} = 19.0 Hz; X denotes impurity. (b) through (d) show the double resonance effect when H_2 is irradiating in the middle of the doublet. There is a small amount of H_2 leakage through the Hewlett Packard mixer used for receiver gating. When the amplitude of H_2 is increased, the resonances of the doublet move further apart due to side band modulation, which is discussed in the text. Spectra (e) through (g) show the multiplet splittings when the lower field line of the doublet is irradiated. In these spectra, the pair of side bands symmetrical about the irradiating frequency can be more clearly identified. (i) and (ii) denote the two pairs of side bands associated with the two resonances of the original doublet.

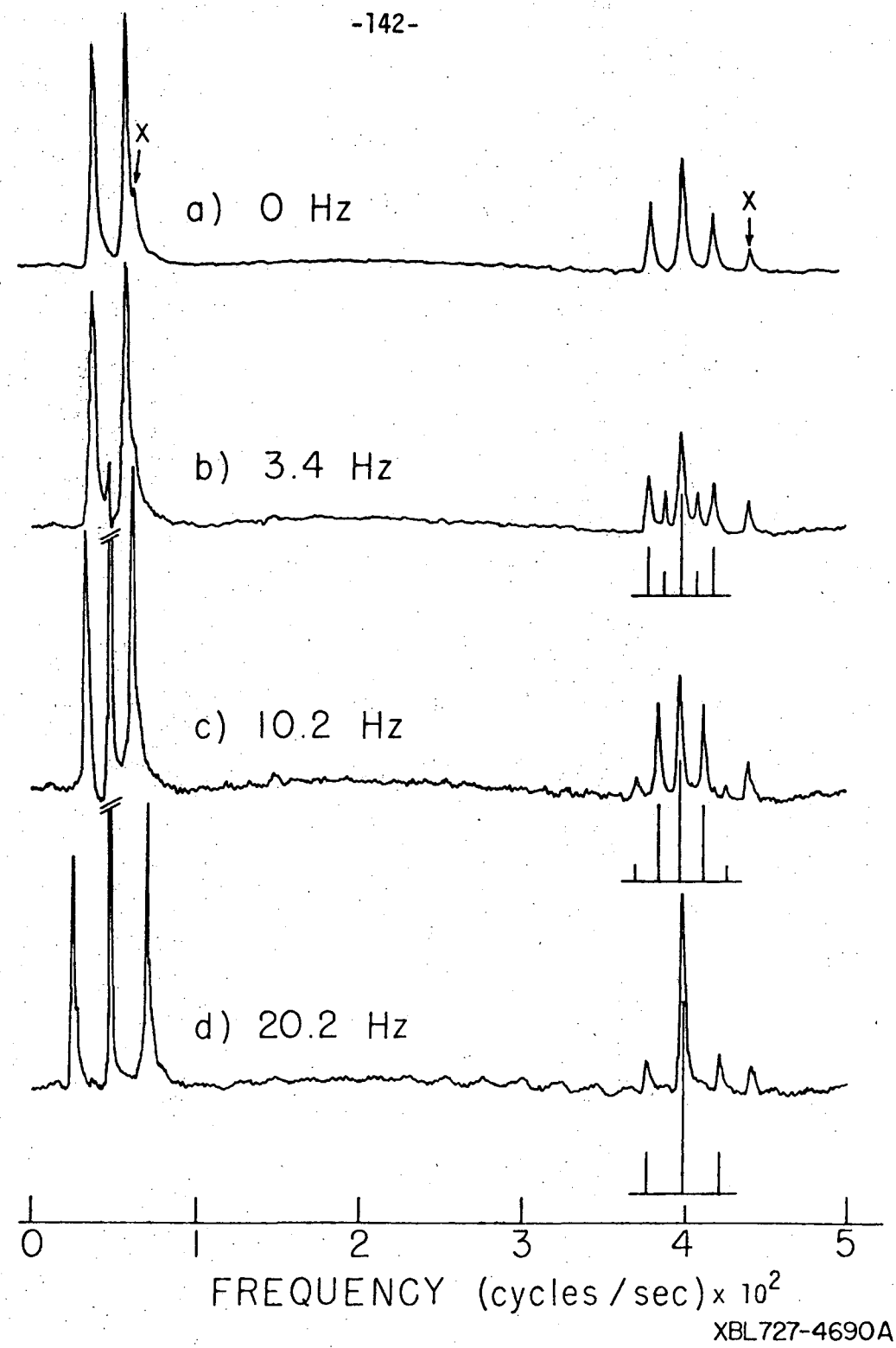
X
a) 0 Hz
X
b) 3.4 Hz
c) 10.2 Hz
d) 20.2 Hz
0
1
2
3
4
5
FREQUENCY (cycles / sec) x 10^2
XBL727-4690A

Figure 2a

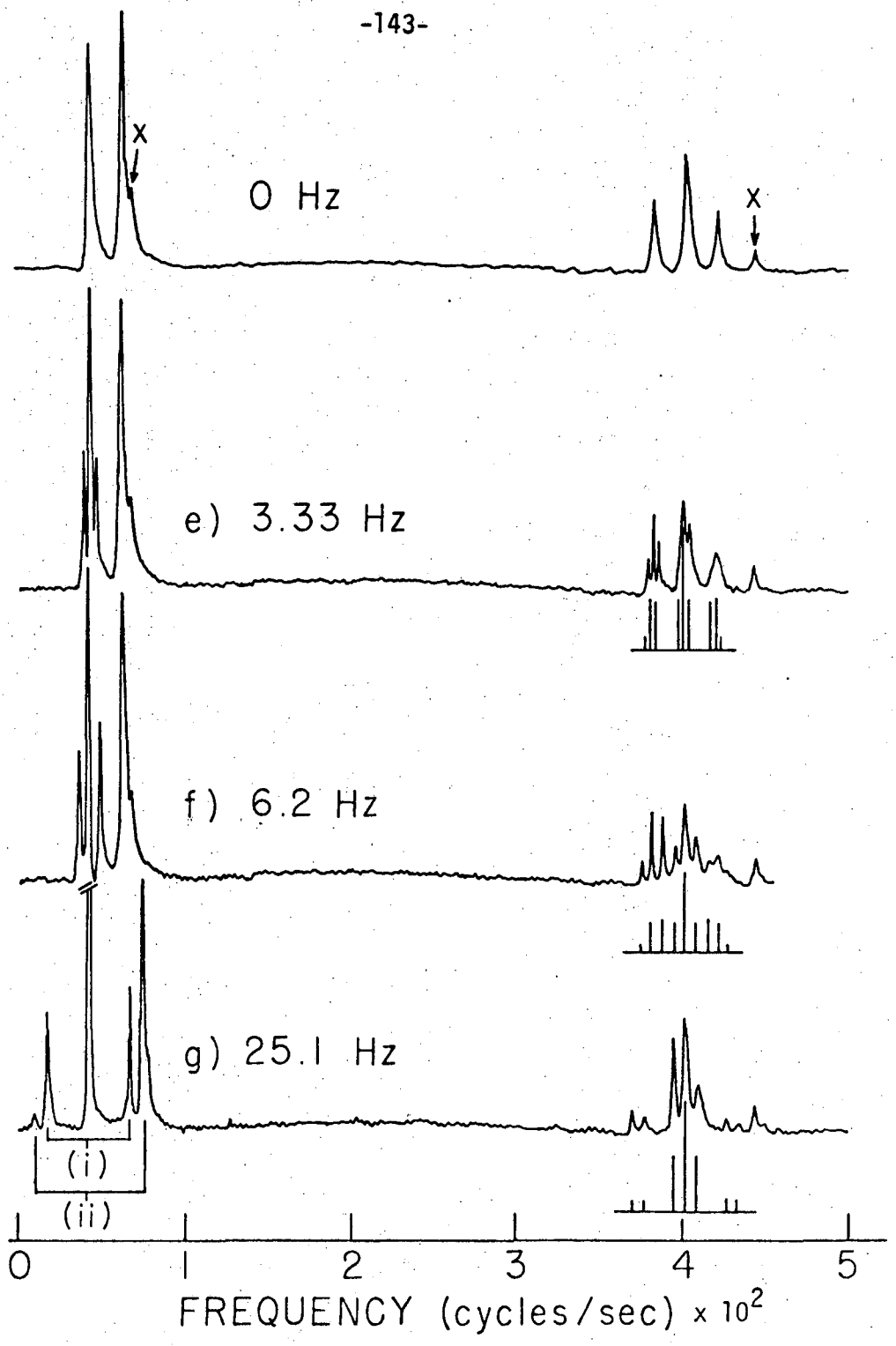

XBL727-4690B

Figure 2b

angular frequency, $\gamma H_{eff}/2\pi$, and amplitudes $M_+ = M_o/2\ (1 + \cos\theta)$, $M_- = M_o/2\ (1 - \cos\theta)$ where $\cos\theta = 2\pi\ (\nu_a - \nu_2)/\gamma H_{eff}$, M_o is the unirradiated intensity. When ν_2 is on resonance the side bands are of equal intensities, but half the magnitude of the unirradiated resonance. When $(\nu_a - \nu_2) >> \frac{\gamma H_2}{2\pi}$, one of the side bands M_- becomes negligibly small, whereas M_+ approaches the unirradiated intensity M_o. The separation of the side bands provides an accurate calibration of the amplitude of the R_f field H_2. Furthermore, knowing the unirradiated splitting of the doublet, the exact resonance condition $\nu_a - \nu_2 = 0$ can be determined precisely.

Figure 2 shows a typical AX_2 spectrum where the chemical shift difference is large compared to the spin-spin coupling. The irradiation of the end phosphorous causes a splitting of the original triplet of the middle phosphorous into submultiplets. These spin multiplets agree reasonably well with theoretical prediction.[7] The total integrated intensity of the multiplets appears to remain constant as H_2 is increased from zero. The relative intensities of the triplet also remain 1:2:1 for weak perturbing field, $\gamma H_2/2\pi \leq 6.5$ Hz.

REFERENCES

1. R. Freeman, J. Chem. Phys. 53, 457 (1970).
2. R. R. Ernst and W. A. Anderson, Rev. Sci. Instr. 31, 93 (1966).
3. R. C. Hewitt, Rev. Sci. Instr. 39, 1066 (1968) and references therein.
4. F. Block, Phys. Rev. 93, 944 (1954); R. Freeman and W. A. Anderson, J. Chem. Phys. 37, 2053 (1962).
5. W. A. Anderson, Phys. Rev. 102, 151 (1956); S. L. Gordon, J. Chem. Phys. 45, 1145 (1966).
6. S. L. Gordon, J. Chem. Phys. 48, 2129 (1968).
7. W. A. Anderson and R. Freeman, J. Chem. Phys. 37, 85 (1962).

APPENDIX IIA

Program ROTSTRN, a Fortran IV program for calculating the rotational strength as a function of bond rotation. The transition moment direction, strength and center are also computed. The program has the option for either monopole approximation or exact integral. Furthermore, the program allows option for self consistent field computation of the polarizable bonds.

```
      PROGRAM ROTSTRN(INPUT,OUTPUT)
C
C
C  DEFINITIONS OF ABOVE VARIABLES/
C     FRAND          ROTATIONAL STRENGTH FOR THIS CONFIG.  (ESU-CGS)
C     TRANMU(I)      I COMPONENT OF TRANSITION MOMENT  (E-ANG)
C     TCENT(I)       I COORD OF CENTER OF TRANSITION MOMENT (ANG)
C     TCENT(4)       FREQUENCY OF TRANSITION    (X1.E-15 RAD/SEC)
C     NDPTS          NUMBER OF DATA POINTS IN COMMON BLOCK
C     POINTS(I,M)    I COMPONENT OF MTH DATA POINT  I=4 FOR SYMBOL
C     KMAX           NUMBER OF POLARIZABILITIES
C     IKPOL.(K)      INDEX FOR .TH POINT OF POLARIZABILITY K
C     XKPOL.(K)      SYMBOL FOR .TH POINT OF POLARIZABILITY K
C     POLPRN(I,K)    PARALLEL(I=1) AND PERP.(I=2) COMPS. OF POLARIZ. K
C     POLPT(I,K)     I COMPONENT OF CENTER OF POLARIZABILITY K
C     XPOL(I,J,K)    I,J COMPONENT OF POLARIZABILITY OF PT K (A**3)
C     RPC(I,K)       I COMPONENT OF VECTOR FROM TCENT TO PT K
C     INMU(I,K)      I COMPONENT OF INDUCED DIPOLE AT PT K (E-A)
C     EFTOT(I)       I COMPONENT OF TOTAL EFF. FIELD AT CURR PT(E/A**2)
C     NTERM          NUMBER OF TERMS IN MULTIPOLE EXPANSION OF FIELD
C                    IF ZERO,MONOPOLE APPROXIMATION IS MADE
C                    IF NEGATIVE, EXACT INTEGRALS+MONOPOLE APPROX.
C     ISCF           IF ZERO, FIELD IS COMPUTED SELF CONSISTENTLY
C     T(I,J)         DIPOLE COUPLING TENSOR BETWEEN TWO CURRENT POINTS
C     A(I,J)         COUPLING TENSOR BETWEEN INMU#S
C     B(I)           VECTOR OF EFTOT#S FOR ALL POINTS
C     NBOND          NUMBER OF BONDS FOR ROTATIONS
C     ICLBRD         CURRENT BOND BEING ROTATED ABOUT
C     BNDID(I,4)     FOUR WORD ID HEADING FOR BOND I
C     X1(I)          SYMBOL FOR POINT ONE OF BOND AXIS I
C     IX1(I)         INDEX FOR POINT ONE OF BOND AXIS I
C     X2(I)          SYMBOL FOR POINT TWO OF BOND AXIS I
C     IX2(I)         INDEX FOR POINT TWO OF BOND AXIS I
C     NTIMES(I)      NO. OF ROTATIONS ABOUT BOND I FOR COMPLETE CIRCLE
C     NRCTS(I)       NUMBER OF ROTATIONS FOR BOND I TO BE PERFORMED
C     ANGLE(I)       ANGLE OF ROTATION FOR BOND I
C     INDEX(I)       COUNTER FOR ROTATIONS ABOUT BOND I
C     NPTS(I)        NUMBER OF POINTS ROTATED ABOUT BOND I
C     XPROTD(J,I)    SYMBOL FOR JTH POINT ROTATED ABOUT BOND I
C     IPROTD(J,I)    INDEX FOR JTH POINT ROTATED ABOUT BOND I
C     INDIC(I)       IF ZERO , NEW DATA FOR THE ITH GROUP IS READ
C                    IF NONZERO, DATA FROM PREVIOUS RUN IS USED
C                              1          DATA
C                              1
C                              2          POINTS
C                              3          FIELD DATA+ TRANS PARAMS
C                              4          FIELD APPROX. PARAM (NTERMS)
C                              5          POLARIZABILITY
C                              6          BOND ROTATION PARAMS
C     IPRINT         IF NON-ZERO, INMU#S ARE PRINTED
C     IPRT2          IF NON-ZERO, COORDS PRINTED AT ALL ORIENTATIONS
C     EPSIL(I,J,K)   COMPLETELY ANTISYMMETRIC 3RD RANK TENSOR
C
      REAL INMU,NEWMU
      COMMON /POINTS/POINTS(4,60) /NDPTS/NDPTS
```

```
      DIMENSION COMMT(25),XPLOT(36),YPLOT(36),EPSIL(3,3,3)
      DIMENSION INDIC(10)
      DIMENSION TRANMU(3),TCENT(4),D(3),EFTOT(3),NEWMU(3),R(3),T(3,3)
      DIMENSION TKPOL1(30),TKPOL2(30),XKPOL1(30),XKPOL2(30),POLPT(3,30),
     $FOLPEN(2,30),XPOL(3,3,30),RHO(3,30),INMU(3,30)
      DIMENSION X1(5),X2(5),NTIMES(5),NPTS(5),IPROTD(30,5),IX1(5),IX2(5)
     $,ANGLE(5),INCEA(5),XPROTD(30,5),BMCID(5,4),NROTS(5)
      DIMENSION A(90,90),B(90)
      DATA PI / 3.1415926535/,ENDFIL/6H$EOF  /
C
901   FORMAT(8(F9.6,1X))
902   FORMAT (16I5)
903   FORMAT(12A6)
904   FORMAT(1H0/,1X,12A6/1X12A6,5X,A10)
905   FORMAT(2(A6,4X),2I5,10X,4A6,6X,I5)
906   FORMAT(1X,I5,5X3(F9.5,2X),5XA6)
907   FORMAT(*  ORIENTATION INDICES=  *,5(I5,5X))
908   FORMAT(*  FINAL VALUE FOR RBAND IN THIS CONFIGURATION = *,E15.8)
909   FORMAT(*0DATA POINTS *,/* PT.NO., COORDS,SYMBOL*)
910   FORMAT(80I1)
911   FORMAT(1X,I5* TERMS WILL BE USED IN THE MULTIPOLE EXPANSION OF THE
     $ POTENTIAL (IF ZERO, MONOPOLE APPROXIMATION IS MADE)*,/
     $70X,*(IF NEGATIVE,EXACT INTEGRALS ARE USED)*)
913   FORMAT (*0BOND ROTATION PARAMS*,/,* BOND NO.,X1,X2,ANGLE,NPTS,NROT
     $S*)
914   FORMAT(1XI3,2X,2(A6,*(*,I3,*)*,2X),E15.8,2(5XI5),10X,4A6 )
915   FORMAT(A6,4X,A6,4X,2F10.6)
916   FORMAT(1X,2(A6,*(*,I3,*)*,1X),2(E15.8,5X))
917   FORMAT(*0POLARIZABILITIES*/* PT1  PT2, PARALLEL,PERPENDICULAR COMP
     $ONENTS*)
918   FORMAT(A6,4X3(F9.5,1X))
919   FORMAT(* FIELDS AT THE RESPECTIVE POLARIZABILITIES WILL COMPUTED
     $SELF-CONSISTENTLY*)
920   FORMAT(8(A6,4X))
921   FORMAT((10X,8(A6,*(*,I3,*)*,2X)))
922   FORMAT(* POINT NUMBER*,I3,* INMU=(*E15.8,1H,,E15.8,1H,,E15.8,1H))
C
C  SET UP EPSILON
C
      DO 101 I=1,3
      DO 101 J=1,3
      DO 101 K=1,3
101   EPSIL(I,J,K)=0.
      EPSIL(1,2,3)=1.
      EPSIL(2,3,1)=1.
C
      EPSIL(3,1,2)=1.
      EPSIL(2,1,3)=-1.
      EPSIL(1,3,2)=-1.
      EPSIL(3,2,1)=-1.
      CALL DATE(COMMT(25))
1000  CONTINUE
      READ 903, (COMMT(I),I=1,24)
      PRINT 904,COMMT
      IF(COMMT(1).EQ.ENDFIL) CALL EXIT
      READ 910, INDIC,IPRINT,IPRT2
```

```
C
C   READ IN COORDINATES
C
      IF(INDIC(2).NE.0) GO TO 401
      READ 902,NCPTS
      DO 301 K=1,NCPTS
      READ 918,POINTS(4,K),(POINTS(I,K),I=1,3)
301   CONTINUE
401   PRINT 909
      DO 351 K=1,NCPTS
      PRINT 906,K,((POINTS(I,K),I=1,4))
351   CONTINUE
C
C   READ IN FIELD PARAMETERS
C
      CALL MFREAD(TRANNU,TCENT,INDIC(3))
      IF(INDIC(4).NE.0) GO TO 403
      READ 902, NTERM ,ISCF
403   PRINT 911,NTERM
      IF(ISCF.EQ.0) PRINT 919
C
C  READ IN POLARIZABILITY DATA
C
      IF(INDIC(5).NE.0) GO TO 404
      READ 902,KMAX
      DO 303 K=1,KMAX
      READ 915 ,XKPOL1(K),XKPOL2(K),(POLPRN(I,K),I=1,2)
      IKPOL1(K)=0
      IKPOL2(K)=0
      DO 304 K2=1,NCPTS
      IF(XKPOL1(K).EQ.POINTS(4,K2))IKPOL1(K)=K2
      IF(XKPOL2(K).EQ.POINTS(4,K2))IKPOL2(K)=K2
304   CONTINUE
      IF((IKPOL1(K).EQ.0).OR.(IKPOL2(K).EQ.0)) GO TO 8000
303   CONTINUE
404   PRINT 917
      DO 305 K=1,KMAX
      PRINT 916,XKPOL1(K),IKPOL1(K),XKPOL2(K),IKPOL2(K),(POLPRN(I,K),I=1
     $,2)
305   CONTINUE
C
C  READ IN BOND ROTATION DATA
C
      IF(INDIC(6).NE.0) GO TO 405
      READ 902,NBOND
      IF(NBOND .EQ.0) GO TO 200
      DO 201 I=1,NBOND
      READ 905,X1(I),X2(I),NTIMES(I),NPTS(I),(BNDID(I,J),J=1,4),NROTS(I)
      IF(NROTS(I).EQ.0) NROTS(I)=NTIMES(I)
      ANGLE(I)=2.*PI/NTIMES(I)
      NROT=NPTS(I)
      IX1(I)=0
      IX2(I)=0
      DO 205 K2=1,NCPTS
      IF(X1(I).EQ.POINTS(4,K2)) IX1(I)=K2
      IF(X2(I).EQ.POINTS(4,K2)) IX2(I)=K2
```

```
205   CONTINUE
      IF(IX1(I).EQ.0.OR.IX2(I).EQ.0) GO TO 8002
      READ 920,(XPROTD(J,I),J=1,JROT)
      DO 203 J=1,JROT
      IPROTD(J,I)=0
      DO 204 K=1,NDPTS
      IF(XPROTD(J,I).EQ.POINTS(4,K))IPROTD(J,I)=K
204   CONTINUE
      IF(IPROTD(J,I).EQ.0) GO TO 8002
203   CONTINUE
201   CONTINUE
      NPLOT=NROTS(NBOND)
      XSTEP=ANGLE(NBOND)*57.29578
      DO 202 I=1,NPLOT
      XPLOT(I)=FLOAT(I-1)*XSTEP
202   CONTINUE
      XPMAX=XPLOT(NPLOT)
      XPINCR=XPMAX/100.
405   IF(NBOND.EQ.0) GO TO 200
      ICURBD=NBOND
      PRINT 913
      DO 210 I=1,NBOND
      INDEX(I)=0
      PRINT 914,I,X1(I),IX1(I),X2(I),IX2(I),ANGLE(I),NPTS(I),NROTS(I),
     $ (BNDID(I,J),J=1,4)
      PRINT 921,(XPROTD(J,I),IPROTD(J,I),J=1,JROT)
210   CONTINUE
200   CONTINUE
      PRINT 904,COMNT
C
C  CALCULATE THEORETICAL ROTATIONAL STRENGTH IN THIS ORIENTATION
C
2000  CONTINUE
      DO 104 K=1,KMAX
      RP=0
      IK1=IKPOL1(K)
      IK2=IKPOL2(K)
      DO 20 I=1,3
      PCLPT(I,K)=0.5*(POINTS(I,IK1)+POINTS(I,IK2))
      RHO(I,K)=PCLPT(I,K)-TCENT(I)
      INMU(I,K)=0.
      D(I)=POINTS(I,IK1)-POINTS(I,IK2)
20    RP=RP+D(I)*D(I)
C
C   EVALUATION OF POLARIZABILITY TENSOR AT POINT K
C
      DIFF=PCLPRN(1,K)-PCLPRN(2,K)
      IF(DIFF.EQ.0.) GO TO 21
      RP=SQRT(RP)
      CTP=D(3)/RP
      STP=SQRT(1.-CTP**2)
      RP=RP*STP
      IF(RP.EQ.0) GO TO 50
      CPP=D(1)/RP
      SPP=D(2)/RP
51    XPCL(1,2,K)=DIFF*(STP*STP*CPP*SPP)
```

```
      XPCL(2,1,K)=XPOL(1,2,K)
      XPCL(2,3,K)=CTFF*STP*CTP*SPP
      XPCL(3,2,K)=XPOL(2,3,K)
      XPCL(1,3,K)=CTFF*STP*CTP*CPP
      XPCL(3,1,K)=XPOL(1,3,K)
      XPCL(1,1,K)=POLPRN(2,K)*((CTP*CPP)**2+SPP**2)+POLPRN(1,K)*(CPP*STP
     S)**2
      XPCL(2,2,K)=POLPRN(2,K)*((CTP*SPP)**2+CPP**2)+POLPRN(1,K)*(STP*SPP
     S)**2
      XPCL(3,3,K)=POLPRN(2,K)*STP**2+POLPRN(1,K)*CTP**2
      GO TO 104
50    SPP=1.
      CPP=0.
      GO TO 51
21    DO 23 L=1,3
      DO 22 M=1,3
22    XPCL(L,M,K)=0.
23    XPCL(L,L,K)=POLPRN(1,K)
104   CONTINUE
C
C   CALCULATION OF INDUCED DIPOLES
C
C  EXTERNAL FIELD PART
      DO 115 K=1,KMAX
      IB=3*K-3
      DO 103 I=1,3
      B(IB+I)=0.
103   EFTOT(I)=0.
      CALL MPFELD(POLPT(1,K),EFTOT,NTERM)
      DO 60 L=1,3
      DO 60 M=1,3
60    B(IB+L)=B(IB+L)+XPOL(L,M,K)*EFTOT(M)
115   CONTINUE
      IF(ISCF.NE.0) GO TO 110
C
C  INTERNAL FIELD COUPLING TENSOR EVALUATION
C
      IF(KMAX.EQ.1) GO TO 110
      IAMX=3*KMAX
      DO 120 I=1,IAMX
      DO 121 J=1,IAMX
121   A(I,J)=0.
120   A(I,I)=1.
      DO 122 K1=2,KMAX
      K2MAX=K1-1
      IAK1=3*K1-3
      DO 122 K2=1,K2MAX
      IAK2=3*K2-3
C
C  CALCULATE T(I,J)
C
      RDIST=0.
      DO 123 I=1,3
      R(I)=PCLPT(I,K)-POLPT(I,K2)
      RDIST=RDIST+R(I)*R(I)
123   CONTINUE
```

```
      RDIST=SQRT(RDIST)
      TDIAG=1./RDIST**3
      DO 124 I=1,3
      DO 125 J=1,3
125   T(I,J)=-3.*R(I)*R(J)/RDIST**5
124   T(I,I)=T(I,I)+TDIAG
      DO 127 II=1,3
      DO 127 JJ=1,3
      DO 127 KK=1,3
      A(IAK2+II,IAK1+JJ)=A(IAK2+II,IAK1+JJ)+XPOL(II,KK,K2)*T(KK,JJ)
      A(IAK1+II,IAK2+JJ)=A(IAK1+II,IAK2+JJ)+XPOL(II,KK,K1)*T(KK,JJ)
127   CONTINUE
122   CONTINUE
C
C  INVERT MATRIX AND SOLVE FOR INMU*S
C
      CALL SIMEQ(A,90,IANX,B,DETERM)
C
C  RECOVER TO INMU*S
C
110   DO 107 K=1,KMAX
      IB=3*K-3
      DO 107 I=1,3
107   INMU(I,K)=B(IB+I)
C
C  EVALUATION OF ROTATIONAL STRENGTH
C
150   RBAND=0
      DO 102 K=1,KMAX
      IF(IPRINT.NE.0) PRINT 922,K,(INMU(I,K),I=1,3)
C
C  TRIPLE PRODUCT
C
      TPROD=0
      DO 70 L=1,3
      DO 70 M=1,3
      DO 70 N=1,3
70    TPROD=TPROD+RNO(L,K)*EPSIL(M,N,L)*TRANMU(M)*INMU(N,K)
      RBAND=RBAND-3.84E-39*TPROD*TCENT(4)
102   CONTINUE
      IF(NBOND.EQ.0) GO TO 30
      IPLOT=INDEX(ICURBD)+1
      YPLOT(IPLOT)=RBAND
C
C  PRINT FINAL VALUE FOR RBAND IN THIS CONFIGURATION
C
30    CONTINUE
      IF(IPRT2.EQ.0) GO TO 32
      PRINT 909
      DO 31 K=1,NDPTS
      PRINT 906,K,(POINTS(I,K),I=1,4)
31    CONTINUE
32    CONTINUE
      PRINT 908 ,RBAND
      IF(NBOND.EQ.0) GO TO 1000
      PRINT 907,(INDEX(I),I=1,NBOND)
```

```
      IF(INDEX(NBOND).NE.NROTS(NBOND)) GO TO 2003
      PRINT 904,COMMT
      CALL PENPLT(XPLOT,YPLOT,XPMAX,XPINCR,YMAX,YINCR,0,1,NPLOT)
      PRINT 907,(INDEX(I),I=1,NBOND)
      PRINT 904 ,COMMT
 2003 INDEX(ICURBD)=INDEX(ICURBD)+1
      IOLD=ICURBD
      IF(INDEX(ICURBD).GT.NROTS(ICURBD)) GO TO 2001
      IX1CUR=IX1(ICURBD)
      IX2CUR=IX2(ICURBD)
      CALL SETROT(POINTS(1,IX1CUR),POINTS(1,IX2CUR),ANGLE(ICURBD))
      IMAX=NPTS(ICURBD)
      DO 2004 I=1,IMAX
      KROT=IPROTD(I,ICURBD)
 2004 CALL ROTATE(POINTS(1,KROT),X,X)
      LBOND=ICURBD+1
      IF(LBOND.GT.NBOND) GO TO 2005
      DO 2006 L=LBOND,NBOND
      INDEX(L)=0
 2006 CONTINUE
      ICURBD=NBOND
 2005 CONTINUE
      GO TO 2000
 2001 ICURBD=ICURBD-1
      IF(ICURBD.EQ.0) GO TO 1000
      GO TO 2003
 8000 PRINT 9800
 9800  FORMAT(*1POLARIZABILITY SYMBOL NOT IN DATA SET*)
      CALL EXIT
 8002 PRINT 9802
 9802 FORMAT(*1ROTATION POINT SYMBOL NOT IN DATA SET*)
      CALL EXIT
      END
```

```
      SUBROUTINE ROTATE(X1,X2,ANGLE)
C    PROGRAM FOR ROTATION ABOUT ARBITRARY AXIS ,ARBITRARY ANGLE IN 3-SPACE
C     RIGHT-HANDED ROTATION AND COORDINATE SYSTEM USED
C
C   CALLING SEQUENCES
C     1)  CALL SETROT(X1,X2,ANGLE)
C              SETS UP TRANSLATION VECTOR AND ROTATION MATRIX FOR ROTATION OF
C              ANGLE #ANGLE# ABOUT AXIS WHOSE + DIRECTION IS DEFINED AS THE
C              VECTOR DIRECTED FROM #X1# TO #X2#
C
C     2)  CALL ROTATE(ATOM,X,X)
C              PERFORMS THE ROTATION DESCRIBED IN THE LAST CALL TO SETROT ON THE
C              POINT #ATOM#
C
      DIMENSION ATOM(3),R(3,3),XTRANS(3),SCRAP(3),X1(3),X2(3),D(3)
      DO 1 I=1,3
1     SCRAP(I)=X1(I)-XTRANS(I)
      DO 2 I=1,3
      X1(I)=XTRANS(I)
      DO 2 J=1,3
2     X1(I)=X1(I)+R(I,J)*SCRAP(J)
      RETURN
C
C   INITIALIZATION ROUTINE
C
      ENTRY SETROT
C
C   ANGLE IS ASSUMED IN RADIANS
C
      SW=SIN(ANGLE)
      CW= COS(ANGLE)
      RAD=0.
      DO 3 I=1,3
      XTRANS(I)=X1(I)
      D(I)=X2(I)-X1(I)
      RAD=RAD+D(I)**2
3     CONTINUE
      RAD=SQRT(RAD)
      CTHETA=D(3)/RAD
      STHETA=SQRT(1.-CTHETA**2)
      IF(STHETA.GT.1.E-06) GO TO 4
      CPHI=1.0
      SPHI=0.
      GO TO 5
4     RAD=RAD*STHETA
      CPHI=D(1)/RAD
      SPHI=D(2)/RAD
5     S2T=STHETA**2
      C2T=1.-S2T
      SCT=STHETA*CTHETA
      S2P=SPHI**2
      C2P=1.-S2P
      SCP=SPHI*CPHI
      R(1,1)=CW*(S2P+C2T*C2P)+S2T*C2P
      R(2,1)=-CW*S2T*SCP+SW*CTHETA+S2T*SCP
      R(3,1)=-CW*SCT*CPHI-SW*STHETA*SPHI+SCT*CPHI
      R(1,2)=-CW*S2T*SCP-SW*CTHETA+S2T*SCP
      R(2,2)=CW*(C2P+C2T*S2P)+S2T*S2P
      R(3,2)=-CW*SCT*SPHI+SW*STHETA*CPHI+SCT*SPHI
      R(1,3)=-CW*SCT*CPHI+SW*STHETA*SPHI+SCT*CPHI
      R(2,3)=-CW*SCT*SPHI-SW*STHETA*CPHI+SCT*SPHI
      R(3,3)=CW*S2T+C2T
      RETURN
      END
```

```
$IBFTC MPOL     LIST,CECK
      SUBROUTINE MPFELD(FPOINT,FIELD,NTERMS)
C
C  MULTIPOLE EXPANSION OF FIELD DUE TO AN ASSEMBLY OF POINT CHARGES
C     THE CALCULATED FIELD IS ADDED TO THE VALUE STORED UPON ENTRY
C     SO CARE MUST BE TAKEN TO INITIALIZE PRIOR TO CALLING MPFELD
C     *NTERMS* TERMS IN THE EXPANSION ARE USED
C    IF NTERMS =0 THE EXACT FIELD FROM THE CHARGES IS COMPUTED,
C       AS WELL AS THE FIELD FROM POINT DIPOLES LOCATED AT THESE SAME
C      POINTS . THE DIPOLES ARE IGNORED IN THE MULTIPOLE EXPANSION
C
C     DEFINITIONS OF VARIABLES USED IN THIS PROGRAM
C   CHARGES ARE IN ESU, DISTANCES IN ANGSTROMS
C
C     FPOINT(I)        I COMPONENT OF THE FIELD POINT
C     FIELD(I) .       I COMPONENT OF CALCULATED FIELD AT ABOVE POINT
C     RZERO(I)         I COMPONENT OF THE CENTER OF ABSOLUTE CHARGE
C     Q.(I,J,...S)     I,J,....,S COMPONENT OF THE 2**. MULTIPOLE
C     NDPTS            NUMBER OF DATA POINTS IN COMMON BLOCK
C     POINTS(I,J)      COORDS AND DESIGNATION FOR JTH DATA POINT
C     JMAX             NUMBER OF FIELD POINTS
C     IFPTS(J)         INDEX FOR JTH FIELD POINT
C     XFPTS(J)         SYMBOL FOR JTH FIELD POINT
C     DIPPT(I,J)       I COMPONENT OF DIPOLE AT FIELD POINT J
C     CPT(J)           CHARGE AT FIELD POINT J
C
      DIMENSION FPOINT(3),FIELD(4)
      DIMENSION Q1(3),Q2(3,3),Q3(3,3,3)
      DIMENSION R(3),RZERO(3),T(3,3)
      DIMENSION QPT(30),DIPPT(3,30),IFPTS(30),XFPTS(30)
      COMMON /POINTS/POINTS(4,60) /NDPTS/NDPTS
C
      DIMENSION F(3)
      REAL INT(3) ,IDOT(3)
      INTEGER ALPHA
C
$01   FORMAT(*0MULTIPOLE EXPANSION ABOUT CENTER OF CHARGE =(*F10.4,*,*,F
     $10.4,*,*,F10.4,*)*  )
$02   FORMAT(16I5)
$03   FORMAT(1H0,10X* MONOPOLE=*,E15.8)
$04   FORMAT(1H0,10X* DIPOLE=*,2(E15.8,1H,),E15.8)
$05   FORMAT(1H0,10X* QUADRUPOLE=*2(E15.8,1H,),E15.8,2(/23X2(E15.8,1H,),
     $E15.8))
$06   FORMAT(1H0,10X* OCTUPOLE=*2(E15.8,1H,),E15.8,8(/21X2(E15.8,1H,),E1
     $5.8))
$07   FORMAT(*0FIELD POINT*,10X,*DIPOLE MOMENT*,16X,*CHARGE* )
$08   FORMAT(1XA6,*(*,I3,*)*5X,3(F8.5,1X),5XF8.5)
$09   FORMAT(A6,4X,4(F9.6,1X))
$10   FORMAT(*0NO MULTIPOLE EXPANSION WILL BE MADE*)
$11   FORMAT(6F10.7)
$12   FORMAT(*0TRANSITION MOMENT=*,3(2XF8.5),2X,*(LENGTH=*,F8.5,*)  CENT
     $ER=*,3(2XF8.5),2X*FREQUENCY=*,2XF8.4,*E+15 CPS*)
$901  FORMAT(1H0,I5* TERMS CANNOT BE USED IN EXPANSION,0 USED*)
C
      IF(NTERMS.LE.0) GO TO 100
```

```
      IF(NHANG.EQ.0) GO TO 500
      RSQ=0.
      DO 1 I=1,3
      R(I)=FPOINT(I)-RZERO(I)
      RSQ=RSQ+R(I)*R(I)
1     CONTINUE
      RAD=SQRT(RSQ)
      GO TO (101,201,301,401)  NTERMS
500   PRINT 9901,NTERMS
      NTERMS =0
      NHANG=1
      GO TO 100
C
C   OCTUPOLE CONTRIBUTION TO FIELD
C
401   CONTINUE
      DO 402 I=1,3
      DO 402 J=1,3
      DO 402 K=1,3
      DO 402 ALPHA=1,3
      GEOM=7.*R(I)*R(J)*R(K)*R(ALPHA)
      IF(I.EQ.ALPHA) GEOM=GEOM-RSQ*R(J)*R(K)
      IF(J.EQ.ALPHA) GEOM=GEOM-RSQ*R(I)*R(K)
      IF(K.EQ.ALPHA) GEOM=GEOM-RSQ*R(I)*R(J)
402   FIELD(ALPHA)=FIELD(ALPHA)+Q3(I,J,K)*GEOM/(6.*RAD**9)
C
C   QUADRUPOLE CONTRIBUTION TO FIELD
C
301   CONTINUE
      DO 302 I=1,3
      DO 302 J=1,3
      DO 302 ALPHA=1,3
      GEOM=5.*R(I)*R(J)*R(ALPHA)
      IF(I.EQ.ALPHA) GEOM=GEOM-RSQ*R(J)
      IF(J.EQ.ALPHA) GEOM=GEOM-RSQ*R(I)
302   FIELD(ALPHA)=FIELD(ALPHA)+Q2(I,J)*GEOM/(2.*RAD**7)
C
C   DIPOLE CONTRIBUTION TO FIELD
C
201   CONTINUE
      DO 202 I=1,3
      DO 202 ALPHA=1,3
      GEOM=3.*R(I)*R(ALPHA)
      IF(I.EQ.ALPHA) GEOM=GEOM-RSQ
202   FIELD(ALPHA)=FIELD(ALPHA)+Q1(I)*GEOM/RAD**5
C
C     MONOPOLE CONTRIBUTION TO FIELD
C
101   CONTINUE
      DO 102 ALPHA=1,3
102   FIELD(ALPHA)=FIELD(ALPHA)+QC*R(ALPHA)/RAD**3
      RETURN
C
C     DIRECT EXPANSION OF POINT MONOPOLES AND DIPOLES
C
100   DO 10 J=1,JMAX
```

```
      JPT=IFPTS(J)
C
C   CALCULATION OF EFFECTIVE FIELD FROM PT J TO FPOINT
C
      RDIST=0
      DO 40 I=1,3
      R(I)=FPOINT(I)-POINTS(I,JPT)
40    RDIST=RDIST+R(I)**2
      RDIST=SQRT(RDIST)
      IF(NTERMS.LT.0) GO TO 700
C
C   IF LESS THAN ZERO EXACT TWO-CENTER INTEGRALS ARE DONE
C
C   DIPOLE COUPLING TENSOR FOR THESE TWO POINTS
C
      DO 50 L=1,3
      DO 50 M=1,3
      T(L,M)=+3.*R(L)*R(M)/RDIST**5
50    CONTINUE
      TDIAG=1./RDIST**3
      DO 51 ALPHA=1,3
      T(ALPHA,ALPHA)=T(ALPHA,ALPHA)-TDIAG
51    FIELD(ALPHA)=FIELD(ALPHA)+QPT(J)*R(ALPHA)/RDIST**3
      DO 53 ALPHA=1,3
      DO 53 I=1,3
53    FIELD(ALPHA)=FIELD(ALPHA)+T(ALPHA,I)*DIPPT(I,J)
      GO TO 10
C
C   EXACT TWO CENTER INTEGRALS
C
700   RHO=1.625*RDIST/0.527
      EXPRHO=EXP(-2.*RHO)
      RHOSQ=RHO**2
      SIG=(1.+3./RHOSQ+EXPRHO*(-3./RHOSQ+2.+3.*RHO+2.*RHOSQ+0.75*RHOSQ
     $*RHO))/RDIST
      PI=(1.-1.5/RHOSQ+EXPRHO*(1.5/RHOSQ-2.5-1.5*RHOSQ-0.25*RHOSQ))/
     $RDIST
      SIGDOT=(-1.-9./RHOSQ+EXPRHO*(-9./RHOSQ-6./RHO-2.-4.*RHOSQ-2.*RHO
     $-2.5*RHOSQ*RHO-1.5*RHOSQ**2))/RDIST**2
      PIDOT=(-1.+4.5/RHOSQ+EXPRHO*(-4.5/RHOSQ-3./RHO+2.5+5.*RHO+2.75*
     $RHOSQ+0.5*RHOSQ*RHO))/RDIST**2
      INT(1)=PI
      INT(2)=PI
      INT(3)=SIG
      IDOT(1)=PIDOT
      IDOT(2)=PIDOT
      IDOT(3)=SIGDOT
      DO 701 ALPHA=1,3
      F(ALPHA)=0.
      DO 702 I=1,3
      F(ALPHA)=R(I)**2*R(ALPHA)*(2./RDIST**4*INT(I)-1./RDIST**3*IDOT(I))
     $+F(ALPHA)
      IF(I.EQ.ALPHA)F(ALPHA)=F(ALPHA)-2.*R(I)/RDIST**2*INT(I)
702   CONTINUE
701   FIELD(ALPHA)=FIELD(ALPHA)+QPT(J)*F(ALPHA)
10    CONTINUE
```

```
      RETURN
C
      ENTRY MPREAD
C     REALLY  MPREAD(TRANMU,TCENT,INDIC)
C  READS IN THE FIELD POINTS,CHARGES AND DIPOLES, AND THEN USING THESE
C     CHARGES ONLY COMPUTES THE CENTER OF ABSOLUTE CHARGE AND THE
C     MONOPOLE,DIPOLE,QUADRUPOLE,OCTUPOLE AND HEXADECAPOLE MOMENTS ABOUT
C     THIS CENTER
C  USES CENTER OF CHARGE FOR TCENT AND DIPOLE MOMENT FOR TRANMU.  READS
C     IN FREQUENCY OF TRANSITION AND TCENT,TRANMU IF ONLY DIPOLES.
C
      IF(NTERMS.NE.0) GO TO 1100
      READ 902,JMAX
      DO 1000 J=1,JMAX
      READ 909,XFPTS(J),(DIPPT(I,J),I=1,3),QPT(J)
      IFPTS(J)=0
      DO 1002 K2=1,NDPTS
      IF(XFPTS(J).EQ.POINTS(4,K2))IFPTS(J)=K2
 1002 CONTINUE
      IF(IFPTS(J).EQ.0) GO TO 8001
 1000 CONTINUE
      READ 911,FIELD(4) ,TMLEN
C
C  COMPUTE MULTIPOLES AND RZERO
C
      DO 1003 I=1,3
      Q1(I)=0.
 1003 RZERO(I)=0.
      QT=0.
      QO=0.
      DO 1010 J=1,JMAX
      JPT=IFPTS(J)
      QT=QT+ABS(QPT(J))
      QO=QO+QPT(J)
      DO 1010 I=1,3
      Q1(I)=Q1(I)+QPT(J)* POINTS(I,JPT)
      RZERO(I)=RZERO(I)+ABS(QPT(J))*POINTS(I,JPT)
 1010  CONTINUE
      IF(QT.EQ.0.) GO TO 1052
      NHANG=1
      TM=Q1(1)**2+Q1(2)**2+Q1(3)**2
      TM=SQRT(TM)
      XFACT=TMLEN/TM
      IF(XFACT.EQ.0.) XFACT=1.
C  IF XFACT COMES OUT ZERO, CONST SCALE
      DO 1012 JJ=1,JMAX
      QPT(JJ)=QPT(JJ)*XFACT
 1012 CONTINUE
      QO=QO*XFACT
      TMLEN=TM*XFACT
      DO 1011 I=1,3
      RZERO(I)=RZERO(I)/QT
      FIELD(I)=RZERO(I)
      Q1(I)=Q1(I)*XFACT-QO*RZERO(I)
 1011 CONTINUE
      DO 1020 I=1,3
```

```
      DO 1020 J=1,3
      Q2(I,J)=0.
      DO 1020 K=1,3
      Q3(I,J,K)=0.
 1020 CONTINUE
      DO 1030 JJ=1,JMAX
      JPT=IFPTS(JJ)
      RSQ=0.
      DO 1031 I=1,3
      R(I)=POINTS(I,JPT)-RZERO(I)
      RSQ=RSQ+R(I)*R(I)
 1031 CONTINUE
      DO 1032 I=1,3
      DO 1032 J=1,3
      GEOM=3.*R(I)*R(J)
      IF(I.EQ.J) GEOM=GEOM-RSQ
      Q2(I,J)=Q2(I,J)+QPT(JJ)*GEOM
      DO 1032 K=1,3
      GEOM=15.*R(I)*R(J)*R(K)
      CON=3.*RSQ
      IF(I.EQ.J) GEOM=GEOM-CON*R(K)
      IF(J.EQ.K) GEOM=GEOM-CON*R(I)
      IF(I.EQ.K) GEOM=GEOM-CON*R(J)
      Q3(I,J,K)=Q3(I,J,K)+QPT(JJ)*GEOM
 1032 CONTINUE
 1030 CONTINUE
      DO 1040 I=1,3
      FPOINT(I)=Q1(I)
 1040 CONTINUE
C
C     PRINT OUT MULTIPOLE EXPANSION
C
 1100  PRINT 907
      DO 1001 J=1,JMAX
      PRINT 908,XFPTS(J),IFPTS(J),(DIPPT(I,J),I=1,3),QPT(J)
 1001 CONTINUE
 1101 IF(CT.EQ.0) GO TO 1050
      PRINT 901,RZERO
      PRINT 903,Q0
      PRINT 904,Q1
      PRINT 905,Q2
      PRINT 906,Q3
 1051 PRINT 912, FPOINT,TMLEN,FIELD
      RETURN
 1050 PRINT 910
      GO TO 1051
 1052 READ 911,FPOINT,(FIELD(I),I=1,3)
      NHANG=0
      GO TO 1050
 8001 PRINT 9801
 9801  FORMAT(*1FIELD POINT SYMBOL NOT IN DATA SET*)
      CALL EXIT
      END
```

```
$IBFTC PRLT     FULTST.DECK
      SUBROUTINE PRNPLT(X,Y,XMAX,XINCR,YMAX,YINCR,ISX,ISY,NPTS)
C  POINTER PLOT ROUTINE
C
C   PLOTS THE *NPTS* POINTS GIVEN BY *X(I),Y(I)* ON A 51 X 101 GRID
C   USING A TOTAL OF 56 LINES ON THE PRINTER
C      IF *ISX* OR *ISY* ARE NON-ZERO, THE CORRESPONDING MAXIMUM AND
C       INCREMENTAL STEP SIZE ARE COMPUTED
C      IF EITHER INCREMENTAL STEP SIZE IS ZERO, THE PROGRAM EXITS
C      NEITHER OF THE INPUT ARRAYS ARE DESTROYED.  IF SCALING IS DONE
C      THE CORRESPONDING NEW VALUES OF MAXIMUM AND STEP SIZE ARE RETURNED
C
      DIMENSION X(NPTS),Y(NPTS),IGRID(105),XAXIS(11)
C
      INTEGER BLANK,DOT,STAR,IGRID,PLUS
      DATA BLANK,DOT,STAR,PLUS / 1H ,1H.,1H*,1H+ /
C
901   FORMAT(14X,105A1)
902   FORMAT(1XE10.3,2X,1H+,105A1,1H+)
903   FORMAT(15X,103(1H.))
904   FORMAT(9X,11E10.3,2H (,I4,5H PTS) )
905   FORMAT(16X,11(1H+,9X))
9800  FORMAT(*1SCALING ERROR IN PRNPLT, EXECUTION TERMINATED*)
C
      IF(ISX.NE.0) CALL PLSCAL(X,XMAX,XINCR,NPTS,100)
      IF(ISY.NE.0) CALL PLSCAL(Y,YMAX,YINCR,NPTS,50)
      IF(XINCR.EQ.0..OR.YINCR.EQ.0.) GO TO 800
      YAXMIN=0.01*YINCR
      XAXMIN=0.01*XINCR
      IZERO=YMAX/YINCR+1.5
      JZERO=103.5-XMAX/XINCR
      IF(JZERO.GT.103.OR.JZERO.LT.4) JZERO=2
      PRINT 905
      PRINT 903
      DO 10 I=1,51
      IF ( I.NE.IZERO) GO TO 16
      DO 14 J=1,105
14    IGRID(J)=PLUS
      GO TO 15
16    DO 11 J=1,105
11    IGRID(J)=BLANK
15    IGRID(JZERO)=PLUS
      IGRID(104)=DOT
      IGRID(2)=DOT
      DO 12 K=1,NPTS
      ITEST =(YMAX-Y(K))/YINCR+1.5
      IF(ITEST .NE.I) GO TO 12
      J=103.5-(XMAX-X(K))/XINCR
      IF(J.GT.103)J=105
      IF(J.LT.3) J=1
      IGRID(J)=STAR
12    CONTINUE
      IF(MOD(I,10).EQ.1) GO TO 13
      PRINT 901,IGRID
      GO TO 10
13    YAXIS=YMAX-(I-1)*YINCR
      IF(ABS(YAXIS).LT.YAXMIN) YAXIS=0.
      PRINT 902,YAXIS,(IGRID(J),J=1,105)
10    CONTINUE
      PRINT 903
      PRINT 905
      DO 20 M=1,11
      XAXIS(M)=XMAX-XINCR*(FLOAT(11-M))*10.0
      IF(ABS(XAXIS(M)).LT.XAXMIN)XAXIS(M)=0.
20    CONTINUE
      PRINT 904,XAXIS,NPTS
      RETURN
800   PRINT 9800
      CALL EXIT
      END
```

```
$IBFTC PLSC     FULIST,DECK
      SUBROUTINE PLSCAL(V,VMAX,VINCR,NPTS,NDIVTS)
C
C     SCALING PROGRAM FOR USE WITH PRNPLT
C   THIS VERSION ADJUSTS THE FULL SCALE TO 2.5,5.0, OR 10. TIMES 10**N
C   AND ADJUSTS THE MAXIMUM POINT TO AN INTEGER MULTIPLE OF 5*VINCR
C
      DIMENSION V(NPTS)
C
      VMIN=V(1)
      VMAX=V(1)
      DO 10 I=1,NPTS
      IF(V(I).LT.VMIN) VMIN=V(I)
      IF(V(I).GT.VMAX) VMAX=V(I)
10    CONTINUE
      QRANGE=0.4342944*ALOG(VMAX-VMIN)
      IF(QRANGE)20,20,30
30    IRANGE=QRANGE
      GO TO 40
20    IRANGE=-QRANGE
      IRANGE=-IRANGE-1
40    QRANGE=QRANGE-FLOAT(IRANGE)
      RANGE=10.**QRANGE
C
C     RANGE IS BETWEEN 1.0 AND 10.0
C
43    IF(RANGE.GT.2.5) GO TO 41
      RANGE=2.5
      GO TO 50
41    IF(RANGE.GT.5.0) GO TO 42
      RANGE=5.0
      GO TO 50
42    RANGE=10.0
50    TRANGE=RANGE*(10.**IRANGE)
C
C   TRANGE IS NOW 2.5,5.0, OR 10.0 TIMES A POWRR OF TEN
C
      VINCR=TRANGE/FLOAT(NDIVIS)
      IF(VMAX)51,51,52
52    IMAX=VMAX/(5.0*VINCR)
      XMAX=5.0*VINCR*FLOAT(IMAX+1)
      GO TO 53
51    IMAX=-VMAX/(5.0*VINCR)
      XMAX=5.0*VINCR*FLOAT(-IMAX+1)
53    IF(VMIN.GT.XMAX-TRANGE) GO TO 100
      RANGE=RANGE*2.0
      IF(RANGE-10.) 43,43,54
54    RANGE=RANGE/10.
      IRANGE=IRANGE+1
      GO TO 43
100   VMAX=XMAX
      VMIN=XMAX-TRANGE
      RETURN
      END
```

APPENDIX IIB

Program TEMROT, weighs the rotational strength by the population distribution at different temperatures. Two versions of integration routines are given.

```
      PROGRAM TEMROT (INPUT, OUTPUT, TAPE 3 = OUTPUT)
C      NELSON TENG      JULY 9, 1970
C      TEMPERATURE DEPENDENCE OF ROTATIONAL STRENGTH
      COMMON/X/X(100)/Y/Y(100)/Z/Z(100)/YZ/YZ(100)/I/N /S/SPOT(100)
      READ 1,L
      DO 30 I= 1,L
      READ 2, (SPOT(I), I=1,8)
    1 FORMAT (I1)
    2 FORMAT (8A10)
      READ 100,N,(Y(I), I=1,N)
      READ 101, N, (Z(I), I=1,N )
  100 FORMAT (I4/ (8F10.4))
  101 FORMAT (I4/ (8E10.4))
      Y(N+1)=Y(1)
      Z(N+1)=Z(1)
      DO 5 J=1,N
      YZ(J)= Y(J)*Z(J)
    5 X(J) = (J-1)*5 - 180
      X(N+1) = -X(1)
      YZ(N+1) = YZ (1)
      M = N+1
      PRINT 200, (X(I), Y(I), Z(I), YZ(I), I=1,M)
  200 FORMAT(*1        DEGREE        PROBABILITY      ROT. STRN        P TIME
     1S R*/(5X, F10.1, 5X, F10.4, 5X, E12.4, 5X, E12.4))
      PRINT 3, (SPOT(I), I=1,8)
    3 FORMAT (1H1, 10X, 8A10)
      SUMY=0
      SUMYZ=0
      DO 20 J=1,N
      SUMY=SUMY+((Y(J)+Y(J+1))*(X(J+1)-X(J)))/2
      SUMYZ=SUMYZ+((YZ(J)+YZ(J+1))*(X(J+1)-X(J)))/2
      JJ=J+1
      PRINT 300, X(JJ), SUMY
      PRINT 400,X(JJ),SUMYZ
  300 FORMAT(*        DEGREE        PROBABILITY INTEGRATED*/
     1(5X, F10.1, 5X, E12.3//))
  400 FORMAT (*        DEGREE        PTIMESR INTEGRATED*/
     1(5X, F10.1, 5X, E12.5  //))
   20 CONTINUE
   30 CONTINUE
      END
```

```
      SUBROUTINE SIMPS (A,B,E,MAXI,XINTG,XIP,INDEX)
      FAFB=XINTG(A)+XINTG(B)
      XH=B-A
      XIR=XH*.5
      XJ=XIR*FAFB
      XNEW=A+XIR
      XHA=XIR/3.
      INDEX=0
 1006 FNEWX=XINTG(XNEW)
 1001 IF (INDEX .GT. 0) GO TO 1003
 1002 INDEX=1
      XI=XHA*(FAFB+FNEWX*4.)
 1004 XJ=(XJ+XI*3.)*.25
      INDEX=INDEX+1
      IF (INDEX .GT. MAXI) GO TO 1009
 1010 XH=XH*.5
      XNEW=A+XH*.5
      S=0.
 1005 IF (XNEW .LT. B) GO TO 1006
 1007 XIP=(XJ+XH*2.*S)/3.
    1 WRITE (3,2) INDEX,XIP
    2 FORMAT (30X,6HINDEX=I4,2X,4HXIP=1PE12.4//)
      IF (ABS (XIP-XI) .LE. ABS (E*XIP)) GO TO 1009
 1008 XI=XIP
      GO TO 1004
 1003 S=S+FNEWX
      XNEW=XNEW+XH
      GO TO 1005
 1009 RETURN
      END
```

```
      PROGRAM TEMPCT (INPUT, OUTPUT, TAPE 3 = OUTPUT)
C      NELSON TENG      JULY 5, 1970
C      TEMPERATURE DEPENDENCE OF ROTATIONAL STRENGTH
      COMMON/X/X(100)/Y/Y(100)/Z/Z(100)/YZ/YZ(100)/I/N /S/SPOT(100)
      EXTERNAL P,PR
      READ 100,N,(Y(I), I=1,N)
      READ 101, N, (Z(I), I=1,N )
  100 FORMAT (I4/ (8F10.4))
  101 FORMAT (I4/ (8E10.4))
      Y(N+1)=Y(1)
      Z(N+1)=Z(1)
      DO 5 J=1,N
      YZ(J)= Y(J)*Z(J)
    5 X(J) = (J-1)*5 - 180
      X(N+1) = -X(1)
      YZ(N+1) = YZ (1)
      N = N+1
      PRINT 200, (X(I), Y(I), Z(I), YZ(I), I=1,N)
  200 FORMAT(*1        DEGREE        PROBABILITY      ROT. STRN        P TIME
     1S R*/(5X, F10.1, 5X, F10.4, 5X, E12.4, 5X, E12.4))
      XSTART = -180.0
      INIT = 0
      DO 10 J= 1, 18
      XX = J*20  -180
      CALL SIMPS ( XSTART, XX, 0.005, 50, P, PFINAL , INDEX )
      IF (INDEX.LT.50) PRINT 300,XX,PFINAL
  300 FORMAT(*        DEGREE        PROBABEILITY INTEGRATED*/
     1(5X, F10.1, 5X, E12.3//))
      IF ( INIT. NE. 0. OR.PFINAL. EQ. 0.0) GO TO 10
      PRINT 500, PFINAL
  500 FORMAT (*        PFINAL EQUAL TO*/(10X,E12.3) )
      INIT = 1
      XSTART = (J-1) * 20 - 180
   10 CONTINUE
      DO 20  J=1,18
      XX = J*20  -180
      IF (XX. LE. XSTART) GO TO 20
      CALL SIMPS ( XSTART, XX, 0.005, 50, PR , PRFINAL, INDEX)
      IF (INDEX.LT.50) PRINT 400, XX, PRFINAL
  400 FORMAT (*        DEGREE        PTIMESR INTEGRATED*/
     1(5X, F10.1, 5X, E12.5  //))
   20 CONTINUE
      END

      FUNCTION P(PHI)
      COMMON/X/X(100)/Y/Y(100)/Z/Z(100)/YZ/YZ(100)/I/N
      DO10 I=1,N
      IF (PHI.GT.X(I+1).OR.PHI.LT.X(I)) GO TO 10
      P=Y(I)+(Y(I+1) - Y(I)) * (PHI-X(I))/(X(I+1)-X(I))
      RETURN
   10 CONTINUE
      END


      FUNCTION PR(PHI)
      COMMON/X/X(100)/Y/Y(100)/Z/Z(100)/YZ/YZ(100)/I/N
      DO10 I=1,N
      IF (PHI.GT.X(I+1).OR.PHI.LT.X(I)) GO TO 10
      PR = YZ(I) +(YZ(I+1) - YZ(I))*(PHI-X(I))/(X(I+1)-X(I))
      RETURN
   10 CONTINUE
      END
```

APPENDIX IIC

Program LESQW, a Fortran IV linear regressive analysis of the Lineweaver and Burk kinetic equation.

```
      PROGRAM LESOK (INPUT,OUTPUT)
C     LEAST SQUARE ANALYSIS OF ENZYME KINETIC DATA
C     WEIGHTED LEAST SQUARE ANALYSIS ON LINE Y = A + B*X
      DIMENSION X(500), Y(500), YPRED(500), YDEV(500),W(500)
      DIMENSION SY(500),SX(500),SVY(500),SI(100), XK(100),SEK(100)
      DIMENSION SNAME(100)
      READ 4 ,(SNAME(I), I=1,8)
    4 FORMAT (8A10)
      PRINT 3,(SNAME(I), I=1,8)
    3 FORMAT (1H1, 8A10)
      J=0
      READ 10, M
      READ 9, (SI(I), I=1, M)
C     READ SUBSTRATE CONCENTRATION
      READ 10, N
      READ 11, (SX(I), I=1,N)
   11 FORMAT (E10.2)
    1 CONTINUE
      J=J+1
      II=0
C     READ SAMPLE SIZE
      READ 10, N
      PRINT 10,N
    9 FORMAT (E10.2)
   10 FORMAT(I3)
      IF (N.EQ.0) GO TO 150
C     READ VELOCITY
      READ 14, (SY(I), W(I), I=1,N)
   14 FORMAT (2F10.5)
C     IF W(I) IS NOT GIVEN SET W(I) = SY(I)**4
      IF(W(1).NE.0.0) GO TO 15
      DO 12 I=1,N
      W(I) = SY(I)**4
   12 CONTINUE
   15 CONTINUE
C     1/V VS. 1/S AND S/V VS. S
      DO 6 I=1,N
      X(I) = 1.0/SX(I)
      Y(I) = 1.0 /SY(I)
      SVY(I) = Y(I) *SX(I)
    6 CONTINUE
    7 CONTINUE
C     DO  CALCULATIONS
      XN = N
      SUMW = 0.0
      SUMWX = 0.0
      SUMWY = 0.0
      SUMWXX = 0.0
      SUMWXY = 0.0
      SUMWYY = 0.0
      SUMZ = 0.0
      DO 20 I=1,N
      SUMW = SUMW + W(I)
      SUMWX = SUMWX + W(I)*X(I)
      SUMWY = SUMWY + W(I)*Y(I)
      SUMWXX = SUMWXX + W(I)*X(I)**2
      SUMWXY = SUMWXY + W(I)*X(I)*Y(I)
      SUMWYY = SUMWYY + W(I)*Y(I)**2
```

```
      SUMZ = SUMZ + Y(I)*SQRT(W(I))
   20 CONTINUE
C     CALCULATE COEFFICIENT B AND INTERCEPT A
      DEN = SUMW*SUMWXX - SUMWX**2
      B = (SUMW*SUMWXY - SUMWX*SUMWY)/DEN
      A = (SUMWXX*SUMWY - SUMWX*SUMWXY)/DEN
C     CALCULATE PREDICTED VALUES, DEVIATIONS AND SUM OF SQUARES
      SS = 0.0
      DO 30 I=1,N
      YPRED(I) = A +B*X(I)
      YDEV(I) = YPRED(I) - Y(I)
      SS = SS + YDEV(I)**2      *W(I)
   30 CONTINUE
      SSQ = SS/(XN - 2.0)
C     CALCULATE STANDARD ERRORS
      SE = SQRT(SUMW*SSQ/DEN)
      SEYINT = SQRT(SUMWXX *SSQ/DEN)
C     CALCULATE CORRELATION COEFFICIENT
      R = SQRT((A*SUMWY+ B*SUMWXY- SUMZ**2/XN)/(SUMWYY- SUMZ**2/XN))
      PRINT 10,N
      PRINT 100, B,A
      PRINT 101, SE
      PRINT 104, SEYINT
      PRINT 102, R
      PRINT 103, (X(I), Y(I), YPRED(I), YDEV(I), W(I), I=1,N)
  101 FORMAT (48HTHE STANDARD ERROR OF THE COEFFICIENT IS S.E. = E16.6)
  100 FORMAT (23HTHE COEFFICIENT IS B = E11.5,27H     THE YINTERCEPT IS
     1A = E11.5)
  102 FORMAT (35HTHE CORRELATION COEFFICIENT IS R = F10.6,/7X,*X*,11X,
     A  3X,*Y*  11X,
     1  *YPRED*,10X,*YDEV*,14X,*W*)
  103 FORMAT (E10.3,5X,E10.3,5X,F10.5,5X,F8.5,7X,E10.3)
  104 FORMAT (52H THE STANDARD ERROR OF THE INTERCEPT IS S.E.(INT) = E16
     1.6)
C     CALCULATION OF K(I) AND STANDARD ERROR FROM S/V VS. S PLOT
      IF (II. EQ. 0 ) GO TO 51
      IF ( SI(J). NE. 0.0 ) GO TO 50
      BV=B
      XK(J) = A
      SQXK = A*A
      SQYINT = SEYINT * SEYINT
      SEK(J) = SEYINT
      GO TO 51
   50 K=1
      XK(J) = SI(J) / (A/XK(K) - 1 )
      SISQ = SI(J)* SI(J)
      DEMO = (A- XK(K) )**4
      SEK(J)=SQRT ((SEYINT**2 *SISQ*SQXK)/DEMO + (SQYINT*SISQ*A*A)/DEMO)
      IF(J. NE. M) GO TO 51
      XK(K) = XK(K)/BV
      PRINT 106
      PRINT 105,( SI(I), XK(I), SEK(I), I=1,M)
  105 FORMAT (E10.3,5X, E10.3,5X, E10.3)
  106 FORMAT (1H1, *INHIBITOR        K(I)      STANDARD ERROR*///)
C     CALCULATION OF AVERAGE K(I) AND STANDARD ERROR
      SXK =0.0
      SSEK = 0.0
      DO 200 I=2,M
```

```
      SXK = SXK + XK(I)
  200 SSEK = SSEK + SEK(I)*SEK(I)
      FXK = SXK/(M-1)
      FSEK = SQRT (SSEK/(M-1)/(M-1))
      PRINT 107
      PRINT 108 , FXK, FSEK
  107 FORMAT (/////,*  FINAL AVE. K(I)        AVE. STANDARD ERROR*)
  108 FORMAT (//,4X, E10.3, 14X, E10.3)
      GO TO 150
   51 II=II+1
      IF (II. GE. 21 GO TO 1
      DO 2 I=1,N
      X(I)=SX(I)
      Y(I)= SVY(I)
      W(I) = W(I) / SX(I) **2
    2 CONTINUE
      GO TO 7
  150 STOP
      END
```

APPENDIX III. REPRINTS

THE JOURNAL OF BIOLOGICAL CHEMISTRY
Vol. 244, No. 20, Issue of October 25, pp. 5656-5662, 1969
Printed in U.S.A.

The 220 MHz Nuclear Magnetic Resonance Study of a Solvent-induced Conformational Change in Flavin Adenine Dinucleotide*

(Received for publication, April 21, 1969

GEORGE KOTOWYCZ,‡ NELSON TENG, MELVIN P. KLEIN, AND MELVIN CALVIN

From the Laboratory of Chemical Biodynamics, Lawrence Radiation Laboratory, University of California, Berkeley, California 94720

SUMMARY

Proton magnetic resonance studies at 220 MHz have shown that the conformation of flavin adenine dinucleotide in D_2O-dioxane-*d*-8 (70:30, v/v) solutions is in agreement with the model proposed by Sarma, Dannies, and Kaplan (*Biochemistry*, 7, 4359 (1968)) for D_2O solution. The determination of the temperature dependence of the FAD, flavin mononucleotide, and adenosine diphosphoribose proton shifts were found to be necessary for a correct assignment of the isoalloxazine protons in FAD and hence for determining the conformation. The FAD proton shifts in D_2O solutions have a sigmoid dependence on temperature which is discussed in terms of a two-state model, where an equilibrium exists between the folded and unfolded states of the molecule. Sigmoid curves are not observed in D_2O-dioxane solutions, suggesting that dioxane lowers the transition temperature. Dioxane decreases the fraction of folded FAD molecules in solution by lowering the energy barrier between the two states and also reduces the intermolecular stacking of FAD and FMN. Line broadening of the adenine AC_8H proton in ADP-ribose is observed and may be interpreted in terms of rotational isomers in solution.

During the course of an investigation of a flavin-containing enzyme, *p*-hydroxybenzoate hydroxylase, the circular dichroism spectrum was observed to exhibit a negative band at 450 nm. Neither the apoprotein (1) nor flavin adenine dinucleotide (Fig. 1) showed any optical activity in this spectral region (1, 2). This 450 nm circular dichroic band may be induced by the particular mode of bonding between the protein and the FAD or by a conformational change in FAD upon binding. The necessity of determining the FAD conformation became imperative for an interpretation of the optical measurements. Nuclear magnetic resonance spectroscopy was chosen since it yields valuable structural and conformational information. For example, the pyridine dinucleotides have been studied alone (3–7) and in a complex formation with several enzymes (5) in solution. While our work was in progress Sarma, Dannies, and Kaplan (8) have published a model for the conformation of FAD in D_2O based on their 60 MHz NMR[1] spectra. In that model, the adenine ring is folded over the isoalloxazine ring and the dinucleotides associate as dimers in solution by way of vertical stacking of the isoalloxazine rings. In the folded dinucleotide conformation the adenine C_2H proton is preferentially located over the aromatic ring (*A* in Fig. 1) of the isoalloxazine of FAD, whereas the isoalloxazine C_6H proton is in the proximity of the pyrimidine portion of adenine.

The present study is concerned with the investigation of the conformation of the folded dinucleotide as a function of temperature in D_2O and D_2O-dioxane solutions. Our chemical shift data support the folded structure for FAD in D_2O which is partially unfolded by D_2O-dioxane solutions or by an increase in temperature. A significant line width change of the adenine C_8H proton, only in the mononucleotide adenosine diphosphoribose with temperature, is discussed in terms of several rotational isomers of this molecule in solution. Finally, we recognize the difficulties in line assignments in FAD and in flavin mononucleotide based solely on chemical shift inferred from electron density calculations.

EXPERIMENTAL PROCEDURE

The NMR spectra were obtained on a Varian high resolution HR 220 MHz spectrometer. The shifts were measured with respect to sodium 2,2-dimethyl-2-silapentane-5-sulfonate (from Merck Sharp and Dohme of Canada) used as an internal reference, and calibrations were carried out by sideband modulation. The precision of the measurements is ±0.5 Hz. Temperatures were calibrated using the temperature-dependent chemical shifts of ethyleneglycol and methanol samples and the calibration charts provided by Varian Associates. The precision of the measurement is ±2.0°. Calibrations were carried out before and after all measurements. High temperatues had no effect on the ambient temperature (17°) spectra of the molecules indicating no irreversible conformational changes or decomposition of the molecules has occurred. All solutions were at neutral pH.

FAD and FMN were obtained from Sigma and K and K Lab-

* This research was supported in part by the United States Atomic Energy Commission.

‡ Holder of a National Research Council of Canada-North Atlantic Treaty Organization Postdoctoral Fellowship.

[1] The abbreviation used is: NMR, nuclear magnetic resonance.

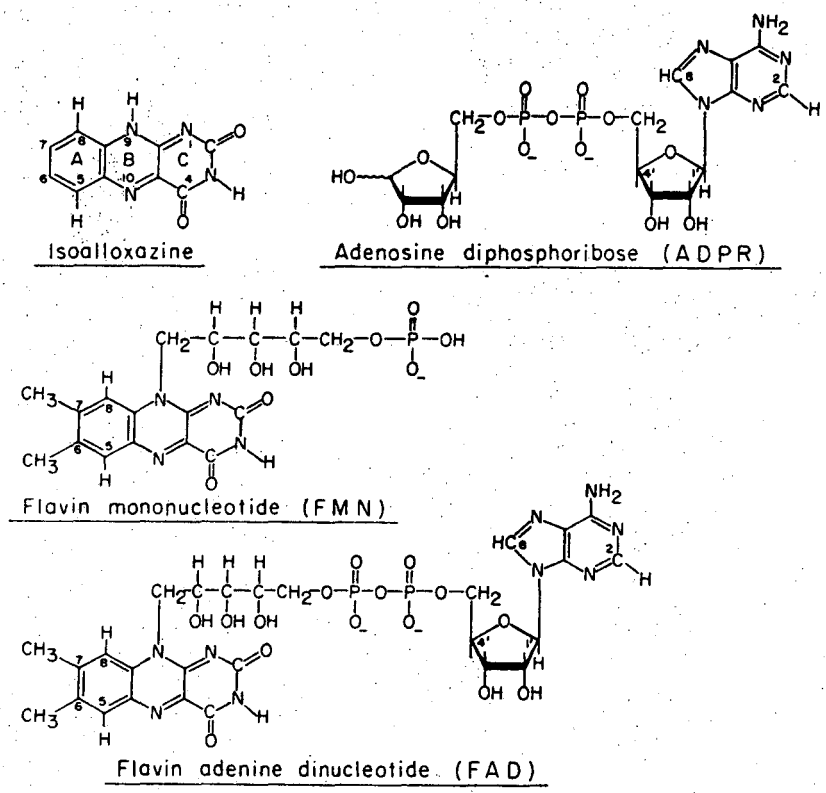

FIG. 1. Structural formulae

oratories; ADP-ribose was obtained from Calbiochem. These compounds were used without further purification but were lyophilized twice from D_2O to remove exchangeable protons. The solvents D_2O, dioxane-*d*-8, and methanol-*d*-4 are from the International Chemical and Nuclear Corporation.

RESULTS AND DISCUSSION

Assignment of Lines—Selected regions of the 220 MHz proton magnetic resonance spectra of ADP-ribose, FMN, and FAD (0.025 M) in a D_2O-dioxane-*d*-8 solution (70:30, v/v) (pH 7.0) are shown in Fig. 2, and the concentration dependence of these proton shifts is illustrated in Fig. 3. The peaks were assigned to their corresponding protons in the following manner. For ADP-ribose the singlet at lower field corresponds to the adenine C_8 proton (AC_8H) as shown by purine exchange experiments with D_2O (9, 10). The singlet at higher field is then assigned to the adenine C_2 proton (AC_2H), while the doublet arises from the C_1' ribose proton in adenosine ($AC_1'H$). The observed splitting corresponds to the coupling constant $J(H_1'-H_2')$ between the ribose protons.

Sarma *et al.* (8) assigned the isoalloxazine protons of FMN and FAD on the basis of the computed π electron densities at the carbon to which the proton is bonded. The uncertainties involved are described. Correlations between π electron densities and aromatic proton chemical shifts have been discussed by several authors (see Reference 11 and references therein). The proton bonded to the highest π electron density carbon experiences the largest diamagnetic (high-field) shift. On this basis, the lower of the two aromatic proton lines was assigned to the isoalloxazine C_5 proton in FMN (FC_5H) (C_5 π electron density, 1.004). The higher field line is then assigned to the C_6 proton (FC_6H) (C_6 π electron density, 1.063). Computed π electron densities at the methyl protons were used to assign the FMN methyl resonances. Hence the C_7 methyl protons (FC_7CH_3) occur to low field of the C_6 methyl protons (FC_6CH_3) (π electron densities, 0.943 and 0.949, respectively). These π electron densities were calculated by Pullman and Pullman (12) for the oxidized form of the isoalloxazine ring of FMN.

The uncertainty in this approach is evident from Figs. 3, 4, and 5. From Fig. 3, the FMN FC_5H and FC_6H proton shifts appear to become equivalent in D_2O-dioxane solutions at infinite dilution. The temperature dependence shows that these two resonances collapse into a single line at 68° in D_2O-dioxane solutions (0.025 M) (Fig. 4) and at 91° in D_2O solutions (0.025 M) (Fig. 5). These results are unexpected from electron density considerations alone.

An unequivocal assignment of the FMN proton resonances has been carried out experimentally by Bullock and Jardetzky (13) who observed the exchange of the FC_7CH_3 protons at 90–95° in D_2O solutions and a consequent decrease in the amplitude of the lower field methyl line.[2] From a comparison of the spectra

[2] In a paper by McAndless and Stewart (14) similar deuterium exchange experiments of the methyl protons in two lumazine derivatives are reported.

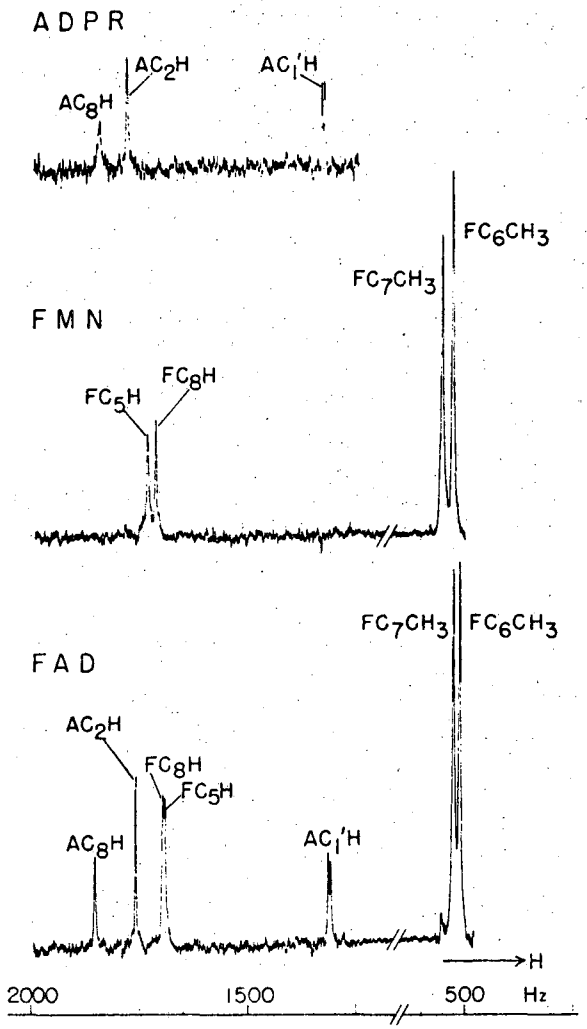

FIG. 2. The 220 MHz proton magnetic resonance spectra of ADP-ribose (*ADPR*), FMN, and FAD (0.025 M) in D_2O-dioxane-*d*-8 (70:30 v/v) at 17° (pH 7.0). Only the aromatic, C'_1-ribose and methyl proton regions of the spectra are shown. All shifts are with respect to internal sodium 2,2-dimethyl-2 silapentane-5-sulfonate.

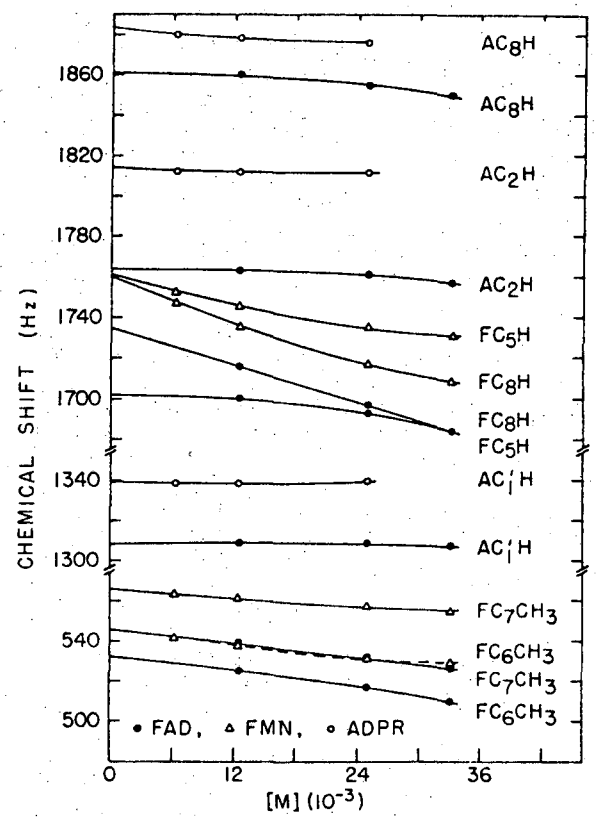

FIG. 3. Concentration dependence of ADP-ribose (*ADPR*), FMN, and FAD chemical shifts in D_2O-dioxane-*d*-8 (70:30 v/v) solutions (pH 7.0, 17°).

of lumiflavin and 8-deuteriolumiflavin, the higher field aromatic proton in the isoalloxazine ring was assigned to the FC_8H proton. This assignment (Fig. 2) is in agreement with that predicted on the basis of the calculations of Pullman.

In FAD, the resonances in the dinucleotide occur at higher fields than they do in the corresponding mononucleotide. This arises from the ring-current diamagnetic shielding effects of the dinucleotide protons in the folded structure as well as from intermolecular ring-current interactions between isoalloxazine rings. The lowest field FAD resonance (Fig. 2) is assigned to the AC_8H proton on the basis of our exchange experiments in which the D_2O-dioxane solution was kept at 85° for 4 hours, resulting in the almost total disappearance of this line. The AC_2H proton is assigned to the next resonance; it is well removed from the flavin peaks and the shift difference between this resonance in FAD and in ADP-ribose decreases as the temperature increases (Figs. 4 and 5). This is interpreted as reflecting a partial unfolding of the dinucleotide with temperature which removes the AC_2H proton from the ring-current shielding influence of the neighboring isoalloxazine ring. The result is that at higher temperatures the FAD AC_2H proton shift tends to approach the observed shift for the corresponding proton in ADP-ribose.

The most difficult assignment was that of the FAD FC_5H and FC_8H protons, and again the requisite information was derived from the temperature measurements. The temperature dependence of the chemical shifts (Figs. 4 and 5) shows that the chemical shift differences between the corresponding AC_8H, AC_2H, and $AC_1'H$ protons in ADP-ribose and FAD decrease with increasing temperature. The shift differences between the FC_6CH_3 and the FC_7CH_3 protons in FMN and FAD also reveal a similar inverse temperature dependence. In fact, at higher temperatures several of the curves for the corresponding protons almost merge. Similar reasoning should also apply to the FAD and FMN FC_5H and FC_8H proton resonances. Using the assignments of the FC_5H and FC_8H proton resonances in FMN, we assigned the corresponding resonances in FAD. A correct assignment of the isoalloxazine protons in FAD would have been very difficult without the temperature measurements. Finally,

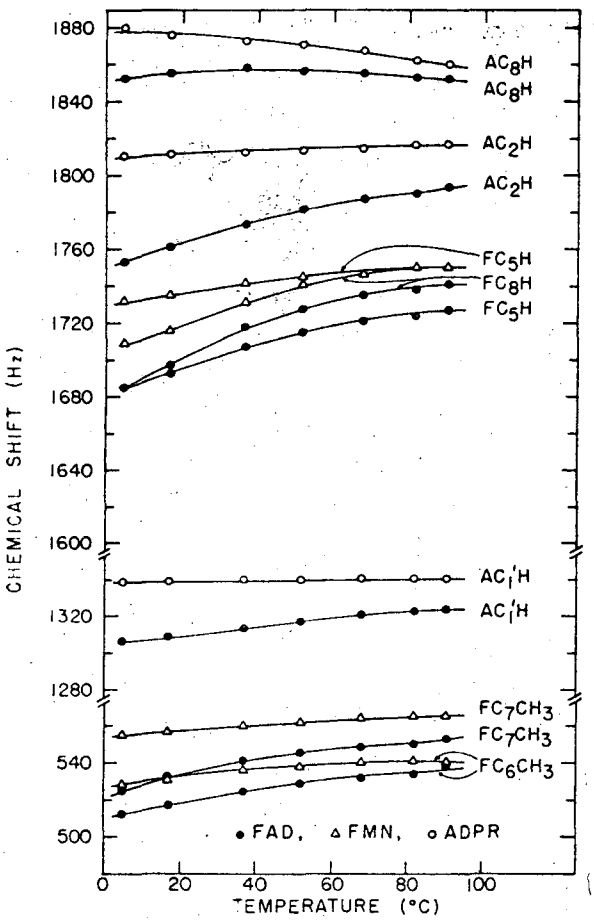

FIG. 4. Temperature dependence of ADP-ribose (*ADPR*), FMN, and FAD chemical shifts in D_2O-dioxane-*d*-8 (70:30 v/v) solutions (0.025 M, pH 7.0).

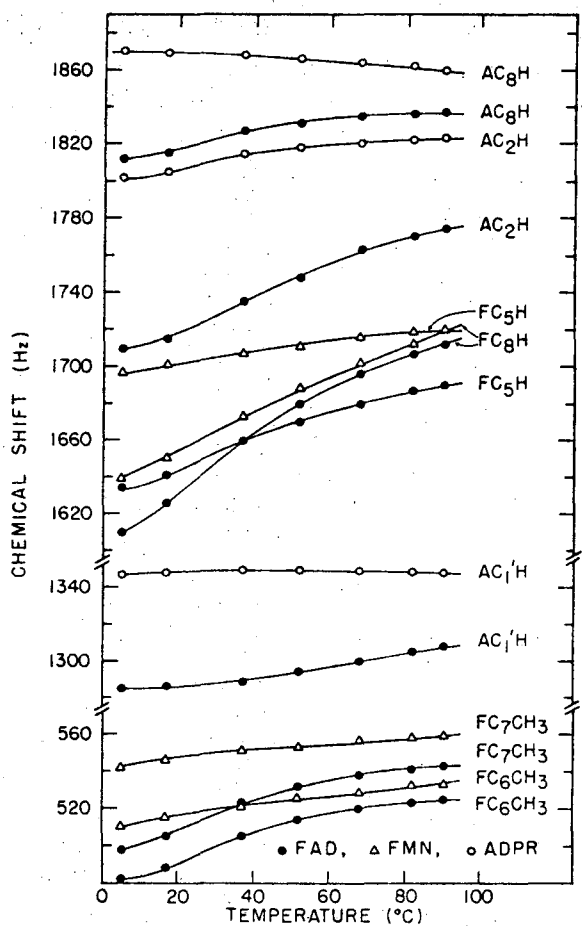

FIG. 5. Temperature dependence of ADP-ribose (*ADPR*), FMN, and FAD chemical shifts in D_2O (0.025 M, pH 7.0).

the FAD AC'_1H, FC_7CH_3, and FC_6CH_3 protons were assigned as in ADP-ribose and FMN.

In order to arrive at a correct model for the folded conformation of FAD or the structure of the FMN and FAD stacked dimers in solution, an unambiguous assignment of the proton resonances is required. An example of an incorrect assignment that could easily be made is seen from the data in Fig. 5. In D_2O solutions at low temperatures the FAD FC_8H resonance occurs to high field of the FC_5H resonance. With an increase in temperature these peaks coalesce and cross with the FC_8H to lower field. Consequently, only at experimental temperatures below 40° can a correct assignment of these FAD proton resonances be made based solely on electron density calculations.

Intermolecular Interactions—Intermolecular interactions may be studied by examining the concentration dependence of FAD, FMN, and ADP-ribose proton shifts in D_2O-dioxane solutions. Table I and Fig. 3 show that the flavin protons are the most sensitive to concentration and must therefore be involved in intermolecular associations. Since the FC_8H proton, both in FAD and FMN, experiences the greatest shift to low field with decreasing concentration, Sarma *et al.* (8) argued that in D_2O these molecules associate by way of vertical stacking of the isoalloxazine rings. On the average, the FC_8H proton of one of the isoalloxazine rings spends a considerable time in the proximity of the aromatic ring A of another isoalloxazine ring, and vice versa. Then these protons experience the largest diamagnetic shielding arising from the ring currents in the A ring. In D_2O-dioxane solutions (Table I), the FC_5H proton also experiences the greatest diamagnetic shift (FAD, 38 Hz; FMN, 44 Hz). The data in Table I are consistent with the stacking model for FAD and FMN proposed for the D_2O solutions. Adenine protons both in ADP-ribose and FAD are insensitive to concentration and therefore are not involved in intermolecular associations.

Intramolecular Interactions—The shielding effect of one ring on the proton resonances of the second ring in FAD may be studied by a comparison of the respective mononucleotide and dinucleotide proton shifts at infinite dilution. This assumes that intermolecular interactions and their effect on the chemical shifts are zero at infinite dilution. The Δ(ADP-ribose-FAD) and Δ(FMN-FAD) values represent the difference in chemical shift between respective protons in the mononucleotides and the di-

TABLE I

Concentration dependence of FAD, FMN, and ADP-ribose proton chemical shifts in D_2O-dioxane-d-8 solutions (70:30, v/v) (17°)

Compound	Concentration	AC_8H	AC_2H	FC_8H	FC_9H	AC'_1H[a]	FC_7CH_3	FC_6CH_3
	M	Hz						
FAD	0.025	1855	1761	1693	1697	1309	531	517
	0.0	1862	1764	1703	1735	1309	546	533
δ[b]		7	3	10	38	0	15	16
FMN	0.025			1735	1716		557	531
	0.0			1762	1760		566	546
δ				27	44		9	15
ADP-ribose	0.025	1876	1812			1339		
	0.0	1883	1815			1339		
δ		7	3			0		

[a] The coupling constant $J(H'_1 - H'_2)$ is 5.5 ± 0.2 Hz in FAD, and 5.8 ± 0.2 Hz in ADP-ribose.

[b] δ signifies shift at 0.0 M − shift at 0.025 M; positive numbers represent a shift to high field.

TABLE II

Difference in chemical shift between respective protons in dinucleotide FAD and mononucleotides FMN and ADP-ribose in D_2O-dioxane-d-8 (70:30, v/v) (17°)

Compound	AC_8H	AC_2H	FC_8H	FC_9H	AC'_1H	FC_7CH_3	FC_6CH_3
	Hz						
Δ(ADP-ribose-FAD),[a] 0.0 M	21	51			30		
Δ(FMN-FAD), 0.0 M			59	25		20	13

[a] Δ represents the difference in the proton shifts at infinite dilution. The positive numbers represent a shift to high field.

nucleotide. In D_2O-dioxane (Table II), all Δ values are positive, indicating that in FAD all protons are diamagnetically shielded. The AC_2H proton is more highly shielded (51 Hz) than the AC_8H proton (21 Hz). The FC_9H proton also experiences a larger diamagnetic shielding (59 Hz) as compared with the FC_8H proton (25 Hz). Therefore, the conformation of FAD in D_2O-dioxane is in agreement with the folded structure proposed for this molecule in D_2O solutions by Sarma *et al.* (8).

Temperature Studies—In Figs. 4 and 5 we have summarized the temperature dependence of the chemical shifts in both D_2O-dioxane and D_2O solutions. With an increase in temperature the proton lines shift to lower field (exception: the AC_8H protons in ADP-ribose in both D_2O-dioxane and D_2O solutions and in FAD in D_2O-dioxane). Changes in temperature will affect both the inter- and intramolecular interactions and associated proton shifts. The shifts to low field may be explained by a decrease in the ring-current diamagnetic shielding of the protons when intermolecular associations decrease by a partial destacking as well as by a partial unfolding of the FAD molecules.

The temperature dependence of the intramolecular interaction in FAD may be deduced by taking the difference between the mononucleotide and dinucleotide proton shifts at every temperature. This assumes that chemical shifts for equivalent protons in both mononucleotides and dinucleotide, arising from any

TABLE III

Temperature dependence of difference in chemical shift between respective protons in dinucleotide FAD and mononucleotides FMN and ADP-ribose

Solvent compounds	AC_8H	AC_2H	FC_8H	FC_9H	AC'_1H	FC_7CH_3	FC_6CH_3
	Hz						
D_2O-dioxane-d-8 (70:30, v/v) (0.025 M) at 5°							
Δ(ADP-ribose-FAD)[a]	28	57			33		
Δ(FMN-FAD)			47	24		30	16
D_2O-dioxane-d-8 (70:30, v/v) (0.025 M) at 90.5°							
Δ(ADP-ribose-FAD)	8	23			17		
Δ(FMN-FAD)			23	9		12	3
D_2O (0.025 M) at 5°C							
Δ(ADP-ribose-FAD)	59	92			62		
Δ(FMN-FAD)			63	29		44	28
D_2O (0.025 M) at 90.5°							
Δ(ADP-ribose-FAD)	23	49			40		
Δ(FMN-FAD)			30	8		16	8

[a] Δ equals the difference in the proton shifts at 0.025 M. Positive numbers represent a shift to high field.

intermolecular associations, have the same dependence on temperature.

Several interesting features are evident from a comparison of the curves in Figs. 4 and 5 and from the data in Table III. The first is the decrease in the chemical shift separation between corresponding protons in the mononucleotides and in FAD as the temperature is increased. For example, the shielding effect on AC_2H in FAD decreases from 92 Hz at 5° to 49 Hz at 90.5° (D_2O) (Table III) as the high temperatures tend to unfold the FAD molecules. However, even at 90.5° the dinucleotide proton resonances are always at higher fields than they are in FMN and ADP-ribose. This indicates that at this temperature adenine-isoalloxazine ring interactions are still present.

Secondly, the FAD temperature curves in D_2O solutions are roughly sigmoidal in shape, with apparent asymptotic limits at both high and low temperatures (Fig. 5). Sigmoid curves are also obtained when the differences in the chemical shifts Δ(ADP-ribose-FAD) and Δ(FMN-FAD) are plotted as a function of temperature (Fig. 6). The sigmoidal dependence of the chemical shifts could arise from changes in the relative conformation of the two rings in FAD. Similar curves were obtained for adenylyl-(3′,5′)-adenosine (ApA) by Chan and Nelson (10).

Sigmoid curves and cooperative transitions have been discussed in terms of the "two-state" hypothesis or "all-or-none" processes. These terms imply a discontinuity in thermodynamic states such that only one thermodynamic state is stable below the "transition temperature" and one above. At any given temperature the molecules in the two states are in equilibrium. The best known two-state processes are the phase changes of solids and liquids and the conformational changes in proteins. The theory, character, and properties of cooperative transitions have been developed for the conformational transitions of proteins together with tests for the validity of the two-state approximation (15).

The melting of dinucleoside monophosphates has been interpreted in terms of this model. The two states correspond to

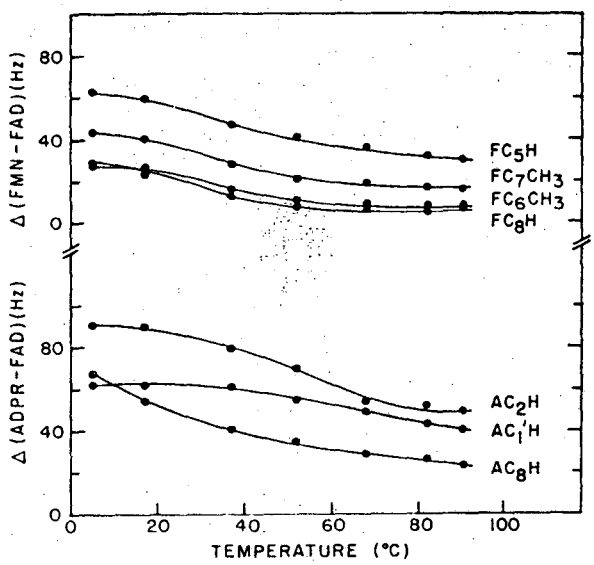

FIG. 6. The correlation between the difference in the proton chemical shifts Δ(ADP-ribose-FAD) and Δ(FMN-FAD) with temperature (0.025 M D_2O solutions, pH 7.0). *ADPR*, adenosine diphosphoribose.

folded and unfolded molecules (16). These results are based on temperature changes in the circular dichroism spectra.

Considering the proton chemical shift *versus* temperature plot (Fig. 6), the shifts at the two asymptotic limits at low and high temperatures approach the chemical shifts of the protons in the folded and unfolded states, respectively. Hence the sigmoid dependence of the shifts on temperature arises mainly from changes in the distance between the two rings, and therefore from changes in the ring-current shielding. The applicability of interpreting ring-current shift changes in ApA in terms of the two-state model has been discussed by Chan and Nelson (10).

Patel (7) has applied NMR in studying the conformation of the coenzyme nicotinamide adenine dinucleotide. He suggests that a rapid equilibrium of open and one folded conformation of NADH favors the open form at higher temperatures and the folded form at lower temperatures. The observed NMR signal at any temperature is the weighted average of open and one folded conformation in rapid equilibrium at that temperature. We therefore suggest that FAD molecules in D_2O solutions are in a rapid equilibrium between a folded and an unfolded state.

Sigmoid curves are not observed in D_2O-dioxane solutions (Fig. 4) nor when the difference in the chemical shifts Δ(ADP-ribose-FAD) and Δ(FMN-FAD) are plotted as a function of temperature. Dioxane must therefore lower the energy barrier and hence the transition temperature between the folded and unfolded states. This results in a decrease in the intramolecular shielding of all FAD protons (Table III). For example, at the lowest and highest temperatures that were studied, the FAD AC_2H proton at 5° in D_2O is shielded by 92 Hz and this shielding decreases to 49 Hz at 90.5°, whereas in D_2O-dioxane the shielding decreases from 57 to 23 Hz over this same temperature region.

Temperature dependences of the coupling constant $J(H_{1'}\text{-}H_{2'})$ have been interpreted in terms of a conformational change of the ribose ring in several dinucleoside monophosphates (17). In ApA this coupling increases from 2.3 to 4.7 Hz (4-71°). In the molecules under consideration the temperature variation of this coupling is small. In D_2O the coupling constant increases from 4.5 to 5.2 Hz in FAD (5-90.5°), and remains at 5.6 Hz in ADP-ribose. In D_2O-dioxane, the coupling constant in FAD is 5.4 Hz but decreases in ADP-ribose from 6.0 to 5.4 Hz (5-90.5°). Because the changes are very small, no appreciable geometrical change in the relationship of $H_{1'}$ and $H_{2'}$ takes place in this temperature range.

Solvent Effects—A comparison of Figs. 4 and 5, together with the data shown in Table IV, show that the addition of dioxane to D_2O solutions of the solute molecules induces a shift to low field for the protons with the exception of the $AC_1'H$ proton in ADP-ribose (17°). These solvent shifts to low field may arise from (*a*) the decrease in the ring-current diamagnetic shielding of protons and (*b*) hydrogen bond formation.

TABLE IV

Solvent effect on FAD, FMN, and ADP-ribose proton shifts

Δ = (D_2O-dioxane-*d*-8 (70:30, v/v))-D_2O proton shifts (0.025 M).

Compound	AC_8H	AC_2H	FC_5H	FC_8H	AC'_1H	FC_7CH_3	FC_6CH_3
			Hz at 17°				
FAD	40	46	52	71	23	27	29
FMN			34	66		11	16
ADP-ribose	6.5	6.5			−9		
			Hz at 90.5°				
FAD	15	20	37	29	16	10	13
FMN			30	30		6	8
ADP-ribose	0	−6			−7		

TABLE V

FAD proton shifts as function of D_2O-dioxane-d-8 ratio (v/v) (0.025 M, 17°)

Solvent ratio	AC_8H	AC_2H	FC_5H	FC_8H	AC'_1H	FC_7CH_3	FC_6CH_3
			Hz				
100:0	1815	1715	1641	1626	1286	505	488
70:30	1855	1761	1693	1697	1309	532	517
50:50	1867	1780	1722	1726	1319	542	526

TABLE VI

Temperature dependence of ADP-ribose proton line widths[a] in three solvent systems

Temperature	D_2O		D_2O-dioxane (70:30, v/v)		D_2O-methanol (50:50, v/v)	
	AC_8H	AC_2H	AC_8H	AC_2H	AC_8H	AC_2H
°	*Hz*		*Hz*		*Hz*	
−29					4.3	3.9
−13.5					4.4	3.8
5	8.0	3.5	8.2	3.0	5.8	3.7
17	6.5	2.5	7.0	3.0	6.0	3.0
37	4.5	3.0	6.5	2.5	8.0	3.5
52	3.0	2.0	5.5	2.0	5.3	2.5
68	2.5	2.0	3.5	2.0	4.0	2.0
82	2.0	2.0	2.5	2.0		
90.5	2.0	2.0	2.0	2.0		

[a] The numbers represent the proton full-line widths at half height.

Solvent shifts of the FAD protons in going from D_2O to D_2O-dioxane arise since dioxane decreases both the fraction of folded molecules (all protons are deshielded and experience a shift to low field) as well as the fraction of intermolecularly stacked FAD molecules in solution (flavin protons experience an additional deshielding). Therefore, from Table IV, the solvent shifts are always greater for the dinucleotide than for the respective mononucleotide protons. For the AC_2H proton, these shifts are 46 and 6.5 Hz for FAD and ADP-ribose, respectively.

Considering the intermolecular solute-solute stacking interactions further, the data in Table IV show that the FC_8H proton undergoes the greatest shift (66 Hz in FMN and 71 Hz in FAD). Since this proton shift is also the most concentration-dependent (Table I) the dioxane must greatly disperse and decrease the fraction of stacked FMN molecules in solution. ADP-ribose proton shifts are only slightly concentration-dependent. Therefore these molecules are not involved in intermolecular associations and experience a very small solvent shift (Table IV). These solvent shifts may be explained by the decrease in the ring-current diamagnetic shielding of protons as neighboring rings are dissociated by dioxane. An increase in temperature also increases the dissociation as evidenced by the smaller (solvent) shifts at 90.5° (Table IV).

FAD proton shifts were also studied in 50:50 (v/v) D_2O-dioxane-*d*-8 solutions (Table V). All protons experience a further shift to low field with increasing concentrations of dioxane. This indicates that all dissociations are further enhanced.

Solvent shifts for the AC_2H, AC_8H, and $AC_1'H$ protons are in agreement with those observed by Hruska *et al.* (18) for purine, 6-methylpurine, and 9-ribosylpurine in D_2O-dioxane solutions for the solvent composition ratios under consideration. Hruska *et al.* also found that the AC_8H protons form hydrogen bonds with the solvent molecules, since the AC_8 carbon is the most electron-deficient center in purines. Protons involved in hydrogen-bonding interactions are invariably shifted to low field (19). The anomalous shifts to high field of the AC_8H proton as a function of temperature in ADP-ribose and FAD in D_2O-dioxane (Fig. 4) and in ADP-ribose in D_2O solutions (Fig. 5) may indicate the presence of this hydrogen bond.[3] Shifts to high field of hydrogen-bonded protons are often observed with increasing temperature and result from a decrease in the fraction of hydrogen-bonded species (20). The NAD AC_8H shift to high field with temperature (D_2O) may then also be ascribed to a decrease in the fraction of hydrogen-bonded species in solution (4).

Temperature Dependence of Line Widths—The line width at half height of the AC_8H proton in ADP-ribose shows a temperature dependence (Table VI) which is not observed for the AC_2H proton in ADP-ribose nor for the FAD protons. In D_2O-methanol, 50:50 (v/v), a sharp AC_8H line is observed at low temperature (−29°), broadens as the temperature is increased, and finally narrows again at temperatures above 60°. In D_2O and D_2O-dioxane solutions this proton line width narrows with an increase in temperature (5–68°). Over this temperature region, the line widths of other protons in ADP-ribose and FAD show a very slight temperature dependence. The ADP-ribose AC_2H proton line width at 5° is 3.0 Hz and decreases to 2.0 Hz at 90.5°. Furthermore, the line width of ADP AC_8H and AC_2H at ambient temperatures (17°) are nearly equal. These observations led us to postulate the presence of rotational isomers in ADP-ribose arising from restricted rotation about the glycosidic C'_1—N_9 bond. At −29° a "freezing in" of a preferred rotational isomer may occur, resulting in a sharp line. With an increase in temperature, the molecules may populate several states each with a slightly different AC_8H proton shift. This will give rise to line broadening (5°). As the temperature is increased above 60° the AC_8H and AC_2H proton line widths are equal, indicating a rapid rotation which will average out the slight variation in AC_8H chemical shifts (21). A temperature dependence of the line width of the AC_8H proton in FAD is not observed, possibly because these molecules are folded and stacked in solution.

[3] The FAD AC_8H proton in D_2O does not exhibit a shift to high field with an increase in temperature. This may arise because contributions to the chemical shift due to hydrogen-bond breaking (a net shift to high field) nearly equal the contributions from a decrease in the ring-current diamagnetic shielding of the protons (a net shift to low field).

Acknowledgments—We thank Dr. W. E. Blumberg for his many helpful suggestions, and Dr. D. J. Patel, Dr. J. M. McAndless, and Dr. R. Stewart for communicating their results prior to publication.

REFERENCES

1. Hesp, B., Calvin, M., and Hosokawa, K., *J. Biol. Chem.*, **244**, 5644 (1969).
2. Miles, D. W., and Urry, D. W., *Biochemistry*, **7**, 2791 (1968).
3. Jardetzky, O., and Wade-Jardetzky, N. G., *J. Biol. Chem.*, **241**, 85 (1966).
4. Sarma, R. H., Ross, V., and Kaplan, N. O., *Biochemistry*, **7**, 3052 (1968).
5. Hollis, D. P., *Biochemistry*, **6**, 2080 (1967).
6. Sarma, R. H., and Kaplan, N. O., *J. Biol. Chem.*, **244**, 771 (1969).
7. Patel, D. J., *Nature*, **221**, 1239 (1969).
8. Sarma, R. H., Dannies, P., and Kaplan, N. O., *Biochemistry*, **7**, 4359 (1968).
9. Schweizer, M. P., Broom, A. D., Ts'o, P. O. P., and Hollis, D. P., *J. Amer. Chem. Soc.*, **90**, 1042 (1968).
10. Chan, S. I., and Nelson, J. H., *J. Amer. Chem. Soc.*, **91**, 168 (1969).
11. Schaefer, T., and Schneider, W. G., *Can. J. Chem.*, **41**, 966 (1963).
12. Pullman, B., and Pullman, A., *Proc. Nat. Acad. Sci. U. S. A.*, **45**, 136 (1959).
13. Bullock, F. J., and Jardetzky, O., *J. Org. Chem.*, **30**, 2056 (1965).
14. McAndless, J. M., and Stewart, R., *J. Amer. Chem. Soc.*, in press.
15. Lumry, R., Biltonen, R., and Brandts, J. F., *Biopolymers*, **4**, 917 (1966).
16. Brahms, J., Maurizot, J. C., and Michelson, A. M., *J. Mol. Biol.*, **25**, 481 (1967).
17. Hruska, F. E., and Danyluk, S. S., *J. Amer. Chem. Soc.*, **90**, 3266 (1968).
18. Hruska, F. E., Bell, C. L., Victor, T. A., and Danyluk, S. S., *Biochemistry*, **7**, 3721 (1968).
19. Pople, J. A., Schneider, W. G., and Bernstein, H. J., *High resolution nuclear magnetic resonance*, McGraw-Hill, Toronto, 1959, Chapter 15.
20. Emsley, J. W., Feeney, J., and Sutcliffe, L. H., *High resolution nuclear magnetic resonance spectroscopy*. Pergamon Press, New York, 1965, Chapter 9, p. 537.
21. Phillips, W. D., *Ann. N. Y. Acad. Sci.*, **70**, 817 (1958).

THE JOURNAL OF BIOLOGICAL CHEMISTRY
Vol. 246, No. 17, Issue of September 10, pp. 5448-5453, 1971
Printed in U.S.A.

Mechanism of Action of *p*-Hydroxybenzoate Hydroxylase from *Pseudomonas putida*

III. THE ENZYME-SUBSTRATE COMPLEX*

(Received for publication, March 29, 1971)

NELSON TENG, GEORGE KOTOWYCZ,‡ AND MELVIN CALVIN

From the Laboratory of Chemical Biodynamics, Lawrence Radiation Laboratory, University of California, Berkeley, California 94720

KEIICHI HOSOKAWA§

From the Space Sciences Laboratory, University of California, Berkeley, California 94720

SUMMARY

The mechanism of action of *p*-hydroxybenzoate hydroxylase from *Pseudomonas putida*, strain M-6, has been investigated. The aromatic substrate analogues, benzoate, *p*-fluorobenzoate, *p*-chlorobenzoate, *p*-nitrobenzoate, *p*-aminobenzoate, and 6-hydroxynicotinate, are found to be competitive inhibitors. This finding differs from the previously reported noncompetitive behavior in a different buffer system.

The optical activity of the enzyme-inhibitor complex has been studied. From the kinetic and circular dichroism (CD) measurements, we have found that the carboxyl moiety is necessary and sufficient for the enzyme-substrate binding, whereas the hydroxyl group alone will not lead to binding. There are two classes of inhibitory analogues: one causes changes in CD spectra of the enzyme similar to those evoked by the substrate, and the other does not cause significant changes. The results indicate that more than one mode of enzyme-inhibitor interaction is involved. The CD of the enzyme-NADPH complex under anaerobic conditions suggests that the oxidized enzyme and reduced pyridine nucleotide form a complex, both in the absence and presence of the substrate, *p*-hydroxybenzoate. Furthermore, evidence for a ternary complex is given.

Hydroxylation plays an important role in the oxidative metabolism of aromatic compounds by bacteria. As a consequence, the mechanisms of action of those enzymes that mediate these hydroxylation reactions have stimulated profound interest. Two mono-oxygenases, *p*-hydroxybenzoate hydroxylase and salicylate hydroxylase, have been purified to homogeneity and investigated actively (1–4). Both mono-oxygenases are inducible. They are flavoproteins requiring FAD and reduced pyridine nucleotides as cofactors; however, they differ in specificity. Salicylate hydroxylase is specific for NADH, whereas *p*-hydroxybenzoate hydroxylase is specific for NADPH (2). The precise role of the flavin prosthetic group and the mechanism of action of the reduced pyridine nucleotide are not clear. Recently, investigation into the nature of the enzyme-substrate ternary complexes of salicylate hydroxylase by fluorometric method has been reported by Takemori *et al.* (5) and Suzuki, Takemori, and Katagiri (6). Higashi *et al.* (7) and Nakamura *et al.* (8) have reported kinetic studies on the reaction mechanism of *p*-hydroxybenzoate hydroxylase from *Pseudomonas desmolytica*.

To elucidate the mechanism of enzymatic catalysis it is pertinent to study the intermediate enzyme-substrate complexes and also the interactions of various analogues. Hesp, Calvin, and Hosokawa (2) reported that the circular dichroism spectrum of *p*-hydroxybenzoate hydroxylase was perturbed significantly upon addition of the substrate, *p*-hydroxybenzoate. CD[1] measurements thus provide a sensitive method of studying the enzyme-substrate complexes. This report presents the results of a kinetic study which indicates the competitive inhibitory behavior of some of the substituted benzoates, and the CD which suggests the interaction of the substrate and the bound FAD.

p-Hydroxybenzoate hydroxylase was induced in *Pseudomonas putida*. The two subspecies, *P. putida* and *P. desmolytica*, have functionally the same *p*-hydroxybenzoate hydroxylases; however, they differ in the subsequent oxidation of protocatechuate. The former uses the *ortho* cleavage pathway, yielding β-carboxy-cis-cis-muconate (9); the latter uses *meta* cleavage, yielding α-hydroxy-γ-carboxy-cis-cis-muconic semialdehyde (10).

EXPERIMENTAL PROCEDURE

Materials—Reagents used routinely for enzyme preparation and assays were the purest grade obtainable and purchased from

* This work was supported by the United States Atomic Energy Commission and by Grant GM-12932 from the National Institutes of Health and Grant NGR 04-003-020 from the National Aeronautics and Space Administration to the University of California, Berkeley, California. Paper I of this series is Reference 1 and Paper II is Reference 2.

‡ Recipient of a National Research Council of Canada-North Atlantic Treaty Organization Postdoctoral Fellowship (1968 to 1969). Present address, Department of Chemistry, The University of Alberta, Edmonton 7, Alberta, Canada.

§ Present address, The Worcester Foundation for Experimental Biology, Shrewsbury, Massachusetts.

[1] The abbreviation used is: CD, circular dichroism.

sources described previously (1). NADPH (grade II), NADH (Sigma grade), $NADP^+$ (grade III), NAD^+ (grade IV), FAD (grade III), *p*-fluorobenzoate, and *p*-aminobenzoate were purchased from Sigma. 6-Hydroxynicotinic acid was obtained from Aldrich. Phenol was from Mallinckrodt Chemical, and *p*-chlorobenzoate and *p*-nitrobenzoate were from Eastman Kodak. All the benzoate derivatives and phenol were twice crystallized from water before use. All other reagents were used directly without further purification.

Enzyme Preparation—*p*-Hydroxybenzoate hydroxylase from *P. putida*, strain M-6 (ATCC 17428), was prepared and purified by a modification of the method described in Paper I of this series. The method is similar to that reported in Paper II. The purified enzyme was stored in a stabilizing mixture at −70° until use, as described previously (2). The enzyme was found to denature slowly over a period of 1 year. The preservation of the enzyme was improved by storing it under an oxygen-free helium atmosphere.

Enzyme Assays—*p*-Hydroxybenzoate hydroxylase was assayed by spectrophotometric measurement of the substrate-dependent oxidation of NADPH. The procedure has been described earlier (1). The standard assay system is slightly modified from the previous method. The standard system contained in 3.0 ml, 67 mmoles of K_2HPO_4-KH_2PO_4 (pH 7.0), 3.3 μmoles of FAD, 0.13 mmole of NADPH, 0.67 mmole of *p*-hydroxybenzoate, enzyme, and deionized water. The unit of enzyme activity is defined as that amount of enzyme which oxidizes 1.0 μmole of NADPH per min under the conditions of the spectrophotometric assay.

Kinetic Measurements—The kinetics were studied spectrophotometrically by measuring the substrate-dependent oxidation of NADPH at 340 nm. Various substrate analogues were incubated for 2 min (or longer) before the measurement. All substrate analogues were adjusted to pH 7.5. All experiments were carried out at 20° ± 1°. Each experiment was repeated at least twice until consistent results were obtained.

Spectroscopic Methods—The absorption spectra were measured in a Cary model 15 spectrometer. The circular dichroism measurements were obtained with a Cary model 60 spectropolarimeter with a standard model 6001 CD accessory attachment. A Cary thermostatable cell compartment was used. CD spectra of the enzyme and the *p*-fluorobenzoate and NADPH complexes with the enzyme were studied at both 20° and 2°. Since spectra at the two temperatures were identical, subsequent inhibitor studies were carried out at 2° ± 0.1° where the enzyme is more stable. The slit width program was set for 15 A resolution and the time constant and scan speed were adjusted for best signal to noise ratio for each individual experiment. In all cases, an optical path length of 1.0 cm was used.

Anaerobic Experiment—We found it difficult to achieve anaerobic conditions efficiently without denaturing the enzyme in a cuvette suitable for optical activity measurement, while still permitting the addition of various reagents. We have used the method described previously (2). The space above the enzyme solution in the cuvette is first flushed with oxygen-free helium for 30 min. The enzyme solution is then bubbled with O_2-free helium at a rate of 1.5 cc per min for 15 min. If it is noticed that the enzyme is undergoing denaturation during the assay procedure, the result is discarded. We have been able to achieve strict anaerobic conditions with a negligible amount of denaturation.

RESULTS

Chemical Structure of Substrate Analogues—Several aromatic compounds which are structurally related to *p*-hydroxybenzoate but cannot serve as a substrate, inhibit the enzyme. The benzoic acid derivatives vary in strength according to the nature of the substituent and its ring position. The relative strength of a substituted benzoic acid is characterized by a substituent constant σ. The more electron-attracting a substituent is, the more positive is its σ value (relative to benzoate as zero). Conversely, the more strongly a substituent donates electrons, the more negative is its σ value. These values for the inhibitory benzoates are given in Table I.

TABLE I

Inhibitory effect of substrate analogues

Substrate analogues	Hammett substituent constants (σ)[a]	Inhibition[b]	K_i[c]
		%	M
p-Nitrobenzoate	0.778 ± 0.02	16	$(4.2 \pm 1.3) \times 10^{-4}$
6-Hydroxynicotinate		17	$(3.1 \pm 0.4) \times 10^{-4}$
p-Chlorobenzoate	0.227 ± 0.02	12	$(1.8 \pm 0.3) \times 10^{-4}$
p-Fluorobenzoate	0.062 ± 0.02	35	$(7.6 \pm 1.9) \times 10^{-5}$
Benzoate	0	25	$(5.9 \pm 0.5) \times 10^{-5}$
p-Aminobenzoate	−0.66 ± 0.1	81	$(4.2 \pm 0.9) \times 10^{-6}$
p-Hydroxybenzoate	−0.37 ± 0.04	0	$K_m = (1.2 \pm 0.5) \times 10^{-5}$

[a] σ values were based on ionization of substituted benzoic acids (11).

[b] Inhibition was measured by the *p*-hydroxybenzoate-dependent oxidation of NADPH in the presence of 3.44 μg of enzyme, 0.1 mM *p*-hydroxybenzoate, and 0.33 mM substrate analogue. The other conditions were the same as the standard assay system mentioned under "Experimental Procedure."

[c] K_i values were calculated, assuming a completely competitive inhibition, by a linear regression analysis of the equation

$$\frac{[S]}{v} = \frac{[S]}{V_{max}} + \frac{K_m}{V_{max}}\left(1 + \frac{[I]}{K_i}\right)$$

where S and I denote the substrate, *p*-hydroxybenzoate, and the inhibitory substrate analogue, respectively, v and V_{max} are the reaction velocity and maximal reaction velocity, K_m is the Michaelis-Menten constant, and K_i is the inhibitor dissociation constant. In our kinetic measurement, the velocity determinations probably are reasonably homogeneous in variance. If the variance of v is σ^2, the variance of $[S]/v$ can be shown to be $\sigma[S]/v^3$ (12). Therefore, in fitting the linear form to the above equation, the proper weight $v^3/[S]^2$ is used. The standard error of K_i is estimated by standard procedure of propagation of error. All computations were done on a CDC 6600 computer.

Kinetic Study—It was reported previously (1) that benzoate and a series of its analogues were inhibitory to the activity of *p*-hydroxybenzoate hydroxylase. With Tris-HCl buffer system for assay, the inhibition was found to be noncompetitive. However, enzyme activity drops very quickly during the assay in Tris buffer system (pH 8.0). Accordingly, there was inaccuracy in determining the initial velocity of the reaction. We could overcome this problem by replacing Tris-HCl buffer with a phosphate buffer system (pH 7.5) in which oxidation of NADPH proceeded almost linearly even at very low concentrations of NADPH and enzyme.

By employing the improved assay system, we have found that benzoate, *p*-fluorobenzoate, *p*-chlorobenzoate, *p*-nitrobenzoate, *p*-aminobenzoate, and 6-hydroxynicotinate are all competitive inhibitors. Fig. 1 shows the Lineweaver-Burk plots of the enzyme activity in the presence of these inhibitors. All of them are typical competitive inhibitions. The K_i values were determined by the method described by Wilkinson (12) and Cleland (14). The results are given Table I.

A Hammett plot of the action of the substituted benzoate derivatives is given in Fig. 2, in which the logarithms of the inhibition constants (K_i) are plotted against their σ values. They fit the Hammett equation very well. The "reaction constant," ρ, which is the slope of the Hammett plot, is estimated to be 1.78. The significance of ρ is that it measures the sensitivity of the reaction to the electrical effects of substituents in the *meta* and *para* positions. A positive ρ value suggests that the inhibition is favored by increasing the nucleophilic reactivity of the carboxyl group.

Phenol shows no inhibition at concentrations below 0.01 M.

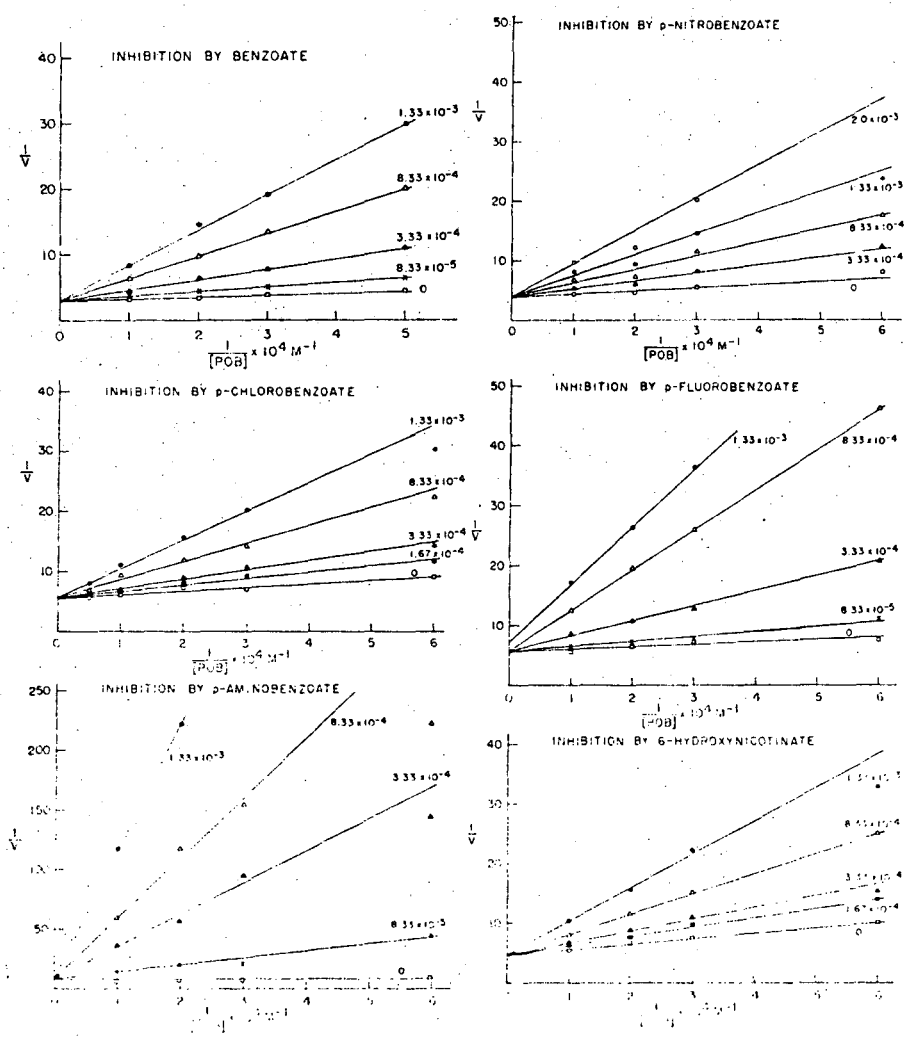

FIG. 1: Effect of benzoate analogues on the activity of *p*-hydroxybenzoate hydroxylase: double reciprocal plot. The data are plotted by the method of Lineweaver and Burk (13). Assay conditions were described under "Experimental Procedure." The reciprocal velocity, $1/v$, is in arbitrary units. The molar concentrations of benzoate are indicated on the plot.

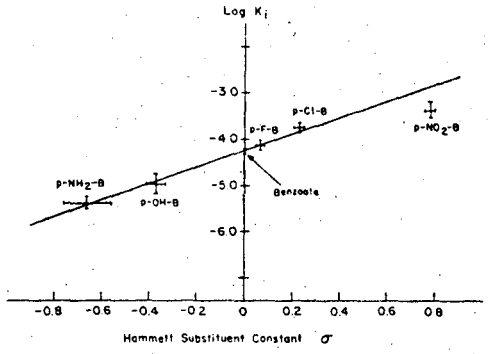

FIG. 2. Action of the substituted benzoate derivatives. K_i represents the inhibition constants evaluated in Table II. The standard errors in log K_i are indicated by the *vertical error bars*. The Hammett substituent constants (σ) are summarized in Table I. The estimated errors of σ are plotted as *horizontal error bars*. The slope of the line is 1.78.

Inhibitory effects occur at concentrations greater than 0.01 M, due presumably to nonspecific binding to the enzyme. The results are given in Table II.

The above findings suggest strongly that the carboxyl group is necessary for the substrate analogues to inhibit the enzyme and possibly is involved in the binding at the active site.

Circular Dichroism Spectra of Enzyme-Inhibitor Complexes—The CD spectrum of the holoenzyme of *p*-hydroxybenzoate hydroxylase has been reported previously (2). The effect of the substrate, *p*-hydroxybenzoate, on the holoenzyme manifests itself in the visible region of the FAD absorption. The perturbation of the holoenzyme CD spectrum upon addition of *p*-hydroxybenzoate was given in Paper II. The CD spectra of the enzyme-bound FAD holoenzyme in the absence and presence of the inhibitors and substrate, *p*-hydroxybenzoate, are given in Figs. 3 and 4. The effect of benzoate on the CD spectrum of *p*-hydroxybenzoate hydroxylase was described earlier (2). A large change was observed in the CD spectrum of *p*-hydroxybenzoate hydroxylase upon addition of benzoate.

p-Fluorobenzoate—The CD spectrum of the enzyme was changed by the addition of 10^{-3} M *p*-fluorobenzoate. The 367 nm CD was slightly shifted and decreased. The 455 nm band also decreased. Addition of 10^{-3} M *p*-hydroxybenzoate to the enzyme *p*-fluorobenzoate system produced the familiar change of the CD spectrum characteristic of the enzyme *p*-hydroxybenzoate complex.

6-Hydroxynicotinate—The effect on the CD spectrum of the enzyme caused by addition of 10^{-3} M 6-hydroxynicotinate was significant. Both the 367 nm and 455 nm CD bands decreased markedly. When 10^{-3} M *p*-hydroxybenzoate was added to the system, enhancement of the 455 nm band was observed. The general appearance of the CD spectrum resembled that of the enzyme *p*-hydroxybenzoate system.

p-Aminobenzoate—In contrast to the effect produced by *p*-fluorobenzoate, benzoate, and 6-hydroxynicotinate, the addition of 10^{-3} M *p*-aminobenzoate caused almost no modification of the CD spectrum of the enzyme except a slight decrease of the shoulder at 340 nm. Even after the addition of 10^{-3} M *p*-hydroxybenzoate, no further change was observed. This experiment was repeated with the order of addition of *p*-aminobenzoate and *p*-hydroxybenzoate reversed. The same final CD spectrum was obtained. Since *p*-aminobenzoate did inhibit the enzyme, this may suggest that the interaction of *p*-aminobenzoate with the enzyme is such that it does not manifest itself in a CD modification. This result indicates the possibility of a different mode of binding between the enzyme and *p*-aminobenzoate from that between the enzyme and *p*-fluorobenzoate.

p-Chlorobenzoate and p-Nitrobenzoate—These substrate analogues have been shown to be the weakest inhibitors (Table I). The CD spectra of the substrate analogue-enzyme mixtures are not significantly modified.

TABLE II

Phenol inhibition

The standard enzyme assay system was utilized with 1 mM *p*-hydroxybenzoate.

Phenol concentration	Inhibition
M	%
10^{-1}	78
5×10^{-2}	51.5
10^{-2}	0
10^{-3}	0
8.3×10^{-4}	0
0	0

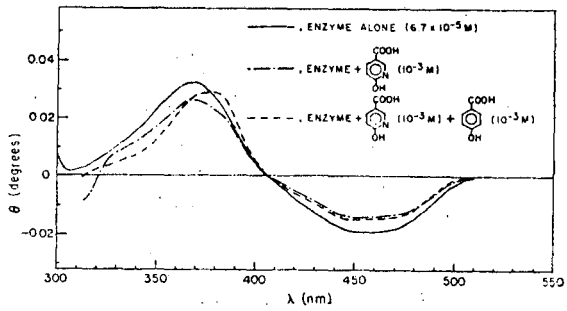

FIG. 3. CD spectrum of *p*-hydroxybenzoate hydroxylase in the presence of 6-hydroxynicotinate and *p*-hydroxybenzoate. The enzyme (6.7×10^{-5} M) is in 0.05 M potassium phosphate buffer, pH 7.5; temperature 2°; path length, 1.0 cm.

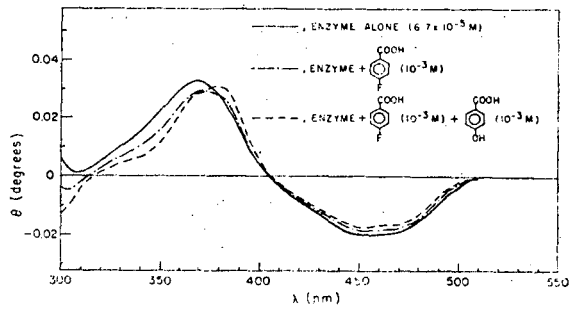

FIG. 4. CD spectrum of *p*-hydroxybenzoate hydroxylase in the presence of *p*-fluorobenzoate and *p*-hydroxybenzoate. The enzyme (6.7×10^{-5} M) is in 0.05 M potassium phosphate buffer, pH 7.5; temperature 2°; path length, 1.0 cm.

TABLE III

Effect of reduced and oxidized pyridine nucleotides on CD spectrum[a] of p-hydroxybenzoate hydroxylase

Condition	p-Hydroxybenzoate	NADPH	NADP	NADH
Aerobic	Absent	No changes, but the conclusion cannot be deduced, because NADPH is oxidized in this system.	No changes.	
	Present	NADPH is oxidized quickly.	Familiar changes.	
Anaerobic	Absent	Marked changes.	No effect.	No significant changes.
	Present	Further changes, more than above.		Slightly affected.

[a] Wave length between 300 and 500 nm.

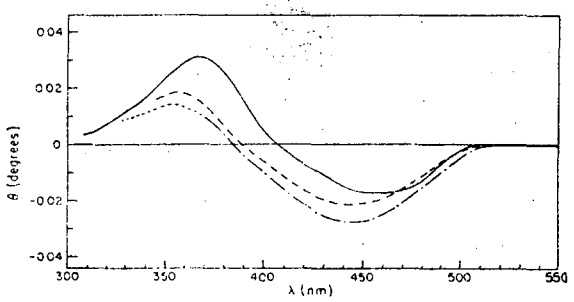

FIG. 5. The effect of NADPH on the CD spectrum of *p*-hydroxybenzoate hydroxylase. The enzyme is in 0.05 M potassium phosphate buffer, pH 7.5; temperature 2°; path length, 1.0 cm; anaerobic conditions. ——, enzyme alone (6.9×10^{-5} M); - - -, enzyme in the presence of 10^{-3} M NADPH; — - —, enzyme in the presence of 10^{-3} M NADPH and 10^{-3} M *p*-hydroxybenzoate. ----, indicates region of the curve where signal to noise ratio is poor.

Evidence for Direct Binding of NADPH to p-Hydroxybenzoate Hydroxylase—Since CD spectra of *p*-hydroxybenzoate hydroxylase served as a sensitive means of detecting the formation of the enzyme-substrate complex, we extended CD measurements to the study of the interaction of NADPH with the enzyme.

Under anaerobic conditions, which were produced by flushing the system with helium, the effect of NADPH on the CD spectra of free *p*-hydroxybenzoate hydroxylase was examined. Upon addition of NADPH, there were marked changes (as shown in Fig. 5) in the CD spectra of the enzyme. In the presence of NADPH, both the negative and positive CD bands of the free enzyme (maxima at 455 nm and 367 nm, respectively) are blue-shifted. In addition, a negative contribution to the optical rotation is observed. When *p*-hydroxybenzoate is added in addition to NADPH under anaerobic conditions, the broad negative band of the CD spectrum of the enzyme-NADPH mixture becomes even more negative. The results suggest that *p*-hydroxybenzoate hydroxylase forms a complex with NADPH both in the absence and presence of *p*-hydroxybenzoate.

In order to find whether NADPH or its oxidation product, NADP, is responsible for this binding, the effect of NADP on the CD spectra of the enzyme was examined. Under anaerobic conditions, there are no significant changes in the CD spectra of the enzyme upon addition of NADP. NADP does not affect the familiar substrate-induced changes in CD spectra of the enzyme under aerobic conditions. These facts indicate that there is probably no interaction between NADP and *p*-hydroxybenzoate hydroxylase or, at least, it does not manifest itself in a CD modification.

NADH does not induce significant changes in CD spectra of free enzyme solution under anaerobic conditions. Therefore, the enzyme-NADPH complex is highly specific, which is consistent with previous reports (1, 2).

From the results described above, we cannot determine the order of the binding of the substrates, NADPH and *p*-hydroxybenzoate, to the holoenzyme in the ternary enzyme-*p*-hydroxybenzoate-NADPH complex. We leave it for future study.

DISCUSSION

As has been reported, discrepancies were found among the modes of inhibition of *p*-hydroxybenzoate hydroxylase by a number of substrate analogues. The analogues, such as *p*-fluorobenzoate, *p*-aminobenzoate, benzoate, and others, inhibited *p*-hydroxybenzoate hydroxylase from *P. putida* A3.12 in a noncompetitive manner (1), whereas these analogues were competitive inhibitors to the *p*-hydroxybenzoate hydroxylase from *P. putida* M-6 (this report) and *P. desmolytica* (7). These discrepancies may be ascribed to the different buffer systems used. In the Tris-HCl buffer, pH optimum is 8.0 as compared to 7.5 (1) and 7.0 (2) found in the potassium phosphate buffer system, and furthermore, the enzyme activity is found to be inhibited, increasingly and markedly, during the assay due to the presence of chloride ion.[2] This inhibitory action of chloride ion made the calculation of enzyme activity inaccurate and resulted earlier in an erroneous interpretation of the mode of inhibition.

The competitive behaviors of the benzoate derivatives indicate strongly that the carboxyl group is essential in the binding. Phenol does not inhibit the enzyme up to a very high concentration at which nonspecific binding may take place. The above findings, in conjunction with the fact that the enzyme will only catalyze *p*-hydroxybenzoate and will not catalyze the other analogues to any significant extent (1), lead to the following hypotheses: the carboxyl moiety participates in binding with the primary site, providing an "anchoring" and, subsequently, the hydroxyl group is bound to a secondary site to facilitate the catalytic activity. This is in agreement with the two binding site model proposed previously (2, 7, 8). The positive "reaction constant" ($\rho = 1.78$) obtained from the Hammett plot (Fig. 2) suggests that the primary binding site is favored by a nucleophilic attack.

Examination of the enzyme-inhibitor complex by CD spectroscopy showed that there are two classes of substrate analogues which competitively inhibit enzyme activity. One class of substrate analogues causes changes in CD spectra, and the

[2] R. G. Kallen and K. Hosokawa, unpublished results.

other class shows no significant changes. *p*-Fluorobenzoate belongs to the former, and *p*-aminobenzoate is an example of the latter.

p-Fluorobenzoate binds to the enzyme, as evidenced by a change in the CD spectrum upon addition to free enzyme. If *p*-hydroxybenzoate is added to the *p*-fluorobenzoate-enzyme complex, the CD spectrum is converted to one similar to the spectrum for the *p*-hydroxybenzoate-enzyme complex. This indicates that *p*-fluorobenzoate binds to the same site as the substrate, and can be displaced by the *p*-hydroxybenzoate. On the other hand, *p*-aminobenzoate does not produce significant changes in the CD spectrum of the free enzyme, although it inhibits the enzyme activity in a competitive manner. *p*-Aminobenzoate may bind to a site other than the one binding *p*-fluorobenzoate, and thus may interfere with the over-all reaction of *p*-hydroxybenzoate hydroxylase. Furthermore, the CD spectrum of the *p*-aminobenzoate-enzyme mixture is not affected significantly upon addition of *p*-hydroxybenzoate. Conversely, the CD spectrum characteristic of the enzyme-substrate complex is converted to the one similar to the free enzyme spectrum by the addition of *p*-aminobenzoate. The results show that the binding of *p*-aminobenzoate to the enzyme causes a secondary effect on the substrate binding site so that *p*-hydroxybenzoate can no longer bind to its site, resulting in the inhibition of activity.

The different modes of binding may be understood in terms of a steric hindrance effect at the hydroxyl binding site. Examination of the CPK space filling models and interatomic distances and configurations (15) of the inhibitors indicates that the class of inhibitors which does not modify the CD spectrum of the enzyme has a benzoate substituent ($-NH_2$, $-NO_2$, $-Cl$) bulkier than that of the other class ($-H$, $-F$, $-OH$).

By CD studies, we obtained evidence that NADPH binds to free *p*-hydroxybenzoate hydroxylase. The binding is so specific that NADH does not become associated with the enzyme. These findings well explain the specific requirement of NADPH for the enzymatic hydroxylation of *p*-hydroxybenzoate.

A preliminary proton magnetic resonance study of the relaxation times of the NADPH protons in the presence of *p*-hydroxybenzoate hydroxylase revealed NADPH binding with the enzyme. This result supports the above-described CD study that NADPH specifically interacts with *p*-hydroxybenzoate hydroxylase.

Acknowledgments—We wish to thank Mrs. Ellen G. Aguayo for her assistance in the purification of *p*-hydroxybenzoate hydroxylase and Dr. Richard M. Lemmon for helpful discussion.

REFERENCES

1. Hosokawa, K., and Stanier, R. Y., *J. Biol. Chem.*, **241**, 2453 (1966).
2. Hesp, B., Calvin, M., and Hosokawa, K., *J. Biol. Chem.*, **244**, 5644 (1969).
3. Yamamoto, S., Katagiri, M., Maeno, H., and Hayaishi, O., *J. Biol. Chem.*, **240**, 3408 (1965).
4. Katagiri, M., Maeno, H., Yamamoto, S., Hayaishi, O., Kitao, T., and Oae, S., *J. Biol. Chem.*, **240**, 3414 (1965).
5. Takemori, S., Yasuda, H., Mihaya, K., Suzuki, K., and Katagiri, M., *Biochim. Biophys. Acta*, **191**, 58, 69 (1969).
6. Suzuki, K., Takemori, S., and Katagiri, M., *Biochim. Biophys. Acta*, **191**, 77 (1969).
7. Higashi, N., Nakamura, S., Yano, K., and Arima, K., *Agr. Biol. Chem.*, **34**, 964 (1970).
8. Nakamura, S., Ogura, Y., Yano, K., Higashi, N., and Arima, K., *Biochemistry*, **9**, 3235 (1970).
9. MacDonald, D. L., Stanier, R. Y., and Ingraham, J. L., *J. Biol. Chem.*, **210**, 809 (1954).
10. Trippett, K. S., Dagley, S., and Stophen, D. A., *Biochem. J.*, **76**, 97 (1968).
11. McDaniel, D. H., and Brown, H. C., *J. Org. Chem.*, **23**, 420 (1958).
12. Wilkinson, G. N., *Biochem. J.*, **80**, 324 (1961).
13. Lineweaver, H., and Burk, D., *J. Amer. Chem. Soc.*, **56**, 658 (1934).
14. Cleland, W. W., *Adv. Enzymol.*, **29**, 1 (1967).
15. Sutton, L. E., *Table of interatomic distances and configuration in molecules and ions*, Special Publication No. 18, The Chemical Society, London, 1965, p. S 1s.

[Reprinted from the Journal of the American Chemical Society, 93, 6257 (1971).]
Copyright 1971 by the American Chemical Society and reprinted by permission of the copyright owner.

Calculation of the Rotational Strengths of Mononucleosides[1]

Nelson N. H. Teng,[2] Martin S. Itzkowitz, and Ignacio Tinoco, Jr.*

Contribution from the Department of Chemistry and the Laboratory of Chemical Biodynamics, Lawrence Radiation Laboratory, University of California, Berkeley, California 94720. *Received February 12, 1971*

Abstract: The rotational strengths of the two longer wavelength transitions, B_{2U} and B_{1U}, of four mononucleosides (adenosine, guanosine, uridine, and cytidine) as a function of the glycosidic rotational angles have been investigated theoretically. The transition in each base is characterized by transition monopoles; the sugar is treated as a sum of bond polarizabilities. The interaction among these polarizabilities is also considered. Rotational strengths were calculated using three different sets of transition monopoles and many combinations of bond polarizabilities. We conclude that adenosine, uridine, and cytidine may have primarily one conformation, but that in guanosine the base is not definitely fixed with respect to the ribose. Calculation on different anomeric nucleosides of adenosine and uridine shows that the configuration at the anomeric carbon C-1′ determines the sign of the optical rotation. The configuration at C-2′ influences the glycosidic angular dependence of rotational strength more profoundly than that at C-3′ and C-5′. These results are in good agreement with experiments. The signs and magnitude of the calculated rotational strengths are in good agreement with experiment for the anti conformation of all the isomers of adenosine. As the conformation of the nucleosides in B-form DNA is quite different from the anti form, we calculate that the rotational strengths of the nucleosides in the polynucleotide are very different from those in solution.

Many workers have measured the circular dichroism (CD) and optical rotatory dispersion (ORD) of polynucleotides, and have shown that optical activity is an important tool for conformational assignments. Theories have been developed to facilitate the interpretation of the spectra of polynucleotides.[3,4] However, in these theories, the CD and ORD of the monomer units themselves have been ignored. Recently, experimental and theoretical studies of the optical activity and conformation of nucleosides have appeared.[5-7] In particular, an extended series of articles by Miles *et al.*,[8] have investigated this problem in detail.

In the present paper we have used an improved version of Kirkwood polarizability theory to include the presence of a classical polarizability near a quantum system. The rotational strengths of mononucleosides are calculated using transition monopoles on the bases interacting with polarizable bonds of the sugars. We try to examine the calculations critically. Three different sets of transition monopoles have been employed with various degrees of success. The effect of different values of bond polarizability and variation of the positions of furanosyl OH groups have also been examined. The calculated rotational strengths as a function of the glycosidic angle are in qualitative agreement

(1) Supported in part by research Grant No. GM 10840 from the National Institutes of Health and by the U. S. Atomic Energy Commission.

(2) University of California Predoctoral Fellowship.

(3) C. A. Bush and I. Tinoco, Jr., *J. Mol. Biol.*, 23, 601 (1967).

(4) W. C. Johnson, Jr., and I. Tinoco, Jr., *Biopolymers*, 7, 727 (1969).

(5) P. A. Hart and J. P. Davis, *J. Amer. Chem. Soc.*, 91, 512 (1969).

(6) G. T. Rogers and T. L. V. Ulbricht, *Biochem. Biophys. Res. Commun.*, 39, 2, 414 (1970).

(7) G. T. Rogers and T. L. V. Ulbricht, *ibid.*, 39, 419 (1970).

(8) D. W. Miles, W. H. Inskeep, M. J. Robins, M. W. Winkley, R. K. Robins, and H. Eyring, *J. Amer. Chem. Soc.*, 92, 3872 (1970), and references therein.

with calculations of Miles, *et al.*, using bond transition dipoles on the bases.

In the next section a detailed description of the theoretical method is given, in section II we discuss the numerical methods and the data used, and in section III we demonstrate the application of the theory to the four mononucleosides found in nucleic acids and to various anomeric isomers of adenosine and uridine.

I. Theory

Rosenfeld[9] characterized the optical rotation by the rotational strength for the optical transition from O to A, $R_{OA} = Im(\mu_{OA} \cdot \mathbf{m}_{AO})$. *Im* denotes the imaginary part of a complex number. μ_{OA} is the electric dipole transition moment vector and $\mathbf{m}_{AO}$ is the magnetic dipole transition moment vector defined as follows

$$\mu_{OA} = \sum_j \langle O|\mu_j|A\rangle \quad (1)$$

$$\mathbf{m}_{AO} = \frac{e}{2mc}\sum_j \mathbf{R}_j \times \langle A|\mathbf{P}_j|O\rangle + \sum_j \langle A|\mathbf{m}_j'|O\rangle \quad (2)$$

where $\mathbf{R}_j$ is the vector distance from an arbitrary origin to the origin of group j; μ_j is the electric dipole moment operator of group j; $\mathbf{P}_j$ is the linear momentum operator of group j; $\mathbf{m}_j'$ is the magnetic moment operator of group j relative to the origin in group j. This origin is usually selected to minimize the contribution of $\mathbf{m}_j'$ to rotational strength. c, e, and m are the usual notations for the speed of light, electronic charge, and electronic mass. The molecular wave functions for states O and A are $|0\rangle$ and $|A\rangle$. If we drop the magnetic dipole term which is expected to be small, the expression for rotational strength is

$$R_{OA} = (-\pi\nu_{OA}/2c)\sum_{i\neq j}\mathbf{R}_{ij}\cdot\langle O|\mu_i|A\rangle \times \langle A|\mu_j|O\rangle \quad (3)$$

where ν_{OA} is the frequency of the transition and $\mathbf{R}_{ij} = \mathbf{R}_j - \mathbf{R}_i$.

It can be seen that the optical activity originates from the interaction between electric transition dipoles located asymmetrically with respect to one another. In eq 3 we have resolved R_{OA} into groups. The obvious separation into groups for mononucleosides would be to treat the base as the major chromophore and the furanose as an asymmetric substituent. The furanose is further subdivided into bonds. For a particular transition O → A of the base, which is far removed in energy from any transitions in the furanose, it is a good approximation to replace the transition dipole from the bonds of the furanose by the dipole that would be induced in a classical polarizability placed within the transition field of the base.

$$\mu_{jAO} = \alpha_j \cdot \mathbf{E}_j^{eff} \quad (4)$$

where α_j is the polarizability tensor of the jth furanose bond and $\mathbf{E}_j^{eff}$ is the effective field at the jth bond due to the transition O → A.

To evaluate the effective field $\mathbf{E}_j^{eff}$, one expands the molecular wave functions in a linear combination of atomic orbitals

$$|O\rangle = \sum_s C_{Os}|s\rangle$$

$$|A\rangle = \sum_s C_{As}|s\rangle$$

We obtain

$$\mathbf{E}_j^{eff} = -\nabla_j\left\langle A\left|\frac{1}{r_j}\right|O\right\rangle = -\nabla_j\sum_{s,t}C_{As}^*C_{Ot}\left\langle s\left|\frac{1}{r_j}\right|t\right\rangle \quad (5)$$

The standard point monopole approximation sets

$$\left\langle s\left|\frac{1}{r_j}\right|t\right\rangle = \delta_{st}\frac{1}{r_{sj}} \quad (6)$$

where δ_{st} is the Kronecker δ.

Alternatively, one may treat $\Psi_O|\Psi_A$ as a charge distribution and do a multipole expansion ($\Sigma_j\mathbf{E}_j^{eff}$) about the center of the charges. The practical limit in terms of computer programming on the CDC 6600 computer used for our calculations is the octupole term, and convergence is poor. We abandoned this method in favor of the use of eq 6. In the hope of increased accuracy we calculated the integrals $\langle s|1/r_i|s\rangle$ in terms of Slater $2p\pi$ orbitals to obtain $\mathbf{E}_j^{eff}$. This was found to make a negligible correction to rotational strengths; we therefore used for a zero-order $\mathbf{E}_j^{eff}$

$$\mathbf{E}_j^{eff} = \sum_s \rho_s\frac{\mathbf{r}_{js}}{|r_{js}|^3} \quad (7)$$

where $\rho_s = C_{As}C_{Os}$ is the monopole charge of atom s due to the base transition O → A. $\mathbf{r}_{js}$ is a position vector from the jth group to the sth monopole. By combining eq 3, 4, and 7, we have an expression for the rotational strength of transition O → A in the base of a nucleoside. The base is represented by transition monopoles on each atom and the furanose is approximated by bond polarizabilities.

$$R_{OA} = \left(-\frac{\pi\nu_{OA}}{2c}\right)\sum_{i\neq j}\sum_s \rho_s\mathbf{R}_{ij}\cdot(\mu_{iAO} \times \alpha_j\cdot r_{js})/|r_{js}|^3 \quad (8)$$

where $\mathbf{R}_{ir}$ is the distance from the base transition dipole (μ_{iAO}) to bond j in the furanose. This is the most commonly used expression for calculating optical activity under conditions mentioned above. However, this expression has only considered the monopole field caused by the base and has ignored the interaction among the furanose bonds. This approximation may be good in situations where the asymmetric perturbation is an aliphatic chain.[10] But in the furanose ring, for the most part, the sugar bonds are much closer to each other than to the base, so each bond will feel the effect of the induced dipoles in all other bonds. To include this effect we replace $\mathbf{E}_j^{eff}$ by a more complete expression

$$\mu_{jAO} = \alpha_j\cdot\mathbf{E}_j^{eff} = \alpha_j\cdot\left[\sum_s \rho_s\frac{\mathbf{r}_{js}}{|r_{js}|^3} - \sum_k \mathbf{T}_{jk}\cdot\mu_{kAO}\right] \quad (9)$$

where $\mathbf{T}_{jk} = (1 - 3\mathbf{r}_{jk}\mathbf{r}_{jk}/r_{jk}^2)(1/r_{jk}^3)$, the dipole interaction tensor, between points j and k.

These coupled linear equations can be solved for μ_{jAO}. Substituting eq 10 in 3, we have the final expression for the rotational strength with the furanose

$$\mu_{jAO} = \sum_k (\mathbf{1} + \alpha\mathbf{T})_{jk}^{-1}\cdot\alpha_k\cdot\sum_s \rho_s\frac{\mathbf{r}_{js}}{|r_{js}|^3} \quad (10)$$

(9) L. Rosenfeld, *Z. Phys.*, 52, 161 (1928).

(10) K. Philipson, S. Tsai, and K. Sauer, *J. Phys. Chem.*, 75, 1440 (1971).

interaction treated self-consistently. For all calculations R_{OA} was evaluated using transition monopoles only, as in eq 8, and also self-consistently including the sugar bond–bond induced dipole coupling as in eq 11.

$$R_{OA} = \left(-\frac{\pi\nu_{OA}}{2c}\right)\sum_{i\neq j}\sum_{k}\sum_{s}\rho_s\mathbf{R}_{ij}\cdot\boldsymbol{\mu}_{iAO}\times (1+\alpha\mathbf{T})_{jk}^{-1}\cdot\boldsymbol{\alpha}_k\cdot\mathbf{r}_{ks}/|r_{ks}|^3 \quad (11)$$

There are other potential contributions to rotational strengths which we do not consider at this time. These include effects of magnetic dipole transition moments and effects of the static fields of the sugar. We think these terms are small, in agreement with the earlier workers,[3] but they should be investigated more thoroughly.

II. Calculation

We consider each base to have two $\pi \rightarrow \pi^*$ transitions with maxima between 240 and 280 mμ. The transition frequency ν_{OA} is taken as the location of the major experimental uv absorption maximum.

Coordinates. The coordinates used in the computation are taken from Spencer[11] for the bases (Table I) and Sundaralingam and Jensen[12] for the 2′-endo ribose and 3′-endo ribose. The coordinates for the α anomers were obtained by reflection from that of β nucleosides about the plane of C-1′, C-2′, and O′ of the furanose. The numbering system and the nomenclature for the pentofuranoses are shown in Figure 1.

Table I.[11] Atomic Coordinates of Purine and Pyrimidine Bases

Atom	X, Å	Y, Å	Atom	X, Å	Y, Å
	Adenine			Cytosine	
N-1	−2.791	4.407	N-1	0.000	1.470
C-2	−3.201	3.134	C-2	−1.207	2.139
N-3	−2.391	2.078	N-3	−1.231	3.489
C-4	−1.079	2.298	C-4	−0.070	4.132
C-5	−0.604	3.583	C-5	1.157	3.504
C-6	−1.500	4.633	C-6	1.181	2.125
N-7	0.763	3.598	O-2	−2.253	1.511
C-8	1.055	2.280	N-4	−0.094	5.472
N-9	0.000	1.470			
N-6	−1.041	5.892			
	Guanine			Uracil	
N-1	−2.799	4.348	N-1	0.000	1.470
C-2	−3.205	3.051	C-2	−1.207	2.139
N-3	−2.378	2.010	N-3	−1.159	3.518
C-4	−1.079	2.298	C-4	0.010	4.251
C-5	−0.604	3.583	C-5	1.205	3.504
C-6	−1.462	4.702	C-6	1.181	2.125
N-7	0.763	3.598	O-2	−2.269	1.538
C-8	1.055	2.280	O-4	0.010	5.471
N-9	0.000	1.470			
N-2	−4.523	2.807			
O-6	−1.045	5.848			

The conformation of the furanose has been the subject of debate.[13-15] We have used the 2′-endo conformation, consistent with the majority of crystal structures of nucleosides, for most of the calculations. The 2′-endo ribose and 3′-endo deoxyribose coordinates are given in Table II. Coordinates of the other sugars were obtained by interchanging H and OH atoms and changing bond lengths. In solution, the positions of the hydroxyl groups of the furanose are not precisely known. In an effort to determine the influence of OH position on R_{OA}, we have rotated the OH groups about their individual CO axes for both adenosine and uridine. The effect on the calculated R_{OA} is small: the shape of the curve when R_{OA} is plotted *vs.* the glycosidic angle (ϕ_{CN}) is not significantly altered. Slight variation in magnitude of R_{OA} is found when the OH at the C-2′

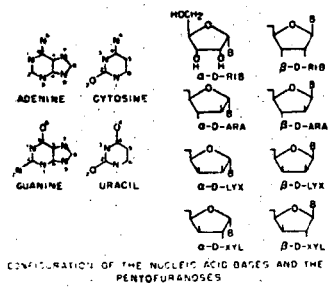

Figure 1. Nomenclatures and configurations of the nucleic acid bases and the pentofuranoses.

Table II. Coordinates of 2′-Endo Ribose and 3′-Endo Deoxyribose[12]

Atoms	x	y	z
	2′-Endo Ribose		
C-1	0.00	0.00	0.00
H-1	−0.51	−0.16	0.74
O-1	1.35	−0.43	0.00
C-2	−0.62	−0.58	−1.25
H-2	−0.26	0.08	−1.89
O-2	−2.02	−0.57	−1.26
OH-2	−2.60	−1.09	−0.59
C-3	0.08	−1.94	−1.31
H-3	0.02	−2.33	−2.02
O-3	−0.53	−2.80	−0.34
OH-3	−0.48	−3.80	−0.42
C-4	1.51	−1.59	−0.86
H-4	1.81	−2.46	−0.38
C-5	2.48	−1.28	−1.97
H-5	3.37	−0.73	−1.40
H-5′	2.98	−2.14	−2.36
O-5	1.95	−0.44	−3.00
OH-5	1.88	−1.15	−3.69
	3′-Endo Deoxyribose		
C-1	0.00	0.00	0.00
H-1	−0.40	−0.53	0.96
O-1	1.37	−0.43	0.00
C-2	−0.68	−0.65	−1.21
H-2	−1.28	−1.47	−1.11
H-2′	−1.35	−0.16	−1.86
C-3	0.52	−1.08	−2.10
H-3	0.87	−0.28	−2.80
O-3	−0.24	−2.16	−2.96
OH-3	0.06	−3.00	−2.40
C-4	1.57	−1.37	−1.08
H-4	1.20	−2.36	−0.70
C-5	3.02	−1.26	−1.52
H-5	3.71	−1.64	−0.80
H-5′	3.28	−1.80	−2.39
O-5	3.27	0.09	−2.04
OH-5	4.06	0.23	−2.73

(11) M. Spencer, *Acta Crystallogr.*, 12, 59 (1969).
(12) M. Sundaralingam and L. H. Jensen, *J. Mol. Biol.*, 13, 914 (1965).
(13) R. C. Davis, Ph.D. Thesis, University of California, Berkeley, 1967, p 128 ff.
(14) D. B. Davies and S. S. Danyluk, 14th Biophysical Society Meeting, Feb 1970.
(15) A. E. V. Haschemeyer and A. Rich, *J. Mol. Biol.*, 27, 369 (1967).

Table III.[a,b] Monopoles for the B_{2U} and B_{1U} Transitions

Atom	Transition B_{2U} SCF-CI[c]	SCF[d]	Bush-DeVoe[e]	Transition B_{1U} SCF-CI	SCF	Bush-DeVoe
Adenine						
N-1	−0.178	0.035	−0.030	0.023	−0.064	
C-2	0.091	−0.072	−0.037	−0.063	−0.050	
N-3	−0.129	0.140	−0.107	0.087	−0.014	
C-4	−0.063	0.018	−0.291	−0.089	−0.051	
C-5	−0.018	0.032	0.126	0.088	0.060	
C-6	0.156	−0.114	0.232	−0.033	0.031	
N-7	0.046	−0.085	0.055	−0.020	0.009	
C-8	−0.180	0.134	−0.106	0.050	0.026	
N-9	0.069	0.031	0.112	0.034	0.023	
N-6	0.206	−0.117	0.046	−0.078	0.030	
Guanine						
N-1	0.051	0.041	−0.032	0.116	0.039	−0.044
C-2	0.100	0.101	0.030	−0.060	−0.013	−0.165
N-3	−0.101	−0.080	−0.050	0.097	0.081	0.075
C-4	0.090	0.060	−0.104	0.108	0.125	−0.151
C-5	−0.112	−0.083	−0.034	−0.045	−0.079	0.165
C-6	−0.013	−0.000	0.035	−0.008	0.007	0.003
N-7	0.009	0.003	0.043	−0.039	−0.063	−0.042
C-8	−0.060	−0.067	−0.291	0.207	0.099	0.127
N-9	−0.009	−0.010	0.249	−0.088	0.000	0.028
O-6	−0.003	−0.002	0.166	−0.243	−0.191	0.054
N-2	0.049	0.039	−0.008	−0.046	−0.005	−0.049
Cytosine						
N-1	−0.202	−0.135	−0.097	0.129	0.095	−0.007
C-2	−0.006	−0.029	0.005	0.011	0.004	0.012
N-3	0.311	0.256	−0.135	0.187	01.05	−0.043
C-4	−0.121	−0.112	0.070	−0.043	−0.043	0.039
C-5	0.167	0.079	0.044	0.021	0.175	−0.061
C-6	−0.156	−0.118	−0.032	0.000	0.047	−0.078
N-4	−0.117	−0.083	0.155	−0.215	−0.136	0.014
O-2	0.123	0.142	−0.011	−0.089	−0.011	−0.111
Uracil						
N-1	0.104	0.080	−0.090	−0.017	−0.085	0.008
C-2	−0.006	−0.001	−0.003	0.000	0.034	0.001
N-3	0.024	0.017	−0.006	0.151	0.292	−0.062
C-4	−0.017	0.030	−0.008	0.054	0.129	−0.021
C-5	−0.286	−0.185	0.262	0.012	0.132	0.001
C-6	0.237	0.179	0.235	0.008	−0.013	−0.017
O-4	−0.063	−0.136	0.086	−0.178	−0.365	−0.001
O-2	0.005	0.016	−0.005	−0.029	−0.124	0.091

[a] The numbering system of the bases is given in Figure 1. [b] The monopoles are scaled to experiments. [c] H. Berthod, C. Giessner-Prettre, and A. Pullman, *Int. J. Quantum Chem.*, **1**, 123 (1967). [d] H. Berthod, C. Giessner-Prettre, and A. Pullman, *Theoret. Chim. Acta*, **5**, 53 (1966). [e] Reference 17.

position is rotated; however, no noticeable change is observed in the case of C-3′ and C-5′. This finding is consistent with our conclusion (section III) about the importance of configuration at the C-2′ position.

Glycosidic Rotation. We have chosen the definition of glycosidic rotation by Donohue and Trueblood.[16] The sugar-base torsion angle ϕ_{CN} is defined as the angle formed by the plane of the base and C-1′-O-1′ bond of the furanose ring when viewed along the C(1)′-N bond. ϕ_{CN} is taken as zero when C-2 of the base is antiplanar to O-1′. Positive rotation is clockwise rotation of C-1′-O-1′ when one looks from C-1′ to N. Donohue and Trueblood define "anti" conformation for $\phi_{CN} = -30 \pm 45°$ and "syn" for $\phi_{CN} = +150 \pm 45°$.

Transition Monopoles and Dipoles. Three sets of monopoles for the various transitions of the four bases were used in the computation. We used monopoles described by Bush[17] and those calculated from self-consistent field with and without configuration interaction.[18] The monopoles obtained from Bush were from an SCF-LCAO-CI calculation by DeVoe of the National Institutes of Health. His method was that of Viellard and Pullman[19] extended to the excited states. The monopoles selected by Bush were not just the lowest energy transitions but were chosen so that the transition moment directions were consistent with experimental directions, or what were inferred to be the most likely directions. Bush's procedure assumes the order of the excited states in energy may be incorrect. The magnitudes of all the monopoles were scaled to give the measured transition moment magnitudes. The scaled monopoles for the B_{2U} and B_{1U} transitions are given in Table III.

The base transition dipoles were calculated from the transition monopoles placed on each nucleus of the base. The point transition dipole is assumed to be at the center of transition charge of the base (Table IV).

The effect of different transition monopoles and the use of a self-consistent treatment of the furanose bond interactions are shown in Figure 2. One sees that the self-consistent theory for induced dipoles in the sugar (eq 11) gives very different results from eq 8. We use eq 11 for all the calculations discussed in this paper.

(16) J. Donohue and K. N. Trueblood, *J. Mol. Biol.*, **2**, 363 (1960).
(17) C. A. Bush, Ph.D. Thesis, University of California, Berkeley, 1965, p 62 ff.
(18) W. C. Johnson, private communication.
(19) A. Viellard and B. Pullman, *J. Theor. Biol.*, **4**, 37 (1963).

Table IV. Data for Transition Moments

Base	Monopoles	Transition energy, eV Theory	Transition energy, eV Exptl[a]	Exptl transition moment magnitude[a] eÅ	Exptl transition moment magnitude[a] D	Calcd transition Vector[b]	Calcd transition eÅ	Transition center,[c] Å X	Transition center,[c] Å Y
Adenine		B_{2U}							
	SCF–CI	4.8	4.77	0.813	3.90	+0.02i	+0.81j	1.24	3.65
	SCF	5.2				−0.14i	−0.80j	1.02	3.47
	Bush–DeVoe	5.6				−0.22i	+0.78j	0.96	3.10
		B_{U1}							
	SCF–CI	5.0	5.17	0.350	1.68	−0.14i	−0.32j	1.21	3.26
	SCF	5.5				−0.34i	+0.08j	1.41	3.47
	Bush–DeVoe								
Guanine		B_{2U}							
	SCF–CI	4.3	4.47	0.514	2.46	+0.51i	+0.07j	1.74	2.92
	SCF	4.4				+0.50i	+0.10j	1.73	2.85
	Bush–DeVoe	5.8				+0.22i	+0.45j	0.34	2.92
		B_{1U}							
	SCF–CI	5.1	4.94	0.806	3.87	−0.21i	−0.78j	1.06	3.44
	SCF	5.4				+0.08i	−0.80j	0.86	3.65
	Bush–DeVoe	4.2				−0.80i	+0.07j	1.33	3.04
Uracil		B_{2U}							
	SCF–CI	4.8	4.72	0.685	3.29	−0.09i	−0.68j	0.76	2.94
	SCF	5.1				−0.06i	−0.68j	0.57	3.27
	Bush–Devoe	5.2				+0.05i	+0.68j	0.80	3.01
		B_{1U}							
	SCF–CI	5.4	5.17	0.241	1.16	−0.08i	−0.23j	−0.50	4.14
	SCF	5.5				+0.04i	−0.24j	−0.43	3.79
	Bush–DeVoe	6.3				−0.15i	−0.18j	−1.29	2.52
Cytosine		B_{2U}							
	SCF–CI	4.1	4.57	0.632	3.04	−0.62i	+0.09j	−0.25	3.02
	SCF	4.2				−0.63i	−0.04j	−0.47	2.95
	Bush–DeVoe	5.4				+0.18i	+0.60j	−0.22	3.64
		B_{1U}							
	SCF–CI	5.1	5.17	0.549	2.63	−0.00i	−0.55j	−0.62	3.49
	SCF	5.3				−0.11i	−0.54j	−0.09	3.52
	Bush–DeVoe	6.8				+0.40i	+0.38j	0.06	2.85

[a] Resolved from spectra of Pabst Laboratories, Milwaukee, Wis. (Circular OR-10, 1967). [b] Transition moment vectors are scaled to experimental magnitude. i, j are unit directional vectors referring to X, Y axes defined in Table I. [c] Coordinates are defined in Table I.

Table V. Bond Polarizabilities (Å³)

Bond	α_{33}[a]	α_{11}[a]
	I[b]	
C–H	0.46	0.77
C–C	0.99	0.27
C–O	1.23	0.27
	II[c]	
C–H	0.8	0.6
C–C	1.85	0.02
	III[d]	
C–H	0.64	0.64
C–C	0.99	0.27
C–O	0.89	0.46
	IV[e]	
C–H	0.77	0.59
C–C	1.35	0.23

[a] α_{33} is along the bond and α_{11} is perpendicular to the bond. [b] See ref 20. [c] See ref 21. [d] R. J. W. Le Fevre, *Adcan. Phys. Org. Chem.*, 3, 1 (1965). [e] R. J. W. Le Fevre, B. J. Orr, and G. L. D. Ritchie, *J. Chem. Soc. B*, 273 (1966).

Polarizabilities. Bond polarizabilities have always been the subject of controversy. The merits of different measurements of polarizability have frequently been discussed, especially by users wanting to evaluate optical activity.[4,3,20] Because of the uncertainties in the bond polarizabilities, the agreement between experiment and the result of any calculation which is sensitive to the values of bond polarizability should be examined critically.

Different sets of values of bond polarizabilities have been published (Table V). These values include those which have been proven satisfactory for other workers,[10] and those existing in the current literature. The rotational strength of uridine resulting from

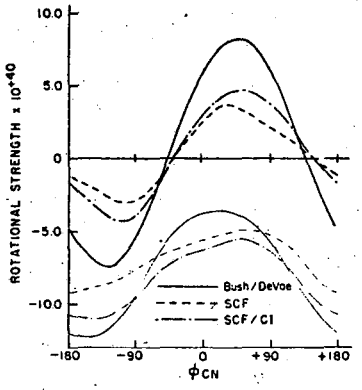

Figure 2. The effect of different transition monopoles and the self-consistent treatment of furanose bonds on $R(B_{2U})$ *vs.* ϕ_{CN} of uridine. The top three curves are self-consistently treated as in eq 11. The bottom three curves are without the self-consistent furanose treatment (eq 8).

different combinations of possible values of bond polarizabilities, using the SCF–CI monopoles, is shown in Figure 3. The calculated R_{OA} is more sensitive to C–O and O–H bond polarizabilities than C–C C–H bonds. The same conclusion is obtained with

(20) C. Houssier and K. Sauer, *J. Amer. Chem. Soc.*, 92, 779 (1970).

Table VI. Calculated Rotational Strengths for Different Monopoles and Furanose Configurations and Conformations[a]

Compound	Exptl $R_{OA} \times 10^{40}$ esu	Monopoles	Theor $R_{OA} \times 10^{40}$ esu B_{2U} Anti	B_{2U} Syn	B_{1U} Anti	B_{1U} Syn
Adenosine	$-2(B_{2U} + B_{1U})$	SCF-CI	−2	+3	+0	+0
		SCF	−2	+3	+2	−4
		Bush-DeVoe	+8	−8		
Guanosine	$-0(B_{2U})$	SCF-CI	+2	−4	−2	+3
	$-1(B_{1U})$	SCF	+2	−4	−2	+2
		Bush-DeVoe	−7	+7	+8	−16
Uridine	$+9(B_{2U})$	SCF-CI	+1	+0	+0	−0
	$-4(B_{1U})$	SCF	+1	+0	−2	+2
		Bush-DeVoe	+2	−1	+0	−1
Cytidine	$+12(B_{2U})$	SCF-CI	+27	−31	−7	+7
	$-6(B_{1U})$	SCF	+19	−24	−5	+5
		Bush-DeVoe	−6	+6	−2	+0
2′-Deoxy A	$-1(B_{2U} + B_{1U})$					
2′ endo		SCF-CI	−2	+4		
3′ endo		SCF-CI	−7	+0		
2′-Deoxy G	$-0(B_{2U})$					
	$-0(B_{1U})$					
2′ endo		SCF-CI	+1	−5		
3′ endo		SCF-CI	+5	−0		
2′-Deoxy U	$+3(B_{2U})$					
2′ endo		SCF-CI	+5	+2		
3′ endo		SCF-CI	+3	+1		
2′-Deoxy C	$+(B_{2U})$					
	$-(B_{1U})$					
2′ endo		SCF-CI	+24	−34		
3′ endo		SCF-CI	+35	+0		

[a] The four ribonucleosides are in the 2′-endo conformation.

the other two sets of monopoles. This is unfortunate because the bond polarizabilities for C–O and O–H bonds are the least well known. For all the computations, unless otherwise stated, we have used Le Fevre's[21]

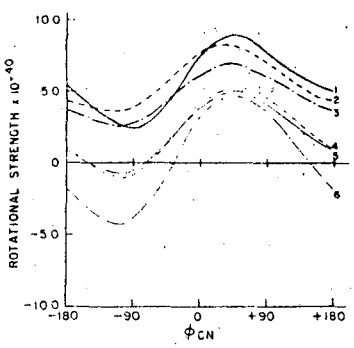

Figure 3. Calculated rotational strengths of B_{2U} transitions of uridine as a function of ϕ_{CN} using different values of polarizabilities. The various sets of polarizabilities are given in Table V: (1) set I, treating OH equivalent to CH; (2) set III, treating OH equivalent to CH; (3) set II, approximating OH by $\alpha_{zz} = 0.8$, $\alpha_{yy} = 0.6$; (4) set IV, treating OH equivalent to CH and CO equivalent to CC; (5) set I, approximating OH by 0.8, 0.6; (6) set II, treating OH equivalent to CH and CO equivalent to CC.

bond polarizabilities (set II in Table V) and treated carbon and oxygen equivalently (curve 6 in Figure 3).

III. Results and Discussion

Results of the calculations are given in Tables VI, VII, and VIII, and Figure 4. The rotational strengths of the B_{2U} and B_{1U} transitions were calculated using eq II for each of the four nucleosides (Table VI). The effect of the 2′-endo and 3′-endo furanose conformation is also

(21) C. G. Le Fevre and R. J. Le Fevre, *Rev. Pure Appl. Chem.*, 5, 261 (1955).

Table VII. Comparison of Calculated and Experimental Rotational Strengths for Different Anomeric Adenosines

Compd	λ_{max}, mμ	Exptl max molar ellipticities[a]	$R_{OA}(B_{2U}) \times 10^{+40}$ esu Exptl[a,b]	Theor[d] Anti	Theor[d] Syn
α-Lyx	260	3750	2.7[c]	3	−7
β-Lyx	256	−3560	−2.7	−2	6
α-Ribo	256	5410	4.4	3	−6
β-Ribo	265	−2970	−2.5[c]	−2	3
α-Ara	258	3570	2.8	1	−6
β-Ara	258	−5380	−4.1	−2	4
α-Xyl	258	6960	6.0	5	−7
β-Xyl	259	−2450	−2.0	−3	5

[a] The experimental results are from Ingwall (personal communication). Molar ellipticities are in units of deg l./(mol cm). [b] The rotational strengths are evaluated by fitting the spectrum by gaussian curves on a DuPont curve resolver and computed using the formula, $R_i = 1.23 \times 10^{-42} (\theta_i \Delta_i / \lambda_i)$ where Δ_i is the half-width of the resolved gaussian. [c] Single gaussian is not possible. Composite gaussian curves are used. [d] SCF-CI monopoles used.

Table VIII. Calculated $R_{OA}(B_{2U})$ of Nucleosides[a] with Glycosidic Angle ϕ_{CN} Present in Polynucleotides

Base	$R_{OA}(B_{2U}) \times 10^{+40}$ esu ϕ_{CN}[b] = −11° (RNA-II)	−14° (DNA-A)	−86° (DNA-B)
A	−3	−3	+5
G	+1	+1	−1
U (T)	+2	+6	+1
C	+31	+32	−25

[a] SCF CI monopoles and the 2′-endo conformation for ribose and deoxyribose were used. [b] ϕ_{CN}'s are from M. Sundaralingam, *Biopolymers*, 7, 821 (1969).

included. From the results, it can be seen that the rotational strength calculation depends critically on the choice of wave functions. However, the rotational strengths from the SCF-CI and SCF monopoles nearly always agree in sign and magnitude with each other. Quantitative comparison with experiment is difficult, because of the uncertainty in assignment and resolution of the CD spectrum into bands. In Table VI the experimental rotational strengths are given to one significant figure, or the sign is simply given. The calculated values are shown for two conformations: anti ($\phi_{CN} = -30°$) and syn ($\phi_{CN} = +150°$). The experimental value, of course, represents an average value over the conformations actually present in solution. With SCF-CI or SCF monopoles the signs of the calculated rotational strengths for the first two transitions are consistent with three of the four mononucleosides in the anti conformation. Calculations for guanosine are not consistent with experiment for either syn or anti conformations.

Figure 4 shows what values of the glycosidic angle give correct results for the calculated signs of the B_{2U} and B_{1U} rotational strengths. For uridine and cytidine, about half the possible range of angles ($+150° > \phi_{CN} > -30°$) give the correct sign for both B_{2U} and B_{1U}. For adenosine only the anti range ($-10° > \phi_{CN} > -90°$) is consistent with the signs of the rotational strengths. For guanosine a very small overlap occurs ($\phi_{CN} \simeq -100°$) between values of ϕ_{CN} which give the correct sign for both B_{2U} and B_{1U} rotational strengths. This probably indicates that guanosine does not exist mainly in one conformation, but instead, includes a wide range of conformations. There is some evidence that the conformation of guanosine depends on pH, as might be expected for a conformationally mobile molecule.

One way of testing this idea further is to calculate an average rotational strength by weighting each calculated rotational strength at angle ϕ_{CN} by the probability of finding the molecule with this value of ϕ_{CN}. We used a probability distribution for the glycosidic bond (ϕ_{CN}), which we had estimated earlier,[22] to obtain an average rotational strength for the B_{2U} transitions for each mononucleoside. Although magnitudes were changed, no signs changed, so a positive B_{2U} rotational strength was still obtained for guanosine in disagreement with experiment.

The temperature dependence of the rotational strengths was also calculated. This gives an increase in rotational strengths with decreasing temperature as expected. It also gives the correct order of magnitude change[13] as the temperature is lowered from +90° to −70°. For cytidine there is a calculated 3% increase, for adenosine a calculated 30% increase.

In Table VII the results for the anomeric cis-trans isomers of adenosine are given. The calculated results for the anti conformation agree well with experiment. The agreement between theory and experiment is excellent when one considers the α and β pairs of the different isomers. The calculation gives not only the correct sign for each one of the pairs, but also provides the correct relative magnitudes. We see that experimentally the sign of the CD for the anomeric adenosine

(22) I. Tinoco, Jr., R. C. Davis, and S. R. Jaskunas, "Molecular Association in Biology," B. Pullman, Ed., Academic Press, New York, N. Y., 1968, p 77.

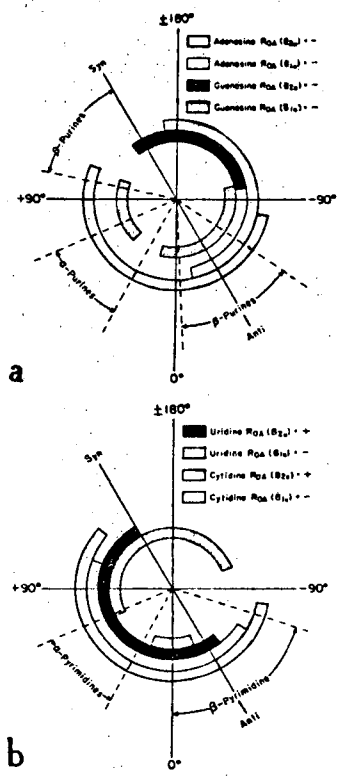

Figure 4. Glycosidic angle (ϕ_{CN}) and calculated sign of the rotational strength. The range of angles labeled α,β-purines and -pyrimidines shown is that found in crystals by X-ray scattering (see Sundaralingam, Table VIII, footnote *b*). The rotational strengths were calculated with SCF-CI monopoles: (a) purines, the measured signs of the rotational strengths are minus for both B_{2U} and B_{1U} transitions of adenosine and guanosine; (b) pyrimidines, the measured signs are plus for the B_{2U} transitions and minus for the B_{1U} transitions of uridine and cytidine.

depends on the configuration at C-1′: α gives a positive CD at high wavelength, β gives a negative CD. The good agreement with the calculated rotational strengths is strong evidence that all eight of these molecules are primarily in the anti conformation.

We also carried out calculations on uracil with different sugars. Experimentally,[23] it was found that the rotational strengths of β-D-ara-U and β-D-lyx-U were similar and approximately twice that of β-D-rib-U. The R_{OA} calculated for these compounds are $+10 \times 10^{-40}$, $+11 \times 10^{-40}$, and $+2 \times 10^{-40}$ for ara-, lyx-, and rib-U, respectively. The Bush-Devoe monopoles were used and anti conformation was assumed.

We have found that a configuration change at the C-2′ position of the furanose alters the glycosidic angular dependence of R_{OA} more significantly than that at the C-3′ position. The calculated R_{OA} *vs.* ϕ_{CN} for ribo and xyl compounds are similar in curve shape and positions of maximum, minimum, and zero crossing, whereas the same holds for ara and lyx compounds.

(23) T. Nishimura, B. Shimizu, and I. Iwai, *Biochim. Biophys. Acta*, **157**, 221 (1968).

Experimentally, it was found that the configuration at C-2′ profoundly affects the magnitude of the Cotton effect.[8,22] It was reported previously[24] that a cis-oriented hydroxyl group at C-2′ interacts with the base and that cis nucleosides gave a Cotton effect larger in magnitude than the trans anomers. It was found that[23] the amplitudes of the Cotton effect of α-D-rib-U and α-D-UMP are larger than their β anomers; however, the magnitudes of α-lyx nucleosides give smaller Cotton effects compared to their β anomers. Examination of molecular models suggests that the C-1′–C-2′ trans configuration allows the base to rotate more freely about the glycosidic bond. By inspection of the R_{OA} *vs.* ϕ_{CN} curve, it can be seen that a range of allowed values of ϕ_{CN} always results in decreasing the amplitude of a trans compound.

The main reason for beginning this study was to estimate the contribution of base–sugar interactions to the CD of polynucleotides. Table VIII shows the calculated B_{U2} rotational strengths for nucleosides with the glycosidic angle found in different double-stranded nucleic acids: A-form DNA,[25] B-form DNA,[26] and RNA-II.[27] One sees that in B-form DNA the calculated rotational strengths are very different from those of A-DNA, or anti mononucleosides. This means one cannot ignore base–sugar interactions in understanding the CD of double-stranded nucleic acids. The CD of the mononucleoside in solution may be very different from its contribution to the CD of the nucleic acid.

Acknowledgments. We wish to thank Dr. W. Curtis Johnson, Jr., for many helpful discussions, and Dr. A. M. Bobst for making some of the calculations. We would also like to express our gratitude to Dr. Joan Ingwall for kindly communicating to us her unpublished results.

(24) T. L. V. Ulbricht, T. R. Emerson, and R. J. Swan, *Biochem. Biophys. Res. Commun.*, 22, 505 (1966).

(25) W. Fuller, M. H. F. Wilkins, R. H. Wilson, and L. D. Hamilton, *J. Mol. Biol.*, 12, 60 (1965).

(26) R. Langridge, D. A. Marvin, W. E. Seeds, H. R. Wilson, C. W. Hooper, M. H. F. Wilkins, and L. D. Hamilton, *ibid.*, 2, 38 (1960).

(27) S. Arnott, M. H. F. Wilkins, W. Fuller, and R. Langridge, *ibid.*, 27, 535 (1967).

LEGAL NOTICE

This report was prepared as an account of work sponsored by the United States Government. Neither the United States nor the United States Atomic Energy Commission, nor any of their employees, nor any of their contractors, subcontractors, or their employees, makes any warranty, express or implied, or assumes any legal liability or responsibility for the accuracy, completeness or usefulness of any information, apparatus, product or process disclosed, or represents that its use would not infringe privately owned rights.

TECHNICAL INFORMATION DIVISION
LAWRENCE BERKELEY LABORATORY
UNIVERSITY OF CALIFORNIA
BERKELEY, CALIFORNIA 94720